Centrum Badań Molekularnych i Makromolekularnych

Polskiej Akademii Nauk

ROZPRAWA DOKTORSKA

„Hybrydowe kompozyty polilaktydu i pochodnych krzemoorganicznych"

Agata Sabrina Herc

Promotor: **dr hab. inż. Anna Kowalewska, prof. CBMiM PAN**

Łódź, 2021

Praca doktorska wykonana w ramach projektu

"Badania oddziaływań supramolekularnych między reaktywnymi nanonapełniaczami wstęgowymi nowego typu a matrycami polimerowymi"

OPUS 11 2016/21/B/ST5/03070

Spis treści

Wykaz ważniejszych skrótów i symboli:

AIBN – azobis(izobutyronitryl)

CX-Vi – 1,3,5,7-tetrametylo-1,3,5,7-tetrawinylocyklotetrasiloksan

DMPA – 2,2-dimetoksy-2-fenyloacetofenon

DMTA – dynamiczna analiza termo-mechniczna, *Dynamic Mechanical Thermal Analysis*

DSC – różnicowa kalorymetria skaningowa, *Differential Scanning Calorimetry*

E' – moduł sprężystości

E" – moduł stratności

EDS – rentgenowska spektroskopia energodyspersyjna, *Energy Dispersive Spectroscopy*

FTIR – spektroskopia fourierowska w podczerwieni, *FourierTransform Infrared*

HMDS – 1,1,1,3,3,3-heksametylodisilazan

LA – laktyd

LAc – kwas 2-hydroksypropionowy, kwas mlekowy

LPSQ – liniowe poli(silseskwioksany), *Linear Poly(Silsesquioxanes)*

M_n – liczbowo średnia masa cząsteczkowa

M_w – wagowo średnia masa cząsteczkowa

NMR – spektroskopia rezonansu magnetycznego, *Nuclear Magnetic Resonance Spectroscopy*

PLA - polilaktyd

PDLA – poli-(D-laktyd)

PLLA – poli-(L-laktyd)

POSS – silseskwioksany poliedryczne, *Polyhedral Oligomeric Silsesquioxanes*

SC-PLA – stereokompleks polilaktydu

SEM – skaningowa mikroskopia elektronowa, *Scanning Electron Microscopy*

T_{cc} – temperatura zimnej krystalizacji

T_g – temperatura zeszklenia

TGA – analiza termograwimetryczna, *Thermogravimetric Analysis*

T_m – temperatura topnienia

UV-VIS – spektroskopia w zakresie światła widzialnego (VIS) i bliskiego ultrafioletu (UV)

V_d – szybkość rozkładu termicznego próbki (w TGA)

W – wydajność procentowa reakcji, molowa

σ_y – granica plastyczności

σ_b – naprężenie przy zerwaniu

ε_b – odkształcenie przy zerwaniu

%wag. - stężenie procentowe, wagowe

I. WPROWADZENIE i Krótki PRZEGLĄD LITERATURY PRZEDMIOTOWEJ

1. Polilaktyd – metody otrzymywania i właściwości:

W ostatnich latach coraz większym problemem staje się zanieczyszczenie środowiska naturalnego odpadami z tworzyw polimerowych, związane z bardzo wolnym rozkładem polimerów syntetycznych, oraz wyczerpywanie się zasobów surowców kopalnych używanych do produkcji tych materiałów. Z tego powodu coraz intensywniej badane są tworzywa wytwarzane z surowców naturalnych – przyjazne dla środowiska naturalnego, które ulegają rozpadowi pod wpływem czynników atmosferycznych lub w pod wpływem enzymów, a jednocześnie zachowują właściwości klasycznych polimerów. Głównym atutem biopolimerów jest ich kompostowalność, biodegradowalność oraz naturalne pochodzenie surowców stosowanych do ich wytwarzania. Wykazują one też dobre właściwości aplikacyjne, są biokompatybilne i nietoksyczne. Ten typ polimerów często określa się też mianem „podwójnie zielonych", wśród których największym zainteresowaniem cieszy się polilaktyd (PLA).
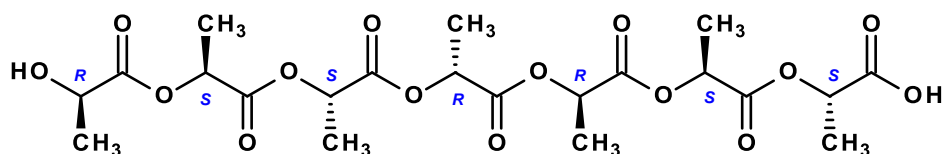
Schemat 1. Budowa łańcucha polilaktydu.

Polilaktyd (Schemat 1) to alifatyczny poliester określany mianem tworzywa XXI wieku. Wyjściowym substratem do jego syntezy jest kwas 2-hydroksypropionowy, zwany kwasem mlekowym (LAc). Jest to najprostszy kwas organiczny zawierający w swojej cząsteczce chiralny atom węgla, dzięki czemu kwas mlekowy występuje w dwóch formach: L(+)kwas mlekowy oraz D(-)kwas mlekowy. Cyklizacja dwóch cząsteczek kwasu mlekowego prowadzi do utworzenia dimeru nazywanego laktydem. Istnieją trzy diastereoizomery laktydu: L-laktyd (L(+)LA), D-laktyd (D(-)LA) oraz LD-*mezo*-laktyd, w cząsteczce którego chiralne atomy węgla mają przeciwną konfigurację.[1-8]

PLA można otrzymać na drodze bezpośredniej polikondensacji kwasu mlekowego, w wyniku której otrzymuje się poli(kwas mlekowy) o małej masie cząsteczkowej, lub poprzez polimeryzację z otwarciem pierścienia (ROP – Ring Opening Polymerization) monomerów laktydowych.[1-8] W wyniku polimeryzacji z otwarciem pierścienia laktydowego można otrzymać PLA o dużej masie cząsteczkowej (ponad 50 000 g/mol). Dzięki odpowiedniemu dobraniu stosunku stężeń inicjatora i monomeru możliwa jest kontrola masy molowej otrzymanych produktów. Jest to najefektywniejszy sposób produkcji PLA o dobrych właściwościach mechanicznych. Ze względu na obecność chiralnego atomu węgla w cząsteczce laktydu, łańcuchy PLA mogą mieć różną konfigurację: poli-L(+)-laktyd (PLLA), poli-D(-)-laktyd (PDLA), poli-*mezo*-laktyd oraz poli-*rac*-laktyd.[1-8]

Łańcuchy PLA mogą tworzyć cztery formy krystaliczne (α, β, δ, γ), w zależności od warunków krystalizacji.[9-14] Najbardziej powszechną formą krystaliczną jest struktura typu α (układ rombowy), która krystalizuje ze stopu lub z roztworów. Makrocząsteczki PLLA lub PDLA przyjmują kształt odpowiednio lewo- lub prawoskrętnej helisy α w konformacji 10_3 co oznacza, że na trzy skręty helisy przypada dziesięć jednostek mleczanowych. Forma δ, nazywana także formą α' powstaje w temperaturach < 120 ºC i wykazuje podobne wartości pików dyfrakcyjnych co forma α. Forma β może powstać podczas szybkiego rozciągania i pod wpływem wysokich temperatur. Forma γ jest głównie otrzymywana poprzez epitaksjalny wzrost na substratach o odpowiedniej strukturze.

Właściwości fizykochemiczne PLA silnie zależą od składu stereochemicznego merów oraz rozmieszczenia ich w łańcuchu głównym.[9-14] Najczęściej spotykany poli(L-laktyd) zawierający niewielką ilość merów typu D, to amorficzny polimer charakteryzujący się temperaturą zeszklenia (T_g) około 60 ºC i temperaturą topnienia (T_m) około 150 ºC (Tabela 1). Wykazuje on gorsze właściwości mechaniczne oraz znacznie łatwiej i szybciej poddaje się degradacji niż PLLA czy PDLA, które wykazują T_g około 60-65 ºC. W przypadku PLLA obserwuje się wyższą T_m (około 170-200 ºC). Temperatura zeszklenia polilaktydu zależy od m.in. masy cząsteczkowej oraz rozłożenia merów w łańcuchu polimerowym. Powyżej T_g łańcuchy polimerowe stają się bardziej mobilne i może rozpocząć się proces krystalizacji frakcji amorficznej polilaktydu - tak zwanej „zimnej krystalizacji". Na termogramach DSC można również często zaobserwować niewielki egzotermiczny sygnał, pojawiający się tuż przed endotermicznym pikiem topnienia. Świadczy on obecności mniej uporządkowanej formy α' i pochodzi od jej przemiany krystalicznej w ciele stałym w bardziej doskonałą fazę α.[9-14] Mieszanina izotaktycznych, homochiralnych łańcuchów PLLA i PDLA jest zdolna do utworzenia stereokompleksów (SC-PLA). Makrocząsteczki PLLA i PDLA w stereokompleksach przyjmują kształt podwójnej helisy β o konformacji 3_1 (na jeden skręt helisy przypadają trzy jednostki mleczanowe), w układzie trójskośnym. SC-PLA odznaczają się wyższą temperaturą topnienia (230 ºC) w porównaniu z homochiralnymi kryształami każdego z jej składników.[9-14]

Tabela 1. Porównanie właściwości PLA (amorficzny), PLLA oraz PDLA[3,15]

Właściwości	PLA	PLLA	PDLA
ρ [g/cm^3]	1,21-1,25	1,24-1,3	1,25-1,27
σ [MPa]	21-60	15,5-150	27,6-50
E [GPa]	0,35-3,5	2,7-4,14	1-3,45
ε_b [%]	2,5-6	3,0-10	2,0-10
σ^* [Nm/g]	16,8-48	40,0-66,8	22,1-39,4
E* [kNm/g]	0,28-2,8	2,23-3,85	0,80-2,36
T_g [ºC]	45-60	55-65	50-60
T_m [ºC]	150-162	170-200	-

ρ [g/cm^3] – gęstość

σ [MPa] – wytrzymałość na rozciąganie

E [GPa] – moduł Younga (moduł sprężystości podłużnej)

ε_b [%] – wydłużenie przy zerwaniu

σ^* [Nm/g] – specyficzna wytrzymałość na rozciąganie

E* [kNm/g] - specyficzny moduł sprężystości

T_g [°C] – temperatura zeszklenia

T_m [°C] – temperatura topnienia

Właściwości mechaniczne oraz zdolność do krystalizacji PLA również zależą od jego masy cząsteczkowej oraz rozkładu merów w łańcuchu.[13,14] Dzięki możliwości kontroli stereochemicznej budowy PLA można kontrolować proces krystalizacji oraz jego mechaniczne właściwości i temperatury przetwórstwa. Wykazano na przykład, że moduł sprężystości PLLA wzrasta dwukrotnie gdy M_w wzrastała od 50 do 100 kDa.[13,14] Wytrzymałość na rozciąganie wraz ze zmianą masy od 50, 150 do 200 kDa wzrastała odpowiednio: 15,5; 80 i 150 MPa.[13,14] Częściowo krystaliczny polilaktyd wykazuje lepsze właściwości mechaniczne w porównaniu do amorficznego. Charakteryzuje się on modułem sprężystości w przybliżeniu równym 3 GPa, wytrzymałość na rozciąganie osiąga wartość w granicach od 50 do 70 MPa, moduł zgięcia 5 GPa, wytrzymałość materiału na zginanie to 100 MPa.[13,14] Jest jednak materiałem kruchym - jego wydłużanie przy zerwaniu wynosi około 4%. Najlepsze mechaniczne właściwości wykazują SC-PLA. Czysty stereokompleks ma nie tylko wyższą temperaturę topnienia, ale też znacznie lepsze właściwości mechaniczne niż czysty polilaktyd.[13,14,16] Wykazano, że w przypadku polilaktydu o niskiej masie cząsteczkowej wytrzymałość na rozciąganie dla SC-PLA wynosi 50 MPa, natomiast dla czystego PLLA około 31 MPa.[13,14,16]

PLA oraz inne biodegradowalne polimery wykorzystuje się głównie w dwóch obszarach. Polimery produkowane wielotonażowo stosowane są w produkcji opakowań i innych produktów jednorazowego użytku oraz w rolnictwie. Drugim obszarem zastosowań biopolimerów są zastosowania specjalistyczne, przede wszystkim w medycynie i inżynierii tkankowej jako bioresorbowalne implanty, nici chirurgiczne jak również nośniki leków.[6,17-19] Mimo swoich dobrych właściwości chemicznych i fizycznych, PLA nie jest materiałem idealnym. Z tego powodu poszukuje się nowych rozwiązań mających na celu utrzymanie biozgodności, a udoskonalenie innych cech użytkowych PLA, takich jak, na przykład, zbyt mała wytrzymałość na rozciąganie, co znacznie ogranicza jego przemysłowe zastosowanie.

2. Kompozyty PLA:

Modyfikacja polilaktydu w celu polepszenia jego właściwości termicznych i mechanicznych oraz zwiększenia jego zdolności do krystalizacji może być przeprowadzana różnymi metodami. Stosowana jest chemiczna modyfikacja PLA poprzez szczepienie łańcuchów bocznych lub kopolimeryzację.[20-23] Jedno ze stosowanych rozwiązań polega na wprowadzeniu napełniaczy/nanonapełniaczy, nukleantów lub plastyfikatorów do matrycy polimerowej co prowadzi do otrzymania tzw. materiałów kompozytowych i mieszanin polimerowych.[20-23] Kompozyty polilaktydu, w zależności od rodzaju dodatku, mogą wykazywać na przykład znacznie wyższą wytrzymałość mechaniczną, zwiększoną stabilność termiczną, lepszą zdolność do krystalizacji czy też niską palność, mimo niewielkiej ilości dodanego napełniacza.[20,22-24] Za czynniki polepszające właściwości PLA zostały uznane różne rodzaje napełniaczy, m.in. dodatki mineralne, dodatki makrocząsteczkowe, nanoceluloza, grafen. Heteroorganiczne modyfikatory PLA można sklasyfikować według sposobu ich otrzymywania,

tj. naturalne, półsyntetyczne i syntetyczne. Jednak zwykle kryterium podziału stanowią wymiary cząstek:[21]

- płytkowe nanowypełniacze (1D) - zwykle o grubości rzędu 1 nm (np. płatki grafenu);
- nanowłókna (2D) - o średnicy poniżej 100 nm (np. nanorurki węglowe, nanoceluloza);
- nanocząstki (3D) - średnie wymiary wynoszą poniżej 100 nm (np. POSS, tlenki metali).

Nanocząstki dodawane do matrycy polimerowej, dzięki znacznie większemu stosunkowi powierzchni do objętości, wykazują większy kontakt z cząsteczkami matrycy. W konsekwencji może to poprawiać właściwości fizykochemiczne lub skutkować pojawieniem się nowych, ciekawych właściwości w porównaniu do wyjściowego polimeru. Kompozyty i nanokompozyty o osnowie polilaktydowej z dodatkiem heterogenicznych napełniaczy można otrzymać metodą mieszania roztworów/zawiesin (a następnie odparowania rozpuszczalnika); mieszania ze stopem polimerowym; na drodze polimeryzacji in situ (dodatki rozpraszane są w ciekłym monomerze lub jego roztworze, następnie prowadzi się polimeryzację w obecności nanowypełniacza); syntezy matrycowej (nanowypełniacze są syntetyzowane z roztworu prekursora przy użyciu polimerów jako matrycy).[21-23]

Aktualnie poszukuje się jak najbardziej efektywnych metod wytwarzania biodegradowalnych materiałów kompozytowych o jak najlepszym rozproszeniu napełniaczy w matrycy polimerowej oraz o jak najkorzystniejszych właściwościach użytkowych. Przykładem klasycznego napełniacza nieorganicznego modyfikującego właściwości osnowy PLA jest talk.[20-23] Jego dodanie powoduje zwiększenie szybkości krystalizacji PLA, zwiększa sztywność oraz termoodporność, polepsza właściwości barierowe oraz ułatwia przetwórstwo PLA. Obecność talku istotnie wpływa na efekt zarodkowania polilaktydu. Według literatury, dodanie 1% wag. talku skutecznie przyspiesza zarodkowanie i szybkość krystalizacji PLA, a dodatek 2% wag. talku zmniejsza prawie 65-krotnie czasy połówkowe izotermicznej krystalizacji.[20-23]

Innym dodatkiem nieorganicznym jest krzemionka (SiO_2), która jest często stosowana w kompozytach polimerowych ze względu na wysoką odporność termiczną i funkcjonalność oraz niski koszt.[20-23] Zaobserwowano, że nanocząstki krzemionki wpływają na efekt enukleacji, zwiększają wytrzymałość polilaktydu na rozciąganie i wydłużenia przy zerwaniu.[20-23] Niewielka ilość krzemionki poprawia wytrzymałość PLA na rozciąganie, natomiast przy większej jej zawartości (10% wag.) obserwowano agregację jej nanocząstek. Jest to związane z małą kompatybilnością nieorganicznego dodatku i osnowy poliestrowej. Rozwiązaniem tego problemu jest zastosowanie poliedrycznych silseskwioksanów (POSS), które mogą być uznane za nanocząstki krzemionki związane kowalencyjnie z grupami organicznymi połączonymi z atomami krzemu. Nanocząstki POSS są monodyspersyjne, co polepsza ich rozproszenie w masie polilaktydu.[20-23] Można wykorzystać je poprzez zmieszanie z polimerem bądź kopolimeryzację, dzięki czemu można uzyskać materiały o lepszych właściwościach mechanicznych, a także zmniejszonej palności. W nanokopozytach PLA/POSS szybkości krystalizacji wzrastały wraz z zawartością POSS i były znacznie wyższe w porównaniu do czystego PLA.[20-23]

W przypadku dodatków organicznych najczęściej badanymi nanowypełniaczami 2D są nanorurki węglowe (CNT).[24] CNT stały się przedmiotem szczególnego zainteresowania ze względu na swoje wyjątkowe właściwości, m.in. takie jak bardzo wysoki moduł Younga, wysoka przewodność elektryczna i cieplna. Dzięki temu CNT mogą stanowić elementy wzmacniające lub przewodzące w kompozytach PLA. Dzięki zwiększeniu stopnia krystaliczności PLA, CNT zmniejszają szybkość biodegradacji polilaktydu. W celu poprawy rozproszenia CNT w matrycy PLA zwykle przeprowadza się ich funkcjonalizację powierzchniową (utlenianie) w celu wytworzenia grup funkcyjnych takich jak COOH, czy OH. Zmodyfikowane w ten sposób CNT mogą oddziaływać poprzez tworzenie wiązań wodorowych z wiązaniem estrowym łańcuchów PLA.[24]

Dużo uwagi poświęcono poprawie zjawiska krystalizacji PLA (zarodkowanie i wzrost kryształów), którą można poprawić za pomocą nukleatorów oraz/lub plastyfikatorów mało- i wielkocząsteczkowych.[20-23] Szczególną klasą dodatków do polilaktydu, są związki organiczne, które mogą wpływać na krystalizację łańcuchów poliestrowych poprzez wykorzystanie oddziaływań supramolekularnych (wiązania wodorowe lub efekty „gość-gospodarz"). Do grupy tej zaliczyć można aminokwasy lub poli(aminokwasy)[25], ftalimid[26], pochodne mocznika[27] lub kwasu glukonowego[28], jak również kwas orotowy[29], kwasów humusowych i fulwowych[30,31], nanocelulozę[32] oraz cyklodekstryny.[33]

Bardzo ciekawe zachowanie obserwowano w przypadku użycia pochodnych arylowych zawierających wiązania amidowe[34] lub hydrazydowe[35] jak również stosując 1,3:2,4-dibenzylideno-D-sorbitol.[36] Substancje te są rozpuszczalne w stopie polilaktydu i w czasie schładzania do temperatur wyższych niż temperatura krystalizacji PLA, krystalizują w formie nanokryształów. Tworzenie wiązań wodorowych pomiędzy wiązaniami estrowymi w łańcuchach PLA i strukturami amidowymi lub hydrazydowymi prowadzą do bardzo efektywnej nukleacji i znacznie przyspieszają proces krystalizacji polilaktydu. Należy jednak podkreślić, że związki te (podobnie jak nukleatory nieorganiczne) nie zmieniają rodzaju struktury krystalicznej (kryształy typu α w osnowie pojedynczych enancjomerów polilaktydu, tj. PLLA lub PDLA).

W przypadku wspomnianych wyżej oddziaływań supramolekularnych przyczyną zwiększenia szybkości krystalizacji PLA jest zmiana mobilności segmentów łańcucha poliestrowego w wyniku interakcji międzycząsteczkowych. Oznacza to, że na krystalizację makrocząsteczek PLA można wpływać jeszcze przed pojawieniem się właściwych zarodków kryształów. Zjawisko to przypomina tworzenie się racemicznej konformacji helikalnej ($3_2/3_1$) pary makrocząsteczek, która pojawia się w stopie mieszany poli(Llaktydu) i poli(D-laktydu), a struktury utworzone w ten sposób są miejscami zarodkowania kryształów stereokompleksów PLLA/PDLA.[37,38]

III. CEL I ZAKRES PRACY

Celem prowadzonych badań było uzyskanie nowych hybrydowych kompozytów polilaktydu z dodatkiem sfunkcjonalizowanych liniowych poli(silseskwioksanów) (LPSQ-R) o ulepszonych właściwościach fizykochemicznych i mechanicznych. Moje główne zadanie badawcze polegało na opracowaniu efektywnych metod funkcjonalizacji liniowych poli(silseskwioksanów) w celu uzyskania makrocząsteczek zdolnych do oddziaływań supramolekularnych z łańcuchami poliestrowej osnowy i zastosowaniu ich, jako napełniaczy/modyfikatorów nowego typu. Zbadanie właściwości uzyskanych materiałów wiązało się z koniecznością analizy charakteru oddziaływań pomiędzy składnikami uzyskanych kompozytów. Wspólną cechą zastosowanych liniowych poli(silseskwioksanów) jest obecność podwójnego łańcucha głównego o drabinkowej budowie, co umożliwia kontrolę rozmieszczenia przestrzennego bocznych grup funkcyjnych znajdujących się przy każdym atomie krzemu. Dzięki temu makrocząsteczki LPSQ-R mogą przypominać w pewnym stopniu supramolekularne kryształy tworzone przez pochodne aryloamidowe w stopie polilaktydu. Aby określić wpływ obecności struktur poli(silseskwioksanowych) na właściwości kompozytów PLA/LPSQ-R, przeprowadzone zostały także badania porównawcze z wykorzystaniem małocząsteczkowych modeli – odpowiednio sfunkcjonalizowanych tetrametylocyklotetrasiloksanów (CX-R). W celu zbadania efektu różnorodnych oddziaływań supramolekularnych na zmianę właściwości osnowy polimerowej, zaprojektowano szereg nowych LPSQ-R oraz CX-R (R = podstawniki zawierające grupy OH, (OH)$_2$, COOH oraz COOMe, lub C$_6$F$_5$, C$_6$H$_4$F, C$_6$H$_4$CF$_3$). Postulowano udział tych grup funkcyjnych w interakcjach z łańcuchami PLA poprzez tworzenie wiązań wodorowych czy oddziaływania typu n-π*, w zależności od struktury przyłączonych podstawników (Schemat 2). Oddziaływania supramolekularne z udziałem cząsteczek zawierających atomy fluoru zostały wykorzystane w inżynierii materiałowej po raz pierwszy.
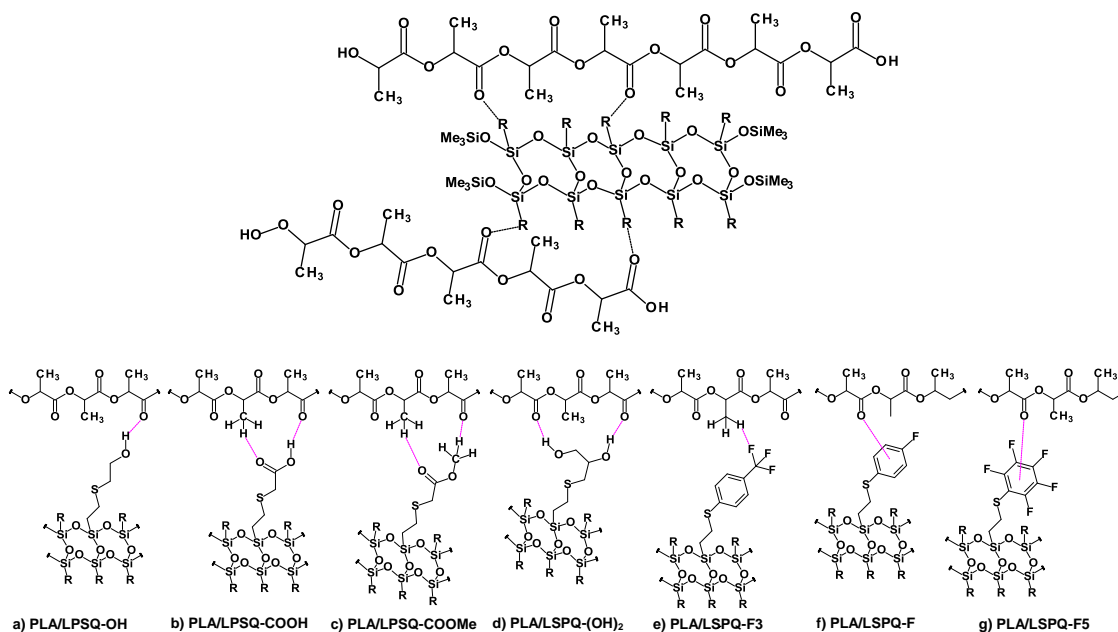
Schemat 2. Postulowane oddziaływania pomiędzy grupami funkcyjnymi LPSQ-R a osnową polilaktydową: (a - e) wiązania wodorowe, (f, g) oddziaływania typu n-π*.

Publikacje wchodzące w skład rozprawy:

I. A.S.Herc, J.Bojda, M.Nowacka, P.Lewiński, W.Maniukiewicz, E.Piorkowska, A.Kowalewska, „Crystallization, structure and properties of polylactide/lader poly(silsesquioxane) blends"
Polymer, 201 (2020) 122563.

II. A.S.Herc, P.Lewiński, S.Kaźmierski, J.Bojda, A.Kowalewska „Hybrid SC-polylactide/poly(silsesquioxane) blends of improved thermal stability."
Thermochimica Acta, 687 (2020) 178592.

III. A.S.Herc, M.Włodarska, M.Nowacka, J.Bojda, W.Szymański, A.Kowalewska „Supramolecular interactions between polylactide and model cyclosiloxanes with hydrogen bonding-capable functional groups."
eXPRESS Polym. Lett., 14 (2020) 134–153.

IV. A.Kowalewska, A.S.Herc, J.Bojda, M.Palusiak, E.Markiewicz, P.Ławniczak, M.Nowacka, J.Sołtysiak; A.Różański, E.Piórkowska „Supramolecular interactions involving fluoroaryl groups in hybrid blends of polylactide and laddder polysilsesquioxanes."
Polymer Testing, 94 (2021) 107033.

IV. WYNIKI BADAŃ

## 1. Synteza i właściwości LPSQ-R oraz CX-R

Pierwszy etap prowadzonych badań syntetycznych obejmował opracowanie i optymalizację sposobów syntezy nowych dodatków modyfikujących właściwości PLA - sfunkcjonalizowanych oligomerycznych silseskwioksanów (prace I, II i IV) oraz modelowych małocząsteczkowych tetrametylocyklotetrasiloksanów (praca III). Zaprojektowano poli(silseskwioksany) LPSQ-R [R = COOH, COOMe, OH, (OH)2] zdolne do tworzenia wiązań wodorowych (silniejszych O-H···O=C i słabszych C-H···O=C), który to typ oddziaływań supramolekularnych jest dobrze znany i opisany w literaturze. Wiązania wodorowe są bardzo często wykorzystywane w trakcie modyfikacji polilaktydu.[39] Nie jest to jednak jedyny możliwy rodzaj oddziaływań niekowalencyjnych, w których mogą uczestniczyć atomy tworzące łańcuchy PLA. Wyniki badań rentgenostrukturalnych białek, jak również małych cząsteczek organicznych i kompleksów metali przejściowych, wykazały, że grupy karbonylowe mogą brać udział nie tylko w tworzeniu wiązań wodorowych, ale także mogą łączyć się z centrami nukleofilowymi poprzez oddziaływania typu n→π*.[40-44] Rozważany był również udział oddziaływań tego typu w tworzeniu helikalnej struktury łańcuchów polilaktydu.[45] Jednak modyfikacja PLA z użyciem dodatków mogących brać udział w oddziaływaniach typu n→π* nie była wcześniej znana w chemii materiałów. Podobnie, oddziaływania supramolekularne z udziałem atomów fluoru są rzadko wykorzystywane w inżynierii materiałowej. Dlatego grupa modyfikatorów polisilseskwioksanowych została rozszerzona o makrocząsteczki z podstawnikami fluoroarylowymi. Elektroujemne atomy fluoru mogą uczestniczyć w tworzeniu wiązań wodorowych C–F···H–C oraz wiązań halogenowych[46-50], a także wpływać na lokalne zmiany rozmieszczenia gęstości elektronów, czego dobrym przykładem jest grupa pentafluorofenylowa.[51-53] Trwałość wiązań C–F···H–C zależy od hybrydyzacji atomów węgli, z którymi połączone są atomy fluoru i wodoru.[54] Wiązania wodorowe $C(sp^3/sp^2)$–H···F–$C(sp^3)$ są silniejsze niż wiązania $C(sp^3/sp^2)$–H···F–$C(sp^2)$. Ugrupowania trifluorometylowe przyłączone do pierścieni fenylowych mogą brać również udział w tworzeniu wiązań halogenowych (C–F···F–C), a także oddziaływań C–F···π.[55] Ponadto, grupa CF_3 jest podstawnikiem silnie odciągającym elektrony i może wpływać na zachowanie sąsiednich fragmentów cząsteczek.[56] W pracy IV przedstawione zostały wyniki modelowania kwantowo-chemicznego (wiązania wodorowe H···F *vs* prawdopodobne oddziaływania typu n→π*) metodami DFT i post-SCF MP2 wykonanego przez pana prof. dr. hab. Marcina Palusiaka (Uniwersytet Łódzki) dla reprezentatywnych modeli małocząsteczkowych. Badania te wykazały, że wzór możliwych preferowanych kontaktów cząstek zawierających grupy 4-(trifluoro)fenylowe różni się od najbardziej korzystnego w przypadku grup 4-fluorofenylowych i pentafluorofenylowych. Z tego względu zaprojektowane zostały również LPSQ posiadające w grupach bocznych podstawniki C_6F_5, C_6H_4F, $C_6H_4CF_3$.

Jako prekursorów użyto liniowych poli(silseskwioksanów) z bocznymi grupami winylowymi (LPSQ-Vi) o małej masie cząsteczkowej (Mn =1 kg/mol, PDI =1,4) oraz 1,3,5,7-

tetrametylotetrawinylocyklotetrasiloksan (CX-Vi). W przeprowadzonych badaniach wykorzystana została metoda syntezy oligomerycznych LPSQ-Vi o regularnej budowie łańcucha głównego, opracowana wcześniej w naszej grupie badawczej.[57] Dzięki obecności grup winylowych możliwa była modyfikacja LPSQ-Vi oraz CX-Vi na drodze addycji eno-tiolowej wybranych merkapto-pochodnych (2-merkaptoetanol, kwas tioglikolowy, tioglikolan metylu, 1-tioglicerol, 4-fluorotiofenol, pentafluorotiofenol, 4-(trifluorometylo)tiofenol) (Schemat 3).

UV, DMTA

LPSQ-OH, LPSQ-(OH)2, LPSQ-COOH,

LPSQ-COOMe, LPSQ-F3

Δ, AIBN

LPSQ-F5, LPSQ-F
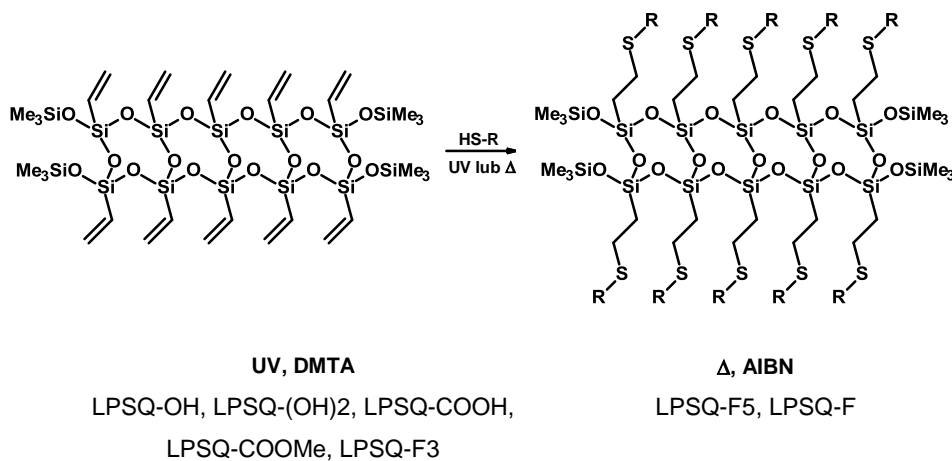
Schemat 3. Synteza sfunkcjonalizowanych LPSQ-R na drodze addycji tioli do LPSQ-Vi
(oznaczenia R jak na Schemacie 2).

Addycja tioli prowadzona była w rozpuszczalniku organicznym (THF), w obecności fotoinicjatora: 2,2-dimetoksy-2-fenyloacetofenonu (DMPA), poprzez naświetlanie mieszaniny reakcyjnej promieniowaniem UV (λ = 356 nm), zgodnie z wcześniej opisaną procedurą.[58] Taka droga syntezy była bardzo efektywna w przypadku addycji kwasu tioglikolowego, tioglikolanu metylu, 1-tioglicerolu, 2-merkaptoetanolu oraz 4-(trifluorometylo)tiofenolu, które udało się otrzymać z dobrą wydajnością. Procedura ta nie sprawdziła się jednak przy próbach addycji pentafluorotiofenolu oraz 4-fluorotiofenolu zarówno do LPSQ-Vi, jak i do CX-Vi. Przeprowadzono szereg testowych reakcji addycji związków fluoroarylowych do 1,3,5,7-tetrametylo-1,3,5,7-tetrawinylocyklotetrasilokanu w obecności DMPA, podjęto próby, w których zmieniano czas naświetlania promieniowaniem UV (od 30 min do 1,5 h), zwiększano ilość fotoinicjatora ($[f]_0/[Vi]_0$ = z 0,02 do 0,055) oraz nadmiar substratu fluoroarylowego (10% - 25%) w stosunku do grup winylowych. Badane tiofenole absorbują światło w nieco szerszym zakresie długości fal niż tiole zawierające grupy karbonylowe (zostało to bardziej szczegółowo przedstawione na Rysunku 7 w podrozdziale 2.2), ich absorbancja jest jednak znacznie większa. Szczególnie wyróżnia się 4-(trifluorometylo)tiofenol. Z tego względu, w kolejnych próbach jako fotoinicjator zastosowano 4,4'-bis(dimetyloamino)-benzofenon. Jego użycie wynikało z różnic pasm absorpcji obu fotoinicjatorów. Maksimum absorpcji DMPA znajduje się przy 330 nm (w MeOH)[59], natomiast w przypadku 4,4'-bis(dimetyloamino)-benzofenonu jest to 370 nm (w EtOH).[60] Niestety, nie przyniosło to pożądanego rezultatu. Wynik ten może wiązać się ze specyficzną strukturą zastosowanych fluoroarylotioli. Tiofenole są bardzo dobrymi donorami atomów wodoru z powodu stabilizacji powstających rodników przez efekt rezonansu.

Energia wiązania S-H w arylotiolach (BDE, *bond dissociation energy*) może jednak zmienić się ze względu na obecność podstawników w pierścieniu. Elektronodonujące grupy w pozycji para zmniejszają energię wiązania S-H.[61] W przypadku arylowych tioli użytych do modyfikacji LPSQ-Vi, dodatkowe znaczenie ma bezpośrednie związanie atomów fluoru z pierścieniem. BDE wiązania S-H w pentafluorotiofenolu wynosi 84,9 kcal/mol a w 4-fluorotiofenolu 82,1 kcal/mol.[62] Natomiast BDE wiązania S-H w 4-(trifluorometylo)tiofenolu wynosi 80,9 kcal/mol (338,6 kJ/mol).[63]

Do przeprowadzenia addycji pentafluorotiofenolu oraz 4-fluorotiofenolu niezbędne było zastosowanie termolabilnego inicjatora reakcji rodnikowych: azobis(izobutyronitrylu) (AIBN) rozkładającego się w temperaturach > 70 °C z utworzeniem rodników 2-cjanoprop-2-ylowych.[64] W wyniku optymalizacji warunków syntezy otrzymano regioselektywnie oczekiwane produkty z ilościową wydajnością. Niezależnie od typu zastosowanego inicjatora, we wszystkich przypadkach addycja eno-tiolowa wybranych związków do grup winylowych przebiegała ilościowo w sposób przeciwny do reguły Markownikowa.

Otrzymane produkty addycji zostały wyizolowane przez wytrącanie z roztworów za pomocą dużej ilości nierozpuszczalnika (w przypadku LPSQ-R) lub za pomocą chromatografii kolumnowej (w przypadku CX-R) z zastosowaniem wypełnień silikażelowych oraz odpowiednio dobranych eluentów. Wyizolowane pochodne zostały po wyodrębnieniu scharakteryzowane za pomocą spektroskopii magnetycznego rezonansu jądrowego (NMR) (Tabela 2). Dokładne przypisanie sygnałów [1]H i [13]C w przypadku LPSQ-OH i LPSQ-(OH)2 zostało ponadto dokonane z zastosowaniem technik korelacyjnych [1]H-[13]C (*heteronuclear single quantum correlation*, HSQC) i [1]H-[1]H (*correlation spectroscopy*, COSY) (praca II). LPSQ-R scharakteryzowano także za pomocą spektroskopii absorpcyjnej w zakresie podczerwieni (FTIR) oraz spektroskopii ramanowskiej (Tabela 3), jak również skaningowej kalorymetrii różnicowej (DSC) oraz analizy termograwimetrycznej (TGA)]. Wszystkie otrzymane LPSQ-R były bardzo lepkimi cieczami/woskami, które nie krystalizowały podczas chłodzenia. Wykazywały się natomiast obecnością charakterystycznego przejścia w stan szklisty. Temperatura zeszklenia (T_g) dla tych polimerów wynosiła odpowiednio: -47 °C (LPSQ-OH), -30 °C (LPSQ-(OH)2); -41 °C (LPSQ-COOMe); -14 °C (LPSQ-COOH) (praca I). Wyższa T_g w przypadku LPSQ-COOH związana jest z możliwością występowania silnych wiązań wodorowych między bocznymi grupami karboksylowymi, analogicznie do dimerycznych struktur tworzących się pomiędzy cząsteczkami kwasów karboksylowych.[58] Temperatura zeszklenia LPSQ-F, LPSQ-F3 i LPSQ-F5 wynosi odpowiednio: -31 °C, -9 °C, -10 °C (praca IV). Należy podkreślić, że charakterystyczna temperatura przejścia LPSQ-Vi w stan szklisty wynosi około -47 °C.[57]

Tabela 2. Przesunięcia chemiczne δ [ppm] charakterystycznych sygnałów w widmach ^{1}H NMR, ^{13}CNMR, ^{29}SiNMR, ^{19}F NMR polisilseskwoksanów LPSQ-R.

LPSQ-R	^{1}H NMR	^{13}C NMR	^{29}Si NMR	^{19}F NMR
LPSQ-COOH [58]	w THF-d$_8$ 0,17 (s, -Si-C$\underline{H}_3$); 1,08 (m, -Si-C$\underline{H}_2$); 2,79 (m, -C$\underline{H}_2$-S-); 3,20 (m, -S-C$\underline{H}_2$-); 8,30 (-COOH).	w CD$_3$OD -0,5 (-Si-$\underline{C}$H$_3$); 11,4 (-Si-$\underline{C}$H$_2$-); 25,3 (-$\underline{C}$H$_2$-S-); 31,6 (-S-$\underline{C}$H$_2$-); 170,9 (-$\underline{C}$OOH).	w CD$_3$OD -70,4 (-CH$_2$SiO$_{3/2}$); 10,9 (OSiMe$_3$).	-
LPSQ-COOMe	w THF-d$_8$ 0,16 (s, -Si-C$\underline{H}_3$); 1,06 (m, -Si-C$\underline{H}_2$); 2,77 (m, -C$\underline{H}_2$-S-); 3,25 (m, -S-C$\underline{H}_2$-); 3,65 (s, -O-C$\underline{H}_3$).	in THF-d$_8$ 0,97 (-Si-$\underline{C}$H$_3$); 13,3 (-Si-$\underline{C}$H$_2$-); 26,6 (-$\underline{C}$H$_2$-S-); 32,3 (-S-$\underline{C}$H$_2$-); 51,4 (-O-$\underline{C}$H$_3$); 170,3 (COO).	in THF-d$_8$ -70,4 (-CH$_2$SiO$_{3/2}$); 10,5 (OSiMe$_3$).	-
LPSQ-OH	w CD$_3$OD 0,16 (s, -Si-C$\underline{H}_3$); 1,03 (m, -Si-C$\underline{H}_2$-); 2,67 (m, -C$\underline{H}_2$-S); 2,67 (m, -S-C$\underline{H}_2$-); 3,68 (m, -C$\underline{H}_2$-OH).	w THF-d$_8$ 1,05 (-Si-$\underline{C}$H$_3$); 14,0 (m, -Si-$\underline{C}$H$_2$-); 26,3 (-$\underline{C}$H$_2$-S-); 34,2 (m, -S-$\underline{C}$H$_2$-); 61,6 (-$\underline{C}$H$_2$-OH).	w CD$_3$OD 10,7 (-O-SiMe$_3$); -70,3 (-CH$_2$-SiO$_{3/2}$).	-
LPSQ-OH$_2$	w CD$_3$OD 0,15 (s, -Si-C$\underline{H}_3$); 1,03 (m,-Si-C$\underline{H}_2$-CH$_2$-S-); 2,59 (m,-Si-CH$_2$-C$\underline{H}_2$-S-); 2,69 (m,-S-C$\underline{H}_2$-CH(OH)-CH$_2$-OH); 3,75 (m,-S-CH$_2$-C$\underline{H}$(OH)-CH$_2$-OH); 3,57 (m,-S-CH$_2$-CH(OH)-C$\underline{H}_2$-OH).	w CD$_3$OD 0,9 (-Si-$\underline{C}$H$_3$); 13,03 (-Si-$\underline{C}$H$_2$-CH$_2$-S-); 34,85 (-Si-CH$_2$-$\underline{C}$H$_2$-S-); 26,72 (-S-$\underline{C}$H$_2$-CH(OH)-CH$_2$-OH); 71,4 (-S-CH$_2$-$\underline{C}$H(OH)-CH$_2$-OH); 64,72 (-S-CH$_2$-CH(OH)-$\underline{C}$H$_2$-OH).	w CD$_3$OD 10,9 (-O-Si-CH$_3$); -70,2 (-CH$_2$-SiO$_{3/2}$).	-
LPSQ-F	w CDCl$_3$ 0,10 (s, -Si-C$\underline{H}_3$); 1,03 (m,-Si-C$\underline{H}_2$-CH$_2$-S-); 2,93 (m,-Si-CH$_2$-C$\underline{H}_2$-S-); 7,01 (s,-S-C$_6\underline{H}_4$F; *meta*); 7,31 (s,-S-C$_6\underline{H}_4$F; *ortho*).	0,9 (-Si-$\underline{C}$H$_3$); 12,96 (-Si-$\underline{C}$H$_2$-CH$_2$-S-); 28,6 (-Si-CH$_2$-$\underline{C}$H$_2$-S-); 115,4 (-S-C-$\underline{C}_5$H$_4$F; *meta*); 130,1 (-S-$\underline{C}$-C$_5$H$_4$F; *ipso*); 131,5 (-S-C-$\underline{C}_5$H$_4$F; *ortho*); 161,2 (-S-C$_5$H$_4$$\underline{C}$-F; *para*; J(C-F) = 247,0 Hz).	11,1 (-O-Si-CH$_3$); -70,3 (-CH$_2$-SiO$_{3/2}$).	-114,16 (-S-C$_6$H$_4$F; *para*)
LPSQ-F3	w CDCl$_3$ 0,16 (m,-Si-C$\underline{H}_3$); 1,22 (m, -Si-C$\underline{H}_2$-CH$_2$-S-); 3,13 (m,-Si-CH$_2$-C$\underline{H}_2$-S-); 7,27 (m,-S-C$_6\underline{H}_4$-CF$_3$; *meta*); 7,44 (m,-S-C$_6\underline{H}_4$-CF$_3$; *ortho*).	0,7 (-Si-$\underline{C}$H$_3$); 12,8 (-Si-$\underline{C}$H$_2$-CH$_2$-S-); 26,8 (-Si-CH$_2$-$\underline{C}$H$_2$-S-); 124,1 (-S-C$_6$H$_4$-$\underline{C}$F$_3$; J(C-F) = 268,7 Hz); 125,8 (-S-$\underline{C}_6$H$_4$-CF$_3$, *meta*); 127,0 (-S-$\underline{C}_6$H$_4$-CF$_3$, *ortho*); 142,0 (-S-$\underline{C}$C$_5$H$_4$$\underline{C}$-CF$_3$, *ipso*).	12,4 (-O-Si-CH$_3$); -70,0 (-CH$_2$-SiO$_{3/2}$).	-61,92 (-S-C$_6$H$_4$-CF$_3$; *para*)
LPSQ-F5	w CDCl$_3$ 0,12 (s, -Si-C$\underline{H}_3$); 1,08 (m, -Si-C$\underline{H}_2$-CH$_2$-S-); 3,00 (m,-Si-CH$_2$-C$\underline{H}_2$-S-).	0,2 (-Si-$\underline{C}$H$_3$); 13,0 (-Si-$\underline{C}$H$_2$-CH$_2$-S-); 28,4 (-Si-CH$_2$-$\underline{C}$H$_2$-S-); 107,8 (-S-$\underline{C}$-C$_5$F$_5$; *ipso*); 137,0 (-S-C-$\underline{C}_5$F$_5$; *meta*, J(C-F) = 254,9 Hz); 140,6 (-S-C-$\underline{C}_5$F$_5$; *para*, J(C-F) = 258,7 Hz); 146,6 (-S-C-$\underline{C}_5$F$_5$; *ortho*, J(C-F) = 247,3 Hz).	14,3 (-O-Si-CH$_3$); -70,5 (-CH$_2$-SiO$_{3/2}$).	-160,30 (-S-C$_6$F$_5$; *ortho*); -151,67 (-S-C$_6$F$_5$; *para*); -132,68 (-S-C$_6$F$_5$; *meta*).

Tabela 3. Charakterystyczne pasma drgań w widmach oscylacyjnych LPSQ-R.

LPSQ-R	spektroskopia	Rodzaje drgań i odpowiadające im liczby falowe [cm^{-1}]
LPSQ-OH	FTIR	v(O-H) 3300; v(C-H) 2950-2850; δ_β(COH) 1410; δ_{as}(CH$_2$) 1409; v(C-O) 1277; δ_s(Si-CH$_3$) 1254; δ(Si-CH$_2$) 1180; v_{as}(Si-O) 1123; v_s(Si-O)1065, 1026; v(O-H) 944; v(Si-C) 758
LPSQ-OH	ramanowska	δ(COH) 1465; δ_{as}(CH$_2$) 1413; ρ(CH$_2$) 1177; v(CCO) w alkoholach 1° 1003; v(CCO) w alkoholach 1° 944; v(C-S) 763, 715, 659
LPSQ-(OH)2	FTIR	v(O-H) 3300; v(C-H) 2950-2860; δ_β(COH) 1409;δ_{as}(CH$_2$) 1409; v(C-O) 1281; δ_s(Si-CH$_2$) 1254; δ(Si-CH$_2$) 1179; v_{as}(Si-O) 1088; v_s(Si-O) 1061, 1025; v(O-H) 925; v(Si-C) 784
LPSQ-(OH)2	ramanowska	δ(COH) 1440; δ_{as}(CH$_2$) 1411; ρ(CH$_2$) 1171; v(CCO) w alkoholach 2° 1070; v(CCO) w alkoholach 2° 873; v(C-S) 757, 715, 632
LPSQ-COOH	FTIR	v(O-H) 3300; v(C-H) 2900-2650; v(C=O) 1700; δ_β(COH) 1414; δ_{as}(CH$_2$) 1409; v(C-O) 1282; δ_s(Si-CH$_2$) 1253; δ(Si-CH$_2$) 1181; v_{as}(Si-O) 1123; v_s(Si-O) 1095, 1040; v(O-H) 842; v(Si-C) 780
LPSQ-COOH	ramanowska	v(C=O) 1700; δ(COH) 1440; δ$_{as}$(CH$_2$) 1406; ρ(CH$_2$) 1180; v(C-COO) 891; v(C-S) 789; 712; 672
LPSQ-COOMe	FTIR	v(C-H) 2950-2900; v(C=O) 1734; δ_{as}(CH2) 1436; v(C-O) 1283; δ_s(Si-CH$_2$) 1254; δ(Si-CH$_2$) 1182; v_{as}(Si-O) 1127; v_s(Si-O) 1046; v(Si-C) 800
LPSQ-COOMe	ramanowska	v(C=O) 1731; δ_{as}(CH$_2$) 1411; ρ(CH$_2$) 1182; v(C-COO) 876; v(C-COO) 902; v(C-S) 789, 709
LPSQ-F	FTIR	v(C-H) 2900-2800; v(C=C) 1590; v(C-F) aryl 1490; v(C-F)+ v(Si-C) 1277; δ_s(Si-CH$_2$) 1175; δ(C-H) w pierścieniach Ar 1087; v(Si-O) 1120; v_{as}(C-F) 1008; δ(C-H) w pierścieniach Ar 829; v(Si-C) 824
LPSQ-F	ramanowska	v(C=C) 1591; v(C-F) aryl 1410; v(C-F)+ v(Si-C) 1272; v(Si-C) 1217; δ(C-H) w pierścieniach Ar 1156; trygonalne oddychanie pierścienia w dwupodstawionych benzenach 1093; v(C-S) 815; pulsacja pierścienia 699; oddychanie pierścienia 629; δ_β(C-F) 515; δ_γ(C-F) 350
LPSQ-F5	FTIR	v(C-H) 2900-2800; v(C=C) 1514; v(C-F) aryl 1485; v(C-F)+ v(Si-C) 1276; v(Si-C) 1183; v(Si-O) 1030; v_{as}(C-F) 979,1090; v(Si-C) 849
LPSQ-F5	ramanowska	v(C=C) 1641; v(C-F) aryl 1403; v(C-F)+ v(Si-C) 1277; v(C-S) 863; pulsacja pierścienia 693; oddychanie pierścienia 584; δ_β(C-F) 441,511; δ_γ(C-F) 384
LPSQ-F3	FTIR	v(C-H) 2900-2800; v(C=C) 1607; v_s(C-F) alkyl 1327; v(C-F)+ v(Si-C) 1275; δ_s(Si-CH2) 1157; δ(C-H) w pierścieniach Ar 1093; v(Si-O) 1115; v_{as}(C-F) 1011, 1062; δ(C-H) w pierścieniach Ar 823; v(Si-C) 821
LPSQ-F3	ramanowska	v(C=C) 1607; v_s(C-F) alkyl 1327; v(C-F)+ v(Si-C) 1267; δ(C-H) w pierścieniach Ar 1190; trygonalne oddychanie pierścienia w dwupodstawionych benzenach 1095; v_{as}(C-F) 1062; v(C-S) 779; pulsacja pierścienia 711; oddychanie pierścienia 626

v – drgania rozciągające (*stretch*); δ – drgania zginające (*bend*); ρ – drgania kołyszące (*rock*); as – antysymetryczne; s – symetryczne; β – zginające w płaszczyźnie (*in-plane*); γ – zginające poza płaszczyznę (*out-of-plane*)

Podwójny szkielet poli(silseskwiokanów) ma istotny wpływ nie tylko na właściwości LPSQ-R i ich odporność termiczną. Analiza TGA (Rysunek 1) wykazała, że zarówno w atmosferze azotu, jak i powietrza LPSQ-R są stabilne termicznie do temperatury 200 °C (praca I). Ponadto polimery te są bardzo dobrze rozpuszczalne w rozpuszczalnikach organicznych (m.in. takich jak chlorek metylenu, tetrahydrofuran, w zależności od typu podstawników R) i można je było połączyć z osnową polilaktydową poprzez mieszanie odpowiednich roztworów.
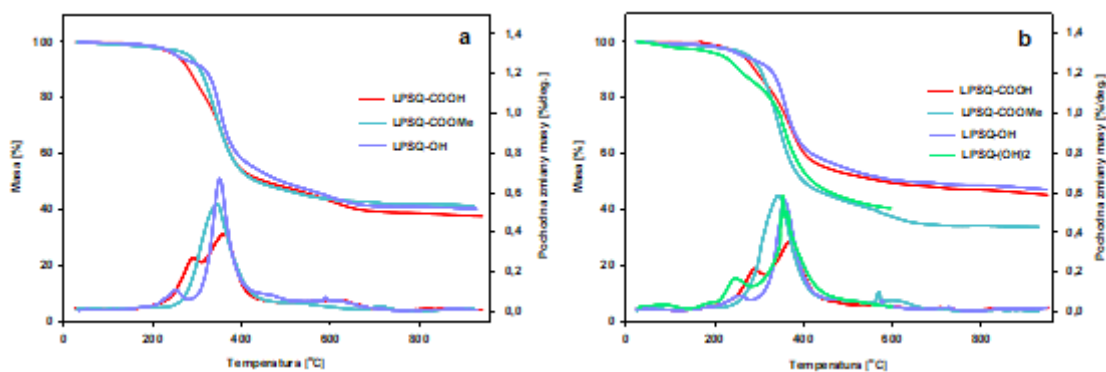
Rysunek 1. Rozkład termiczny LPSQ-R (a) w powietrzu i (b) w N_2 (10 °C/min).

W celu oszacowania roli liniowych struktur polisilseskwioksanowych na właściwości otrzymanych kompozytów konieczne było dokonanie badań porównawczych z użyciem modeli sfunkcjonalizowanych w ten sam sposób co LPSQ, mających jednak charakter małocząsteczkowy. Pochodne 1,3,5,7-tetrametylo-1,3,5,7-tetrawinylocyklotetrasiloksanu były najlepszą opcją, ponieważ strukturalnie przypominają dimeryczne jednostki powtarzalne w LPSQ. Modyfikacja CX-Vi została przeprowadzona dokładnie w ten sam sposób, co funkcjonalizacja LPSQ-Vi (prace III i IV). Cyklotetrasiloksany zawierające dwa różne podstawniki przy atomach krzemu zazwyczaj są mieszaninami czterech izomerów: all-*cis*, *cis-cis-trans*, *cis-trans-cis* i all-*trans* o różnej zawartości molowej.[65] W przypadku CX-COOH w trakcie oczyszczania produktów reakcji metodą chromatografii kolumnowej udało się wyodrębnić frakcję z przeważającą większością izomeru *cis-cis-trans* (praca III). Ze względu na giętkość wiązań siloksanowych i łańcuchów alkilowych, rodzaj izomerów dodanych do PLA nie wpływał zasadniczo na właściwości kompozytów. Jednak fakt wyizolowania izomerów małocząsteczkowych cyklicznych siloksanów jest warty odnotowania ze względu na możliwość ich zastosowania w syntezie nowych materiałów.

W kolejnym etapie prowadzonych badań przygotowane zostały (metodą mieszania składników w roztworze rozpuszczalników organicznych) mieszaniny zawierające LPSQ-R, w których matrycę stanowił komercyjnie dostępny polilaktyd (NW 2003D: M_w = 196 kg/mol, M_w/M_n = 1,7 lub NW 4032D: M_w = 130 kg/mol, M_w/M_n = 1,9; zawierające odpowiednio 3,2% mol. i 1,2% mol. jednostek D-laktydowych). Do badań użyte zostały również PLLA oraz PDLA otrzymane przez polimeryzację z otwarciem pierścienia L-laktydu i D-laktydu (PLLA: M_w = 6400 g/mol, M_w/M_n = 1,42; PDLA: M_w = 7200g/mol, M_w/M_n = 1,36). Dwa ostatnie polimery o stereoregularnej budowie łańcuchów zostały użyte do przygotowania mieszanin

21

zawierających stereokompleksy polilaktydu. Przygotowane mieszaniny zawierały różne ilości sfunkcjonalizowanych LPSQ-R lub CX-R (bardziej szczegółowo omówione w kolejnych rozdziałach). Po swobodnym odparowaniu rozpuszczalników w temperaturze pokojowej, otrzymane hybrydowe mieszaniny zostały dokładnie wysuszone w suszarce próżniowej, a następnie zbadano ich właściwości fizykochemiczne i mechaniczne.

2. Wpływ LPSQ-R oraz CX-R na właściwości polilaktydu

2.1. Oddziaływania supramolekularne w mieszaninach PLA/LPSQ-R – badania za pomocą metod spektroskopii oscylacyjnej

Analiza LPSQ-R za pomocą spektroskopii absorpcyjnej w zakresie podczerwieni (FTIR) (Rysunki 2-4) (prace I, II i IV) oraz spektroskopii ramanowskiej (Rysunki 5 i 6) (praca IV) dostarczyła informacji odnośnie budowy chemicznej tych polimerów. Wpływ hybrydowych dodatków silseskwioksanowych oceniano poprzez porównanie intensywności drgań IR charakterystycznych dla grup funkcyjnych LPSQ-R jak również polilaktydu, w tym sygnałów świadczących o obecności określonych struktur krystalicznych [utworzenie kryształów α lub α' (helisa 10_3)[66] w przypadku homopolimerów lub helisy 3_1 w przypadku stereokompleksów polilaktydu[67]). Zastosowane zostało również matematyczne przekształcenie widm FTIR do ich drugich pochodnych w celu oszacowania zmian położenia poszczególnych składowych pasma νC=O polilaktydu oraz odróżnienia ich, w przypadku LPSQ-COOH i LPSQ-COOMe, od pasm νC=O dodatków. Spektroskopia Ramana została zastosowana, jako metoda komplementarna dla FTIR, w celu oceny zmian położenia charakterystycznych drgań grup funkcyjnych, które nie są aktywne w podczerwieni. Technika ta pozwala na analizę nie tylko wiązań chemicznych w cząsteczkach, ale także o ich polaryzowalności oraz umożliwia badanie ruchu segmentów wiązań. Obydwie metody wykazały też różnice krystaliczności mieszanin PLA/LPSQ-R. Badania spektroskopowe oddziaływań supramolekularnych w mieszaninach PLA/LPSQ przeprowadzono dla próbek P/100-R zawierających składniki makrocząsteczkowe w proporcji 50% wag.), co odpowiada proporcji molowej grup funkcyjnych w LPSQ do jednostek laktydowych w łańcuchu [R]/[La] odpowiednio 0,5; 0,46; 0,51 i 0,46 dla P/100-OH, P/100-(OH)2, P/100-COOH i P/100-COOMe (badania niepublikowane) oraz 0,35; 0,28 i 0,26 dla P/100-F, P/100-F3 i P/100-F5 (praca IV). Dzięki zwiększeniu zawartości LPSQ-R w PLA możliwa była obserwacja przesunięć niektórych charakterystycznych drgań w widmach IR (Rysunki 2 i 3) oraz Ramana (Rysunki 5 i 6).

Takie analizy nie były możliwe w przypadku próbek mieszanin przeznaczonych do badań właściwości użytkowych (termicznych i mechanicznych) ze względu na zbyt małe stężenie dodatków. Do badań zastosowano PLA NW 2003 D zawierający 3,2% mol. jednostek D-laktydowych, który oczyszczono dokładnie z dodatków stabilizujących poprzez kilkukrotne wytrącanie z roztworu w CH_2Cl_2 za pomocą metanolu. Widma FT-IR cienkich warstw amorficznych mieszanin umieszczonych pomiędzy płytkami NaCl rejestrowano w trybie transmisji. Znaczna część widm PLA (1200-1000 cm^{-1}) pokrywała się z pasmami

charakterystycznych drgań pochodzących od LPSQ-R, szczególnie v(Si-O). Jednakże w przypadku wszystkich mieszanin PLA/100-R obserwowano zmniejszenie intensywności pasma drgań przy 1211 cm^{-1} (odpowiadających v_{as}(COC) i r_{as}CH$_3$ w szkielecie PLA). Zwykle wraz ze wzrostem ilości frakcji krystalicznej w PLA intensywność tego pasma zwiększa się wraz z pojawieniem się charakterystycznych drgań świadczących o powstawaniu struktury krystalicznej typu α (920 cm^{-1}) lub α' (922 cm^{-1}). Zostało to zaobserwowano w widmie czystego PLA po 30 min izotermicznej krystalizacji w 110 °C (linia przerywana, Rysunki 2 i 3).

W czasie analizy widm zaobserwowano także, że obszar drgań odpowiadających v(C=O) po zmieszaniu PLA z LPSQ-R przesunął się w stronę niższych liczb falowych i uległ zwężeniu. Największy efekt odnotowano dla P/100-F5, P/100-OH i P/100-(OH)2, dla których FWHM (full width at half maximum) wynosi odpowiednio 41,6 cm^{-1}, 41,8 cm^{-1} i 38,1 cm^{-1} w przeciwieństwie do P/100-COOMe, P/100-F, P/100-COOH i P/100-F3, w dla których FWHM wynosiła odpowiednio 60,2 cm^{-1}, 55,6 cm^{-1}, 53,4 cm^{-1} i 47,6 cm^{-1}, co oznacza, że efekt zwężenia tego pasma był nieco mniejszy (FWHM v(C=O) czystego PLA wynosi 59 cm^{-1}). Pasmo drgań v(C=O) pochodzących od LPSQ-COOH i LPSQ-COOMe w P/100-COOH oraz P/100-COOMe pokrywało się częściowo z v(C=O) w PLA (1720-1690 cm^{-1}).
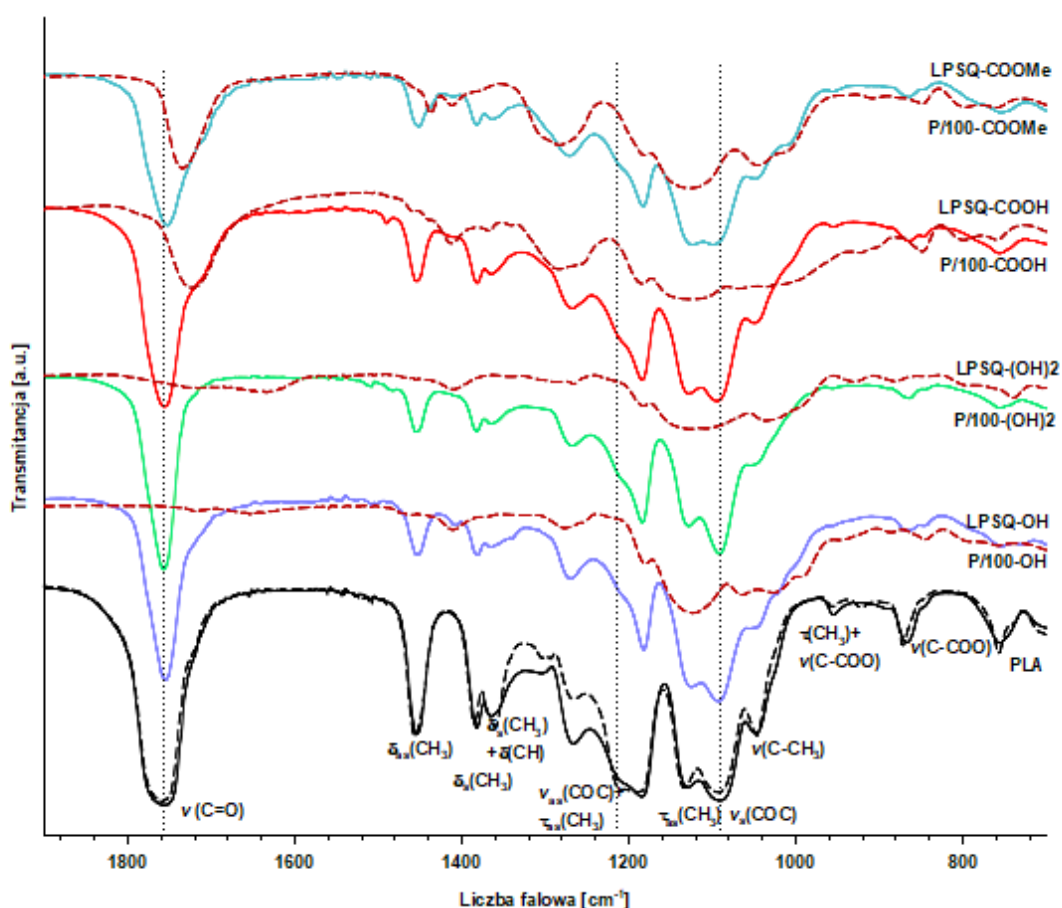
Rysunek 2. Widma FT-IR mieszanin PLA i P/100-R (— próbki amorficzne schłodzone ze stopu do 110°C; --- widma FTIR odpowiednich LPSQ-R; --- czysty PLA krystalizowany izotermicznie w 110°C przez 30 min.).
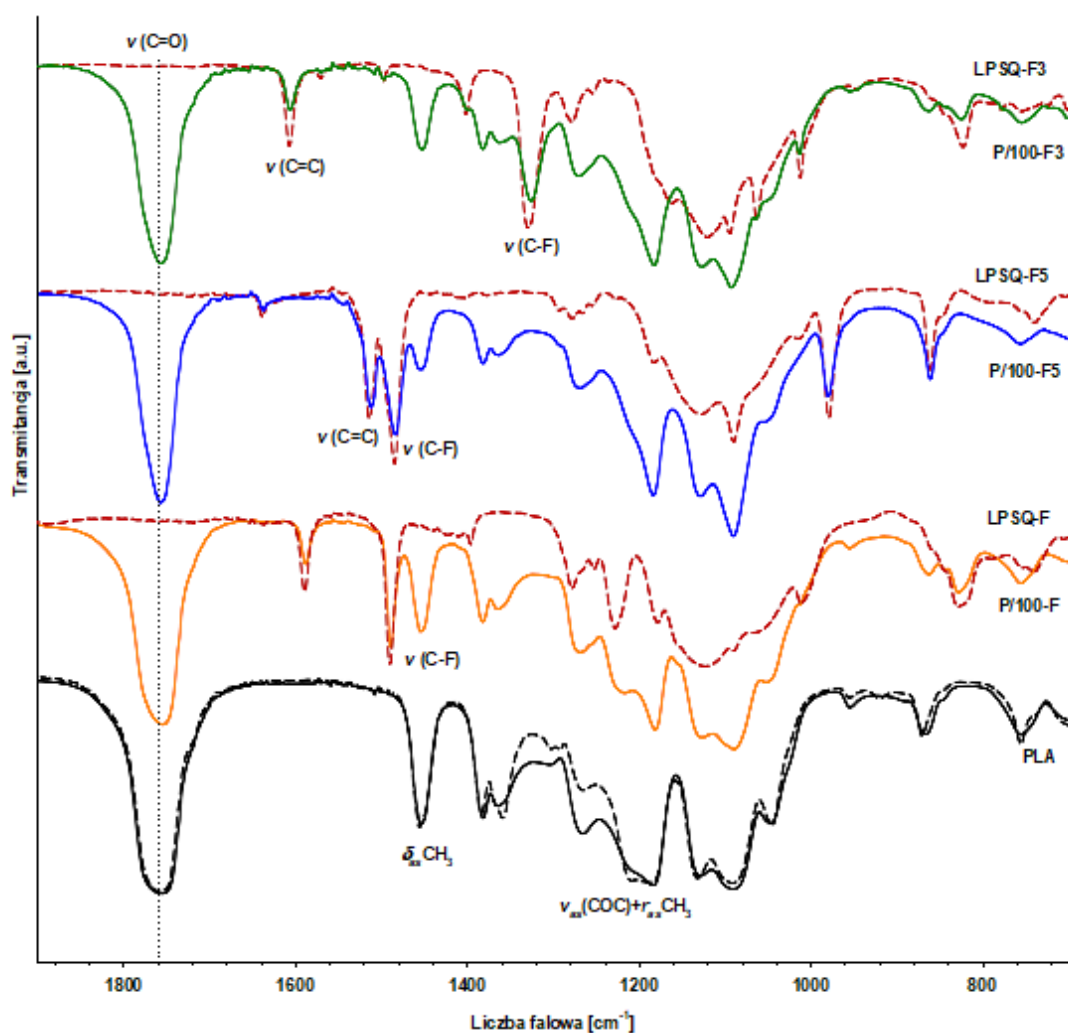
Rysunek 3. Widma FT-IR mieszanin PLA i P/100-R (— próbki amorficzne schłodzone ze stopu do 110°C; --- widma FTIR fluoroarylowych LPSQ-R; --- czysty PLA krystalizowany izotermicznie w 110°C przez 30 min.).

Obliczenie drugiej pochodnej widm IR pozwoliło na dokładne wyznaczenie składowych sygnałów pasma drgań v(C=O) (Rysunek 4). W amorficznym PLA obserwowano dwa główne piki odpowiadające konformerom *gg* prz 1778 cm^{-1} oraz konformerom *gt* przy 1742 cm^{-1}.[68-71] Gdy niedomieszkowany PLA był poddawany izotermicznej krystalizacji w 110°C sygnały ulegały niewielkim przesunięciom (1776 cm^{-1} i 1745 cm^{-1}). Wzrost intensywności pasma *gt* odnotowano dla próbek P/100-F5 (1750 cm^{-1}), P/100-F3 (1747 cm^{-1}), P/100-OH (1751 cm^{-1}) i P/100-(OH)2 (1752 cm^{-1}). W przypadku konformerów *gt* w mieszaninach P/100-COOH i P/100-COOMe (~ 1750 cm^{-1}) obserwowano wyraźnie mniejszy wzrost ich intensywności oraz niewielką asymetryczność. Można przypuszczać, że efekty obserwowane dla P/100-R mogą być prawdopodobnie związane z tworzeniem się supramolekularnych kompleksów między grupami funkcyjnymi pochodzącymi od LPSQ-R a ugrupowaniami karbonylowymi należącymi do konformerów *gt*.
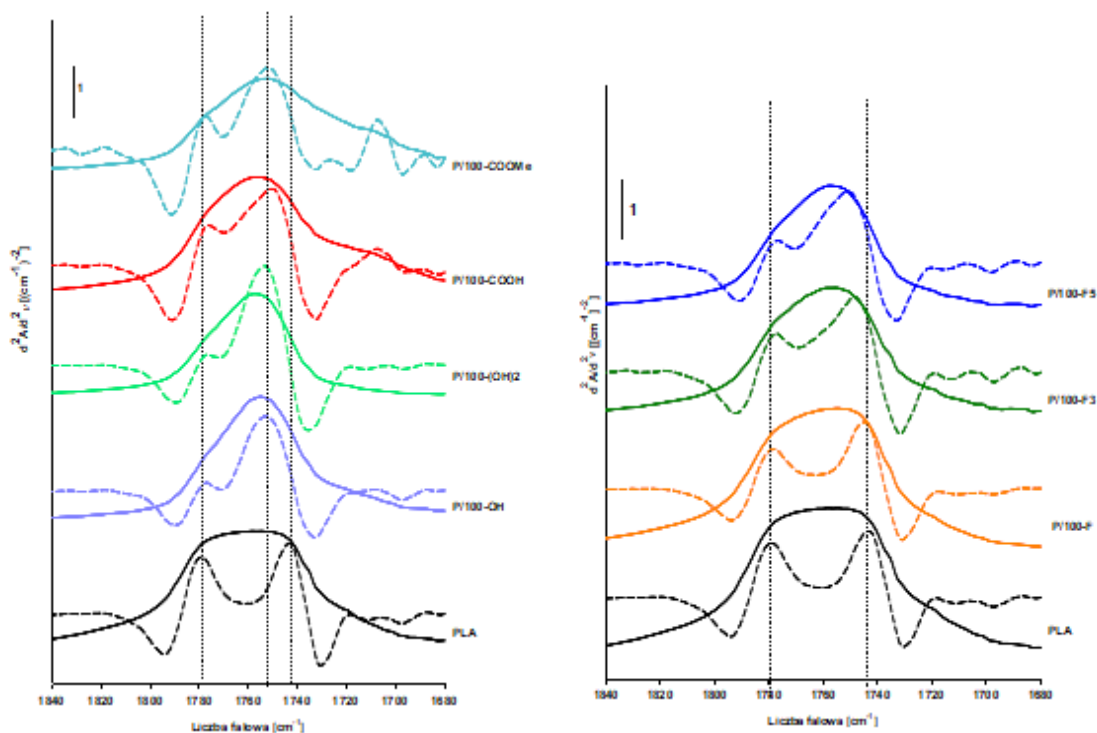
Rysunek 4. Porównanie drgań v(C=O) w PLA i P/100-R schłodzonych ze stopu do 110 °C (linie ciągłe - widma absorpcyjne; linie przerywane - ich drugie pochodne).

Mieszaniny PLA i LPSQ-R (przygotowane przez wylewanie roztworów mieszanin i swobodne odparowywanie a następnie suszenie próbek) badano także przy użyciu spektroskopii Ramana. Wiele drgań ramanowskich charakterystycznych dla PLA i LPSQ-R częściowo pokrywało się. Główne różnice pomiędzy PLA i P/100-R zaobserwowano dla drgań v(C=O) PLA (1750-1800 cm^{-1}) i v(C-S) LPSQ-R (600-850 cm^{-1}). Rozszczepienie linii Ramana w regionie v(C=O) jest wrażliwe na zmiany morfologii próbek i konformacji łańcuchów. Kister i in.[72] opisali ewolucję składowych drgań pasm A (1749 cm^{-1}), B (1763 cm^{-1}), E1 (1769 cm^{-1}) i E2 (1773 cm^{-1}) symetrii dla częściowo krystalicznego PLA. Pasmo pochodzące od v(C=O) w amorficznym PLA jest szerokie i można wyróżnić w nim dwa sygnały przy 1768 cm^{-1} i 1749 cm^{-1}. W badanej próbce PLA również obserwowano dwa pasma w regionie v(C=O), co jest związane z obecnością jednostek D w głównej matrycy poliestrowej. Pasma δ(CCO) zarówno w czystym PLA, jak i P/100-R (R = OH, (OH)2, COOH i COOMe) obserwowane są jako dublet przy 392 i 395 cm^{-1}, co świadczy o krystaliczności badanych próbek. Znacznie lepiej rozdzielone są też składowe pasma v(C=O), co także wskazuje na większą krystaliczność próbek z dodatkiem LPSQ. Na Rysunku 5 przedstawiono jako przykład zestawienie widm Ramana dla czystego PLA, LPSQ-OH oraz mieszaniny P/100-OH. Obserwuje się zmianę intensywności drgań v(C-S) dla mieszaniny P/100-OH w porównaniu do czystego LPSQ-OH. Pozwala to przypuszczać, że zmiana ta może być wynikiem powstawania wiązań wodorowych, co powoduje trudniejszą rotację wiązań w podstawnikach bocznych LPSQ.
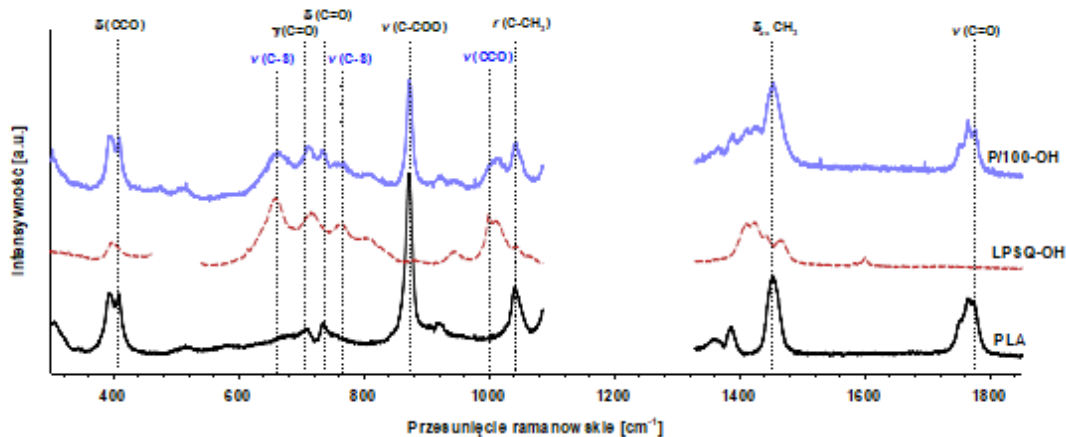
Rysunek 5. Zestawienie widm Ramana PLA, LPSQ-OH oraz mieszaniny P/100-OH.
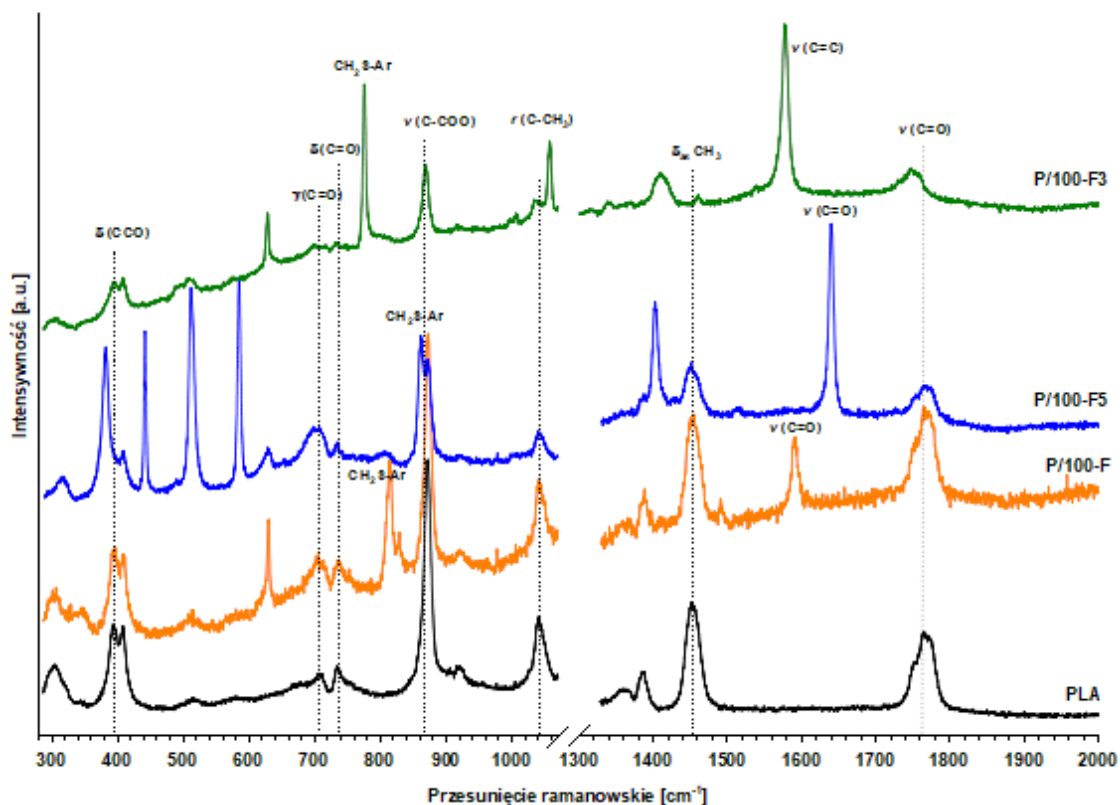
Rysunek 6. Zestawienie widm Ramana PLA oraz P/100-R zawierających fluorowane LPSQ.

Pasma drgań v(C-S) LPSQ-R w P/100-F, P/100-F3 i P/100-F5 również nakładały się w widmach Ramana na pasma odpowiadające drganiom $γ$(C=O) i $δ$(C=O) pochodzące od PLA (Rysunek 6; publikacja IV). Niemniej jednak można zaobserwować niewielką (~ 2 cm^{-1}) zmianę względnej intensywności i kształtu drgań v(C-S) po zmieszaniu z matrycą poliestrową. Może to sugerować tworzenie wiązań wodorowych, których rezultatem jest utrudnienie swobodnej rotacji

wiązań w grupach bocznych. Przesunięcie pasm oddychania pierścieni arylowych (*ring breathing*) (586 cm^{-1}) jak również drgań C–F w płaszczyźnie [*a* (511 cm^{-1}) i *e* (441 cm^{-1})] oraz deformacyjnych poza płaszczyzną (384 cm^{-1}) w widmach ramanowskich P/100-F5 może również wskazywać na istnienie oddziaływań pomiędzy łańcuchami PLA a grupami pentafluorofenylowymi. Największy efekt (przesunięcie o ~4 cm^{-1} w kierunku mniejszych liczb falowych) odnotowano jednak dla drgań rozciągających IR wiązania C-F w LPSQ-F3 [v_{sym}(C-F) 1327 cm^{-1} w czystym LPSQ-F3 wobec 1323 cm^{-1} w P/100-F3], co może być związane z tworzeniem się wiązań wodorowych F···H.

2.2. Morfologia mieszanin PLA/LPSQ-R i PLA/CX-R oraz ich właściwości optyczne

Badania struktury mieszanin PLA/LPSQ-R oraz PLA/CX-R przy użyciu mikroskopii skaningowej SEM oraz mikrofotografie mapowania krzemu metodą SEM-EDS, zostały przeprowadzone we współpracy z zespołem pani prof. dr hab. Ewy Piórkowskiej (CBMiM PAN). Wykazały one separację faz, która zależała od rodzaju grupy funkcyjnej R oraz od typu i ilości krzemoorganicznych dodatków. W przypadku LPSQ-R najlepszą dyspersję otrzymano dla PLA/LPSQ-COOMe (2% wag.), w którym widoczne są tylko wtrącenia submikronowe (praca I). Zwiększenie zawartości LPSQ-COOMe do 5% wag. skutkowało pojawieniem się takich wtrąceń w większej ilości i w postaci nieco większych ziaren. Mikrofotografie SEM/SEM-EDS pozostałych mieszanin świadczą o otrzymaniu struktur częściowo mieszalnych i częściowo rozdzielonych fazowo. W przypadku mieszanin PLA/LPSQ-(OH)2 obserwowano wtrącenia submikronowe. Z kolei mieszaniny PLA/LPSQ-COOH oraz PLA/LPSQ-OH (praca I) zawierały nieznacznie większe wtrącenia dodatków (odpowiednio 10-20 μm i 6-10 μm), a ich średnica zwiększała się wraz ze wzrostem zawartości LPSQ-R. Dodatki polisilseskwioksanowe zawierające podstawniki fluoroarylowe koncentrowały się we wtrąceniach o wielkości 1-3 μm, które były rozproszone w matrycy polimerowej (praca IV). Najlepiej mieszalnym dodatkiem fluoroarylowym był LPSQ-F, który przy zawartości 5% wag. w osnowie PLA pozostawał dobrze zdyspergowany. LPSQ-F3, zdolny do tworzenia wiązań wodorowych i halogenowych z udziałem atomów fluoru z grupy trifluorometylowej, tworzył skupiska mniejszych wtrąceń.

Przy założeniu istnienia oddziaływań supramolekularnych w mieszaninach zawierających sfunkcjonalizowane LPSQ-R, struktura polimerowa tych makrocząsteczek może znacząco wpływać na stopień rozproszenia. Dlatego wykonane zostały badania porównawcze z użyciem małocząsteczkowych cyklosiloksanów CX-R (praca III). W przypadku mieszanin PLA i CX-COOH widoczne były heterogeniczne wtrącenia, które zwiększały się wraz z ilością krzemoorganicznego dodatku. Cyklosiloksany CX-COOMe i CX-OH (jak również niesfunkcjonalizowany CX-Vi) były jednak dobrze zdyspergowane w matrycy polimerowej. Dyspersja CX-(OH)2 była dość dobra, jednak obserwowane były małe wtrącenia o nieco wyższym stężeniu tego dodatku. Porównanie wyników uzyskanych dla mieszanin z dodatkiem LPSQ-R i CX-R potwierdziło istotny wpływ struktury polimerowej liniowych silseskwioksanów dla ich mieszalności z PLA.

Struktura fazowa i skład hybrydowych kompozytów miały odzwierciedlenie w ich charakterystycznych właściwościach, w tym we właściwościach optycznych, co wykazały badania przenikalności światła przez cienkie filmy mieszanin PLA/LPSQ-R (prace I, III i IV). W przypadku mieszanin PLA i LPSQ-R [R = COOH, OH i (OH)2] (praca I), transmitancja próbek była niższa niż czystego PLA (Rysunek 7). Obecność większych wtrąceń bogatych w heterogeniczne dodatki skutkowało rozpraszaniem światła, stąd zmniejszenie przezroczystości i spadek transmitancji próbek. Jedynym wyjątkiem była mieszanina zawierająca 2% wag. LPSQ-COOMe, gdzie bardzo dobre rozproszenie dodatku skutkowało wysoką transmitancją próbki, zbliżoną do czystego PLA. Kompozyt PLA/LPSQ-COOMe (5% wag.) zawierający większą ilość submikronowych wtrąceń również charakteryzował się dosyć dobrą przezroczystością.
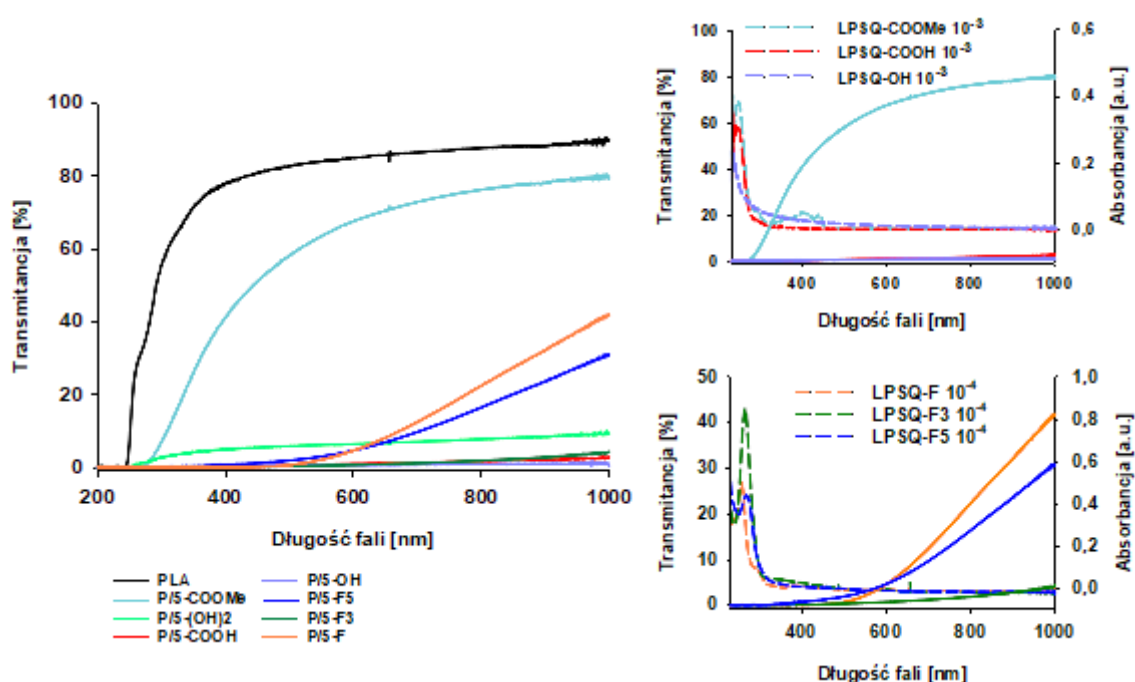
Rysunek 7. Widma UV P/LPSQ-R (5% wag.) oraz czystych LPSQ-R.

Małocząsteczkowe dodatki CX-R były lepiej mieszalne z polilaktydem i dlatego przejrzystość próbek PLA/CX-Vi (2% wag.) i PLA/CX-OH (1% wag.) była zbliżona do PLA (praca III). Większa zawartość CX-OH w PLA powodowała zmniejszenie przejrzystości próbek, jednak była ona wciąż relatywnie wysoka. Wprowadzenie CX-(OH)2 prowadziło do znacznego spadku przepuszczalności światła, a zwiększenie jego zawartości w PLA do 4% wag. sprawiło, że materiał ten stał się nieprzezroczysty w całym zakresie UV/Vis. Obecność wtrąceń CX-COOH w PLA, potwierdzona za pomocą SEM-EDS, powodowała duży spadek przepuszczalności światła. Cienkie filmy mieszanin PLA i CX-COOMe (zawartości ≤ 5% wag.), podobnie jak miało to miejsce w przypadku LPSQ-COOMe, charakteryzowały się przejrzystością taką jak czysty PLA. Dodanie 10% wag. CX-COOMe spowodowało tylko niewielkie zmniejszenie transparentności (około 10% przy λ = 600 nm). Co ciekawe, okazało się, że wszystkie badane dodatki zawierające grupy karbonylowe absorbują światło przy

28

długości fali 250-340 nm. Zakres ten znajduje się w obrębie najbardziej energetycznego pasma naturalnego światła UV odpowiadającego za fotochemiczną degradację materiałów (UV-B). Przejrzystość mieszanin PLA z LPSQ-COOMe i CX-COOMe oraz absorpcja światła o określonej długości fali mogą być potencjalnie korzystne w zastosowaniu takich kompozytów, jako materiałów opakowaniowych.

Zmniejszenie przenikalności światła w zakresie 250–340 nm (UV–B) zostało również zaobserwowane dla PLA zawierającego fluorowane LPSQ (praca IV). Jednak w przypadku mieszanin polilaktydu zawierających LPSQ z grupami fluoroarylowymi znaczny spadek przezroczystości widoczny był nawet przy małej ich zawartości. Co prawda, próbka zawierająca 1% wag. LPSQ-F okazała się niemal tak samo przezroczysta jak czysty PLA, co potwierdziło obserwacje z SEM i SEM-EDS, o bardzo dobrej mieszalności tego dodatku. Dodatek 1% wag. LPSQ-F5 powodował zmniejszenie przezroczystości osnowy o 10% przy λ = 600 nm, a obecność 1% wag. dodatku LPSQ-F3 zmniejszała transmitancję próbki przy λ = 600 nm już o 50%. Jednak 5% dodatku LPSQ-F spowodowało zmniejszenie DLT przy λ = 600 nm o około 95%. Podobny efekt zaobserwowano dla PLA zawierającego 5% wag. LPSQ-F5 (Rysunek 7). Próbka zawierająca 5% wag. LPSQ-F3 była całkowicie nieprzezroczysta. Przyczyną różnic w transmitancji tych próbek są dodatkowo różne właściwości spektroskopowe czystych dodatków fluoroarylowych. Wyższa absorpcja LPSQ-F3, w porównaniu do LPSQ-F i LPSQ-F5, może być związana ze zmniejszeniem transmitancji oraz przezroczystości próbek mieszanin polilaktydu z tym dodatkiem.

2.3. Swobodna krystalizacja mieszanin PLA/LPSQ-R

Sferolity polilaktydu tworzą się poprzez promieniowy wzrost lameli na zewnątrz, od centrum nukleacji.[14,66] Dodatek nukleatorów i/lub plastyfikatorów może powodować przyspieszenie krystalizacji oraz mieć różny wpływ na strukturę tworzących się kryształów. Przykładem może być zmienność struktury sferolitów PLA w mikroskali, w obecności niektórych dodatków polimerowych do matrycy poliestrowej, W wyniku krystalizacji PLLA w obecności dużych ilości amorficznego poli(winylofenolu)[73] lub ataktycznego poli(metakrylanu metylu)[74] uzyskano różnego typu morfologie sferolityczne (sferolity „o powierzchni sektorowej"). Amorficzne LPSQ mogą powodować w czasie krystalizacji PLA znaczące efekty makroskopowe, w zależności od rodzaju grup funkcyjnych R i ich oddziaływań z łańcuchami poliestrowymi. W związku z tym zbadano również morfologię struktur tworzących się w trakcie swobodnego odparowywania rozpuszczalników z mieszanin polilaktydu zawierających duże ilości sfunkcjonalizowanych polisilseskwioksanów LPSQ-R (R = OH, COOH, COOMe) (w proporcji 1:1 wag.). Wszystkie roztwory, niezależnie od składu, zawierały dokładnie takie same ilości rozpuszczalników (CH_2Cl_2 został użyty do rozpuszczenia PLA, natomiast THF był rozpuszczalnikiem LPSQ-R). Do próbki czystego PLA dodano również THF, aby wyeliminować różnice w kinetyce krystalizacji, które mogłyby wynikać z różnych szybkości odparowania mieszanin rozpuszczalników. Górną powierzchnię tak uzyskanych próbek analizowano przy użyciu skaningowego mikroskopu elektronowego (SEM). Zaobserwowano tworzenie się

hierarchicznych struktur makroskopowych w niektórych ze skrystalizowanych hybrydowych materiałów.

Pomimo tego, że wszystkie LPSQ-R są lepkimi cieczami o niskiej temperaturze zeszklenia, struktury tworzące się w czasie krystalizacji z roztworów mieszanin PLA i LPSQ-COOH i LPSQ-OH miały zupełnie inną morfologię. Czysty PLA tworzył jednorodne sferolity o gładkiej powierzchni i średnicy około 100 µm (Rysunek 8a), które były połączone ze sobą w związku z mało efektywną nukleacją i powolnym wzrostem. Sferolity powstające w obecności LPSQ-COOMe były tylko nieco większe niż te tworzące się w roztworze czystego PLA (Rysunek 8b). Nie tworzyły jednak pełnych sfer i charakteryzowały się obecnością pustych przestrzeni i zagłębień. Efekt ten może być związany z małą siłą wiązań wodorowych mogących tworzyć się między atomami wodoru w grupie estrowej LPSQ-COOMe oraz grupami karbonylowymi w łańcuchach polilaktydu. LPSQ-COOMe odgrywa rolę plastyfikatora, który w zbyt dużych ilościach, przeszkadza w równomiernym wzroście sferolitów. Mimo, że przy niskich stężeniach (≤ 5% wag.) LPSQ-COOMe był znacznie lepiej zdyspergowany w matrycy polilaktydowej niż LPSQ-COOH i LPSQ-OH, jego duże ilości nie mieszają się dobrze z PLA.
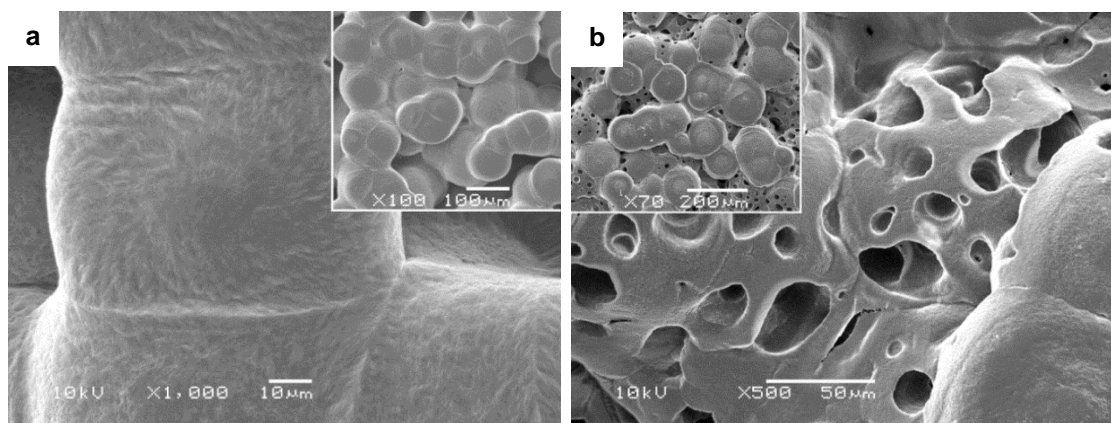
Rysunek 8. Mikrofotografie SEM PLA/THF (a) oraz P/100-COOMe (b).

Kuliste kryształy powstające w P/100-COOH były dwukrotnie mniejsze w porównaniu do sferolitów czystego PLA (średnica ~ 50 µm) (Rysunek 9). Były również jednolite, ale znacznie lepiej separowane a ich powierzchnia była mniej gładka. Niektóre z nich wzrastały w postaci hemisfer, dzięki czemu można było mieć wgląd w sposób ich powstawania. Od dosyć zwartego centrum tych sferolitów odchodzą w sposób radialny krótkie lamele. Można sądzić, że LPSQ-COOH tworzy wtrącenia, które dzięki tworzeniu wiązań wodorowych z udziałem grup karboksylowych (zarówno między LPSQ-COOH i łańcuchami PLA jak i między cząsteczkami LPSQ-COOH w inkluzjach) nie powodują nadmiernego uplastycznienia osnowy polilaktydowej. Sprzyja to zarówno nukleacji (o czym świadczy większa ilość sferolitów w próbce i ich mniejszy rozmiar), jak i wzrostowi sferolitów. W celu selektywnego usunięcia dodatków z matrycy poliestrowej próbki wytrawiono poprzez spęcznianie w oparach MeOH, a następnie zanurzenie na krótki czas w MeOH. Na mikrofotografiach SEM zaobserwowano, że struktura powierzchni PLA i P/100-COOMe nie uległa większym zmianom. Można sądzić, że większa część LPSQ-COOMe znajdowała się w zagłębieniach i mogła być łatwo wymywana. Jak można

zauważyć (Rysunek 9 c, d), wytrawianie MeOH próbki P/100-COOH nie doprowadziło do istotnego zwiększenia pustych przestrzeni w centralnej części sferolitów.
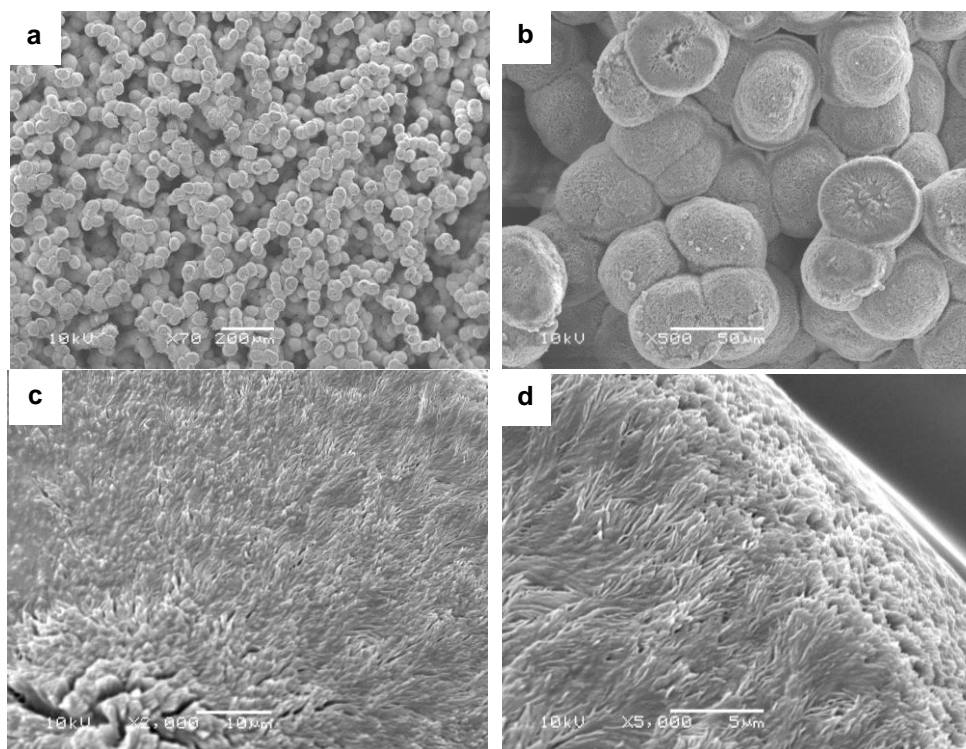
Rysunek 9. Mikrografie SEM P/100-COOH (a, b) oraz centralny fragment (c) i fragment krawędzi (d) przykładowego sferolitu P/100-COOH wytrawionego MeOH.

Najciekawszą morfologię zaobserwowano w przypadku mieszaniny P/LPSQ-OH, która po odparowaniu rozpuszczalników krystalizowała w sposób szczególny i tworzyła unikalną makrostrukturę hierarchiczną 3D (Rysunek 10). W próbkach P/100-OH i możliwa była obserwacja ich wewnętrznej struktury. Takich wyników nie obserwowano dla czystego polilaktydu ani jego mieszanek z innymi dodatkami. Utworzone krystality były małe (~ 25 μm) i nie miały kulistej budowy, charakterystycznej dla sferolitów PLA, a raczej eliptyczny, płaski kształt. Wskazuje to na przyspieszenie nukleacji PLA w obecności LPSQ-OH, którego grupy boczne są donorami wiązań wodorowych łączących makrocząsteczki polisilseskwioksanów z łańcuchami PLA. Są to jednak wiązania słabsze niż tworzone przez grupy COOH. Dzięki temu utworzone krystality przypominały raczej hedryty (nazywane inaczej aksjalitami), w których centrum znajdują się osiowo połączone lamele, które początkowo narastają równolegle, aby po etapie jednokierunkowego wzrostu utworzyć stopniowo dendrytyczną strukturę.[75] W centrum hedrytów połączone lamele są mniej więcej równoległe w formie wiązki Mikrofotografie SEM krystalitów trawionych działaniem MeOH (Rysunki 10c oraz 11) wskazują, że budowa hierarchiczna P/100-OH nie uległa dużej zmianie, co sugeruje dobrą mieszalność składników kompozytu i trwałość solwolityczną tego połączenia. Wolne przestrzenie obserwowane po wytrawieniu próbki za pomocą MeOH świadczą o tym, że LPSQ-OH znajdował się zarówno w centralnej, jak i w zewnętrznej części sferolitów. Większe powiększenia wskazują na

warstwowy wzrost lameli, co może wyjaśniać łączenie poprzez zazębianie się ich brzegów i tworzenie struktur 3D w trakcie wzrostu kryształów.
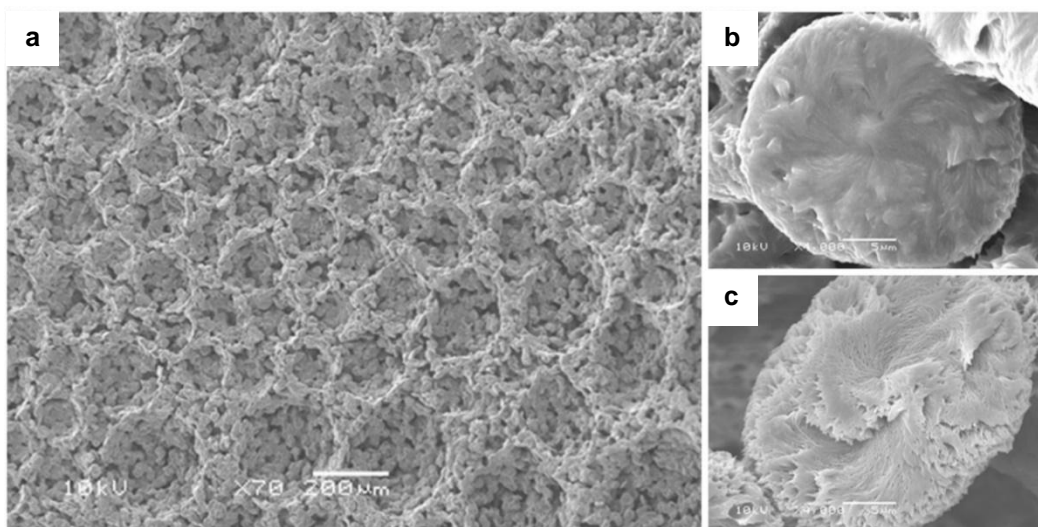
Rysunek 10. Powierzchnia hierarchicznych makrostruktur utworzonych w wyniku krystalizacji z roztworu mieszaniny P/100-OH (a) oraz pojedynczego sferolitu P/100-OH przed (b) i po wytrawieniu MeOH (c).
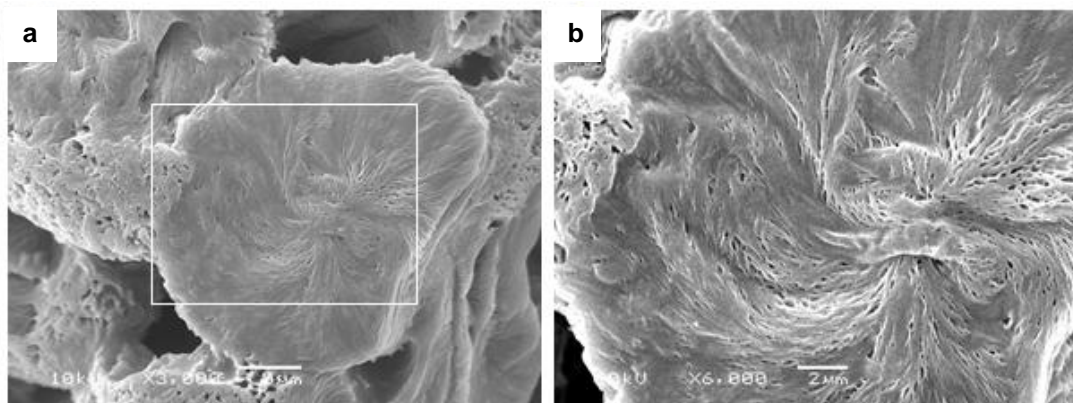
Rysunek 11. Mikrografie SEM P/100-OH wytrawionego MeOH (różne powiększenia) pokazujące makroskopową organizację sferolitów i ich strukturę wewnętrzną.

2.4. Właściwości termiczne mieszanin PLA/LPSQ-R oraz PLA/CX-R

2.4.1. Analiza wpływu LPSQ-R i CX-R na zdolność polilaktydu do krystalizacji

Zbadany został wpływ dodatków krzemoorganicznych na właściwości termiczne kompozytów PLA/LPSQ-R, w tym temperaturę zeszklenia, zdolność do krystalizacji ze stopu oraz krystalizacji fazy amorficznej (tak zwanej „zimnej krystalizacji") (prace I, III i IV). Zwiększenie temperatury przejścia w stan szklisty oraz stopnia krystaliczności polilaktydu jest korzystne ze względu na poszerzenie temperaturowego zakresu użyteczności, polepszenie stabilności kształtu i właściwości barierowych. Nie udało się jednak osiągnąć znaczącego polepszenia tych cech poprzez zastosowanie LPSQ-R w przypadku handlowo dostępnych polilaktydów. Badania przeprowadzone za pomocą różnicowej kalorymetrii skaningowej DSC

przy stałym naroście temperatury (10 °C/min) wykazały (Rysunek 12), że temperatura zeszklenia otrzymanych mieszanin PLA i LPSQ-R jest zbliżona do czystego PLA (około 60 °C). Jest to jednak ciekawy rezultat, ponieważ LPSQ-R są lepkimi cieczami i ich dodatek mógłby spowodować znaczące obniżenie temperatury zeszklenia. Jednak zarówno tworzenie oddziaływań supramolekularnych pomiędzy grupami R a łańcuchami PLA, jak również struktura podwójnego łańcucha LPSQ powodują brak takiego efektu. Wskazuje na to zarówno nieznaczne obniżenie T_g w przypadku słabo oddziałującego dodatku LPSQ-COOMe (Rysunek 12) jak też znaczące obniżenie T_g w mieszaninach zawierających sfunkcjonalizowane cyklosiloksanowe analogi (publikacja III).
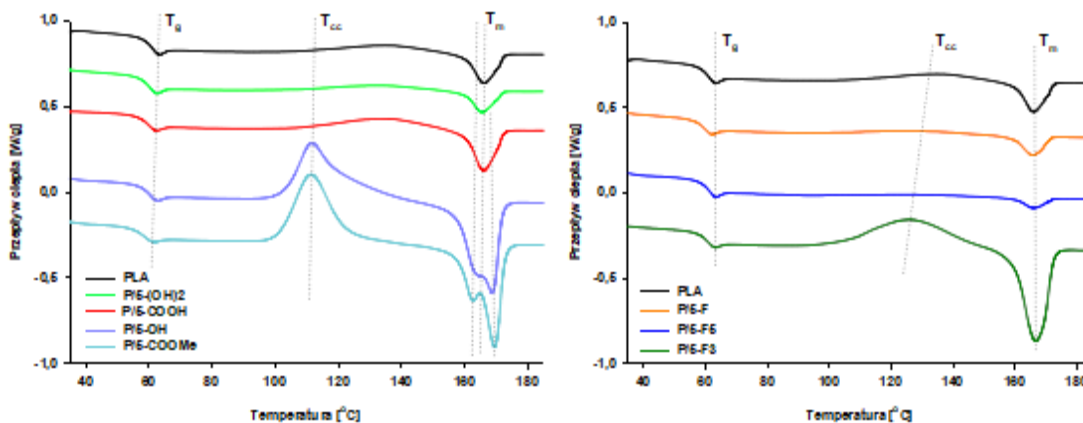
Rysunek 12. Termogramy DSC zarejestrowane dla P/LPSQ-R (5% wag.), II przebieg; 10°C/min.

Termogramy DSC mieszanin LPSQ-R i CX-R z PLA nie wykazały też krystalizacji w czasie chłodzenia ze stopu, jak również znaczącej zmiany temperatury topnienia T_m. Należy jednak podkreślić, że dodatek 2% wag. LPSQ-R [R = COOH, COOMe, OH] zdolnych do tworzenia wiązań wodorowych spowodował zwiększenie zawartości frakcji krystalicznej w mieszaninach z enancjomerycznie czystym poli(L-laktydem) (o ~5%) i zmniejszenie temperatury krystalizacji w czasie schładzania stopu polimerowego z szybkością 10 °C/min (praca I). Zaobserwowane zostało również przyspieszenie zimnej krystalizacji fazy amorficznej w czasie stopniowego ogrzewania tych częściowo skrystalizowanych próbek. Zimna krystalizacja jest bardzo ważnym zjawiskiem, które może mieć duże znaczenie, na przykład, w polepszeniu właściwości mechanicznych obiektów wytwarzanych w procesach drukowania 3D za pomocą polimerów termoplastycznych. Przebiega ona z wykorzystaniem zarodków krystalizacji w osnowie polimeru. Zwiększenie liczby takich zarodków zmniejsza rozmiar krystalitów, co jest korzystne ze względu na własności mechaniczne materiałów polimerowych. Uplastycznienie polimeru zwiększa ruchliwość łańcuchów i również ułatwia przyrost struktur krystalicznych w amorficznym materiale polimerowym. Taka skłonność do krystalizacji frakcji amorficznej w trakcie powtórnego ogrzewania schłodzonego stopu zaobserwowana została zaobserwowana w mieszaninach niektórych LPSQ-R i komercyjnych polilaktydów zawierających niewielkie ilości jednostek D-laktydowych (prace I i IV). Entalpia tej egzotermicznej przemiany była równa entalpii topnienia, co wskazuje na brak krystaliczności materiałów schłodzonych ze stopu (Rysunek 12). Materiały zawierające dodatki LPSQ-COOMe

oraz LPSQ-OH ulegały bardziej intensywnej krystalizacji w trakcie ogrzewania [większe ciepło przemiany oraz niższa temperatura jej występowania (T_{cc})] z powodu, odpowiednio, plastyfikacji polilaktydu lub bardziej intensywnego zarodkowania. Efekt ten wzrastał, w badanym zakresie stężeń, wraz z zawartością LPSQ-R. Niewielkie ilości LPSQ-COOH (2% wag.) polepszały krystalizację amorficznego PLA w małym stopniu (Rysunek 12). Jednak zwiększenie zawartości dodatku LPSQ-COOH nie ułatwiało procesu zimnej krystalizacji amorficznego polilaktydu. Podobny efekt zaobserwowano w przypadku LPSQ(OH)2. Wyjaśnieniem tego zjawiska może być zahamowanie krystalizacji PLA przez zbyt intensywne tworzenie sieci wiązań wodorowych, analogicznie do mechanizmów i przykładów opisywanych literaturze.[77]

Potwierdzeniem tej tezy są wyniki uzyskane z zastosowaniem sfunkcjonalizowanych cyklosiloksanów (praca III). Dodanie CX-R [R = COOH, OH, (OH)2, COOMe] również nie poprawiało krystalizacji PLA ze stopu, jednak dodatki wyraźnie wpływały na proces zimnej krystalizacji. CX-Vi nie powodował znaczących efektów (oprócz zauważalnego zmniejszenia T_g PLA), jednak obecność dodatków CX-COOMe, CX-OH i CX-(OH)2 indukowała zimną krystalizację już w temperaturach T_{cc} niższych średnio o 15 °C od charakterystycznych dla badanego PLA. Zwiększenie ilości CX-OH jak i CX-(OH)2 skutkowało intensyfikacją krystalizacji, o czym świadczyło zwiększenie entalpii procesu. Jednak pomimo większej ilości grup hydroksylowych w CX-(OH)2 efekt ten był słabszy niż osiągany przy zastosowaniu CX-OH. W przypadku CX-COOH, podobnie jak innych CX-R, jego niewielka ilość sprzyjała zimnej krystalizacji PLA. Jednak, gdy jego stężenie wynosiło ≥ 5% wag. krystalizacja fazy amorficznej PLA stawała się utrudniona na skutek znacznego udziału grup karboksylowych w oddziaływaniach międzycząsteczkowych (pomiędzy CX-COOH) i międzyfazowych (pomiędzy CX-COOH i PLA). Dodatkowo różnica w T_g mieszanin PLA/CX-COOH 2% i 5% wynosiła 3 °C, podczas gdy w kompozytach PLA/CX-R [R = OH, (OH)2, COOMe] wraz ze wzrostem zawartości dodatku obserwowano obniżenie temperatury zeszklenia o ~ 4 °C. Największy jej spadek (~ 6 °C) odnotowano dla kompozytu PLA/CX-COOMe (10% wag), co ma związek z bardzo słabym oddziaływaniem grup COOMe z łańcuchami PLA i plastyfikacją osnowy poliestrowej. Jednak efekt entalpowy indukowanej termicznie krystalizacji fazy amorficznej PLA/CX-COOMe nie zależał (pomijając obniżenie T_{cc}) od ilości dodatku.

Znaczenie tworzenia wiązań wodorowych dla zintensyfikowania nukleacji w osnowie PLA potwierdziły wyniki uzyskane dla mieszaniny PLA/LPSQ-F3, gdzie zimna krystalizacja była intensywniejsza niż w przypadku czystego PLA (praca IV). Stopień krystaliczności tego materiału wyniósł 30%. Dodatek LPSQ-F3 jak również CX-F3 wyraźnie indukował zimną krystalizację PLA, co zostało przypisane powstawaniu centrów nukleacji na skutek tworzenia się wiązań wodorowych pomiędzy atomami fluoru w grupach CF_3 a wodorami ugrupowań metylowych i/lub metinowych polilaktydu. W przypadku dodatku LPSQ-F3 możliwe jest też tworzenie wiązań C-F···F-C we wtrąceniach, co może pośrednio wzmacniać zarodkowanie kryształów PLA. Krystalizacji na zimno nie obserwowano jednak dla mieszanin PLA z LPSQ-F5 oraz z LPSQ-F, niezależnie od ich zawartości w matrycy. Efekt entalpowy był mniejszy niż dla czystego PLA. Termogramy DSC kompozytów PLA/CX-F oraz PLA/CX-F5 również nie

34

wskazywały na występowanie tego zjawiska, także w przypadku zwiększenia stężeń dodatków w mieszaninach. W przeciwieństwie do swych cyklosiloksanowych analogów, LPSQ-F i LPSQ-F5 nie powodowały zmniejszenia T_g wskazującego na plastyfikację. W związku z tym, jako wyjaśnienie nietypowego zachowania, postulowany został wpływ labilnych oddziaływań n-π* pomiędzy grupami karbonylowymi PLA a podstawnikami fluoroarylowymi i mała efektywność oddziaływań $C(sp^3)$–H···F–$C(sp^2)$. O znaczeniu różnic w interakcjach pomiędzy LPSQ-F i LPSQ-F5 a LPSQ-F3 świadczą również wyniki badań mechanicznych (opisane w podrozdziale 2.6).

Wyniki uzyskane za pomocą kalorymetrii różnicowej korelują ze zmianami procesów relaksacyjnych PLA pod wpływem obecności LPSQ posiadających grupy fluoroarylowe (praca IV), jak również w obecności CX-COOH oraz CX-OH (praca III), co wykazano za pomocą szerokopasmowej spektroskopii dielektrycznej. Badania te zostały wykonane we współpracy z panią dr hab. Ewą Markiewicz i dr. Pawłem Ławniczakiem (Instytut Fizyki Molekularnej Polskiej Akademii Nauk) oraz panią dr Magdaleną Włodarską (Politechnika Łódzka). Amorficzny polilaktyd wykazuje obecność procesów relaksacyjnych, których zmiany mogą być obserwowane za pomocą spektroskopii dielektrycznej. Dwa najważniejsze to relaksacja α odpowiadająca przejściu szklistemu oraz relaksacja β związana z lokalnymi drganiami cząsteczki.[78] Oddziaływania PLA z udziałem grup fluoroarylowych odgrywają ważną rolę w modyfikacji osnowy poliestrowej, o czym świadczy istnienie dodatkowych procesów relaksacji w mieszaninach zawierających dodatki LPSQ-F, LPSQ-F5 oraz LPSQ-F3 (relaksacja typu „*normal mode*" związana z dynamiką globalną łańcuchów). W mieszaninach PLA/CX-R, w których dodatki siloksanowe posiadały grupy karboksylowe lub hydroksylowe, modyfikacja procesów relaksacji zależała od rodzaju wiązań wodorowych. Niezależnie od R, proces relaksacji α był prawie identyczny jak w czystym PLA. Relaksacja β ulegała modyfikacjom w obecności CX-OH. Dodatek CX-COOH powodował pojawienie się dodatkowej relaksacji (proces γ) w zakresie niskich temperatur, innej niż proces β, której amplituda zwiększała się wraz ze wzrostem zawartości CX-COOH.

Rezultaty badań kalorymetrycznych zostały również porównane z wynikami uzyskanymi metodą dynamicznej analizy termo-mechanicznej (DMTA) (prace I i IV), które zostały wykonane we współpracy z zespołem pani prof. dr hab. Ewy Piórkowskiej (CBMiM PAN). Przebieg zmian zależności modułu stratności E'' od temperatury dla czystego PLA wykazał tylko obecność przejścia szklistego przy 63°C, natomiast dla PLA z dodatkami LPSQ obserwowano dwa sygnały, co świadczy o częściowej mieszalności i częściowej separacji faz. Szeroki sygnał w temperaturach zbliżonych od temperatury zeszklenia dodatków polisilseskwioksanowych zwiększa swoją intensywność wraz ze wzrostem zawartości LPSQ-R. Nieznaczny spadek temperatury głównego przejścia szklistego w porównaniu do czystego PLA obserwowany jest dla każdego PLA z dodatkiem LPSQ-R i świadczy o niewielkim uplastycznieniu polilaktydu. Nie zależał on znacząco od zawartości LPSQ-R w kompozycie. Moduł sprężystości E' mieszanin PLA i LPSQ-R malał wraz ze wzrostem temperatury, a jego wartość gwałtownie spadała w zakresie temperatury zeszklenia PLA. E' mieszanin zawierających dodatki LPSQ-COOH,

LPSQ-COOMe i LPSQ-OH, w przeciwieństwie do mieszanin z dodatkami fluorowanymi, zmniejszał się wraz ze wzrostem temperatury oraz zwiększeniem stężenia dodatków.

2.4.2. Wpływ LPSQ-R na proces stereokompleksacji PLLA i PDLA

Tworzenie kryształów stereokompleksów PLLA/PDLA jest jedną z nabardziej efektywnych metod polepszania właściwości mechanicznych materiałów polilaktydowych oraz zwiększania ich odporności termicznej i hydrolitycznej, a także właściwości barierowych.[38,64] Różnorodne dodatki mogą być dodawane do mieszaniny PLLA/PDLA, aby usprawnić ten proces i zwiększyć zawartość kryształów SC-PLA w materiale. Środki nukleujące działają, jako zarodki krystalizacji, podczas gdy dodatki plastyfikujące polepszają dyfuzję łańcuchów polimerów i zwiększają szybkość wzrostu kryształów. Przykładem może być PEG.[79] Ze względu na hybrydową strukturę, polimerowy charakter oraz obecność grup funkcyjnych mogących brać udział w tworzeniu wiązań wodorowych, LPSQ-R [R = OH, (OH)2, COOH, COOMe] mogą być dobrymi promotorami procesu stereokompleksowania poli(L-laktydu) i poli(D-laktydu) (praca II). Przeprowadzone zostały badania dla szerokiego zakresu stężeń LPSQ-R w mieszaninie PLLA/PDLA, aby oprócz ich zdolności do nukleacji SC-PLA oszacować również wpływ sfunkcjonalizowanych poli(silseskwioksanów) na właściwości stereo-kompleksów.

Charakterystyczna struktura stereokompleksów w materiałach SC-PLA/LPSQ-R otrzymanych przez swobodne odparowywanie rozpuszczalników z roztworów mieszanin PLLA/PDLA/LPSQ-R, została potwierdzona metodami rentgenostrukturalnymi oraz spektroskopowymi (FTIR, NMR). Została ona zachowana w badanych mieszaninach, gdzie [R]/[La] wynosiło od 0,01 do 0,5. Szczegółowa analiza właściwości termicznych metodą kalorymetrii różnicowej pozwoliła na określenie stopnia krystaliczności tych materiałów, potwierdzenie rodzaju tworzących się struktur oraz oszacowanie zmian przebiegu krystalizacji stereokompleksów w zależności od rodzaju LPSQ-R. W termogramach DSC badanych mieszanin PLLA/PDLA/LPSQ-R nie obserwowano przejścia szklistego. Oznacza to dobre upakowanie molekularne w badanych próbkach oraz istnienie interakcji między łańcuchami PLA specyficznych dla tworzenia się stereokompleksów. Temperatury krystalizacji SC-PLA/LPSQ-R w trakcie chłodzenia stopu hybrydowej mieszaniny są niższe w porównaniu do czystego SC-PLA. Może to być wyjaśnione koniecznością pojawienia się oddziaływań z LPSQ-R (wiązania wodorowe), które mogą być wystarczająco trwałe w niższych temperaturach. To obniżenie T_c SC jest jednak zbyt małe, aby można je przypisać tylko uplastycznieniu osnowy. Ponadto różni się dla różnych LPSQ-R. Zarówno krystalizacja jak i topnienie w trójskładnikowych mieszaninach PLLA/PDLA/LPSQ-R przebiega w szerszym zakresie temperatur niż obserwowane dla SC-PLA. Jednak temperatura topnienia hybrydowych stereokompleksów była bardzo podobna do T_{mSC}. Entalpia krystalizacji SC-PLA/LPSQ-R, zmniejszała się wraz ze wzrostem ilości dodatku, ale stopień krystaliczności określany na podstawie ciepła topnienia kryształów był znacznie wyższy (Rysunek 13). Wyjątkiem były mieszaniny SC-PLA/LPSQ-COOMe, zawierające polisilseskwioksany mogące brać udział

w tworzeniu bardzo słabych wiązań wodorowych C=H···O=C. Dodatek LPSQ-COOMe zmniejszył nieznacznie zdolność do stereokompleksowania mieszaniny PLLA/PDLA. Jednak, w przeciwieństwie do mieszaniny PLLA/PDLA w czasie ogrzewania skrystalizowanej próbki nie obserwowano pików topnienia charakterystycznych dla homokryształów PLLA/PDLA, które pojawiły się w próbce niedomieszkowanego SC-PLA w zakresie temperatur 150-170 °C. Przyczyną tego może być spowolnienie procesu stereokompleksowania w stopie PLLA/PDLA/LPSQ-R. SC-PLA/LPSQ-R wykazywały się również lepszą odpornością termiczną, co zostało szczegółowo omówione w rozdziale 2.5.
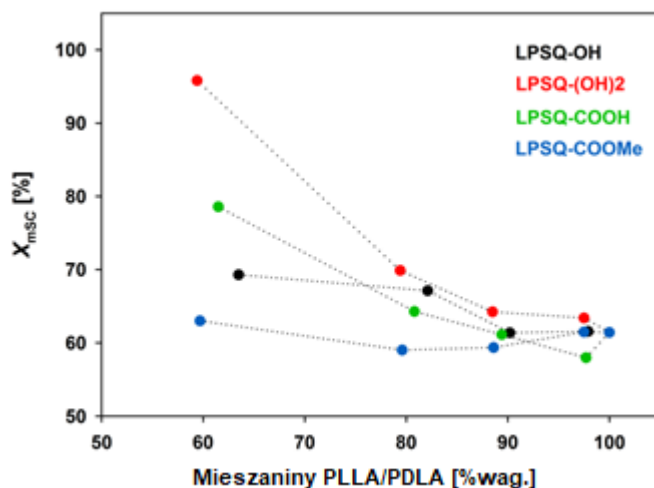
Rysunek 13. Zmiany stopnia krystaliczności (X_{mSC}) mieszanin PLLA/PDLA zawierających różne ilości LPSQ-R i krystalizowanych w czasie chłodzenia stopu z szybkością 10 °C/min (DSC, II grzanie, 10 °C/min).

Tworzenie struktury stereokompleksu w mieszaninach PLLA/PDLA i PLLA/PDLA/LPSQ-R (R = OH, (OH)2, COOH, COOMe) ([R]/[La] = 0,5; co odpowiada 44-48% wag. zawartości LPSQ-R w próbce) badano również przy użyciu spektroskopii FTIR podczas ich izotermicznej krystalizacji ze stopu w 175 °C (praca II). W kryształach stereokompleksu polilaktydu w układzie trójskośnym łańcuchy PLLA oraz PDLA mają konformację 3_1 β-helikalną i charakteryzują się określonymi częstotliwościami pasm IR (około 908 cm^{-1} [ρ(CH$_3$) + v(C-COO)] w temperaturze pokojowej[80]). Wpływ hybrydowych dodatków silseskwioksanowych oceniano poprzez porównanie intensywności wybranych pasm IR. Zaobserwowano, że pasma drgań δ_{as}(CH$_3$) (1455 cm^{-1}) i δ_s(CH$_3$) (1382 cm^{-1}) nie ulegały zmianie w trakcie analizy, co wskazuje na dobrą stabilność badanych próbek w wysokiej temperaturze. Struktury β-helisy powstawały z różną szybkością w niedomieszkowanym SC-PLA i jego hybrydowych analogach zawierających LPSQ. Intensywność pasma drgań [v_{as}(COC) + ρ_{as}(CH$_3$)] przy 1215 cm^{-1} w hybrydowych SC wzrastała szybciej niż w czystym SC-PLA. Sugeruje to, że sfunkcjonalizowane silseskwioksany mogą wpływać na ruchliwość segmentów łańcuchów polilaktydowych poprzez tworzenie wiązań wodorowych. Interesujące wyniki otrzymano w przypadku PLLA/PDLA/LPSQ(OH)2. Próbka ta szybko krystalizowała a pasma wibracyjne przy 1382 cm^{-1} i 1215 cm^{-1} były intensywne już na wczesnych etapach procesu. Wzrost intensywności pasma [v_{as}(COC) + ρ_{as}(CH$_3$)] w trakcie krystalizacji próbek zawierających LPSQ-OH, LPSQ-COOH i LPSQ-COOMe był wolniejszy.

Pomimo to końcowy efekt zaobserwowany w widmach FTIR próbek skrystalizowanych i schłodzonych następnie do temperatury pokojowej jest zbieżny z wynikami uzyskanymi za pomocą różnicowej kalorymetrii skaningowej.

Najlepszy efekt dodatków z grupami hydroksylowymi potwierdzono dodatkowo prowadząc badania wpływu obecności CX-R (2% wag.) na przebieg izotermicznej krystalizacji ze stopu. Badano tworzenie się kryształów typu α oraz α' (helisa typu 10_3) w PLA NW 2003 D zawierającym 3,2% mol. jednostek D-laktydowych (praca III). Obserwowano zmiany pasm charakterystycznych w zakresie liczb falowych 1300-700 cm^{-1} ze szczególnym uwzględnieniem sygnałów w zakresie 920 i 922 cm^{-1}, związanych z drganiami $\rho(CH_3)$ oraz $\nu(C–COO)$ w kryształach typu α i α'. Dodatek CX-OH przyspieszył krystalizację PLA w 100 °C, na co wskazywał wyraźny wzrost pasma przy 1213 cm^{-1}, któremu towarzyszył wzrost pasma drgań $\nu(C–CH_3)$ przy 1042 cm^{-1} oraz spadek intensywności pasma fazy amorficznej przy 955 cm^{-1}. Podobny efekt obserwowano wcześniej, ale dla enancjomerycznie czystego PLLA i tylko w T > 110 °C [81,82]. Nieco wolniejszą krystalizację PLA/CX–OH obserwowano w 110 i 120 °C. Podobne (ale mniej wyraźne) efekty zanotowano dla CX–COOH (2% wag.). Krystalizacja PLA w obecności CX–COOMe (2% wag.) była najszybsza w temperaturze 110 °C.

2.5. Wpływ LPSQ-R na odporność termiczną PLA

Polilaktyd rozkłada się w trakcie ogrzewania w atmosferze azotu poprzez depolimeryzację z utworzeniem cyklicznych oligomerów, laktydu, aldehydu octowego, CO_2 oraz CO.[83] Termiczna degradacja ma miejsce w zakresie temperatur 350-400 °C. Z uwagi na szerokie zastosowanie PLA, jako termoplastycznego materiału w technikach druku 3D bardzo ważne jest zwiększenie jego odporności termicznej jak również użycie do modyfikacji dodatków, które będą ulepszały właściwości osnowy. Termoodporne materiały na osnowie polilaktydu mają zwykle dużą zawartość fazy krystalicznej lub wykazują zmniejszoną ruchliwość segmentów łańcucha w wyniku, na przykład, sieciowania.[84] Odporność termiczna stereokompleksów polilaktydu jest większa niż homopolimerów.[38,85] Dzięki silnym oddziaływaniom pomiędzy sekwencjami komplementarnych jednostek L-laktydowych i D-laktydowych temperatura topnienia kryształów jest wyższa o 40 °C niż homokryształów. Zmniejszenie ruchliwości takich kompleksów utrudnia degradację termiczną, aczkolwiek w trakcie ogrzewania ze stałą szybkością następuje ona według tego samego mechanizmu jak degradacja pojedynczych enancjomerów PLA. Ogrzewanie izotermiczne powoduje rozkład SC-PLA dopiero w temperaturach znacznie wyższych niż temperatura topnienia.[85]

Jak wspomniano, sfunkcjonalizowane LPSQ-R są odporne na degradację termiczną do temperatury 200 °C. Dlatego mogły zostać bez przeszkód użyte do modyfikacji PLA. Przeprowadzona analiza termograwimetryczna czystego PLA i jego mieszanin z CX-R (1-4% wag.) wykazała, że ich stabilność termiczna jest zbliżona (praca III). Nie zaobserwowano również zmian przebiegu degradacji termicznej PLA w obecności LPSQ z podstawnikami fluoroarylowymi (praca IV). Ciekawy efekt został zaobserwowany natomiast w przypadku mieszanin polilaktydu i LPSQ-R [R = COOH, COOMe, OH oraz (OH)2] (Rysunek 14). Dodatek

nawet niewielkiej ilości (0.25% wag.) LPSQ-COOH lub LPSQ-COOMe powodował zwiększenie temperatury rozkładu osnowy poliestrowej o około 20 °C (praca I). Podobny efekt uzyskano w przypadku zwiększenia ilości tych polisilseskwioksanów do 5% wag. próbki PLA. Dodatki te nie miały jednak wpływu na szybkość rozkładu próbki.
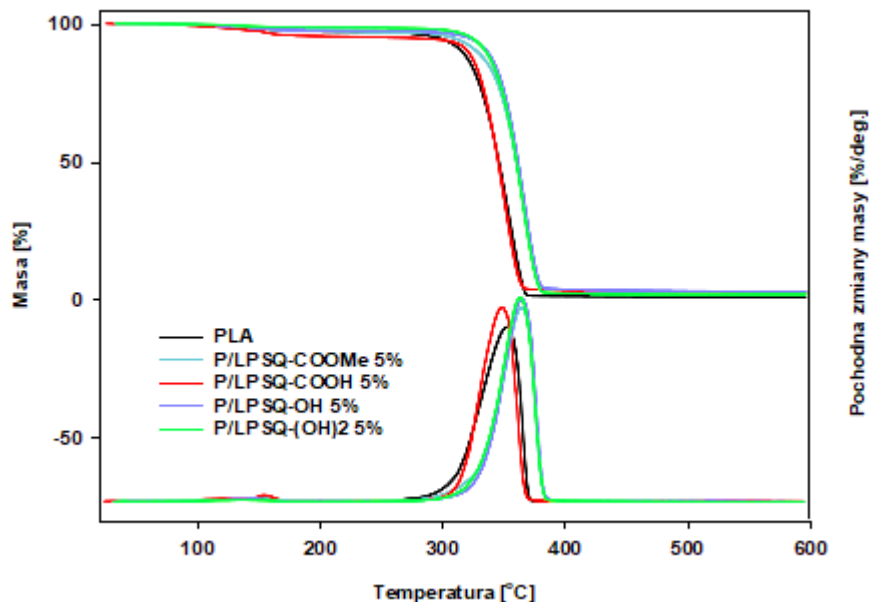
Rysunek 14. Termogramy TGA mieszanin P/LPSQ-R (5% wag.) (10 °C/min w N_2).

Zwiększenie odporności termicznej PLA może być tłumaczone sieciowaniem matrycy polimerowej w podwyższonych temperaturach w obecności tych LPSQ. Jest ono prawdopodobnie powodowane występowaniem reakcji transestryfikacji pomiędzy łańcuchami polilaktydu a grupami hydroksylowymi, karboksylowymi jak również estrowymi, znajdującymi się w łańcuchach bocznych LPSQ. Z uwagi na niewielką wagowo ilość dodatków nie miało to odzwierciedlenia w pozostałości zebranej po zakończeniu ogrzewania, było jednak wystarczające do zmniejszenia ruchliwości części łańcuchów PLA.

Potwierdzeniem tej tezy są wyniki uzyskane w trakcie badań termoodporności hybrydowych stereokompleksów PLLA/PDLA zawierających LPSQ-R [R = COOH, COOMe, OH oraz (OH)2] (praca II). Mieszaniny SC-PLA/LPSQ-R wykazywały większą stabilność termiczną w porównaniu do czystego SC-PLA. Obecność nawet małych ilości LPSQ-R w badanych materiałach (~ 2% wag.) zwiększała temperaturę rozkładu termicznego o około 20-30 °C w zależności od LPSQ-R. Proces degradacji przebiegał w jednym, głównym etapie ubytku masy, którego szybkość zmniejszała się wraz ze wzrostem ilości LPSQ-R w mieszaninie. Zaobserwowano, że odporność termiczna zależy od rodzaju dodatku i siły oddziaływań z osnową polilaktydową. W porównaniu z mieszaninami z LPSQ-OH oraz LPSQ-COOMe, degradacja materiałów zawierających 20% wag. LPSQ-COOH i LPSQ-OH$_2$ zachodziła w wyższych temperaturach, jednak szybkość tych procesów (V_d). Dla wszystkich

polisilseskwioksanów zaobserwowane zostało zmniejszanie się V_d wraz ze wzrostem zawartości LPSQ-R w mieszaninie.

Porównanie procesów degradacji termicznej czystych LPSQ-R i SC-PLA oraz SC-PLA/LPSQ-R (praca II) wskazuje, że składniki mieszanin nie ulegają dekompozycji oddzielnie. Wyniki badań rozkładu termicznego mieszanin SC-PLA/LPSQ-R zawierających około 40% wag. polisilseskwioksanów również sugerują, że ich rozkład termiczny może polegać na transestryfikacji pomiędzy dodatkami LPSQ-R a łańcuchami polilaktydu, powodując sieciowanie osnowy polilaktydowej. Postulowany proces transestryfikacji wydaje się być wolniejszy w obecności LPSQ-COOMe, a mieszanina zawierająca ten dodatek wykazuje rozkład w szerszym zakresie temperatur. Zjawisko transestryfikacji w przypadku mieszanin zawierających LPSQ-COOMe, LPSQ-OH i LPSQ-(OH)2 wydaje się jednak mieć miejsce w podwyższonych temperaturach. Pomiary mas cząsteczkowych mieszanin PLA/LPSQ-R za pomocą chromatografii żelowej przeprowadzone po dłuższym czasie przechowywania próbek w temperaturze pokojowej wykazały, że tak sfunkcjonalizowane polisilseskwioksany nie powodują zasadniczych zmian w wielkości makrocząsteczek ani w rozrzutach mas cząsteczkowych. Wyjątkiem jest LPSQ-COOH, który po dłuższym czasie powodował pogorszenie rozpuszczalności próbki, co było również bardziej wyraźne wraz ze wzrostem jego zawartości w kompozycie.

Dodanie większej ilości dodatków krzemoorganicznych do mieszaniny (około 40% wag.) spowodowało zwiększenie ilości stałej pozostałości po procesie degradacji do temperatury 600°C. Przeprowadzone zostały również badania odporności termicznej SC-PLA/LPSQ-R w trakcie izotermicznej degradacji w atmosferze azotu. Hybrydowe stereokompleksy były dużo bardziej trwałe w wybranych temperaturach (260 °C, 280 °C i 300 °C), a szybkość ich rozkładu znacznie się zmniejszała w porównaniu do wyników uzyskanych z SC-PLA (praca II).

2.6. Wpływ LPSQ-R na właściwości mechaniczne i barierowe PLA

Wyniki badań przeprowadzonych w statycznych próbach jednoosiowego rozciągania zostały przeprowadzone we współpracy z zespołem pani prof. dr hab. Ewy Piórkowskiej (CBMiM PAN) (prace I i IV). Wykazały one, że obecność LPSQ-R wpływa na właściwości mechaniczne PLA (Rysunek 15). Czysty PLA (NW4032D), który również stanowił osnowę badanych kompozytach, wykazywał granicę plastyczności (σ_y) 44 MPa, a jego naprężenie (σ_b) i odkształcenie przy zerwaniu (ε_b) wynosiło odpowiednio 41 MPa i 30 %. Właściwości te ulegały modyfikacji w zależności od rodzaju grup funkcyjnych LPSQ-R, jak również były zależne od mieszalności i stopnia dyspersji krzemoorganicznych dodatków. Zaobserwowana została zależność zdolności materiału do odkształcenia plastycznego od wielkości hybrydowych wtrąceń. Obecność bardzo małych inkluzji zawierających LPSQ-R i uplastyczniających osnowę poliestrową, powodowało polepszenie ciągliwości kompozytów. Należy podkreślić, że mechanizm tego procesu nie wiązał się ze znaczącym zmniejszeniem temperatury zeszklenia materiału, obserwowanym dla innych kompozytów PLA.[23,87,88]
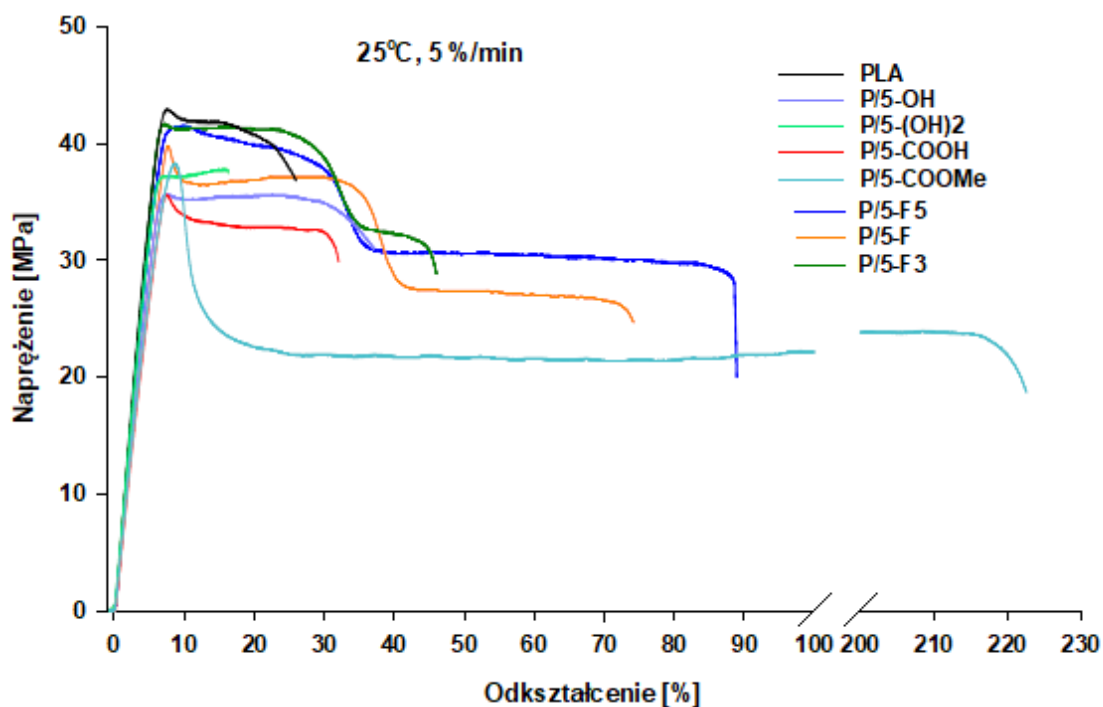
Rysunek 15. Rozciąganie jednoosiowe P/LPSQ-R (5% wag.).

Dzięki bardzo dobrej dyspersji modyfikatora w PLA/LPSQ-COOMe (5% wag.) uzyskany został plastyczny hybrydowy kompozyt, o czym świadczyło prawie 230% wydłużenie przy zerwaniu, przy zachowaniu stosunkowo wysokiej granicy plastyczności ~ 40 MPa (praca I). Interesujące wyniki otrzymano również dla mieszanin PLA i fluoroarylowanych LPSQ (5% wag.) (praca IV). Dla wszystkich trzech dodatków (LPSQ-F, LPSQ-F3 oraz LPSQ-F-5) obserwowano charakterystyczne dwustopniowe odkształcenie, które świadczyło o zwiększeniu podatności materiału na rozciąganie. W pierwszym etapie nie następowało zerwanie, natomiast przejście do drugiego etapu odkształcenia plastycznego przebiegał z tzw. „szyjkowaniem", które występowało najwcześniej w przypadku mieszaniny z LPSQ-F3. Całkowita ciągliwość tej mieszaniny była trochę mniejsza niż pozostałych z tej serii, pomimo bardzo zbliżonych wartości T_g. Może to być związane z nieznacznie większym rozmiarem wtrąceń. Biorąc jednak pod uwagę brak zależności przebiegu pierwszego etapu odkształcenia PLA od temperatury zeszklenia LPSQ-COOMe i LPSQ-F przy podobnej wielkości wtrąceń (Tabela 4), wydaje się, że zwiększenie ciągliwości może być wypadkową kilku czynników. Jednym z nich mogą być różnice w niespecyficznych oddziaływaniach grup funkcyjnych R i łańcuchów poliestrowych. Ponadto, pomimo tego, że temperatura zeszklenia mieszanin polilaktydu zawierających LPSQ-COOH, LPSQ-OH i LPSQ-(OH)2 jest podobna omówionych powyżej, to jednak obecność oraz zwiększenie stężenia tych dodatków nie poprawiło znacznie ciągliwości PLA i wytrzymałości na zerwanie (praca I). Można to przypisać gorszej mieszalności, związanej prawdopodobnie również z tworzeniem wiązań wodorowych między grupami funkcyjnymi a atomami tlenu grup karbonylowych PLA. Dzięki temu uplastycznienie wtrąceń jest mniejsze, co wpływa na całościowe właściwości mechaniczne tych materiałów. Dodanie mniejszych ilości LPSQ-

COOMe, LPSQ-F, LPSQ-F3 i LPSQ-F5 także nie było wystarczające dla poprawienia właściwości mechanicznych PLA.

Tabela 4. Zestawienie temperatury zeszklenia LPSQ-R i średniej wielkości wtrąceń mieszaninach PLA zawierających 5% wag. LPSQ-R.

LPSQ-R	T_g [°C]	d [µm]	σ_y [MPa]	σ_b [MPa]	ε_b [%]
PLA	60	-	42	38	22
LPSQ-COOH	-14	10-20	36	33	29
LPSQ-OH	-47	6-10	36	35	28
LPSQ-COOMe	-41	1	40	22	230
LPSQ-(OH)2	-30	2-4	37	38	17
LPSQ-F	-31	1	40,5	(36) 26	63
LPSQ-F5	-10	1-3	41	(38) 29	87
LPSQ-F3	-9	1-3	41	(40) 31	44

T_g – temperatura zeszklenia czystych substancji
d – średni rozmiar wtrąceń oszacowany na podstawie SEM

σ_y – granica plastyczności
σ_b – naprężenie przy zerwaniu
ε_b –odkształcenie przy zerwaniu

Obecność atomów fluoru spowodowała ponadto zmniejszenie energii powierzchniowej mieszanin polilaktydu i fluorowanych LPSQ oraz poprawiła ich właściwości barierowe (praca IV). Zaobserwowano znaczne zmniejszenie przepuszczalności tlenu przez całkowicie amorficzne folie wykonane z mieszanin zawierających 1 i 5 % wag. fluorowanych LPSQ-R, w porównaniu z czystym PLA (badania prowadzone we współpracy z panem dr. hab. Arturem Różańskim, CBMiM PAN). Zaobserwowane różnice w przepuszczalności były związane z rodzajem grup funkcyjnych i mieszalnością polisilseskwioksanów z osnową poliestrową. Największy efekt został zaobserwowany dla PLA/LPSQ-F3. Zbliżony efekt uzyskano także dla PLA/LPSQ-F5. Zwiększenie ich ilości do 5% wag. powodowało jednak wzrost przenikalności tlenu przez membrany. Z kolei w przypadku PLA/LPSQ-F wraz ze wzrostem zawartości dobrze mieszalnego LPSQ-F zanotowano zwiększenie właściwości barierowych. Uzyskane wyniki mogą wskazywać na wpływ separacji faz w tych mieszaninach na właściwości barierowe.
Ta unikalna kombinacja właściwości mechanicznych i barierowych może stanowić o przydatności hydrofobowych mieszanin polilaktydu i fluorowanych LPSQ, jako materiałów opakowaniowych. Dodanie plastyfikatorów do PLA powoduje podwyższenie ruchliwości łańcucha polimeru, jednak zwykle wpływa na pogorszenie jego właściwości barierowych.[89] Należy podkreślić, że wcześniejsze przykłady zmniejszenia przenikalności PLA polegały na generowaniu przeszkód na drodze dyfuzji gazów w osnowie poliestrowej (dodatek warstwowych minerałów[89], grafenu[90] lub zwiększenie stopnia krystaliczności PLA[91]). Wzrost stopnia krystaliczności może wiązać się jednak ze zwiększeniem objętości wykluczonej, co może przyspieszać transport cząsteczek gazów w pobliżu kryształów PLA[92]. Ponadto, wpływa niekorzystnie na wytrzymałość PLA na rozciąganie.

V. PODSUMOWANIE I WNIOSKI

W trakcie przeprowadzonych badań przygotowano hybrydowe kompozyty polimerowe zawierające polilaktyd jako osnowę polimerową oraz dodatki nowego typu: sfunkcjonalizowane liniowe polisilseskwioksany (LPSQ-R) oraz ich małocząsteczkowe odpowiedniki – cyklotetra-siloksany (CX-R) z podstawnikami bocznymi (R = OH, $(OH)2$, COOH, COOMe, C_6F_5, C_6H_4F, $C_6H_4CF_3$) zdolnymi do oddziaływań supramolekularnych. Opracowano metody otrzymywania i scharakteryzowano właściwości pochodnych krzemoorganicznych użytych jako modyfikatory. W zależności od siły interakcji supramolekularnych, LPSQ-R i CX-R były w różnym stopniu zdyspergowane w matrycy poliestrowej. Postulowano tworzenie wiązań wodorowych, w których grupy funkcyjne mogły pełnić rolę akceptora lub donora, jak również oddziaływania typu n-π*.

Uzyskane materiały hybrydowe wykazywały różne właściwości w zależności od rodzaju i zawartości krzemoorganicznych dodatków. Zbadano ich wpływ na zimną krystalizację polilaktydu, a także na właściwości mechaniczne i termiczne przygotowanych kompozytów. Dodanie do PLA LPSQ-R posiadających grupy boczne zdolne do wzięcia udziału w reakcjach transestryfikacji (OH, COOH, COOMe) spowodowało wzrost odporności termicznej hybrydowych materiałów. Wprowadzenie ich małocząsteczkowych analogów, jak również LPSQ z podstawnikami fluoroarylowymi, nie zmieniło stabilności termicznej polilaktydu.

Dzięki bardzo dobrej dyspersji w osnowie, małe ilości LPSQ-COOMe znacząco zwiększyły plastyczność PLA, co znalazło odzwierciedlenie w prawie 230% wydłużeniu przy zerwaniu, przy zachowaniu granicy plastyczności ~ 40 MPa. Dodatek LPSQ z grupami fluoroarylowymi również polepszył właściwości mechaniczne PLA. Modyfikatory krzemoorganiczne sfunkcjonalizowane podstawnikami tworzącymi silniejsze wiązania wodorowe, na przykład LPSQ-OH, nie wykazywały takich właściwości. Przyspieszały jednak zarodkowanie wzmacniając proces zimnej krystalizacji. Wykazano także, że dodatek LPSQ-R (R = OH, $(OH)2$, COOH, COOMe) do mieszaniny poli(L-laktydu) i poli(D-laktydu) spowodował powstanie stereokompleksów o zwiększonej stabilności termicznej. Co więcej, stereokompleksacja łańcuchów PLLA i PDLA przebiegała efektywnie nawet w obecności znacznych ilości tych polisilseskwioksanów. Z kolei dodatki CX-R (R = OH, COOMe, $C_6H_4CF_3$) mimo bardzo niskiego współczynnika kształtu skutecznie działały jako zarodki krystalizacji PLA. W przeciwieństwie do LPSQ, powodowały jednak zauważalne obniżenie temperatury zeszklenia osnowy polilaktydowej.

Badane materiały z domieszką fluoroarylowanych LPSQ wykazały także istotną poprawę właściwości barierowych w stanie amorficznym – obserwowano znaczny spadek szybkości przenikania tlenu oraz wzrost hydrofobowości. Charakteryzowały się one również znaczącym wzrostem absorpcji światła w zakresie UV-B. Dodatek pochodnych krzemoorganicznych zawierających w łańcuchach bocznych grupy karbonylowe powodował podobny efekt, nawet w przypadku całkowicie przezroczystych próbek. Te specyficzne cechy mogą okazać się cenne w projektowaniu zastosowań tych materiałów.

VI. STRESZCZENIE

Tematem rozprawy doktorskiej są *„Hybrydowe kompozyty polilaktydu i pochodnych krzemoorganicznych".* Celem prowadzonych badań było zbadanie możliwości wykorzystania pochodnych krzemoorganicznych: polisiloseskwioksanów oraz cyklotetrasiloksanów sfunkcjonalizowanych podstawnikami zdolnymi do oddziaływań supramolekularnych (wiązania wodorowe oraz oddziaływania typu n-π*) jako modyfikatorów polilaktydu (PLA). Polilaktyd, jako „podwojnie zielony" biopolimer, cieszy się ogromnym zainteresowaniem ze względu na naturalne pochodzenie, biokompatybilność, biodegradowalność oraz kompostowalność. Tego typu materiały są niezwykle ważne ze względu na zwiększające się zanieczyszczenie środowiska naturalnego odpadami z tworzyw polimerowych oraz wyczerpywaniem się zasobów surowców kopalnych. PLA wymaga jednak modyfikacji w celu polepszenia jego właściwości użytkowych, szczególnie termicznych i mechanicznych. Dlatego poszukuje się jak najbardziej efektywnych metod wytwarzania biodegradowalnych materiałów kompozytowych o jak najkorzystniejszych właściwościach użytkowych. Interesującym przykładem może być zastosowanie amidowych lub hydrazydowych pochodnych arylowych, które tworzą nanokryształy w trakcie schładzania stopu domieszkowanego PLA. Tworzenie wiązań wodorowych pomiędzy wiązaniami estrowymi w łańcuchach PLA i strukturami amidowymi lub hydrazydowymi prowadzi do efektywnej nukleacji PLA.

Liniowe poli(silseskwioksany) (LPSQ-R) sfunkcjonalizowane podstawnikami zawierającymi grupy boczne (COOH, COOMe, OH, C_6H_4F, $C_6H_4CF_3$, C_6F_5), mogące oddziaływać z ugrupowaniami poliestrowymi, zostały zaprojektowane jako nowe modyfikatory PLA. Ich wspólną cechą jest obecność podwójnego łańcucha głównego o drabinkowej budowie, co umożliwia kontrolę rozmieszczenia przestrzennego bocznych grup funkcyjnych znajdujących się przy każdym atomie krzemu (podobnie jak ma to miejsce w supramolekularnych kryształach tworzonych przez pochodne amido/hydrazydo-arylowe w stopie polilaktydu). Ich małocząsteczkowe analogi – cyklotetrasiloksany (CX-R) – zostały zastosowane w celu oszacowania wpływu struktury LPSQ na właściwości hybrydowych materiałów. Substancje te były częściowo mieszalne z osnową PLA a siła ich interakcji z matrycą poliestrową, jak również morfologia (makrocząsteczki lub związki małocząsteczkowe), określały ich stopień dyspersji w matrycy poliestrowej. Uzyskane w ten sposób materiały hybrydowe wykazywały różne właściwości fizykochemiczne i mechaniczne, w zależności od rodzaju i zawartości LPSQ-R oraz CX-R. Dodatki LPSQ-R, w zależności od rodzaju grupy funkcyjnej R, wpływały na przebieg krystalizacji fazy amorficznej w trakcie ogrzewania oraz stereokompleksacji, jak również na właściwości optyczne i mechaniczne. Należy podkreślić znaczny wzrost ciągliwości materiału w obecności LPSQ z podstawnikami COOMe, C_6H_4F, $C_6H_4CF_3$ i C_6F_5 przy zachowaniu wysokiej granicy plastyczności. Z kolei dodanie LPSQ-COOH, LPSQ-COOMe oraz LPSQ-OH znacząco poprawiało odporność termiczną PLA. Należy podkreślić, że związki tworzące wiązania wodorowe oraz oddziaływania typu n-π* z atomami fluoru zastosowano do modyfikacji PLA po raz pierwszy. Dzięki temu udało się znacząco polepszyć właściwości barierowe w amorficznych foliach wykonanych z domieszkowanego polilaktydu.

VII. SUMMARY

The topic of my doctoral thesis is "Hybrid composites of polylactide and organosilicon derivatives". The aim of the research was to investigate the possibility of using organosilicon derivatives: polysilsesquioxanes and cyclotetrasiloxanes functionalized with substituents capable of supramolecular interactions (hydrogen bonds and n-π* interactions) as polylactide (PLA) modifiers. Polylactide, as a "double green" biopolymer, is of great interest due to the natural origin of the raw materials used for its production, biocompatibility, biodegradability and compostability. Such materials become extremely important due to the increasing pollution of the natural environment with polymer waste and the depletion of fossil resources. Despite the advantages, PLA requires modification in order to improve its thermal and mechanical performance. Therefore, the new methods of its modification are sought for the production of biodegradable composites with enhanced properties. Application of aryl amide or hydrazide derivatives as additives that can form nanocrystals on cooling of the PLA melt is an interesting example. Formation of hydrogen bonds between PLA chains and these supramolecular structures leads to an effective nucleation of PLA.

Linear poly(silsesquioxanes) (LPSQ-R) functionalized with substituents containing side groups (COOH, COOMe, OH, C6H4F, C6H4CF3, C6F5), which can interact with polyesters were designed as PLA modifiers. Their unique feature is the presence of a double main chain of ladder structure. It allows controlling the spatial distribution of functional groups grafted to silicon atoms, analogously to the effect exerted by supramolecular crystals of aryl amido/hydrazide derivatives in PLA melt. Their small-molecule analogs - cyclotetrasiloxanes (CX-R) - were used to estimate the influence of the structure of ladder polysilsesquioxanes on the properties of hybrid materials. The organosilicon derivatives were partially miscible with PLA and the strength of their interactions with the polyester matrix as well as their morphology (macromolecules or low molecular weight compounds) determined the degree of dispersion in PLA. Hybrid composite materials obtained in this way exhibited various physicochemical and mechanical properties, depending on the type and content of LPSQ-R and CX-R. Addition of LPSQ-R, depending on the type of the R functional group, influenced the course of the crystallization of the amorphous phase during heating and stereocomplexation, as well as the optical and mechanical properties of the blends. It should be emphasized that the material toughness increased significantly in the presence of LPSQ with COOMe, C6H4F, C6H4CF3 and C6F5 groups while maintaining the high yield point of PLA. In turn, the addition of LPSQ-COOH, LPSQ-COOMe and LPSQ-OH significantly improved the thermal resistance of PLA. It is worth noting that compounds forming hydrogen bonds with fluorine atoms and n-π* interactions were used for the first time for modification of PLA. As a result, a significant improvement of barrier properties in amorphous films of PLA-based composites was achieved.

VIII. LITERATURA

1. S. Slomkowski, S. Penczek, A. Duda „Polylactides – an overview", *Polym. Adv. Technol.*, 25 (2014) 436–447.

2. J. Pretula, S. Slomkowski, S. Penczek "Polylactides—Methods of synthesis and characterization", *Adv. Drug Deliv. Rev.* 107 (2016) 3–16.

3. S. Farah, D.G. Anderson, R. Langer "Physical and mechanical properties of PLA, and their functions in widespread applications — A comprehensive review", *Adv. Drug Deliv. Rev.,* 107 (2016) 367–392.

4. A. Duda, S. Penczek „Polilaktyd [poli(kwas mlekowy)]: synteza, właściwości i zastosowania", *Polimery*, 1 (2003) 48.

5. K. Masutani, Y. Kimura "Present Situation and Future Perspectives of Poly(lactid acid) [w:] M.L. di Lorenzo, R. Androsch "Synthesis, structure and properties of poly(lactic acid)", *Adv. Polym. Sci.* 279 (2017) 1-26.

6. S. Corneillie, M. Smet "PLA architectures: the role of branching", *Polym. Chem.*, 6 (2015) 850–867.

7. X. Pang, X. Zhuang, Z. Tang, X. Chen "Polylactic acid (PLA): Research, development and industrialization", *Biotechnol. J.*, 5 (2010) 1125–1136.

8. A.P. Gupta, V. Kumar "New emerging trends in synthetic biodegradable polymers – Polylactide: A critique", *Eur. Polym. J.*, 43 (2007) 4053–4074.

9. J. Zhang, K. Tashiro, H. Tsuji, A.J. Domb "Disorder-to Order Phase Transition and Multiple Melting Behavior of Poly(L-lactide) Investigated by Simultaneous Measurements of WAXD and DSC", *Macromolecules*, 41 (2008) 1352-1357.

10. K. Wasanasuk, K. Tashiro "Crystal structure and disorder in Poly(L-lactic acid) α form (α' form) and the phase transition mechanism to the ordered α form", *Polymer*, 52 (2011) 6097-6109.

11. R. Androsch, M.L. Di Lorenzo „Effect of molar mass on the α'/ α -transition in poly (L-lactic acid)", *Polymer*, 114 (2017) 144-148.

12. L. Aliotta, P. Cinelli M.B. Coltelli, M.C. Righetti, M. Gazzano, A. Lazzeri "Effect of nucleating agents on crystallinity and properties of poly(lactic acid) (PLA)", *Eur. Polym. J.*, 93 (2017) 822-832.

13. A. Magoń, M. Pyda "Study of crystalline and amorphous phases of biodegradable poly(lactic acid) by advanced thermal analysis", *Polymer,* 50 (2009) 3967–3973.

14. S. Saeidlou, M.A. Huneault, H. Li, C.B. Park "Poly(lactic acid) crystallization", *Progr. Polym. Sci.*, 37 (2012) 1657–1677.

15. K. Van de Velde, P. Kiekens "Biopolymers: overview of several properties and consequences on their applications", *Polym. Test.*, 21 (2002) 433-442.

16. L. Jiang, T. Shen, P. Xu, X. Zhao, X. Li, W. Dong, P. Ma, M. Chen "Crystallization modification of poly(lactide) by using nucleating agents and stereocomplexation", *e-Polymers*, 16 (2016) 1–13.

17. K. Madhavan Nampoothiri, N.R. Nair, R.P. John "An overview of the recent developments in polylactide (PLA) research" *Bioresource Technol.*, 101 (2010) 8493–8501.

18. T. Mukherjee, N. Kao "PLA Based Biopolymer Reinforced with Natural Fibre: A Review", *J. Polym Environ*, 19 (2011) 714–725.

19. V. DeStefano, S. Khan, A. Tabada "Applications of PLA in modern medicine", *Eng. Reg.*, 1 (2020) 76-87.

20. M. Murariu, P. Dubois "PLA composites: From production to properties", *Adv. Drug Deliv. Rev.*, 107 (2016) 17–46.

21. J.-M. Raquez, Y. Habibi, M. Murariu, P. Dubois "Polylactide (PLA)-based nanocomposites", *Progr. Polym. Sci.*, 38 (2013) 1504– 1542.

22. A. Basu, M. Nazarkovsky, R. Ghadi, W. Khan, A.J. Domb "Poly(lactic acid)-based nanocomposites", *Polym. Adv. Technol.*, 28 (2017) 919–930.

23. M. Nofar, D. Sacligil, P.J. Carreau, M.R. Kamal, M.-C. Heuzey "Poly (lactic acid) blends: Processing, properties and applications", *Int. J. Biol. Macromol.*, 125 (2019) 307–360.

24. T. Maharana, S. Pattanaik, A. Routaray, N. Nathb, A. Kumar Sutar "Synthesis and characterization of poly(lactic acid) based graft copolymers", *React. Funct. Polym.*, 93 (2015) 47–67.

25. M.J. Carbone, M. Vanhalle, B. Goderis, P. Van Puyvelde "Amino acids and poly(amino acids) as nucleating agents for poly(lactic acid)", *J. Polym. Eng.*, 35 (2015) 169-180.

26. Y. Zhou, L. Lei, B. Yang, J. Li, J. Ren "Preparation and characterization of polylactic acid (PLA) carbon nanotube nanocomposites", *Polym. Test.*, 68 (2018) 34-38.

27. Y. Xu, L. Wu "Synthesis of organic bisurea compounds and their roles as crystallization nucleating agents of poly(L-lactic acid)", *Eur. Polym. J.*, 49 (2013) 865-872.

28. X. Zheng, H. Luo, S. Chen, B. Zhang, B. Sun, M.-F. Zhu, B. Zhang, X.-K. Ren, J. Song "Conformation variation induced crystallization enhancement of poly(L-lactic acid) by gluconic derivatives", *Cryst. Growth Des.*, 20 (2020) 653–660.

29. P. Song, L. Sang, L. Zheng, C. Wang, K. Liu, Z. Wei "Insight into the role of bound water of a nucleating agent in polymer nucleation: a comparative study of anhydrous and monohydrated orotic acid on crystallization of poly(L-lactic acid)", *RSC Adv.*, 7 (2017) 27150–27161.

30. X. Xu, W. Zhen "Preparation, performance and non-isothermal crystallization kinetics of poly(lactic acid)/amidated humic acid composites", *Polym. Bull.*, 75 (2018) 3753–3780.

31. P. Liu, W. Zhen, S. Bian, X. Wang "Preparation and performance of poly (lactic acid)/fulvic acid benzhydrazide composites", *Adv. Polym. Technol.*, 37 (2018) 2788–2798.

32. R. Scaffaro, L. Botta, F. Lopresti, A. Maio, F. Sutera "Polysaccharide nanocrystals as fillers for PLA based nanocomposites", *Cellulose*, 24 (2017) 447–478.

33. R. Zhang, Y. Wang, K. Wang, G. Zheng, Q. Li, C. Shen "Crystallization of poly(lactic acid) accelerated by cyclodextrin complex as nucleating agent", *Polym. Bull.*, 70 (2013) 195–206.

34. H. Zhang, S. Wang, S. Zhang, R. Ma, Y. Wang, W. Cao, C Liu, C. Shen "Crystallization behavior of poly(lactic acid) with a self-assembly aryl amide nucleating agent probed by real-time infrared spectroscopy and X-ray diffraction" *Polym. Test.*, 64 (2017) 12–19.

35. T. Xu, A. Zhang, Y. Zhao, Z. Han, L. Xue "Crystallization kinetics and morphology of biodegradable poly(lactic acid) with a hydrazide nucleating agent", *Polym. Test.*, 45 (2015) 101-106.

36. W.-C. Lai "The effect of self-assembled nanofibrils on the morphology and microstructure of poly(L-lactic acid)", *Soft Matter*, 7 (2011) 3844–3851.

37. C.-F. Yang, Y.-F. Huang, J. Ruan, A.C. Su "Extensive development of precursory helical pairs prior to formation of stereocomplex crystals in racemic polylactide melt mixture" *Macromolecules*, 45 (2012) 872−878.

38. H. Tsuji "Poly(lactic acid) stereocomplexes: A decade of progress", *Adv. Drug Deliv. Rev.*, 107 (2016) 97-135.

39. A. Kowalewska, M. Nowacka „Supramolecular Interactions in Hybrid Polylactide Blends—The Structures, Mechanisms and Properties", *Molecules*, 25 (2020) 3351.

40. R.W. Newberry, R.T. Raines "The $n \rightarrow \pi^*$ Interaction", *Acc. Chem. Res.,* 50 (2017) 1838-1846.

41. S.K. Singh, A. Das "The $n \rightarrow \pi^*$ interaction: a rapidly emerging non-covalent interaction" *Phys. Chem. Chem. Phys.*, 17 (2015) 9596-9612.

42. A. Rahim, P. Saha, K.K. Jha, N. Sukumar, B.K. Sarma „Reciprocal carbonyl-carbonyl interactions in small molecules and proteins", *Nature Comm.*, 8, 78 (2017)

43. S.K. Singh, P.R. Joshi, R.A. Shaw, J.G. Hill, A. Das "Interplay between hydrogen bonding and n → π* interaction in an analgesic drug salicin", *Phys. Chem. Chem. Phys.*, 20 (2018) 18361-18373.

44. J. Echeverria "Intermolecular Carbonyl···Carbonyl Interactions in Transition-Metal Complexes", *Inorg. Chem.*, 57 (2018) 5429-5437.

45. R.W. Newberry, R.T. Raines "*n → π** interactions in poly(lactic acid) suggest a role in protein folding", *Chem. Comm.*, 49 (2013) 7699-7701.

46. P. Panini, D. Chopra „Understanding of noncovalent interactions involving organic fluorine. Chapter 2, *Hydrogen Bonded Supramolecular Structures. Lecture Notes in Chemistry*, 87 (2015).

47. V.R. Thalladi, H.-C. Weiss, D. Bläser, R. Boese, A. Nangia, G.R. Desiraju "C-H···F Interactions in the Crystal Structures of Some Fluorobenzenes", *J. Am. Chem. Soc.,* 120 (1998) 8702-8710.

48. P. Panini, D. Chopra "Quantitive insights into energy contributions of intermolecular interactions in fluorine and trifluoromethyl substituted isomeric *N*-phenylacetamides and *N*-methylbenzamides", *CrystEngComm*, 15 (2013) 3711-3733.

49. H.-J. Schneider "Hydrogen bonds with fluorine. Studies in solution, in gas phase and by computations, conflicting conclusions from crystallographic analyses", *Chem. Sci.*, 3 (2012) 1381-1394.

50. P.A. Champagne, J. Desroches, J.-F. Paquin "Organic Fluorine as a Hydrogen-Bond Acceptor: Recent Examples and Applications", *Synthesis*, 47 (2015) 306-322.

51. P. Metrangolo, J.S. Murray, T. Pilati, P. Politzer, G. Resnati, G. Terraneo "The fluorine atom as a halogen bond donor, *viz*. a positive site", *CrystEngComm*, 13 (2011) 6593-6596.

52. P. Metrangolo, J.S. Murray, T. Pilati, P. Politzer, G. Resnati, G. Terraneo "Fluorine centered halogen bonding: a factor in recognition phenomena and reactivity", *Cryst. Growth Des.*, 11 (2011) 4238-4246.

53. M.S. Pavan, K.D. Prasad, T.N.G. Row "Halogen bonding in fluorine: experimental charge density study on intermolecular FF and FS donor-acceptor contacts", *Chem. Comm.*, 49 (2013) 7558-7560.

54. J.A.K. Howard, V.J. Hoy, D. O'Hagan, G.T. Smith "How good is fluorine as a hydrogen bond acceptor?", *Tetrahedron*, 52 (1996) 12613-12622.

55. P. Panini, D. Chopra "Role of intermolecular interactions involving organic fluorine in trifluoromethylated benzanilides", *CrystEngComm*, 14 (2012), 1972-1989.

56. V.R. Hathwar, D. Chopra, P. Panini, T.N.G. Row "Revealing the polarizability of organic fluorine in the trifluoromethyl group: implications in supramolecular chemistry", *Cryst. Growth Des.*, 14 (2014) 5366-5369.

57. A. Kowalewska, M. Nowacka „Synthesis of Ladder Silsesquioxanes by *in* situ Polycondensation of Cyclic Tetravinylsiloxanetetraols" *Silicon*, 7 (2015) 133-146.

58. A. Kowalewska, M. Nowacka, A. Tracz, T. Makowski „Supramolecular self-assembly of linear oligosilsesquioxanes on mica – AFM surface imaging and hydrophilicity studies", *Soft Matter*, 11 (2015) 4818-4829.

59. N.F. Ayub, S. Hashim, J. Jamaluddin, N. Adrus "New UV LED curing approach for polyacrylamide and poly(N-isopropylacrylamide) hydrogels", *New J. Chem.*, 41 (2017) 5613-5619.

60. R. W. Castelino, G. Hallas "Electronic Absorption Spectra of Some Analogues and Derivatives of Michler's Ketone", J. Chem. Soc. B, (1971) 1468-1471.

61. F. Dénès, M. Pichowicz, G. Povie, P. Renaud "Thiyl Radicals in Organic Synthesis", *Chem. Rev.,* 114 (2014) 2587–2693.

62. J.L. Heidbrink, L.E. Ramírez-Arizmendi, K.K. Thoen, L. Guler, H.I. Kenttämaa "Polar Effects Control Hydrogen-Abstraction Reactions of Charged, Substituted Phenyl Radicals", *J. Phys. Chem. A*, 105 (2001) 7875–7884.

63. E.T. Denisov, T. Denisova Handbook of Antioxidants: Bond Dissociation Energies, Rate Constants, Activation Energies, and Enthalpies of Reactions, 2nd Edition, CRC Press, (1999) str. 97.

64. B. Roduit, M. Hartmann, P. Folly, A. Sarbach, P.Brodard, R. Baltensperger "Thermal decomposition of AIBN, Part B: Simulation of SADT value based on DSC results and large scale tests according to conventional and new kinetic merging approach", *Thermochim. Acta*, 621 (2015) 6-24.

65. E. Pelletier, J.F. Harrod „Cyclosiloxanes as frameworks for multimetallic compounds. 3. Proton NMR spectra of some substituted methylcyclosiloxanes", *Organometallics*, 3 (1984) 1070–1075.

66. A.J. Muller, M. Avila, G. Saenz, J. Salazar "Crystallization of PLA-based materials", A. Jumenez, M. Peltzer, R. Ruseckaite (Eds.), *Poly(lactic Acid) Science and Technology: Processing, Properties, Additives and Applications, RSC Polymer Chemistry Series, Royal Society of Chemistry, Cambridge*, (2015) 66-98.

67. H. Tsuji, I. Fukui "Enhanced thermal stability of poly(lactide)s in the melt by enantiomeric polymer blending", *Polymer*, 44 (2003) 2891-2896.

68. E. Meaurio, N. López-Rodriguez, J.R. Sarasua "Infrared spectrum of poly(L-lactide): application to crystallinity studies", *Macromolecules*, 39 (2006) 9291-9301.

69. D.A. Brant, A.E. Tonnelli, P.J. Flory "The configurational statistics of random poly(lactic acid) Chamins. II. Theory", *Macromolecules*, 2)1969) 228-235.

70. Y. Sasanuma, D. Togue "Configurational statistics of poly(L-lactide) and poly(DL-lactide) chains, *Polymer*, 55 (2014) 1901-1911.

71. E. Meaurio, E. Zuza, N. López-Rodriguez, J.R. Sarasua "Conformational behavior of poly(L-lactide) studied by infrared spectroscopy", *J. Phys. Chem. B*, 110 (2006) 5790-5800.

72. G. Kister, G. Cassanas, M. Vert "Effect of morphology, conformation and configuration on the IR and Raman spectra of various poly(lactic acid)s", *Polymer*, 39 (1998) 267-273.

73. S. Nurkhamidah, E.M. Woo "Mechanisms of Multiple Types of Lamellae and Spherulites in Poly(L-lactic acid) Interacting with Poly(4-vinyl phenol)" *Macromol. Chem. Phys.*, 214 (2013) 2345-2354.

74. G. Lugito, S. Nagarajan, E.M. Woo "Explosive Fibonacci sequence growth into unusual sector face morphology in poly(L-lactic acid) crystallized with polymeric diluents" *Sci. Rep.*, 10 (2020) 10811.

75. N. Siti, E.M. Woo, Y.-T. Yeh, F. Luo, V. Katiyar "Lamellae Assembly in Dendritic Spherulites of Poly(L-lactic Acid) Crystallized with Poly(p-Vinyl Phenol)", *Polymers,* 10 (2018) 545.

76. E.M. Woo, G. Lugito, S. Nagarajan "Dendritic polymer spherulites: birefringence correlating with lamellae assembly and origins of superimposed ring bands", *J. Polym. Res.,* 27 (2020) 7.

77. J. Shi, W. Wang, Z. Feng, D. Zhang, Z. Zhou, Q. Li „Multiple influences of hydrogen bonding interactions on PLLA crystallization behaviors in PLLA/TSOS hybrid blending systems", *Polymer*, 175 (2019) 152–160.

78. M. Pluta, J.K. Jeszka, G. Boiteux „Polylactide/montmorillonite nanocomposites: Structure, dielectric, viscoelastic and thermal properties", *Eur. Polym. J.*, 43 (2007) 2819–2835.

79. R.Y. Bao, W. Yang, X.F. Wei, B.H. Xie, M.B. Yang „Enhanced formation of stereocomplex crystallites of high molecular weight poly(L-lactide)/poly(D-lactide) blends from melt by using poly(ethylene glycol)" *ACS Sustainable Chem. Eng.*, 2 (2014) 2301–2309.

80. P. Pan, J. Yang, G. Shan, Y Bao, Z. Weng, A. Cao, K. Yazawa, Y. Inoue "Temperature-Variable FTIR and Solid-State ^{13}C NMR Investigations on Crystalline Structure and Molecular Dynamics of Polymorphic Poly(L-lactide) and Poly(L-lactide)/Poly(D-lactide) Stereocomplex", *Macromolecules*, 45 (2012) 189-197.

81. P. Pan, B. Zhu, W. Kai, T. Dong, Y. Inoue "Effect of crystallization temperature on crystal modifications and crystallization kinetics of poly(L-lacide)", *J. Appl. Polym. Sci.*, 107 (2008) 54-62.

82. P. Pan, Z. Liang, B. Zhu, T. Dong, Y. Inoue "Blending effects on polymorphic crystallization of poly(L-lactide)", *Macromolecules*, 42 (2009) 3374-3380.

83. H. Zou, C. Yi, L. Wang, H. Liu, W. Xu „Thermal degradation of poly(lactic acid) measured by thermogravimetry coupled to Fourier transform infrared spectroscopy", *J. Therm. Anal. Calorim.*, 97 (2009) 929–935.

84. T.M. Quynh, H. Mitomo, M. Yoneyama, N.Q. Hien „Properties of radiation-induced crosslinking stereocomplexes derived from poly(L-lactide) and different poly(D-lactide)", *Polym. Eng. Sci.*, 49 (2009) 970–976.

85. H. Tsuji „Poly(lactide) stereocomplexes: formation, structure, properties, degradation, and applications", *Macromol. Biosci.*, 5 (2005) 569–597.

86. M. Hirata, Y. Kimura, Structure and properties of stereocomplex-type poly(lactic acid). Chapter 5 w *Poly(lactic acid): Synthesis, structures, properties, processing, and applications*, w: R.A. Auras, L.-T. Lim, S.E.M. Selke, H. Tsuji (Eds.), RSC, 2011.

87. M. Baiardo, G. Frisoni, M. Scandola, M. Rimelen, D. Lips, K. Ruffieux, E. Wintermantel „Thermal and mechanical properties of plasticized poly(L-lactic acid)", *J. Appl. Polym. Sci.*, 90 (2003) 1731–1738.

88. S. Phattarateera, C. Pattamaprom "Comparative performance of functional rubbers on toughness and thermal property improvement of polylactic acid", *Materials Today Comm.*, 19 (2019) 374–382.

89. A.J. Svagan, A. Åkesson, S. Bulut, J.C. Knudsen, J. Risbo, D. Plackett „Transparent films based on PLA and montmorillonite with tunable oxygen barrier properties", *Biomacromolecules*, 13 (2012) 397–405.

90. A.M. Pinto, J. Cabral, D.A.P. Tanaka, A.M. Mendes, F.D. Magalh˜aes „Effect of incorporation of graphene oxide and graphene nanoplatelets on mechanical and gas permeability properties of poly(lactic acid) films", *Polym. Int.*, 62 (2013) 33–40.

91. S. Domenek, S. Fernandes-Nassar, V. Ducruet "Rheology, mechanical properties, and barrier properties of poly(lactic acid)", *Adv. Polym. Sci.*, (2017) 303–341.

92. A. Guinault, C. Sollogoub, V. Ducruet, S. Domenek „Impact of crystallinity of poly(lactide) on helium and oxygen barrier properties", *Eur. Polym. J.*, 48 (2012) 779–788.

IX. PUBLIKACJE I OŚWIADCZENIA WSPÓŁAUTORÓW
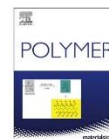
Crystallization, structure and properties of polylactide/ladder poly (silsesquioxane) blends

Agata S. Herc [a], Joanna Bojda [a], Maria Nowacka [a], Piotr Lewiński [a], Waldemar Maniukiewicz [b], Ewa Piorkowska [a,*], Anna Kowalewska [a,**]

[a] Centre of Molecular and Macromolecular Studies, Polish Academy of Sciences, Sienkiewicza 112, 90-363, Lodz, Poland
[b] Institute of General and Ecological Chemistry, Lodz University of Technology, Żeromskiego 116, 90-924, Lodz, Poland

ABSTRACT

Oligomeric ladder silsesquioxanes (LPSQ-R) with side substituents (R = COOH, COOMe, OH) capable of acceptor/donor interactions through hydrogen bonds were used for the preparation of blends with polylactide (PLA). Depending on the strength of their interactions with the PLA, LPSQ-R were differently dispersed in the polyester matrix. The blends exhibited different properties and crystallization behaviour depending on the type and content of LPSQ-R. PLA/LPSQ-COOMe exhibited good transparency. Owing to very good dispersion of the modifier, PLA with 5 wt% of LPSQ-COOMe was ductile, which was reflected in nearly 230% elongation at break, retaining however relatively high yield strength of nearly 40 MPa. Moreover, the spherulite growth rate was accelerated in PLA/LPSQ-COOMe, which caused enhancement of the cold-crystallization. In turn, cold-crystallization of PLA/LPSQ-OH was enhanced by strong nucleation.

1. Introduction

Polymers obtained from renewable natural sources are of high demand, especially in the light of regulations and restrictions regarding the limited use of petrol derived polymers. Polylactide/poly(lactic acid) (PLA) and its composites or blends with improved properties are one of the most promising biodegradable materials [1,2].

The applications of neat PLA may be limited by its stiffness (modulus of elasticity around 3–3.5 GPa) and brittleness, as well as rather poor crystallization rate. In order to improve the properties of PLAs, including mechanical performance and crystallizability, various modification routes are applied, including copolymerization, chain extension, plasticization, blending with other polymers, fillers, nanofillers, fibers, and nucleating agents [2–10]. Efficient plasticization of PLA requires a decrease of T_g to at least 35 °C [11]. It increases PLA ductility, although simultaneously strongly decreases its yield stress and elastic modulus. Moreover, a drawback of plasticized PLAs is its ageing having an adverse effect on the physical properties. It is connected with migration of a plasticizer, phase separation, crystallization of both, plasticizer and PLA [12–15]. Immiscible PLA blends with other polymers also exhibit improved ductility, whereas their elastic modulus and yield strength exceed those of the plasticized PLA [2,3,6]. The decrease of T_g of the PLA matrix is usually insignificant but the presence of the dispersed phase results in loss of transparency. Moreover, to enhance the ductility and impact resistance, compatibilization is often required.

Crystallinity of PLA decreases its ductility and slows down biodegradation. However, it can improve barrier properties, broadens a temperature range of applicability and stabilizes shapes of products during processing. Depending on crystallization temperature PLA chains crystallize from melt in the α or α' orthorhombic form with a characteristic 10_3 helical chain conformation [16,17]. Crystallization of PLA is affected both by its chemical structure, especially enantiomeric composition, and molecular mass. The process in neat PLA is slow, especially if the share of units of different chirality is large enough to disturb a proper sequence ordering along the chain axis.

Crystallization of PLA can be promoted by shear [18,19] or addition of nucleating agents including talc, N,N'-ethylenebis(12-hydroxystearamide), derivatives of 1,3,5-benzene tricaboxyamide, and orotic acid among others [16]. It was also demonstrated that poly(L-lactide)/poly (D-lactide) stereocomplex nanocrystals can serve as efficient nucleation sites for PLA [20,21]. The nucleation rate of poly(L-lactide) (PLLA) shows a maximum at around 100 °C; it slows down at lower

* Corresponding author.
** Corresponding author.
E-mail addresses: cpiorkowska@cbmm.lodz.pl, epiorkow@cbmm.lodz.pl (E. Piorkowska), anko@cbmm.lodz.pl (A. Kowalewska).

temperatures due to hindrance of segment mobility and at higher temperatures due to the increased size of critical nuclei of crystallization [22]. Slowly crystallizing PLAs can be cooled to the glassy state and crystallized during subsequent heating via "cold crystallization". However, even if crystallization is not clearly detectable, primary crystallization nuclei can form during cooling and subsequent annealing in the glassy state, and their number depends on the cooling rate and the temperature and time of annealing. The thus-formed nuclei can enhance cold crystallization on subsequent heating [22]. An increase of the number of nucleation sites accelerates crystallization and reduces sizes of polycrystalline aggregates, which is advantageous for the polymer properties. Plasticization also enhances the crystallization of PLA by increasing chain mobility and facilitating chain transport to the existing crystals. As a consequence, spherulite growth is accelerated in isothermal conditions, and cold crystallization peak is sharpened and shifted to lower temperature [16].

The cold crystallization is very important, for example for the rapidly developing technique of fused deposition modelling (FDM) in 3D printing with PLA thermoplastics [23,24]. Thermal annealing may even out the mechanical stress in 3D printed parts and increase their strength due to the formation of small crystallites in the course of cold crystallization. Shifting cold crystallization of PLA towards lower temperatures can be beneficial for both the printed objects and the reduction of energy. The choice of additives modifying the properties of biodegradable polymers used for 3D printing of objects designed for the use in regenerative medicine is a very important problem. They should not only exhibit nucleation activity, be well miscible/dispersible with the polymer, thermally resistant and non-toxic but also biocompatible.

Among others, silicon compounds and minerals have been used to modify PLA. A number of publications concern modification of PLA with polyhedral oligomeric silsesquioxanes (POSS) and their derivatives [25–31]. Usually, POSS molecules dispersed in PLA formed solid aggregates with sizes dependent on POSS functionalization and content. A decrease of T_g by up to a few degrees was observed [26,28,29]. POSS exhibited nucleation activity that enhanced crystallization of PLA [25–27,29]. The presence of aminopropylheptaisobutyl- and aminopropylheptaisooctyl-POSS in PLA increased the Young's modulus and the yield stress, while decreasing the elongation at break [26]. An increase of the storage modulus was reported for PLA with octaisobutyl POSS [27]. On the contrary, the addition of aminopropylisobutyl-,

glycidylisobutyl-, trisilanolisobutyl-, and octaisobutyl-POSS to PLA resulted in a decrease of the elastic modulus and the yield strength, while the impact strength and the elongation at break increased, although the latter did not exceed 20% [28]. Interestingly, composites with octa(3-chloropropylsilsesquioxane) exhibited a decrease of the yield stress and an increase of the elongation at break, to about 16 MPa and 90%, respectively, at 15 wt% POSS content [29]. In turn, POSS grafted with poly(ethylene glycol) arms acted as an efficient plasticizer for PLA, both amorphous and semicrystalline [5,30,31]. Recently, enhancement of cold-crystallization was reported for PLA modified with functionalized cyclotetrasiloxanes [32]. Shi et al. [33] reported that in PLA/trisilanolheptaphenyl POSS nanocomposites cold-crystallization was enhanced due to nucleating activity of POSS, whereas overall crystallization rate in the melt crystallization decreased because of hydrogen bonding that impeded mobility and folding of PLA macromolecules.

In the study PLA was modified by blending with oligomeric linear ladder-like polysilsesquioxanes (LPSQ) bearing side groups capable of hydrogen bonding (Scheme 1). The alignment of side substituents in LPSQ-R makes them similar, even at very low concentrations, to the organic nucleating agents that form crystals *in situ* on cooling the PLA matrix [34–39]. LPSQ-R are well defined macromolecules of a double chain siloxane backbone, which makes them more rigid than typical polysiloxanes and limits their coiling in solutions. The specific structure of LPSQ backbone can impose linear organization of the side groups in a quasi-rod system. Their solubility is governed by the type of side groups [40,41]. We have previously shown that LPSQ-R can adsorb on reactive surfaces and form superhydrophilic self-assembling layers (PSAMs type), well organized due to the specific hydrogen bonding of macromolecules [42,43]. The LPSQ-R described in this report are viscous amorphous substances of good thermal stability, well soluble in organic solvents. They can be solution- or melt-blended with PLA. Despite the interesting properties of LPSQ-R and possibility of their various functionalization, the opportunity to use them as modifiers of PLA properties and crystallization behaviour has not been explored so far. Only Herc et al. [44] recently demonstrated that LPSQ-R (R = side substituents containing COOH, COOMe and OH groups) enhanced thermal stability of PLLA/poly(D-lactide) blends. The formation of hydrogen bonds between LPSQ-R and carbonyl groups of PLA was also evidenced. In the present study we have analysed the effect of those LPSQ-R on properties
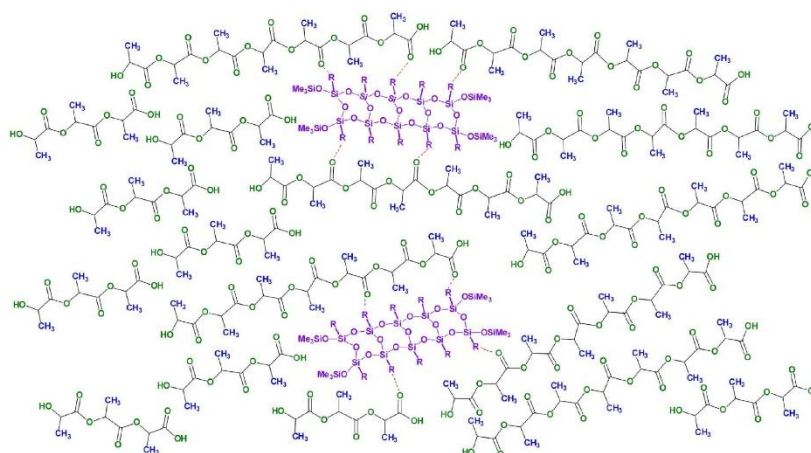
Scheme 1. Supramolecular interactions of PLA with LPSQ-R.

and crystallization of commercially available PLA as well as PLLA.

2. Experimental

2.1. Materials

Oligomeric linear polysilsesquioxanes LPSQ-R of ladder-like, double-strand backbone terminated with trimethylsilyl groups were prepared by photoinitiated thiol-ene addition of selected mercapto-compounds (Scheme 2), analogously to earlier published procedures [32,42]. Thioglycolic acid, methyl thioglycolate, 2-mercaptoethanol and thioglycerol were grafted to linear poly(vinylsilsesquioxane) precursors (LPSQ-Vi, M_n = 1 kg mol^{-1}, M_w/M_n = 1.4 [45]) in the presence of 2, 2-dimethoxy-2-phenylacetophenone (DMPA) as a photoinitiator, giving respectively LPSQ-COOH, LPSQ-COOMe and LPSQ-OH. The detailed synthetic procedure and products characterization can be found in ESI. Commercially available reagents: thioglycolic acid (Sigma-Aldrich, 98%), methyl thioglycolate (Acros Organics, 95%), 2-mercaptoethanol (Sigma-Aldrich, 99%), 1-thioglycerol (Sigma-Aldrich, 99%) and 2, 2-dimethoxy-2-phenylacetophenone (DMPA, Acros Organics, 99%) were used as received. Solvents were purified following literature procedures [46].

Polylactides used in the studies were PLLA (weight average molar mass M_w = 194.6 kg mol^{-1}, dispersity M_w/M_n = 1.9, prepared as described in ESI) and a commercially available PLA (NW4032D grade from NatureWorks LLC, Minnetonka, USA; M_w = 130 kg mol^{-1}, M_w/M_n = 1.9) containing 1.2 mol% of D-lactide units. PLLA was additionally stabilized with additives: 0.2 wt% of Irganox 1010 [pentaerythriol tetrakis (3-(3,5-di-tert-butyl-4-hydroxyphenyl)propionate)] (Sigma-Aldrich) and 0.2 wt% of Irganox 1024 [2′,3-bis[[3-[3,5-di-tert-butyl-4-hydroxyphenyl]propionyl]]propionohydrazide] (BASF).

Compositions of PLA NW4032D with 0.25, 0.5, 1, 2 and 5 wt% of LPSQ-R were prepared. In addition, PLLA was mixed with 2 wt% of LPSQ-R. In general, the polymer was dissolved in CH$_2$Cl$_2$, to obtain 10 wt% solution. After 24 h a specifiied volume of LPSQ-R 10 wt% solution in THF was added dropwise. The mixtures containing smaller amounts of LPSQ-R than 5 wt%, were admixed with pure THF, in order to have the same concentration of THF in all compositions. The mixtures were stirred magnetically for 0.5 h at room temperature (RT). The mixtures containing LPSQ-COOH and LPSQ-OH became cloudy in a short time (less than 1 min) after the addition of the polysilsesquioxanes, and remained turbid on prolonged stirring. The effect was not observed for LPSQ-COOMe. No increase of viscosity of the mixtures was observed. The prepared compositions were then poured into Petri dishes and left for free solvent evaporation. Solid products were carefully dried for 24 h at 80 °C under high vacuum (0.01 Torr) and analysed with

Scheme 2. Synthesis of functionalized LPSQ.

thermogravimetry (TGA). For further studies, 0.5 mm and 1 mm thick films were compression moulded at 190 °C and rapidly quenched at 0 °C. All films were amorphous, which was evidenced by differential scanning calorimetry.

The PLA blends are referred to through this paper as, for example P/5-R nad PL/5-R, where the number stands for the LPSQ-R weight content, P and PL denote PLA and PLLA, respectively.

2.2. Analytic methods

LPSQ-R were characterized with liquid state ^{1}H, ^{13}C and ^{29}Si NMR spectroscopy (Table ESI-1). The spectra were recorded on a Bruker DRX-500 MHz spectrometer using THF-d8 or CD$_3$OD as deuterated solvents.

M_w of PLLA and PLA were determined by size-exclusion chromatography (SEC) with a multi-angle laser light scattering (MALLS) detector in CH$_2$Cl$_2$.

Thermogravimetric analysis (TGA) of the blends was carried out at a rate of 10 °C/min in nitrogen atmosphere and in air using a Hi-Res TGA 2950 Thermogravimetric Analyzer (TA Instruments, New Castle, USA).

To have an insight into their internal structure, the amorphous films of neat and modified PLA were cryo-fractured, then sputtered with gold using a Jeol Fine Coater 1200 (Tokyo, Japan) and analysed with scanning electron microscopy (SEM) using SEM Jeol 5500LV operating in the high vacuum mode at 10 kV. The distribution of silicon atoms of LPSQ-R in the studied samples was examined with SEM equipped with energy dispersive spectroscopy (SEM-EDS, Jeol JSM-6010LA) operating in the high vacuum mode at an accelerating voltage 8 kV. The surfaces were sputtered with carbon using a coater Q150R ES (Quorum Technologies).

Dynamic mechanical thermal analysis (DMTA) was carried out on 1 mm thick rectangular specimens, 17.5 mm × 12 mm, in single cantilever bending mode, using a DMTA TA Q-800 Thermal Analyser (TA Instruments, New Castle, USA) at a frequency of 1 Hz and a heating rate of 2 °C/min from −70 to 140 °C, under a fixed deformation of 0.5%.

Direct light transmittance (DLT) through 0.5 mm thick films of neat and modified PLA was measured using a UV–VIS SPECORD S 600 diode array spectrophotometer (Analytik Jena AG) at RT in the wavelength (λ) range from 200 to 1000 nm, with a resolution of 0.5 nm and using air as a reference. Data were averaged for 3 runs for each film.

Tensile properties were measured using Linkam Tensile Stress Testing System TST 350 (Linkam, UK). At last five 0.5 mm thick oar-shaped specimens, with 3.81 mm gauge length, and width of 1.59 mm were drawn to fracture at a rate of 5%/min, at 25 °C. The average values of mechanical parameters were calculated.

Thermal properties and crystallization of the materials were analysed with a differential scanning calorimetry (DSC) using DSC Q20 (TA Instruments). Thermal characteristics of LPSQ-R were obtained during heating from RT to 100 °C and cooling down to −100 °C, followed by heating to 100 °C at 10 °C/min. PLA/LPSQ-R were heated to 190 °C, held at this temperature for 3 min, cooled at 10 °C/min to RT and heated again at 10 °C/min. To study isothermal crystallization, the specimens were heated to 190 °C, kept at this tempeearature for 3 min and cooled at 30 °C/min to selected temperatures, crystallized isothermally and then cooled to RT at 30 °C/min. Melting of these specimens was analysed during heating at 10 °C/min. In addition, the spherulite growth was measured in 10 μm thick films prepared by compression molding at 190 °C and crystallized isothermally. The crystallization of the films was carried out using a Linkam CSS450 hot stage and observed by polarized light microscopy (PLM). In each case the increase of spherulite radius in time was measured for at least three spherulites in each case, and an average value of the growth rate was calculated. Additionally, the selected films were cooled to RT and cold crystallized during heating to 130 °C at 10 °C/min and holding at this temperature until completion of crystallization.

Wide-angle X-ray diffraction data were collected using a PANalytical X'Pert Pro diffractometer equipped with an Anton Paar XRK900 reactor

3
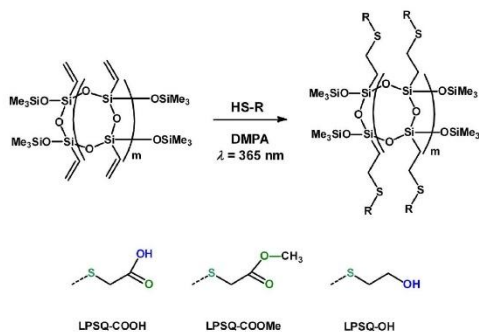
chamber. The electrical heater of the reactor chamber is designed to heat the sample with a minimum temperature gradient. The X-ray source was a copper long fine focus X-ray diffraction tube operating at 40 kV and 30 mA. Amorphous samples (~150 mg) were packed in the glass ceramics (Macor) sample holder and heated at 10 °C/min. Samples were scanned from 5° to 40° 2θ with step of 0.0167° and exposition per one step of 100 s. Diffractograms were collected every 10 °C starting from 70 °C and ending at 140 °C. A curved graphite monochromator on the receiving side was used to eliminate CuK$_\beta$ radiation. A PANalytical X'Celerator detector based on Real Time Multiple Strip technology capable of simultaneously measuring the intensities in the 2θ range of 2.122° was used.

3. Results and discussion

3.1. Synthesis and properties of LPSQ-R

Linear polysilsesquioxanes with heterorganic groups being either donors or acceptors of hydrogen bonds were prepared by grafting appropriate mercapto-compounds onto the backbone of poly(vinyl-silsesquioxanes) of ladder structure through thiol-ene addition (Scheme 2). All the obtained LPSQ-R were viscous substances that vitrified but did not crystallize on cooling and devitrified on heating. T$_g$ of LPSQ-OH and LPSQ-COOMe, determined during heating at 10 °C/min was at −47 °C and −41 °C, respectively, as shown in Fig. ESI-1. The higher T$_g$ observed for LPSQ-COOH, at −14 °C, can be linked to the more extensive hydrogen bonding between their side functional groups. The

structure of the double siloxane backbone strongly affects the LPSQ properties and their thermal stability. Contrary to linear poly(siloxanes), LPSQ-R do not suffer from thermal depolymerization at temperatures < 200 °C. TGA analysis (both in nitrogen atmosphere and in air, Fig. ESI-2) showed that they are thermally stable at 200 °C, which allows for their use in melt blending.

3.2. Phase structure of PLA/LPSQ-R

Fig. 1 compares exemplary SEM micrographs of PLA modified with LPSQ-R. The micrographs evidence the phase separated structure, although dependent on the LPSQ-R type and content. On the micro-graphs of cryo-fractured P/2-OH small submicron inclusions are visible accompanied by occasionally seen larger ones, with a diameter of up to 6 μm. At 5 wt% content of LPSQ-OH the maximum inclusion size increased to about 10 μm. However, those few large particles are accompanied by numerous much smaller ones of micron- or submicron-sizes. The dispersion of additive was different in PLA/LPSQ-COOH blends, where at 2 and 5 wt% of LPSQ-COOH content particles with sizes up to several micrometers were visible. However, the best disper-sion was achieved in PLA/LPSQ-COOMe, in which only submicron in-clusions are seen, very few in P/2-COOMe and numerous in P/5-COOMe.

Silicon mapping with SEM-EDS evidenced partial miscibility of LPSQ-R with PLA and phase separation. The images of PLA/LPSQ-OH and PLA/LPSQ-COOH, in Fig. 2a and b show inclusions dispersed in matrices. The silicon containing compounds are concentrated in the
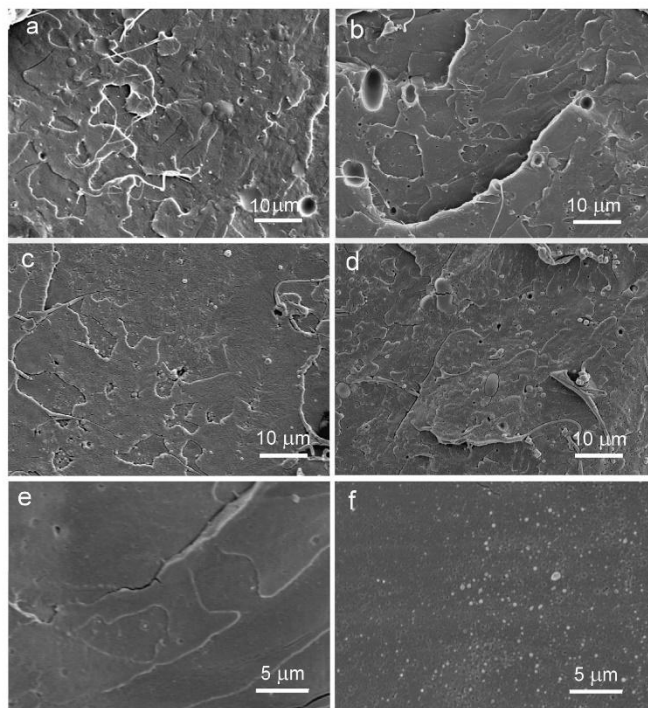

Fig. 1. SEM micrographs of P/2-OH (a), P/5-OH (b), P/2-COOH (c), P/5-COOH (d), P/2-COOMe (e), P/5-COOMe (f).
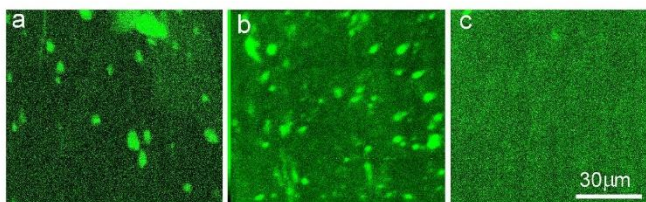
Fig. 2. Silicon mapping of PLA/LPSQ-R blends: P/5-OH (a), P/5-COOH (b), P/5-COOMe (c).

inclusions but are also dispersed in PLA-rich matrix. In LPSQ-COOMe the inclusions are not seen in Fig. 2c because of their too small submicron size.

Figs. 3 and 4 show the loss modulus (E″) and storage modulus (E′) of the materials. E″ temperature dependence of PLA exhibits a single peak, corresponding to the glass transition, with a maximum at 63 °C. E″ temperature dependencies of 2 wt% blends are also featured by single peaks, at 57 °C for P/2-OH, and 56 °C for P/2-COOH and P/2-COOMe. The temperature of E″ peak did not change with an increase of LPSQ-OH content to 5 wt%. However, for P/5-COOH and P/5-COOMe it decreased to 55 °C and also additional, low and broad peaks appeared on the E″ plots, with maxima at −7 and −11 °C, respectively. A trace of broad peak with a maximum at −37 °C was also observed for P/5-OH.

The decrease of the main peak temperature indicates plasticization of PLA by LPSQ-R, whereas the low temperature peaks evidence the phase separation in the blends. Judging from the temperatures of these peaks in comparison to T_gs of the respective LPSQ-R, the peaks reflect glass transition not in pure LPSQ-R but in LPSQ-R rich phases. This especially applies to P/5-COOMe. The results corroborate SEM and SEM-EDS observations. In the blends with 2 wt% content of LPSQ-R the phase separated amount of LPSQ-R was obviously too small to be reflected in low temperature E″ peaks.

Similarly to E′ of PLA, E′ of the blends decreases with increasing temperature and sharply drops in the glass transition region. However, E′ of the 2 wt% blends is below that of PLA and further decreases with increasing LPSQ-R content. At 25 °C E′ is equal to 3.4 GPa and 2.9–3.1 GPa, for neat PLA and 2 wt% blends, respectively, whereas 2.6 GPa for
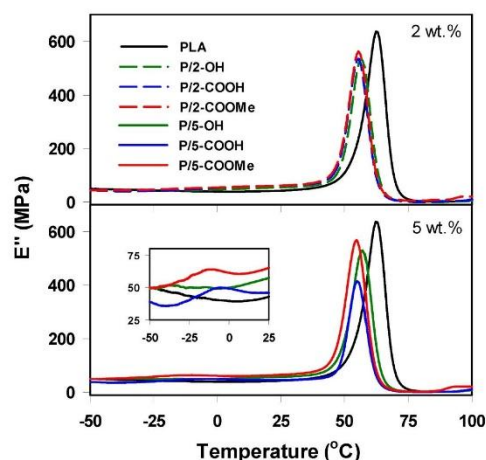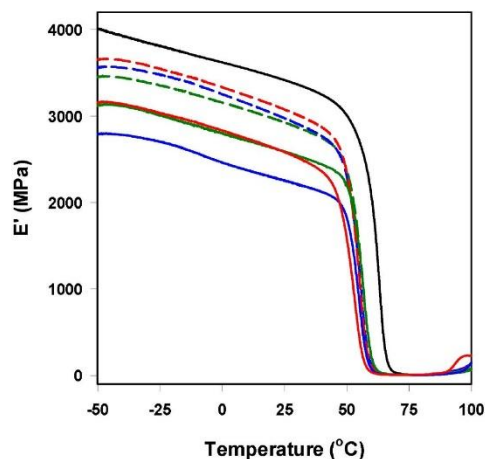

Fig. 4. Storage modulus (E′) of PLA and PLA/LPSQ-R blends vs. temperature. Meaning of lines as in Fig. 3.

P/5-OH and P/5-COOMe, and 2.3 for P/5-COOH. The sharp drop of E′ of the blends occurs at lower temperature than that of neat PLA, which indicates a decrease of T_g due to plasticization of PLA with LPSQ-R. The decrease of E′ is also suggestive of plasticization of PLA matrix, but can also result from the presence of phase separated modifier-rich inclusions with low T_g.

The dispersion of LPSQ-R in PLA may be explained by the specific structure of LPSQ-R and the presence of hydrogen bond donating groups at each silicon atom in the double-strand chains. There are several factors that should be taken into account: the nature of side substituents, their congestion along the polymer chains and the type of solvents used for the preparation of PLA/LPSQ-R blends. In the compositions containing polar groups –COOH and –OH the interactions between the side groups compete with hydrogen bonds to the polyester backbone. Solvation of LPSQ-COOH and LPSQ-OH by THF molecules allows for their complete dissolution, but they seem to agglomerate on solvent evaporation from the mixture. The effect was observed regardless of the amount of LPSQ-R (Fig. ESI-3″). Macromolecules of LPSQ-COOMe were very well dispersed and their compositions with PLA were fairly clear. We have previously shown for compositions of PLA and cyclotetrasiloxanes having the same functional groups that species bearing R = OH and COOMe were evenly distributed in the studied samples [32]. On the contrary, dispersion of the organosilicon additives in blends of PLA with 1,3,5,7-[2-(carboxymethylthio)ethyl]-1,3,5,7-tetramethylcyclotetra-siloxanes was not uniform. It was attributed to a preferential

Fig. 3. Loss modulus (E″) of PLA and PLA/LPSQ-R blends vs. temperature.

5

formation of dimeric structures linking two –COOH moieties.

3.3. Optical and mechanical properties

The composition and phase structure of the blends is reflected in their optical properties, as shown in Fig. 5.

DLT of the PLA/LPSQ-R, shown in Fig. 5, corroborates the SEM results. Except for P/2-COOMe, the transmittance of the blends is below that of neat PLA. The decrease of the transmittance is caused by scattering on LPSQ-R rich inclusions dispersed in PLA rich matrix and can be correlated with the content and dispersion of LPSQ-R. Small amount of phase separated LPSQ-COOMe in P/2-COOMe resulted in high DLT, nearly the same as for neat PLA. DLT of P/5-COOMe was slightly worse due stronger to scattering on the inclusions. A decrease of DLT of these two materials in the wavelength range of 250–340 nm (UV–B region of light, linked with photochemical degradation of materials) can be explained as related to absorption caused by carbonyl groups [32]. The specific features of PLA/LPSQ-COOMe (transparency, absorption of UV-B) can be valuable in packaging applications. For other PLA/LPSQ-R the optical clarity was poorer and depended on the type of functional groups and the concentration of the additive (Fig. ESI-4).

Fig. 6 presents exemplary engineering stress-engineering strain relationships of PLA and PLA/LPSQ-R materials. Neat PLA exhibited yield stress (σ_y) of 44 MPa, stress (σ_b) and strain (ε_b) at break of 41 MPa and 29%, respectively. The properties of blends with 2 wt% of LPSQ-R were not improved in comparison to those of neat PLA; σ_y of 36–40 MPa, σ_b of 33–38 MPa, and ε_b of 26–28%. The increase of content of LPSQ-OH and LPSQ-COOH did not result in a significant change of the tensile behaviour. σ_y remained at the similar level of 36–38 MPa and only a small increase in ε_b was observed, to 35–37%, which was accompanied by a decrease of σ_b to 33–34 MPa. However, a strong improvement of drawability was achieved for P/5-COOMe, without a significant reduction of σ_y, which remained relatively high, 39 MPa. Beyond the yield strain the stress strongly decreased, and a large ε_b of 230% was reached, at σ_b of 22 MPaa

During drawing of P/5-COOMe the formation of neck was observed. Although PLM examination of the deformed specimen evidenced the presence of distorted and diffused crazes perpendicular to the drawing
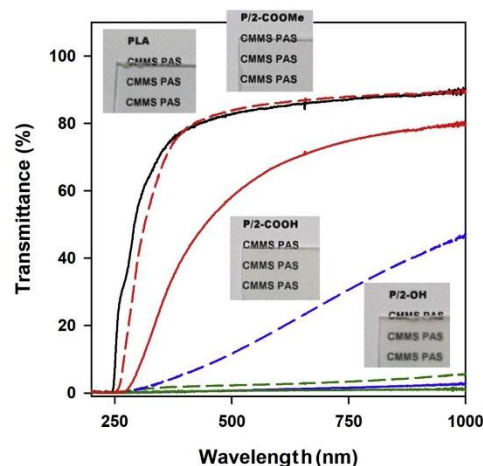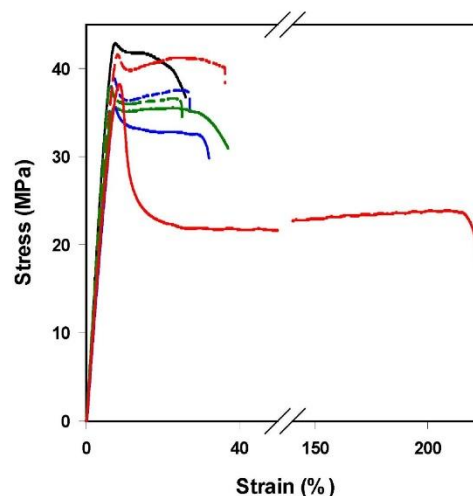

Fig. 6. Engineering stress vs. engineering strain dependencies of PLA and PLA/LPSQ-R blends. Meaning of lines as in Fig.3.

direction in the neck region (Fig. ESI-5), the occurrence of necking allows to conclude that shear yielding was responsible for the onset of the plastic deformation. Crazes were also visible in the region adjacent to the neck evidencing that crazing occurred before the necking. It should be added that no visible worsening of transparency and no whitening of the neck were observed.

Toughening of PLA can be achieved by plasticization or by taking advantage of "rubber toughening" mechanism, which is active in phase separated blends [2,47]. The plasticization of PLA, although undoubtedly facilitated the plastic deformation, cannot be solely responsible for the improved drawability of P/5-COOMe since ε_b of P/2-COOMe was much worse despite nearly the same T_g. Moreover, a decrease of T_g to about 35 °C is required to improve the drawability of plasticized PLA [11]. This indicates the important role of LPSQ-COOMe rich inclusions dispersed in PLA-rich matrix, which obviously promoted shear yielding and further deformation, similarly as observed in other systems [e.g. 6]. The improved drawability of P/5-COOMe in comparison to the other PLA blends results from very good dispersion of LPSQ-COOMe in PLA as the presence of too large inclusions in the rubber toughened blends can cause premature fracture. Undoubtedly, the presence of submicron inclusions rich in LPSQ-COOMe facilitated plastic deformation of the PLA rich matrix, thus improving the drawability of the blend without a significant decrease of the yield strength. It is thus concluded that both molecularly dispersed fraction of the modifier, plasticizing the continuous phase, and its phase separated fraction forming fine inclusions contributed to the enhanced ability to the plastic deformation of the partially miscible and phase separated blend, which was reflected in the improved drawability and the tensile toughness, similarly as observed and discussed e.g. in Refs. [30,48].

3.4. Thermal properties and crystallization

From a point of view of melt processing an important feature of the modified PLA is its thermal stability. TGA experiments in nitrogen atmosphere demonstrated that LPSQ-R did not deteriorate the stability of the 2 and 5 wt% blends. DTGA thermograms were featured by single peaks (shown in Fig. ESI-6), with peak temperature of 354 °C for PLA

Fig. 5. Direct light transmittance of PLA and PLA/LPSQ-R vs. wavelength. Meaning of lines as in Fig. 3. Insets illustrate transparency of 0.5 mm thick films to visible light.

and 350–366 °C for the blends. Temperature of 5 wt% weight loss of the blends was in the range of 302–322 °C, exceeding that of PLA, 295 °C, with the only exception of P/5-COOH, for which this temperature was 257 °C (Table ESI-2). Nevertheless, even in the last case the thermal stability is sufficient for melt processing.

DSC thermograms of PLA and PLA/LPSQ-R, recorded during the second heating, are shown in Fig. 7. During cooling at 10 °C/min the materials did not crystallize. The heating thermograms exhibited glass transition, cold-crystallization exotherms and melting endotherms. T_g of neat PLA was at 60 °C. T_g of PLA/LPSQ-R was at 59–60 °C and 57–59 °C for 2 and 5 wt% blends, respectively. In each case the cold crystallization enthalpy (ΔH_{cc}) was equal to the melting enthalpy (ΔH_m) evidencing that the materials were amorphous before the heating. The cold-crystallization of neat PLA was weak, with ΔH_{cc} of 9 J/g and peak rate temperature (T_{cc}) of 135 °C. Crystallization of PLA/LPSQ-R was stronger, especially that of PLA with LPSQ-OH and LPSQ-COOMe. The decrease of T_{cc} corresponded with ΔH_{cc} increase. P/2-OH and P/2-COOMe exhibited T_{cc} of 116 and 130 °C, and ΔH_{cc} of 34 and 27 J/g, respectively, whereas P/5-OH and P/5-COOMe 112 and 109 °C, and 33 and 34 J/g, respectively. Similar tendency was observed for PLLA blends with LPSQ-R as shown in ESI (Fig. ESI-7). The melting of the cold-crystallized materials reflected their crystallization temperature ranges. PLA's melting peak was centered at T_m of 166 °C. The thermograms of blends, whose T_{cc} was above 120 °C, were also featured by single melting peaks with the same T_m, whereas the blends crystallized at lower temperature exhibited double-peak melting behaviour with T_ms at 162–164 °C and 169 °C. Such melting of PLA is attributed to the melting-recrystallization behaviour [49].

To have a more detailed insight into crystallization of the blends, their isothermal crystallization was studied. Exemplary DSC thermograms recorded during crystallization at 120 °C are shown in Fig. ESI-8. The crystallization half-time is plotted against crystallization temperature (T_c) in Fig. 8. It appears that the crystallization half-times of PLA/LPSQ-COOH were similar to that of PLA. Crystallization of two other
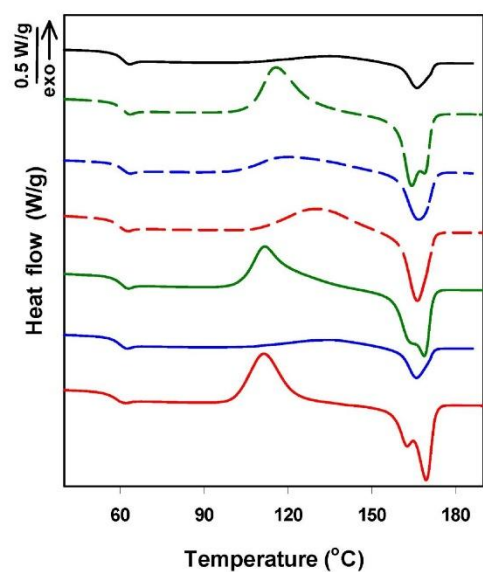
blends was longer in T_c range of 100–120 °C. It must be mentioned that the half-time values at 90 °C are only approximate; as can be judged from the respective thermograms, the crystallization started before the temperature was stabilized.

The slowing down of the overall crystallization rate can result from a decrease of the crystal growth rate or/and of the nucleation density. The crystallization of all the materials was spherulitic. Fig. 9 shows exemplary PLM micrographs of spherulites in the materials at T_c of 125 °C and 145 °C. The presence of inclusions trapped inside the spherulites and also in the melt outside of the spherulites evidences that crystallization occurred in the phase separated blends. The inclusions, presumably liquid, are well visible in P/5-OH and P/5-COOH. The fine droplets in P/5-COOMe are shown in Fig. 10.

It is worth mentioning that the plots of spherulite radii against time were linear in each case, evidencing a constant growth rate. The results of the growth rate measurements are plotted in Fig. 11. It appears that the growth rate was significantly accelerated only in P/2-COOMe and P/5-COOMe in 115–130 °C and 115–140 °C, respectively. In the other blends it was the same or nearly the same as in PLA. Most possibly, the increase of the growth rate was related to increase of the segment mobility of PLA in PLA/LPSQ-COOMe in the high temperature range. We hypothesize that very good dispersion of LPSQ-COOMe rich inclusions in the blend, that increased the amount of interphase in which segments of PLA chain were more mobile, could contribute to this effect.

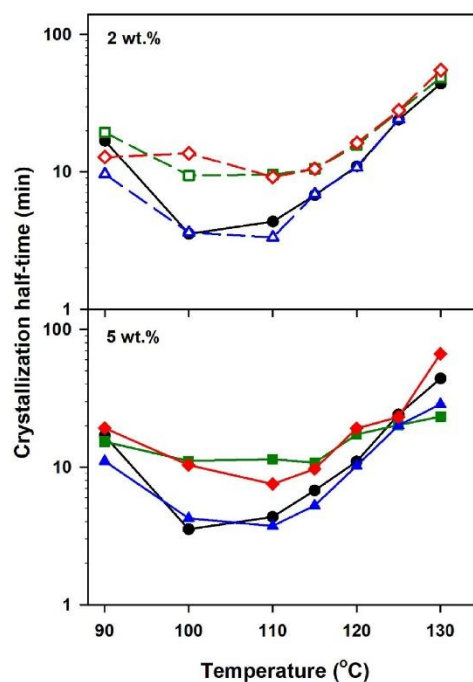Considering the faster or the same as in PLA crystal growth rate, the

Fig. 8. Crystallization half-times of PLA and PLA/LPSQ-R vs. crystallization temperature. Empty symbols - 2 wt% blends, full symbols - 5 wt% blends. Meaning of lines and colors as in Fig. 3. (For interpretation of the references to color in this figure legend, the reader is referred to the Web version of this article.)
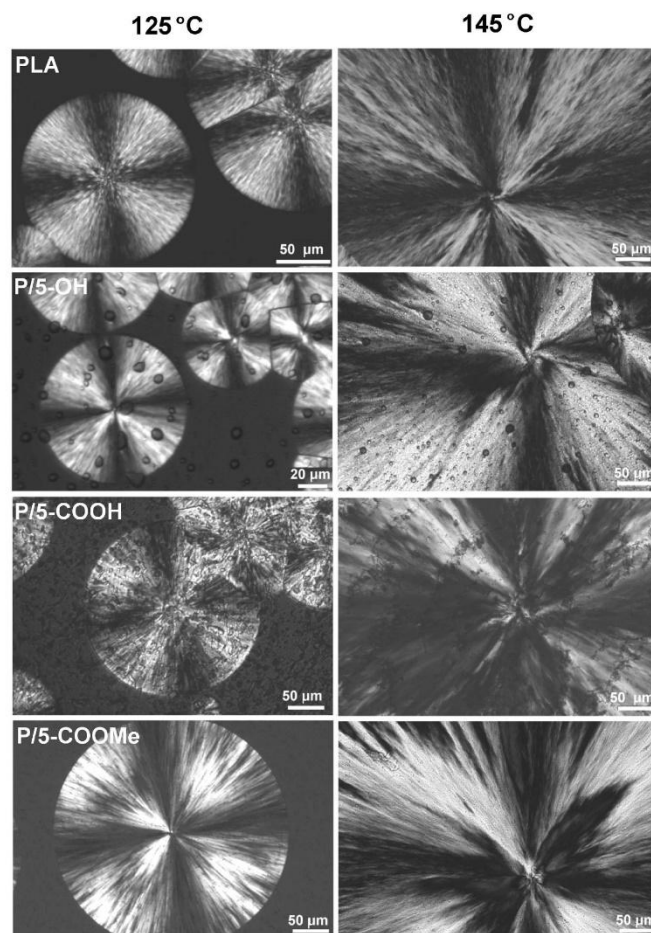

Fig. 7. DSC thermograms of PLA and PLA/LPSQ-R recorded during the second heating at 10 °C/min. Meaning of lines as in Fig. 3.

Fig. 9. PLM micrographs of spherulites at 125 °C and 145 °C.

slower overall crystallization, especially in PLA/LPSQ-COOMe can only result from the less intense nucleation. This is evidenced in PLM micrographs of thin films of PLA and P/5-COOMe crystallized at 120 °C, shown in Fig. 12. The increased macromolecular mobility might not be beneficial for the nucleation in the relatively high temperature range. Moreover, the nucleation at low and medium undercooling is usually heterogeneous and possibility of migration of nucleating impurities to the phase separated inclusions should be taken into account [50], which could be facilitated by good dispersion and larger content of LPSQ-R increasing the surface area of inclusions. The nucleation density was obviously decreased also in PLA/LPSQ-OH blends.

However, the cold-crystallization during heating was enhanced in both PLA/LPSQ-OH and PLA/LPSQ-COOMe blends. In PLA/LPSQ-COOMe it can result from the faster growth of crystals homogeneously nucleated in the low temperature range. However, in PLA/LPSQ-OH, which crystal growth rate was nearly the same as of neat PLA, the

enhancement of cold-crystallization can result only from intensification of the low temperature nucleation. Fig. 13 compares spherulitic structures of cold-crystallized thin films of PLA and P/5-OH; the films were cooled from 190 °C at 30 °C/min to RT then heated to 130 °C at 10 °C/min and held at this temperature until completion of crystallization. It is clearly seen that the nucleation in P/5-OH was much more intense than in PLA. Shi et al. [33] postulated that hydrogen bonds between carbonyl groups of PLA and hydroxyl groups of semicrystalline trisilanolheptaphenyl-POSS intensified POSS particles ability to nucleate cold crystallization. LPSQ-OH is an amorphous substance with low T_g at −47 °C, it is dispersed in PLA rich matrix and also forms LPSQ-OH rich inclusions. It can be thus postulated that in the temperature range, where nucleation rate decreases due to hindrance of segment mobility [22], interactions with LPSQ-OH, enhanced by the hydrogen bonds formed with PLA carbonyl groups, increase locally the segment mobility and intensify the nucleation. The same could also
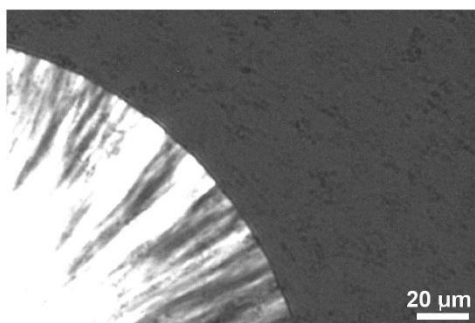
8

Fig. 10. Inclusions of LPSQ-COOMe rich phase in P/5-COOMe at 125 °C.

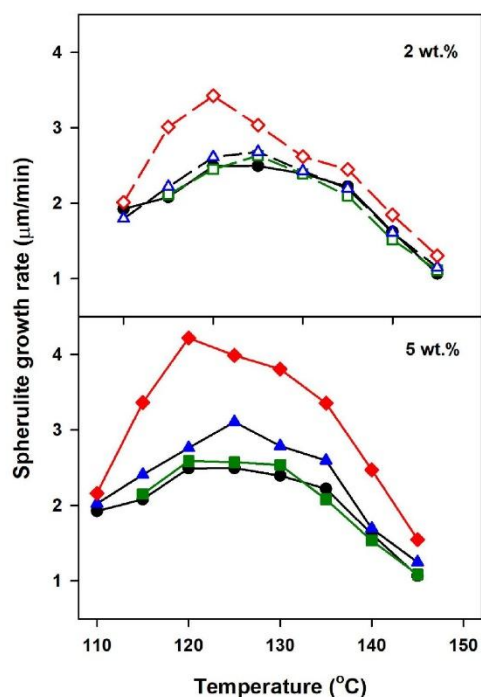**Fig. 11.** Spherulite growth rate in PLA and PLA/LPSQ-R vs. crystallization temperature. Meaning of lines and symbols as in Fig. 3 and Fig. 8.

Fig. 12. PLM micrographs of spherulitic structure in PLA and P/5-COOMe crystallized isothermally at 120 °C.

apply to PLA/LPSQ-COOMe blends.

Melting behaviour of the isothermally crystallized PLA/LPSQ-R was similar to that of PLA (Fig. ESI-9). T_m and ΔH_m of 5 wt% PLA/LPSQ-R blends are plotted in Fig. 15. The melting behaviour of 2 wt% blends was very similar, hence it is not discussed. The thermograms of the materials crystallized at 90 °C exhibited exothermic pre-melting peaks at about 150 °C followed by melting peaks with T_m at 164–166 °C. The
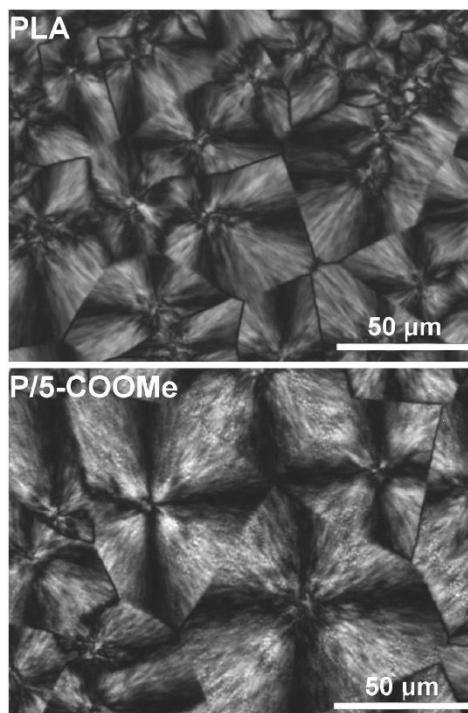
exothermic pre-melting effect is attributed to transition of the disordered α' to the ordered α form [49]. The melting endotherms of samples crystallized at 100 and 110 °C exhibited either two peaks or peaks with shoulders, at lower T_m of 157–158 °C and 161–162 °C, respectively, and at higher T_m of 167-167 °C, evidencing reorganization in the α phase. Higher T_c resulted in single melting peaks with T_m increasing with increasing T_c. ΔH_m of the materials also increased with increasing T_c as illustrated in Fig. 14.

WAXD examination of PLA and 2 wt% PLA/LPSQ-R blends after cold-crystallization at 90 °C for 30 min (Fig. 15) have features generally attributed to the disorder orthorhombic α' phase [49,51–53], which is primarily reflected in the absence or very weak (010) and (210) peaks characteristic of the order orthorhombic α phase. The strong (200)/(110) and (203) peaks are significantly more pronounced for the blends than for neat PLA, indicating more intense crystallization. With increasing temperature, the peak position of the observed reflections shifted to lower 2θ angles due to the thermal expansion of the lattice prior to the α'- α transition (Fig. ESI-10). Similar phenomenon was reported by Zhang et al. who studied changes of WAXD of PLLA samples crystallized at various temperatures [49]. A slight sharpening and intensity increase of some reflections during the thermal annealing of both PLA and PLA/LPSQ-R blends indicate a gradual perfecting of the α' form, although the degree of ordering is rather low and larger domains of the α phase were not formed during the experiment even at high temperatures.
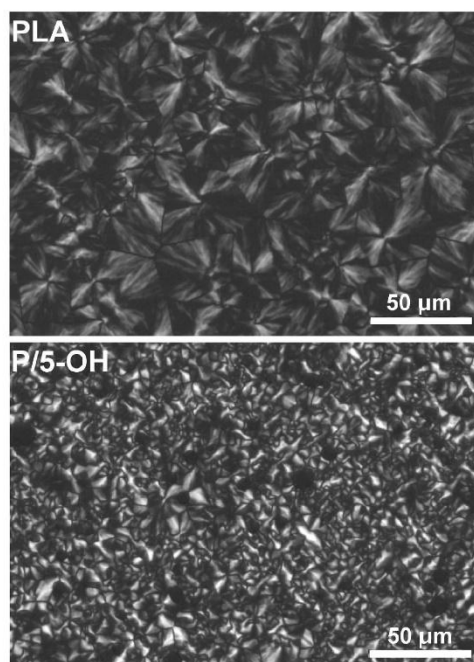
Fig. 13. PLM micrographs of thin films of PLA and P/5-OH heated from the glassy state to 130 °C at 10 °C/min and held at this temperature until completion of crystallization.

4. Conclusions

Addition of functionalized LPSQ-R to the PLA did not affect adversely its thermal stability. Depending on the strength of their interactions with the polyester backbone, LPSQ-R were differently dispersed in PLA matrix. Those interactions were governed by the R = side substituents containing COOH, COOMe and OH groups, and could be influenced by hydrogen bonds between R and carbonyl groups of PLA.

The blends exhibited different properties and crystallization behaviour depending on the type and content of LPSQ-R. The blends were partially miscible and phase separated. The best dispersion was achieved in PLA/LPSQ-COOMe, in which inclusions of LPSQ-COOMe rich phase were of submicron size. PLA/LPSQ-COOMe exhibited good transparency. Owing to very good dispersion of the modifier, PLA with 5 wt% of LPSQ-COOMe was ductile, which was reflected in nearly 230% elongation at break, retaining however relatively high yield strength of nearly 40 MPa.

The crystallization in all blends was spherulitic. The spherulite growth rate was accelerated in 115–130 °C and 115–140 °C in PLA/LPSQ-COOMe with 2 and 5 wt% of the modifier, respectively. The increase of the growth rate resulted most probably from enhanced mobility of PLA chains in the blends at high temperature. Faster growth rate caused enhancement of the cold-crystallization of PLA/LPSQ-COOMe. In turn, cold-crystallization in PLA/LPSQ-OH was intensified by strong nucleation in the low temperature range, which was possibly related to the hydrogen bonds formed by side groups of LPSQ-OH.
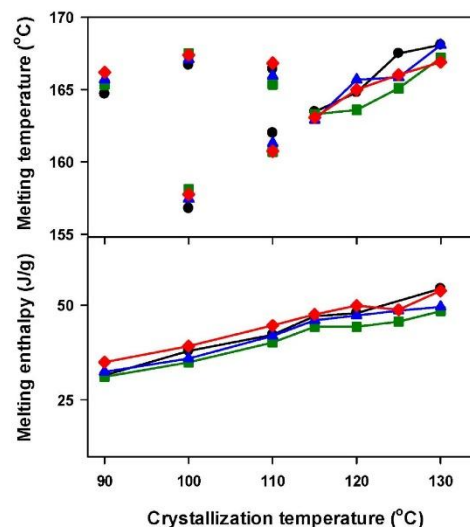

Fig. 14. Melting peak temperature and melting enthalpy of PLA and 5 wt% PLA/LPSQ-R blends vs. crystallization temperature. Meaning of lines and symbols as in Fig. 3 and Fig. 8. Exothermic pre-melting peak enthalpy was subtracted from the melting enthalpy of samples crystallized at 90 °C.
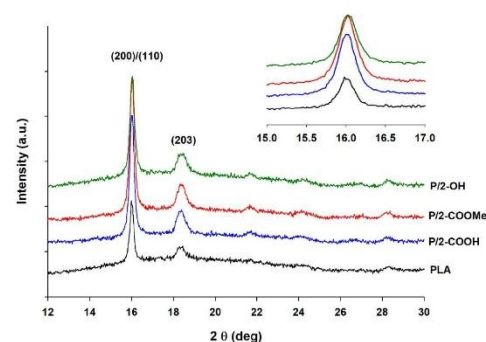

Fig. 15. WAXD curves recorded after 30 min of crystallization at 90 °C for PLA and PLA blends with 2 wt% of PLA/LPSQ-R.

Declaration of competing interest

The authors declare that they have no known competing financial interests or personal relationships that could have appeared to influence the work reported in this paper.

CRediT authorship contribution statement

Agata S. Herc: Investigation, Formal analysis. **Joanna Bojda:** Investigation, Formal analysis. **Maria Nowacka:** Investigation. **Piotr Lewiński:** Investigation. **Waldemar Maniukiewicz:** Investigation. **Ewa Piorkowska:** Conceptualization, Supervision, Writing - original draft.

10

Anna Kowalewska: Conceptualization, Supervision, Writing - original draft.

Appendix A. Supplementary data

Supplementary data to this article can be found online at https://doi.org/10.1016/j.polymer.2020.122563.

References

[1] K. Masutani, Y. Kimura, Present situation and future perspectives of poly(lactic acid), Adv. Polym. Sci. 279 (2018) 1–25, https://doi.org/10.1007/12_2016_16.
[2] H. Liu, J. Zhang, Research progress in toughening modification of poly(lactic acid), J. Polym. Sci., Part B: Polym. Phys. 49 (2011) 1051–1083, https://doi.org/10.1002/polb.22283.
[3] S. Domenek, S. Fernandes-Nassar, V. Ducruet, Rheology, mechanical properties, and barrier properties of poly(lactic acid), Adv. Polym. Sci. 279 (2018) 202–341, https://doi.org/10.1007/12_2016_17.
[4] E. Lezak, Z. Kulinski, R. Masirek, E. Piorkowska, M. Pracella, K. Gadzinowska, Mechanical and thermal properties of green polylactide composites with natural fillers, Macromol. Biosci. 8 (2008) 1190–1200, https://doi.org/10.1002/mabi.200800040.
[5] A. Zubrowska, E. Piorkowska, J. Bojda, Novel tough crystalline blends of polylactide with ethylene glycol derivative of POSS, J. Polym. Environ. 26 (2018) 145–151, https://doi.org/10.1007/s10924-016-0920-2.
[6] M. Kowalczyk, E. Piorkowska, S. Dutkiewicz, P. Sowinski, Toughening of polylactide by blending with a novel random aliphatic-aromatic copolyester, Eur. Polym. J. 59 (2014) 59–68, https://doi.org/10.1016/j.eurpolymj.2014.07.002.
[7] R. Siakeng, M. Jawaid, H. Ariffin, S.M. Sapuan, M. Asim, N. Saba, Natural fiber reinforced polylactic acid composites: a review, Polym. Compos. 40 (2019) 446–463, https://doi.org/10.1002/pc.24747.
[8] K. Piekarska, P. Sowinski, E. Piorkowska, M.M. Ul Haque, M. Pracella, Structure and properties of hybrid PLA nanocomposites with inorganic nanofillers and cellulose fibers, Composites Part A – Appl. Sci. Manuf. 82 (2016) 34–41, https://doi.org/10.1016/j.compositesa.2015.11.019.
[9] C. Goncalves, I.C. Goncalves, F.D. Magalhaes, A.M. Pinto, Poly(lactic acid) composites containing carbon-based nanomaterials: a review, Polymers 9 (2017), 269, https://doi.org/10.3390/polym9070269.
[10] M. Murariu, P. Dubois, PLA composites: from production to properties, Adv. Drug Deliv. Rev. 107 (2016) 17–46, https://doi.org/10.1016/j.addr.2016.04.003.
[11] M. Baiardo, G. Frisoni, M. Scandola, M. Rimelen, D. Lips, K. Ruffieux, E. Wintermantel, Thermal and mechanical properties of plasticized poly(L-lactic acid), J. Appl. Polym. Sci. 90 (2003) 1731–1738, https://doi.org/10.1002/app.12549.
[12] Y. Hu, Y.S. Hu, V. Topolkaraev, A. Hiltner, E. Baer, Crystallization and phase separation in blends of high stereoregular poly(lactide) with poly(ethylene glycol), Polymer 44 (2003) 5681–5689, https://doi.org/10.1016/S0032-3861(03)00609-8.
[13] Y. Hu, M. Rogunova, V. Topolkaraev, A. Hiltner, E. Baer, Aging of poly(lactide)/poly(ethylene glycol) blends. Part 1. Poly(lactide) with low stereoregularity, Polymer 44 (2003) 5701–5710, https://doi.org/10.1016/S0032-3861(03)00614-1.
[14] Y. Hu, Y.S. Hu, V. Topolkaraev, A. Hiltner, E. Baer, Aging of poly(lactide)/poly(ethylene glycol) blends. Part 2. Poly(lactide) with high stereoregularity, Polymer 44 (2003) 5711–5720, https://doi.org/10.1016/S0032-3861(03)00615-3.
[15] M. Pluta, M.A. Paul, M. Alexandre, P. Dubois, Plasticized polylactide/clay nanocomposites. II. The effect of aging on structure and properties in relation to the filler content and the nature of its organo-modification, J. Polym. Sci., Part B: Polym. Phys. 44 (2006) 312–325, https://doi.org/10.1002/polb.20697.
[16] S. Saeidlou, M.A. Huneault, H. Li, C.B. Park, Poly(lactic acid) crystallization, Prog. Polym. Sci. 37 (2012) 1657–1677, https://doi.org/10.1016/j.progpolymsci.2012.07.005.
[17] A.J. Muller, M. Avila, G. Saenz, J. Salazar, Crystallization of PLA-based materials, in: A. Jimenez, M. Peltzer, R. Ruseckaite (Eds.), Poly(lactic Acid) Science and Technology: Processing, Properties, Additives and Applications, RSC Polymer Chemistry Series, Royal Society of Chemistry, Cambridge, 2015, pp. 66–98.
[18] J. Bojda, E. Piorkowska, Shear-induced nonisothermal crystallization of two grades of PLA, Polym. Test. 50 (2016) 172–181, https://doi.org/10.1016/j.polymertesting.2016.01.006.
[19] A. Rhoades, R. Pantani, Poly(lactic acid): flow-induced crystallization, Adv. Polym. Sci. 283 (2019) 87–117, https://doi.org/10.1007/12_2019_49.
[20] S.C. Schmidt, M.A. Hillmyer, Polylactide stereocomplex crystallites as nucleating agents for isotactic polylactide, J. Polym. Sci., Part B: Polym. Phys. 39 (2001) 300–313, https://doi.org/10.1002/1099-0488(20010201)39:3%3C300::aid-polb1002%3E3.0.co;2-m.

[21] K.S. Anderson, M.A. Hillmyer, Melt preparation and nucleation efficiency of polylactide stereocomplex crystallites, Polymer 47 (2006) 2030–2035, https://doi.org/10.1016/j.polymer.2006.01.062.
[22] R. Androsch, C. Schick, M.L. di Lorenzo, Kinetics of nucleation and growth of crystals of poly(L-lactic acid), Adv. Polym. Sci. 279 (2018) 235–272, https://doi.org/10.1007/12_2016_13.
[23] I. Chiulan, A.N. Frone, C. Brandabur, D.M. Panaitescu, Recent advances in 3D printing of aliphatic polyesters, Bioengineering 5 (2018), 2, https://doi.org/10.3390/bioengineering5010002.
[24] B. Coppola, N. Cappetti, L. Di Maio, P. Scarfato, L. Incarnato, 3D printing of PLA/clay nanocomposites: influence of printing temperature on printed samples properties, Materials 11 (2018), 1947, https://doi.org/10.3390/ma11101947.
[25] J. Yu, Z. Qiu, Effect of low octavinyl-polyhedral oligomeric silsesquioxanes loadings on the melt crystallization and morphology of biodegradable poly(L-lactide), Thermochim. Acta 519 (2011) 90–95, https://doi.org/10.1016/j.tca.2011.03.009.
[26] M.D. Fernandez, M.J. Fernandez, M. Cobos, Effect of polyhedral oligomeric silsesquioxane (POSS) derivative on the morphology, thermal, mechanical and surface properties of poly(lactic acid)-based nanocomposites, J. Mater. Sci. 51 (2016) 3628–3642, https://doi.org/10.1007/s10853-015-9686-5.
[27] H. Pan, Z. Qiu, Biodegradable poly(L-lactide)/polyhedral oligomeric silsesquioxanes nanocomposites: enhanced crystallization, mechanical properties, and hydrolytic degradation, Macromolecules 43 (2010) 1499–1506, https://doi.org/10.1021/ma9023685.
[28] H. Sirin, M. Kodal, G. Ozkoc, The influence of POSS type on the properties of PLA, Polym. Compos 37 (2016) 1497–1506, https://doi.org/10.1002/pc.23319.
[29] X. Zhang, J. Sun, S. Fang, X. Han, Y. Li, C. Zhang, Thermal, crystalline, and mechanical properties of octa(3-chloropropylsilsesquioxane)/poly(L-lactic acid) hybrid films, J. Appl. Polym. Sci. 122 (2011) 296–303, https://doi.org/10.1002/app.34059.
[30] A. Zubrowska, E. Piorkowska, A. Kowalewska, M. Cichorek, Novel blends of polylactide with ethylene glycol derivatives of POSS, Colloid Polym. Sci. 293 (2015) 23–33, https://doi.org/10.1007/s00396-014-3344-3.
[31] L. Tang, Z. Qiu, Effect of poly(ethylene glycol)-polyhedral oligomeric silsesquioxanes on the thermal and mechanical properties of biodegradable poly(L-lactide), Compos. Commun. 3 (2017) 11–13, https://doi.org/10.1016/j.coco.2016.11.003.
[32] A.S. Herc, M. Wlodarska, M. Nowacka, J. Bojda, W. Szymański, A. Kowalewska, Supramolecular interactions between polylactide and model cyclosiloxanes with hydrogen bonding-capable functional groups, Express Polym. Lett. 14 (2020) 134–153, https://doi.org/10.3144/expresspolymlett.2020.12.
[33] J. Shi, W. Wang, Z. Feng, D. Zhang, Z. Zhou, Q. Li, Multiple influences of hydrogen bonding interactions on PLLA crystallization behaviors in PLLA/TSOS hybrid blending systems, Polymer 175 (2019) 152–160, https://doi.org/10.1016/j.polymer.2019.05.008.
[34] J.Y. Nam, M. Okamoto, H. Okamoto, M. Nakano, A. Usuki, M. Matsuda, Morphology and crystallization kinetics in a mixture of low-molecular weight aliphatic amide and polylactide, Polymer 47 (2006) 1340–1347, https://doi.org/10.1016/j.polymer.2005.12.066.
[35] H. Bai, C. Huang, H. Xiu, Q. Zhang, H. Deng, K. Wang, F. Chen, Q. Fu, Significantly improving oxygen barrier properties of polylactide via constructing parallel-aligned shish-kebab-like crystals with well-interlocked boundaries, Biomacromolecules 15 (2014) 1507–1514, https://doi.org/10.1021/bm500167u.
[36] Q. Xie, L. Han, G. Shan, Y. Bao, P. Pan, Polymorphic crystalline structure and crystal morphology of enantiomeric poly(lactic acid) blends tailored by a self-assemblable aryl amide nucleator, ACS Sustain. Chem. Eng. 4 (2016) 2680–2688, https://doi.org/10.1021/acssuschemeng.6b00191.
[37] C. Li, S. Luo, J. Wang, H. Wu, S. Guo, X. Zhang, Conformational regulation and crystalline manipulation of PLLA through a self-assembly nucleator, Biomacromolecules 18 (2017) 1440–1448, https://doi.org/10.1021/acs.biomac.7b00367.
[38] Y. Feng, P. Ma, P. Xu, R. Wang, W. Dong, M. Chen, C. Joziasse, The crystallization behavior of poly(lactic acid) with different types of nucleating agents, Int. J. Biol. Macromol. 106 (2018) 955–962, https://doi.org/10.1016/j.ijbiomac.2017.08.095.
[39] W.-C. Lai, Thermal behavior and crystal structure of poly(l-lactic acid) with 1,3:2,4-dibenzylidene-D-sorbitol, J. Phys. Chem. B 115 (2011) 11029–11037, https://doi.org/10.1021/jp2037312.
[40] M. Nowacka, A. Kowalewska, T. Makowski, Nanostructured surfaces by supramolecular self-assembly of linear oligosilsesquioxanes with biocompatible side groups, Beilstein J. Nanotechnol. 6 (2015) 2377–2387, https://doi.org/10.3762/bjnano.6.244.
[41] M. Nowacka, A. Rygała, D. Kręgiel, A. Kowalewska, Poly(silsesquioxanes) and poly(siloxanes) grafted with N-acetylcysteine for eradicating mature bacterial biofilms in water environment, Colloids Surf. B Biointerfaces 172 (2018) 627–634, https://doi.org/10.1016/j.colsurfb.2018.09.017.
[42] A. Kowalewska, M. Nowacka, A. Tracz, T. Makowski, Supramolecular self-assembly of linear oligosilsesquioxanes on mica-AFM surface imaging and hydrophilicity studies, Soft Matter 11 (2015) 4818–4829, https://doi.org/10.1039/c5sm00787a.
[43] A. Kowalewska, M. Nowacka, T. Makowski, A. Michalski, Thermal stability of self-assembled surfaces and micropatterns made of ladder polysilsesquioxanes, Polymer 90 (2016) 147–155, https://doi.org/10.1016/j.polymer.2016.03.002.
[44] A.S. Herc, P. Lewiński, S. Kaźmierski, J. Bojda, A. Kowalewska, Hybrid SC-polylactide/poly(silsesquioxane) blends of improved thermal stability, Thermochim. Acta 687 (2020), 178592, https://doi.org/10.1016/j.tca.2020.178592.

11

[45] A. Kowalewska, M. Nowacka, Synthesis of ladder silsesquioxanes by in situ polycondensation of cyclic tetravinylsiloxanetetraols, Silicon 7 (2015) 133–146, https://doi.org/10.1007/s12633-014-9209-z.

[46] W.L.F. Armarego, Ch.L.L. Chai, Purification of Laboratory Chemicals, Butterworth-Heinemann, Bodmin, 2003.

[47] H. Hu, X. Zhao, X. Wang, X. Yu, W. Zhou, S. Peng, Super tough poly(lactic acid) blends: a comprehensive review, RSC Adv. 10 (2020) 13316–13368, https://doi.org/10.1039/d0ra01801e.

[48] M. Pluta, E. Piorkowska, Tough and transparent blends of polylactide with block copolymers of ethylene glycol and propylene glycol, Polym. Test. 41 (2015) 209–218, https://doi.org/10.1016/j.polymertesting.2014.11.011.

[49] J. Zhang, K. Tashiro, H. Tsuji, A.J. Domb, Disorder-to-order phase transition and multiple melting behavior of poly(L-lactide) investigated by simultaneous measurements of WAXD and DSC, Macromolecules 41 (2008) 1352–1357, https://doi.org/10.1021/ma0706071.

[50] A. Galeski, Z. Bartczak, M. Pracella, Spherulite nucleation in polypropylene blends with low density polyethylene, Polymer 25 (1984) 1323–1326, https://doi.org/10.1016/0032-3861(84)90384-7.

[51] T. Kawai, N. Rahman, G. Matsuba, K. Nishida, T. Kanaya, M. Nakano, H. Okamoto, J. Kawada, A. Usuki, N. Honma, K. Nakajima, M. Matsuda, Crystallization and melting behavior of poly (L-lactic acid), Macromolecules 40 (2007) 9463–9469, https://doi.org/10.1021/ma070082c.

[52] P. Pan, B. Zhu, W. Kai, T. Dong, Y. Inoue, Polymorphic transition in disordered poly (L-lactide) crystals induced by annealing at elevated temperatures, Macromolecules 41 (2008) 4296–4304, https://doi.org/10.1021/ma800343g.

[53] M. Cocca, M.L. Di Lorenzo, M. Malinconico, V. Frezza, Influence of crystal polymorphism on mechanical and barrier properties of poly(L-lactic acid), Eur. Polym. J. 47 (2011) 1073–1080, https://doi.org/10.1016/j.eurpolymj.2011.02.009.

Crystallization, structure and properties of polylactide/ladder poly(silsesquioxane) blends

Agata S. Herc, Joanna Bojda, Maria Nowacka, Piotr Lewiński, Waldemar Maniukiewicz,

Ewa Piorkowska*, Anna Kowalewska*

Electronic Supporting Information

1.1. Synthesis of LPSQ-R

In general a thiol derivative was added (at $[HS]_0/[Vi]_0 = 1.4$) to the solution of LPSQ-Vi in dry THF (containing LPSQ-Vi at 8% wt) placed in a quartz crucible. 2,2-dimethoxy-2-phenylacetophenone (DMPA) ($[Vi]_0/[DMPA]_0 = 50$) was added with stirring to the solution of reagents. The mixture was irradiated for 15 min with UV light ($\lambda = 365$ nm). ^1H NMR analysis of the products thus prepared showed complete conversion of the vinyl groups in LPSQ-Vi. Volatiles were then removed under reduced pressure and the residue was dissolved in a small amount of THF and precipitated into a large amount of a non-solvent (cyclohexane for LPSQ-COOH and LPSQ-COOMe or hexane/ethyl acetate (1:1 v/v) in the case of LPSQ-OH). The purification procedure was repeated twice. The purified precipitates were dried under high vacuum at room temperature to the constant weight. The products were characterized using DSC and NMR spectroscopies (Table ESI-1).

Table ESI-1. NMR characteristics of LPSQ-R.

| LPSQ-R	Chemical name	Y [%]	^1H NMR δ [ppm]	^{13}C NMR δ [ppm]	^{29}Si NMR δ [ppm]
LPSQ-OH	poly[2-(hydroxyethylthio)-ethylsilsesquioxane]	76	in CD_3OD 0.16 (s. $OSiMe_3$), 1.03 (m. $SiCH_2$), 2.67 (m. CH_2S), 2.67 (m. SCH_2), 3.68 (m. CH_2OH)	in THF-d8 1.05 ($OSiMe_3$), 14.0 (m. $SiCH_2$), 26.3 (CH_2S), 34.2 (m. SCH_2), 61.6 (CH_2OH)	in CD_3OD -70.3 (-$CH_2SiO_{3/2}$), 10.7 ($OSiMe_3$)
LPSQ-COOMe	poly[2-(methylthioglycolate)-ethylsilsesquioxane]	91	in THF-d8 0.16 (s. $OSiMe_3$), 1.06 (m. $SiCH_2$), 2.77 (m. CH_2S), 3.25 (m. SCH_2), 3.65 (s. OCH_3)	in THF-d8 0.97 ($OSiMe_3$), 13.3 ($SiCH_2$), 26.6 (CH_2S), 32.3 (SCH_2), 51.4 (OCH_3), 170.3 (COO)	in THF-d8 -70.4 (-$CH_2SiO_{3/2}$), 10.5 ($OSiMe_3$)
LPSQ-COOH	poly[2-(carboxymethylothio)-ethylsilsesquioxane]	98	in THF-d8 0.17 (s. $OSiMe_3$), 1.08 (m. $SiCH_2$), 2.79 (CH_2S), 3.20 (m. SCH_2), 8.30 (COOH)	in CD_3OD -0.5 ($OSiMe_3$), 11.4 ($SiCH_2$), 25.3 (CH_2S), 31.6 (SCH_2), 170.9 (COOH)	in CD_3OD −70.4 (-$CH_2SiO_{3/2}$), 10.9 ($OSiMe_3$)

Y - reaction yield (after purification)

1
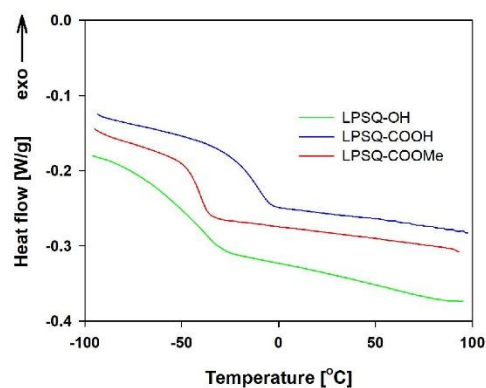
Figure ESI-1. DSC traces of LPSQ-R recorded during the second heating at 10 °C/min (after the first heating to 100 °C at 10 °C/min and cooling down to -100 °C).
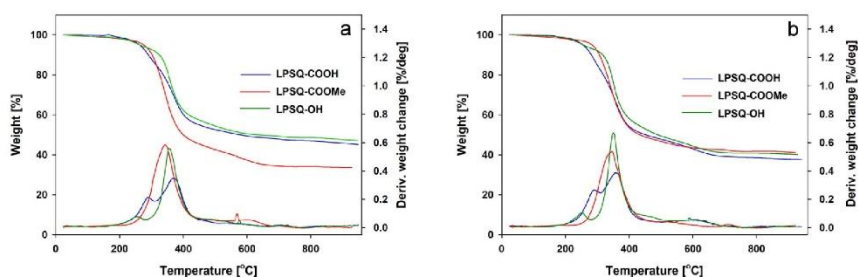
Figure ESI-2. TGA thermograms recorded for LPSQ-R during heating at 10 °C/min: a) in N_2 and b) in air.

1.2. Synthesis of PLLA

L-lactide (L-LA) (Boehringer-Ingelheim, Germany) was crystallized from dry 2-propanol, sublimed in vacuum, distributed into glass ampoules with break-seals, dried and sealed off. Tin (2-ethylhexanoate) $Sn(Oct)_2$ (95%, Aldrich, USA) was first distilled (10^{-3} mbar, 413 K) into a glass ampoule with Rotaflo® stopcock. Next a portion of the catalyst was transferred in vacuum into a heart-shaped flask and distilled (also in vacuum) into glass ampoules with break-seals.

2

L-LA (13.0387 g, 0.09 mol) was placed in a custom glass vessel with an arm with break-seal containing Sn(Oct)$_2$ (0.0957 g, 2.4·10^{-4} mol) attached. The ampule was connected to a vacuum line and after 2.5 h of drying sealed off. Next the break-seal containing Sn(Oct)$_2$ was broken and the vessel was placed in 140 °C until L-LA melted. The reagents were then mixed and the vessel was again placed in 140 °C for 20 h. The crude product was dissolved in 270 ml of CH$_2$Cl$_2$ and precipitated into 2700 ml of methanol. Resulting PLA was filtered, washed with methanol and dried to a constant weight.

Dichloromethane (DCM, CH$_2$Cl$_2$; P.P.H. "STANLAB" Sp.J.) was used as received. Methanol (analytical grade, Chempur, Poland) was used as received. 2-propanol (analytical grade, Chempur, Poland) was distilled from over sodium metal chips.
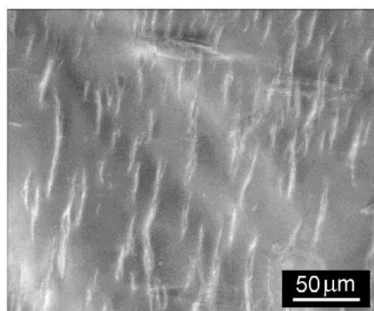
1.3. Structure, properties and crystallization of PLA and PLLA blends with LPSQ-R
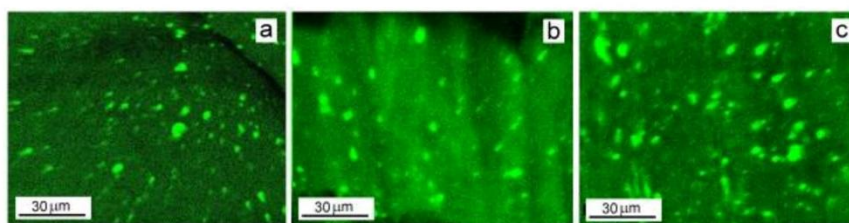
Figure ESI-3. SEM-EDS (Si mapping) of PLA blends with LPSQ-COOH: a) P/1-COOH, b) P/2-COOH and c) P/5-COOH.
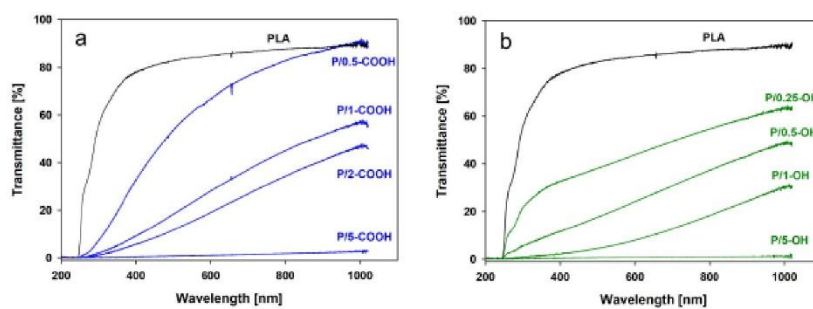
Figure ESI-4. Direct light transmittance through 0.5 mm thick samples of: a) PLA/LPSQ-COOH, b) PLA/LPSQ-OH.

3

Figure ESI-5. Polarized light micrograph of the neck region of P/5-COOMe drawn uniaxially to 400%. Drawing direction – horizontal.
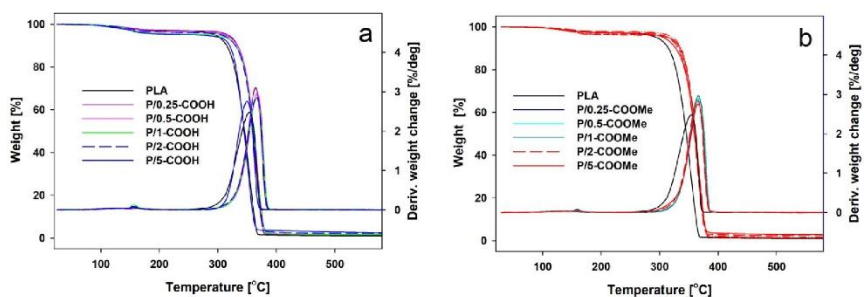
Figure ESI-6. TGA thermograms recorded for PLA/LPSQ-COOH (a) and PLA/LPSQ-COOMe (b) (N_2, 10 °C/min).

The initial small weight loss near 150-160 °C, visible on TGA thermograms in Figure ESI-5, results most possibly from sublimation of cyclic oligomers of low molecular weight present in PLA. The sublimation could be facilitated by reduction of entanglement density due to dissolution of PLA. It is worth noting that the temperature of this event is too high to be caused by evaporation of residual solvent.

4

Table ESI-2. TGA characteristics of PLA blends with LPSQ-R. T_d denotes the temperature of maximum weight loss rate (peak of deriv. weight change), $T_{5\%}$ denotes the temperature of 5% weight loss. $\Delta T_{5\%} = T_{5\%}$ PLA-$T_{5\%}$ PLA/LPSQ-R

| Sample code	LPSQ [wt%]	T_d [ºC]	$T_{5\%}$ [ºC]	$\Delta T_{5\%}$ [ºC]
PLA	-	354.2	309.2	0
P/0.25-OH	0.25	365.4	331.1	21.9
P/0.5-OH	0.5	367.9	331.5	22.3
P/2-OH	1	366.1	328.7	19.5
P/2-OH	2	366.0	330.9	21.7
P/5-OH	5	365.9	330.2	21.0
P/0.25-COOH	0.25	364.4	331.7	22.5
P/0.5-COOH	0.5	367.0	329.5	20.3
P/1-COOH	1	366.0	328.9	19.7
P/2-COOH	2	365.9	326.5	17.3
P/5-COOH	5	349.5	319.1	9.9
P/0.25-COOMe	0.25	367.3	331.8	22.6
P/0.5-COOMe	0.5	366.9	331.4	22.2
P/1-COOMe	1	366.5	330.8	21.6
P/2-COOMe	2	364.2	324.9	15.7
P/5-COOMe	5	365.8	320.6	11.4
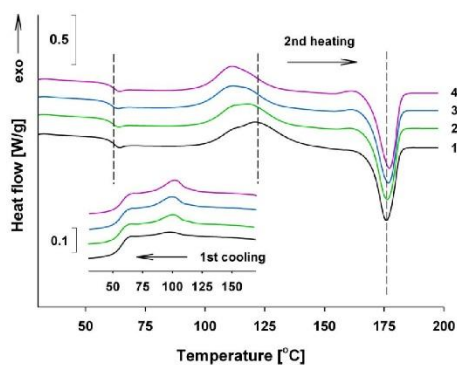
Figure ESI 7. DSC traces (second heating runs at 10ºC/min) of neat PLLA and PLLA blends with 2 wt% of LPSQ-R: 1 - PLLA, 2 - PL/2-OH, 3 - PL/2-COOMe and 4 - PL/2-COOH. The inset shows traces recorded on cooling at 10 ºC/min.

5

68
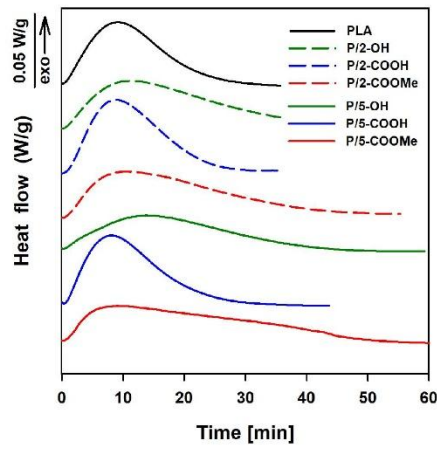
Figure ESI-8. DSC thermograms or PLA and PLA blends with 2 wt% and 5 wt% of LPSQ-R recorded during isothermal crystallization at 120 °C.
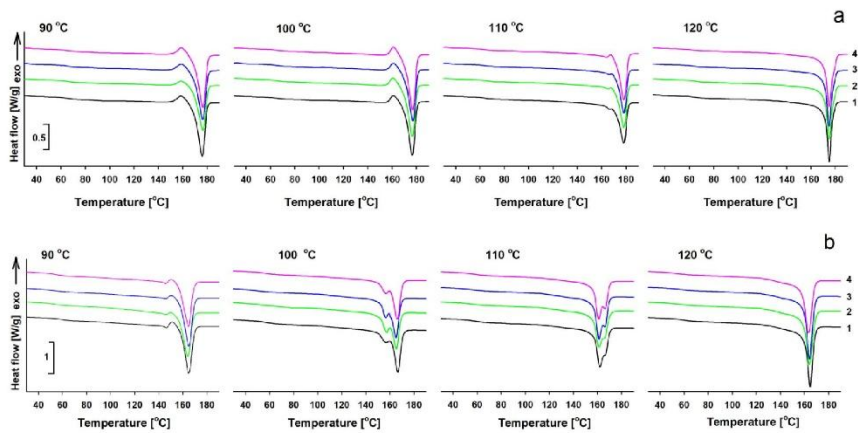
Figure ESI-9. DSC heating thermograms (at 10 °C/min) of isothermally crystallized PLLA and PLA NW4032D, and their blends with 2 wt% of LPSQ-R: a) 1 – PLLA, 2 – PL/2-OH, 3 – PL/2-COOMe, 4 – PL/2-COOH, b) 1 – PLA, 2 – P/2-OH, 3 – P/2-COOMe, 4 – P/2-COOH.

6

Table ESI-3. The melting enthalpy (ΔH_m) and crystallinity (X) of isothermally crystallized PLLA blends wit 2 wt% of LPSQ-R, the latter calculated assuming ΔH_m of PLLA crystals of 93.1 J/g.

Crystallization temperature [ºC]	PLLA		PL/2-COOH		PL/2-COOMe		PL/2-OH	
	ΔH_m [J/g]	X[wt%]	ΔH_m [J/g]	X[wt%]	ΔH_m [J/g]	X [wt%]	ΔH_m [J/g]	X [wt%]
90	44.8	48.1	45.5	48.9	43.2	46.4	41.3	44.4
100	42.6	45.8	44.8	48.1	42.5	45.7	42.1	45.2
110	45.5	48.9	45.5	48.9	45.0	48.3	44.4	47.7
120	49.6	53.3	49.8	53.5	45.8	49.2	45.3	48.7
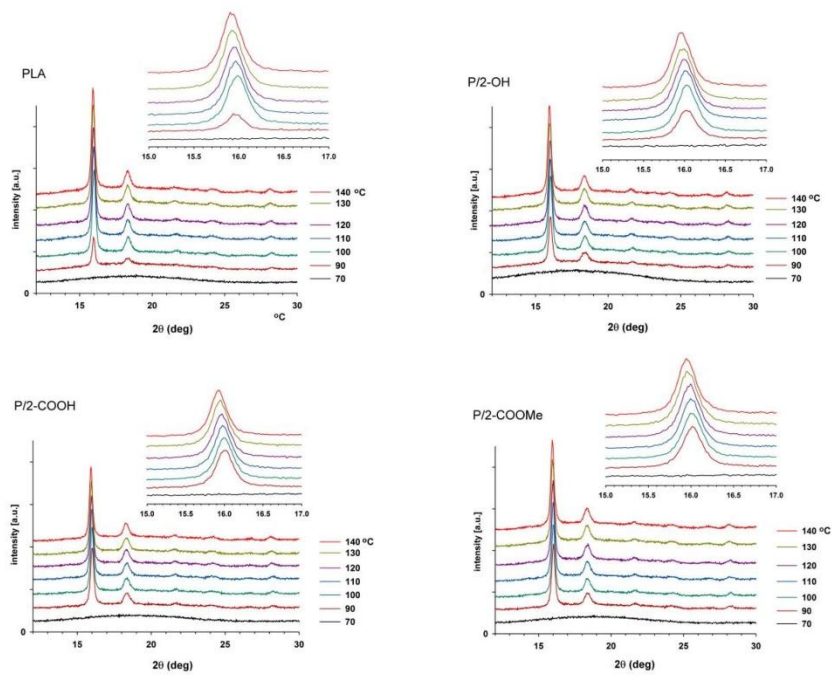
Figure ESI-10. WAXS curves of PLA and PLA blends with 2 wt% of LPSQ-R annealed at indicated temperatures.

7

70

Hybrid SC-polylactide/poly(silsesquioxane) blends of improved thermal stability

Agata S. Herc, Piotr Lewiński, Sławomir Kaźmierski, Joanna Bojda, Anna Kowalewska*

Centre of Molecular and Macromolecular Studies, Polish Academy of Sciences, Sienkiewicza 112, 90-363, Łódź, Poland

ARTICLE INFO

ABSTRACT

Hybrid blends of poly(L-lactide)/poly(D-lactide) (PLLA/PDLA) and hydrogen bonds donating/accepting oligomeric ladder silsesquioxanes (LPSQ-R; R=OH, (OH)2, COOH, COOMe) exhibited higher thermal stability at $T > 533$ K. Temperature of decomposition (T_d) increased by 20–30 K comparing to neat PLLA/PDLA, even when small amounts of the additives were used. Stereocomplexation in PLLA/PDLA blends was improved with the addition of H-bond donating LPSQ-R, even in the presence of substantial amounts of the additives, and only slightly disturbed by LPSQ-COOMe. Vibrational spectroscopic analysis was used to follow the crystal structure evolution at 448 K. The modes characteristic of 3_1 β-helical structures were observed in the studied samples. LPSQ-R grafted with thioglycerol moieties, significantly increased the stereocomplexation rate. Nuclear magnetic resonance spectroscopy (NMR) and wide-angle X-ray scattering (WAXS) measurements confirmed the stereocomplex structure of the hybrid blends. All the observed effects may be related to the specific structure of polysilsesquioxanes and R groups.

1. Introduction

Durable polymeric materials having high biobased content are of an unceasing interest for multiuse long-term practical applications, *e.g.* in electronics or automotive industries. Apart for being tough and strong, durable biomaterials should also exhibit good thermal stability defined as the ability to maintain their intrinsic properties (heat deflection and softening) at increased temperatures. Polylactic acid (PLA) has been widely studied for its applicative potential in this area [1,2]. The heat resistance of amorphous PLA is quite difficult to improve since its glass transition occurs at relatively low temperatures (~ 333 K). Interchain interactions and packing of molecular chains in the crystalline phase strongly influence physical properties of PLA-based materials. Thermal resistance of PLA depends also on the amount of rigid amorphous fraction (RAF) and the mobile amorphous fraction (MAF). Heat resistant PLA-based materials should preferably have large amounts of crystalline and rigid amorphous fractions as well as exhibit reduced chain mobility. Apart from improved mechanical properties, PLA should also be resistant to thermal degradation. This can be achieved by addition of PLA-crystal nucleating agents and formation of stereocomplexes (SC), or blending the polyester matrix with heat resistant species or reinforcing additives. Stereocomplexation is one of the most effective methods to improve heat resistance, hydrolytic resistance,

mechanical performance and barrier properties of PLA-based materials [3–5]. Owing to the strong interactions between L-lactyl and D-lactyl unit sequences, SC formed from mixtures of poly(L-lactide) (PLLA) and poly(D-lactide) (PDLA) melt at temperatures higher than those characteristic of PLA homocrystals (~ 503 K *vs* ~ 463 K). They can act as nucleating agents for epitaxial growth of ordered structures in PLA matrix.

The exceptionally strong interactions between L-lactide chains and D-lactide chains in 3_1 helical conformation have a significant effect in reducing the molecular mobility and may hinder the thermal degradation. Nevertheless, at high temperatures, neat SC PLA tend to decompose quite abruptly through the same mechanism as any of the single enantiomeric forms. Comparative thermogravimetric studies showed a very small difference between the degradation curves of neat PLLA and PDLA as well as SC PLLA/PDLA blend in heat scanning at a constant rate, whereas at fixed temperatures of 523 K and 533 K [T > temperature of melting SC (T_{mSC})] the blend had higher stability than the components [6]. Thermal degradation in the melt is disturbed by blending PLLA and PDLA chains, even though they no longer form SC crystallites but are in the amorphous melted state. However, at $T >> T_{mSC}$ the helical conformation disappears and a rather rapid thermal degradation proceeds through mechanisms of unzipping, lactide elimination, and random degradation [3]. Incorporation of

---

aromatic groups at terminal positions of low molecular weight chains in PLLA/PDLA blends improved the thermal properties in both T_m and 10 % weight loss temperature (T_{10}) [7]. Thermal an mechanical properties as well as resistance towards an enzymatic degradation of PLLA/PDLA blends can be also improved by crosslinking [8–11].

Various additives (nucleating agents, plasticizers and compatibilizers) were used to promote SC nucleation by generation of clusters of helical PLLA/PDLA pairs [3,5]. In general, highly active nucleating agents provide heterogeneous surfaces, whereas plasticizers improve diffusion of polymer chains and therefore promote the crystal growth. We have found that linear polysilsesquioxanes (LPSQ-R) with features characteristic of hybrid inorganic-organic polysilsesquioxane materials, and bearing hydrogen bond donating/accepting groups (−COOH, −COOMe, −OH), combine these two trends. The range of additives concentration in the blends was chosen to study the effect of LPSQ-R as both nucleants and structural components. Addition of LPSQ-R to the mixture of PLLA and PDLA, results in formation of hybrid materials of increased thermal stability. The stereocomplex structure was retained, even in the presence of substantial amounts of LPSQ-R. In some hybrid blends the degree of crystallinity of neat polylactide was larger than that of SC PLLA/PDLA. The temperature of melting of SC formed in the hybrid materials was approximately the same as T_{mSC} in the neat mixture of PLLA and PDLA. LPSQ-R (R = COOH, OH, (OH)2) interacting with polylactide chains caused effects that could not be ascribed solely to the matrix plastification as only a small decrease of crystallization temperature (T_{cSC}) was observed on cooling from melt. Side ester groups of LPSQ-COOMe may be only donors of weak C−H···O=C bonds and therefore this additive acted less effectively. Notwithstanding, its influence on the rate of thermal degradation of PLA was rather similar to that of other LPSQ-R. The presented results may have an important applicative aspect.

2. Experimental

2.1. Materials

Well-defined polylactides, PLLA (M_w = 6400 g/mol, M_w/M_n = 1.42) and PDLA (M_w = 7200 g/mol, M_w/M_n = 1.36), used for the studies were prepared by ring-opening polymerization (ROP) of enantiomeric lactides: L-lactide (L-LA) and D-lactide (D-LA) (Boehringer-Ingelheim, Germany). The procedure and characteristics of the polymers can be found in ESI. Oligomeric linear polysilsesquioxanes LPSQ-R of ladder-like, double-strand backbone terminated with trimethylsilyl

groups were prepared by photoinitiated thiol-ene addition of selected mercapto-compounds (Scheme 1), analogously to earlier published procedures [12,13]. A general description including structural characteristics obtained by NMR spectroscopy is presented in ESI. Thioglycolic acid (Sigma-Aldrich, 98 %), methyl thioglycolate (Acros Organics, 95 %), 2-mercaptoethanol (Sigma-Aldrich, 99 %) or thioglycerol (Sigma-Aldrich, 99 %) were grafted to linear poly(vinylsilsesquioxane) precursors (LPSQ-Vi, M_n = 1000 g/mol, M_w/M_n = 1.4, prepared by in situ condensation of 2,4,6,8-tetrahydroxy-2,4,6,8-tetravinyl-cyclotetrasiloxanes [14]) giving respectively LPSQ−COOH, LPSQ-COOMe, LPSQ-OH and LPSQ(OH)2. 2,2-Dimethoxy-2-phenylacetophenone (DMPA; Acros Organics, 99 %) was used as a photoinitiator. Commercially available reagents were used as received. Solvents were purified according to the literature procedures [15].

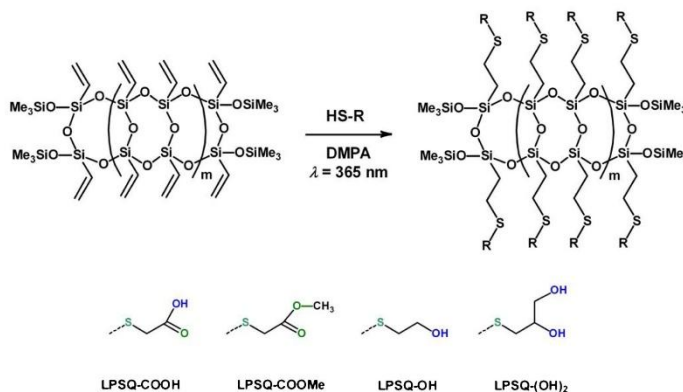### 2.2. Preparation of PLLA/PDLA/LPSQ-R blends

PLLA and PDLA were dissolved in a mixture of CH$_2$Cl$_2$/THF. LPSQ-R were dissolved in tetrahydrofuran (THF) [or MeOH in case of LPSQ-(OH)2] at the given concentrations (Table 1). Compositions containing PLLA, PDLA and LPSQ-R were prepared at room temperature, following three different procedures in order to find the most suitable one to promote the effective interactions between the components.

SC-1: Solutions of PLLA and PDLA [concentration of lactide units (C_L) 0.434 mol/dm^3 each] in a mixture of CH$_2$Cl$_2$ and THF (6:10 v/v) were mixed for 5 min under magnetic stirring. The initially clear mixture became slightly turbid after that time. It was added dropwise to a solution of LPSQ-R in THF [or MeOH in the case of LPSQ-(OH)2] (C_R = 2.5 mol/dm^3) under vigorous stirring at room temperature.

SC-2: Solutions of PLLA and PDLA (in CH$_2$Cl$_2$; C_L = 0.435 mol/dm^3) were mixed for 2 min and then a solution of LPSQ-R (C_R = 2.5 mol/dm^3) in THF [or MeOH in the case of LPSQ-(OH)2] was added dropwise under magnetic stirring. The resulting mixture was stirred for additional 30 min.

SC-3: A solution containing LPSQ-R (C_R = 2.5 mol/dm^3) in THF (or MeOH) was added dropwise to the solution of PLLA (in 18.6:16 v/v mixture of CH$_2$Cl$_2$ and THF; C_L = 0.323 mol/dm^3) and the mixture was left with stirring for 5 min. The solution of PDLA (C_L = 0.323 mol/dm^3; in a mixture of CH$_2$Cl$_2$ and THF) was then added dropwise. The resulting mixture was stirred for 30 min.

Blends with low amount of LPSQ-R were prepared following the procedure SC-3. Samples obtained at [R]/[La] (the initial molar ratio of functional groups R to the amount of lactide segments) equal to 0.1,

Scheme 1. Structure of LPSQ-R used for modification of PLLA/PDLA blends.

Table 1
The composition of solutions used for the preparation of PLLA/PDLA/LPSQ-R.

sample	R	[R]/[La]	wt.%	V_{LPSQ} [ml]	V_{PLLA} [ml]	V_{PDLA} [ml]	ΣC_R [mol/dm^3]	ΣC_L [mol/dm^3]	v/v
SC-1-1	–	0	100.0	–	2.0	2.0	0	0.434	0.6
SC-1-2	OH	0.25	64.7	0.26	3.0	3.0	0.104	0.415	0.56
SC-1-3	(OH)2	0.50	43.6	0.57	3.3	3.3	0.199	0.399	0.53
SC-1-4	COOH	0.25	63.4	0.15	1.8	1.8	0.101	0.416	0.56
SC-1-5	COOMe	0.25	61.1	0.30	3.5	3.5	0.103	0.416	0.56
SC-2-1	–	0	100.0	0.85*	5.6	5.6	0	0.404	13.2
SC-2-2	OH	0.50	47.9	0.85	5.0	5.0	0.200	0.401	11.8
SC-2-3	(OH)2	0.50	43.6	0.86**	5.0	5.0	0.200	0.401	11.6
SC-2-4	COOH	0.50	45.8	0.85	5.0	5.0	0.200	0.401	11.8
SC-2-5	COOMe	0.50	43.8	0.87	5.0	5.0	0.200	0.400	11.5
SC-3-1	–	0	100.0	0.40*	5.3	5.3	0	0.309	1.07
SC-3-2-0.01	OH	0.01	97.9	0.11	6.0	6.0	0.003	0.318	1.12
SC-3-2-0.05	OH	0.05	90.2	0.55	6.0	6.0	0.014	0.309	0.97
SC-3-2-0.1	OH	0.10	82.1	0.15	6.0	6.0	0.027	0.319	1.11
SC-3-2	OH	0.26	63.5	0.39	6.0	6.0	0.081	0.307	1.08
SC-3-3-0.01	(OH)2	0.01	97.5	0.12**	6.0	6.0	0.003	0.320	1.17
SC-3-3-0.05	(OH)2	0.05	88.5	0.60**	6.0	6.0	0.015	0.308	1.17
SC-3-3-0.1	(OH)2	0.10	79.4	0.18**	6.0	6.0	0.032	0.318	1.17
SC-3-3	(OH)2	0.26	59.4	0.40**	6.0	6.0	0.081	0.307	1.08
SC-3-4-0.01	COOH	0.01	97.7	0.12	6.0	6.0	0.003	0.320	1.12
SC-3-4-0.05	COOH	0.05	89.4	0.60	6.0	6.0	0.015	0.308	0.96
SC-3-4-0.1	COOH	0.10	80.8	0.17	6.0	6.0	0.030	0.319	1.10
SC-3-4	COOH	0.26	61.5	0.39	6.0	6.0	0.081	0.307	1.08
SC-3-5-0.01	COOMe	0.01	97.5	0.12	6.0	6.0	0.003	0.320	1.12
SC-3-5-0.05	COOMe	0.05	88.6	0.60	6.0	6.0	0.015	0.308	0.96
SC-3-5-0.1	COOMe	0.10	79.6	0.18	6.0	6.0	0.030	0.318	1.10
SC-3-5	COOMe	0.26	59.7	0.40	6.0	6.0	0.081	0.307	1.08

[R]/[La] – mixing molar ratio of functional groups R to the amount of lactide segments.
wt.% – weight content of polylactide in PLLA/PDLA/LPSQ-R blend.
ΣC_R – molar concentration of functional groups R in the mixture.
ΣC_L – molar concentration of lactide units in the mixture.
v/v – the volume ratio of CH_2Cl_2 and THF in the mixture.
* addition of pure THF.
** solution of LPSQ-(OH)2 in MeOH.

0.01 and 0.05 were prepared with more diluted solutions of LPSQ-R (C_R = 2.15 mol/dm^3, 0.32 mol/dm^3 and 0.32 mol/dm^3, respectively).

Each of the blending procedures was applied to prepare neat SC as structural standard. Mixtures of appropriate PLLA and PDLA solutions (1:1 M ratio) were used. Additional amounts of THF were added to compositions of SC 2-1 (0.85 ml) and SC 3-1 (0.4 ml) to equalize the concentrations with respect to those in mixtures containing PLLA/PDLA/LPSQ-R.

The prepared compositions were then left for free solvent evaporation without stirring. Solid products were carefully dried for 24 h at 353 K under high vacuum (0.01 Torr), crushed using an agate mortar and analysed.

2.3. Analytic methods

^{13}C NMR cross polarization magic angle spinning (CP MAS) experiments in solid-state for PLLA/PDLA as well as PLLA/PDLA/LPQ-R mixtures were performed on BRUKER Avance III 400 spectrometer operating at 100.61 MHz. During the measurements the samples were spun at 8000 MAS frequency, a sample of glycine was used for setting the Hartmann-Hahn condition, and adamantane was used as a secondary chemical shift reference; resonances at δ = 38.48 ppm and 29.46 ppm from the external tetramethylsilane [16]. ^{13}C CP MAS spectra were accumulated with proton 90° pulse of 5.0 μs in length and a contact time of 2 ms. The repetition delay was 4 s, and the spectral width was 21.5 kHz. The FIDs were accumulated with a time domain size of 2 K data points 64 scans each and a SPINAL sequence was applied for ^{1}H decoupling [17].

The morphologies of SC-containing samples of PLLA/PDLA and PLLA/PDLA/LPSQ-R were characterized using scanning electron microscopy (SEM) (Jeol 5500 L V, Tokyo, Japan) operating in the high vacuum mode and at an accelerating voltage of 10 kV. Samples of crushed precipitates were mounted on brass stubs using double-sided adhesive tape and sputtered with gold using a Jeol Fine Coater 1200.

Phase transitions in the native PLLA and PDLA as well as the prepared PLLA/PDLA blends and compositions PLLA/PDLA/LPSQ-R were studied in bulk using a DSC 2920 Modulated thermal analysis system (TA Instruments; New Castle, DE, United States). Thermograms were taken for samples (sealed in aluminium pans) heated at 10 K/min from room temperature to 523 K, kept at this temperature (5 min) for clearing off crystals and cooled down to room temperature at the same temperature ramp. The characteristic transition temperatures and enthalpies were obtained during both cooling and heating runs (Table ESI-1 a/b). The degree of crystallinity (X_c) was estimated from both the endothermic (melting, X_{c-m}) and exothermic (crystallization, X_{c-c}) peaks and calculated from the Eq. (1) or Eq. (2):

$$X_c = \frac{\Delta H_m}{\Delta H_0} \tag{1}$$

$$X_c = \frac{\Delta H_c}{\Delta H_0} \tag{2}$$

where ΔH_m and ΔH_c are, respectively, enthalpies of fusion and crystallization for a sample (corrected for the neat PLA) and ΔH_0 is the enthalpy of fusion of 100 % crystalline polylactide. The ΔH_0 used for the 100 % crystalline stereocomplex was 155 J/g, as determined by Sawai et al. [18] and for the 100 % crystalline homocomplex ΔH_0 was 93 J/g (enthalpy of melting of α-crystals) [19].

Thermal degradation processes were studied for the components and the blends. Analyses were carried out in N_2 atmosphere (heating rate 10 K/min, resolution 3, sensitivity 3) using a Hi-Res TGA 2950 Thermogravimetric Analyzer (TA Instruments, New Castle, DE, United States). The 10 % weight loss temperature (T_{10}) as well as peak

3

Table 2
Thermal degradation of hybrid PLLA/PDLA/LPSQ-R blends (N_2, 10 K/min).

sample	LPSQ-R	[R]/[La]	T_{10} [K]	T_d [K]	V_d [%min/K]	R_{600} [%]	R_{600-c} [%]
SC-1-1	–	0	526	544	9.9	0.8	0
SC-1-2	OH	0.25	542	555	7.7	15.9	11.7
SC-1-3	OH2	0.50	546	572	7.0	20.6	15.7
SC-1-4	COOH	0.25	563	600	7.4	16.5	11.3
SC-1-5	COOMe	0.25	544	575	7.5	18.0	11.0
SC-2-1	–	0	531	547	9.8	0.6	0
SC-2-2	OH	0.50	548	568	7.7	14.8	17.3
SC-2-3	OH2	0.50	554	575	7.5	16.6	15.7
SC-2-4	COOH	0.50	569	596	7.9	15.5	16.5
SC-2-5	COOMe	0.50	540	550	7.3	19.7	15.8
SC-3-1	–	0	535	550	9.8	0.8	0
SC-3-2-0.01	OH	0.01	553	569	9.4	1.3	0.7
SC-3-2-0.05	OH	0.05	566	580	8.7	3.0	3.3
SC-3-2-0.1	OH	0.10	562	579	8.4	4.8	5.9
SC-3-2	OH	0.26	541	558	7.5	13.0	12.0
SC-3-3-0.01	OH2	0.01	553	571	9.5	0.5	0.7
SC-3-3-0.05	OH2	0.05	560	577	8.9	1.4	3.2
SC-3-3-0.1	OH2	0.10	567	585	8.7	2.6	5.7
SC-3-3	OH2	0.26	560	582	8.0	10.0	11.2
SC-3-4-0.01	COOH	0.01	553	570	9.1	1.0	0.7
SC-3-4-0.05	COOH	0.05	558	575	8.8	2.1	3.2
SC-3-4-0.1	COOH	0.10	552	574	8.5	4.2	5.8
SC-3-4	COOH	0.26	552	581	7.6	12.7	11.6
SC-3-5-0.01	COOMe	0.01	556	572	9.3	1.0	0.7
SC-3-5-0.05	COOMe	0.05	556	574	8.4	3.9	3.2
SC-3-5-0.1	COOMe	0.10	555	574	7.9	7.0	5.7
SC-3-5	COOMe	0.26	537	548	7.6	15.0	11.3

T_{10} – 10 % weight loss temperature.
T_d – peak temperature of weight loss derivative.
V_d – rate of weight loss at major decomposition step.
R_{600} – residue at 873 K.
R_{600-c} – residue calculated for the complete abstraction of organic part.

temperature of weight loss derivative (T_d) with respect to temperature (DTGA) were determined (Table 2). Isothermal decomposition of the studied materials was carried out at 533 K, 553 K and 573 K. The heating (10 K/min ramp) was started at room temperature until the isotherm was reached. Samples were kept at the chosen temperature until no weight decrease was observed.

Fourier transform infrared (FTIR) spectra were recorded using Nicolet 380 FTIR spectrometer (Thermo Fisher Scientific; Waltham, Massachusetts, United States), equipped with a heated cell and Harrick ATC/low voltage controller (Harrick Scientific Products, Inc. Pleasantville, New York, United States)] for thin films cast on NaCl crystal windows from 0.5 wt% solutions of LPSQ-R in CH_2Cl_2. Samples of PLLA/PDLA and PLLA/PDLA/LPSQ-R were grounded into fine powders using an agate mortar. The powders were suspended in CH_2Cl_2

(at 0.5 wt%) and cast on NaCl windows. The samples were left for slow solvent evaporation and then dried under high vacuum at room temperature. FTIR spectra were collected at given intervals by adding 16 scans at 4 cm^{-1} resolution. Isothermal crystallizations were studied for samples melted isothermally at 523 K (5 min) for complete clearing of crystals. The samples were then cooled down to 448 K and kept at this temperature for 30 min. Comparative analysis was carried out for spectra recorded every 1 min in transmission mode as well as for their second derivatives. The second derivatives were also used to estimate the position of the characteristic IR modes.

Analysis of crystalline structure of the obtained materials was performed using wide-angle X-ray scattering measurements (WAXS) by means of a computer controlled goniometer coupled to a sealed-tube source of CuK$_\alpha$ radiation (Philips), operating at 30 kV and 50 mA. The
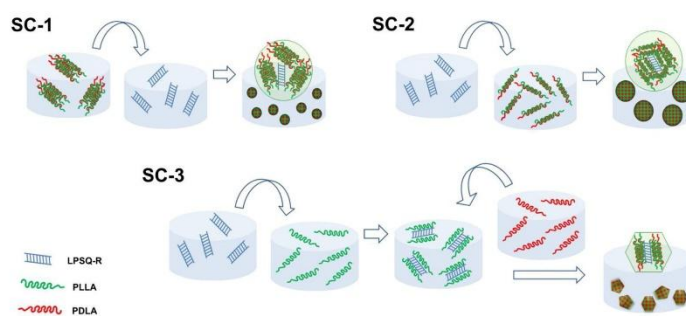
Scheme 2. Synthetic approach for the preparation of PLLA/PDLA/LPSQ-R hybrids (SC-1, SC-2 and SC-3).
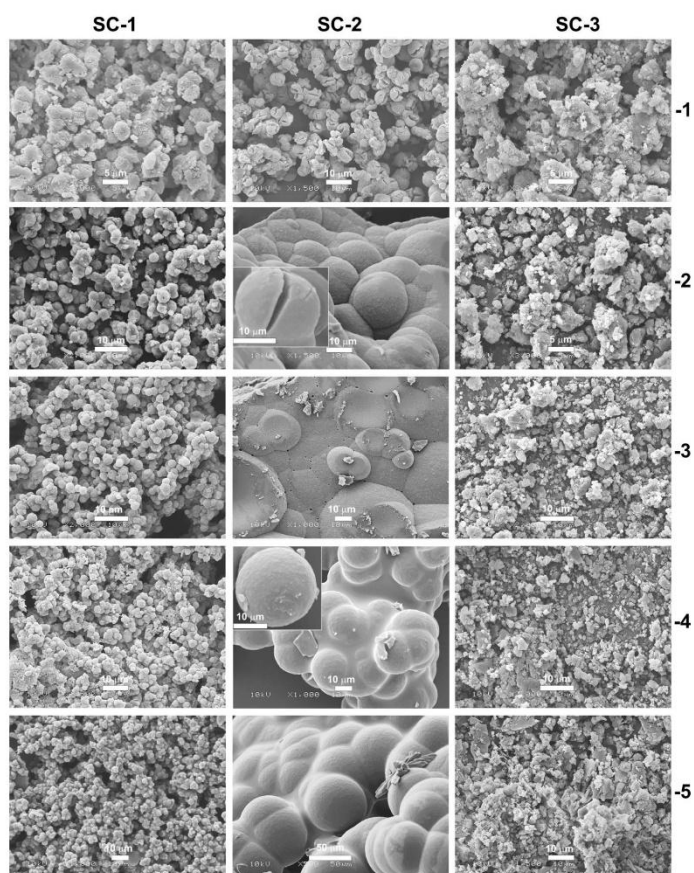
Fig. 1. SEM micrographs of particles formed during experiments SC-1 (left), SC-2 (middle) and SC-3 (right): (1) neat SC PLLA/PDLA and blends containing (2) LPSQ-OH, (3) LPSQ-(OH)2, (4) LPSQ-COOH and (5) LPSQ-COOMe.

CuK$_\alpha$ line was filtered using electronic filtering and the usual thin Ni filter. The data were collected at room temperature. The scans were preformed within the range of $2\theta = 5$ to $50°$ with a scanning step of $0.05°$.

3. Results and discussion

3.1. Preparation of PLLA/PDLA/LPSQ-R blends

The materials containing stereocomplexed PLLA/PDLA and LPSQ-R were prepared in solution. Parameters affecting the formation of SC structures are the mixing ratio ([R]/[La]) that represents the molar ratio of functional groups R to the total number of polyester segments, and the order of addition of the reaction mixture components (Table 1). The ratio of L-lactyl and D-lactyl units was equimolar, but the used solvents and the concentration of the mixture components varied between samples.

Three different experimental procedures were chosen to study the effect of the incorporation of LPSQ-R (Scheme 2). The first one (SC-1) was based on the addition of suspension containing preformed neat stereocomplex of PLLA and PDLA into solutions containing LPSQ-R. A smaller amount of PLLA/PDLA was admixed into the solution of LPSQ-(OH)2 due to the formation of a white precipitate that became well dispersed after prolonged stirring (30 min). The effect was not observed with other LPSQ-R.

The second procedure (SC-2) involved addition of LPSQ-R into freshly prepared clear solution of PLLA and PDLA (before the characteristic SC-turbidity appeared). The mixtures containing LPSQ-COOH, LPSQ-OH and LPSQ-(OH)2 became cloudy in a short time (less than 1 min after the addition of polysilsesquioxanes) and remained turbid on prolonged stirring. The effect was not observed for LPSQ-COOMe (for about 30 min) but the precipitate was formed on solvents evaporation.

In first step of the third procedure (SC-3) solutions of PLLA and LPSQ-R were mixed. The solutions were clear and fine turbidity appeared only in the mixture containing LPSQ-(OH)2. The solution
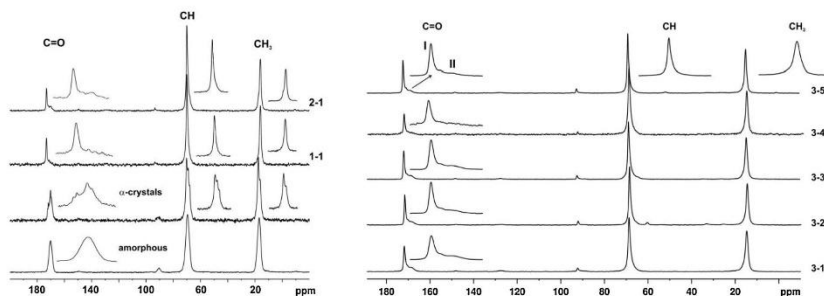
5

Fig. 2. ^{13}C NMR spectra of selected hybrid products and neat PLLA/PDLA compared to PLA containing α-type crystals and amorphous phase.

containing PDLA was added to the mixture of PLLA/LPSQ-R and pre-cipitation of SC occurred quite rapidly.

The morphology of precipitates formed during the free evaporation of solvents was studied with scanning electron microscopy (Fig. 1). The solvents composition played a significant role in the evolution of crystal structure, even in the absence of LPSQ-R. SC particles prepared in the medium containing high volume ratio of CH_2Cl_2 to THF (SC-2-1) are spherical ($\varphi = 2-8\,\mu m$) of rather high size polydispersity. A mixture of particles of spherical and irregular shape was obtained with larger amounts of THF (SC-1-1 and SC-3-1). The presence of LPSQ-R changed the structure of SC precipitates. The effect depended on the strength of hydrogen bonds formed between the functional groups R and the polyester backbone. Spherical crystals were obtained by procedure SC-1. Their size is similar to that of SC-1-1 ($\varphi = 2-4\,\mu m$), except for SC-1-3 containing LPSQ-(OH)2 that were somewhat smaller ($\varphi = 2-3\,\mu m$).

On the other hand, particles of PLLA/PDLA/LPSQ-R formed in experiments SC-3-(2–5) completely lack spherical structures that can be noticed among irregular particles in sample SC-3-1. Apparently, the interactions of PLLA chains with the side functional groups linked to the double siloxane backbone in the first step of procedure SC-3 hindered the typical growth of spherulitic SC crystals. A peculiar effect was observed in experiments carried out in medium with high content of CH_2Cl_2 [experiments SC-2-(2–5)]. Addition of LPSQ-R to the mixture of PLLA and PDLA resulted in the formation of large spherical objects ($\varphi = 20-50\,\mu m$), built of smaller microspheres ($\varphi = 2-10\,\mu m$) that coalesced during the solvents evaporation. In the case of PLLA/PDLA/LPSQ-(OH)2, the particles were rather planar and small pores could be seen on the surface. It was caused by the presence of MeOH that had to be used to dissolve the polar LPSQ-(OH)2. The large size of particles in experiments SC-2-(2–5) can be explained in terms of growth on LPSQ-R macromolecules added to the solution containing PLLA and PDLA before the critical size of SC particles was reached. Moreover, di-chloromethane is a better solvent for polylactides than for LPSQ-R which could result in micro-precipitation of the latter and growth of the SC layers on the micro-droplets of LPSQ-R.

3.2. NMR and WAXS analysis of PLLA/PDLA/LPSQ-R blends

^{13}C NMR spectroscopy can be an effective tool for identification of PLA crystals and tracing SC formation in PLLA/PDLA mixtures [20–22]. Different crystalline forms of polylactide (SC crystals of 3_1 helical conformation, α and α' 10_3 crystals) have characteristic resonance line shapes and splitting in their ^{13}C NMR spectra in solid state. Comparative analysis of ^{13}C NMR spectra recorded for SC-PLLA/PDLA/LPSQ-R, amorphous PLA and α-type PLA obtained after annealing at 393 K for 5 h proved that the presence of LPSQ-R did not disturb formation of stereocomplex structures (Fig. 2). Materials containing SC crystals exhibit a characteristic C=O signal at about 173.3 ppm (marked as **I**)
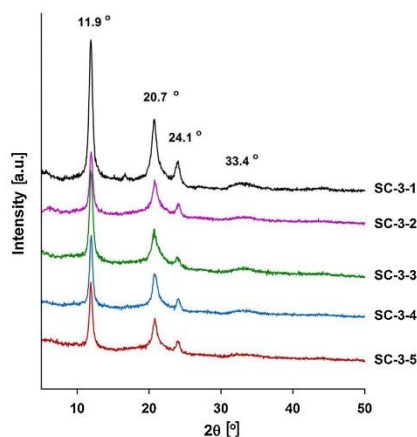

Fig. 3. X-ray diffractograms of selected PLLA/PDLA/LPSQ-R blends prepared following procedure SC-3.

which represents both SC chains in a rigid state and SC chains in a disordered state. The region corresponding to methine and methyl carbons is less sensitive. No specific resonance lines appear, but the signals shift to lower field. A decrease of the peak half width can be also observed.

Component analysis of the carbonyl carbon resonance line in ^{13}C CP MAS NMR spectra was carried out for the obtained PLLA/PDLA/LPSQ-R blends. The results revealed that despite the presence of substantial amounts of polysilsesquixanes, the spectra of all the obtained products are characteristic of polylactide SC. A broad resonance signal at 169.7 ppm (**II**) appeared as a shoulder to the main peak. It indicates contribution of a noncrystalline component of amorphous phase and can be related to the entrapment of PLA chains in the amorphous regions [22]. Polylactide chains in homo-crystalline regions should give a signal at 172.0 ppm [22]. Such a resonance line is present in the group of carbonyl resonances in SC 2-1 that is a mixture of PLLA and PDLA prepared in the solution containing high volume ratio of CH_2Cl_2. These results corroborate the data obtained from differential calorimetric analysis (part 3.3).

Wide-angle X-ray scattering profiles of the selected PLLA/PDLA/LPSQ-R blends are given in Fig. 3. Regardless of the sample, the main diffraction peaks appeared at 2θ values of 11.9°, 20.7° and 24.1°, which is characteristic of stereocomplexed PLLA/PDLA (a triclinic unit cell, in
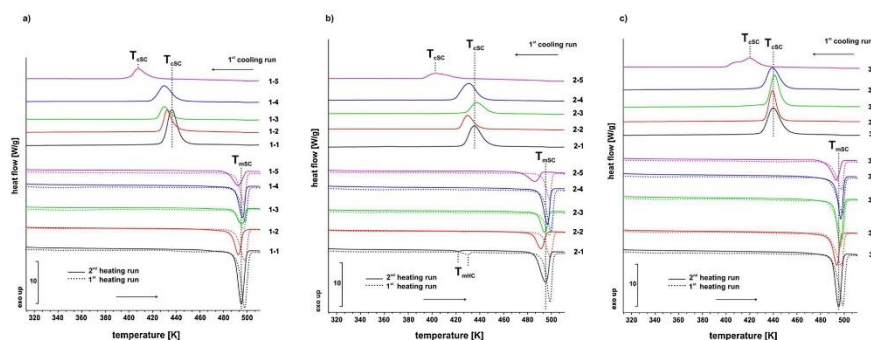
Fig. 4. DSC heating/cooling curves of SC PLLA/PDLA/LPSQ-R blends (10 K/min).
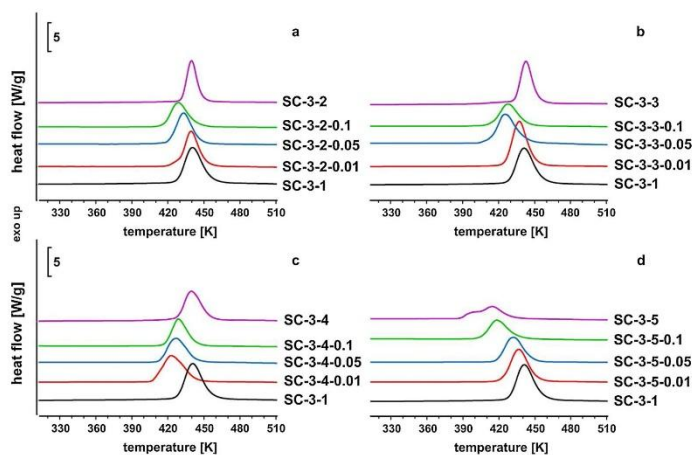

Fig. 5. Changes in T_{cSC} of PLLA/PDLA blends containing different amounts of LPSQ-R.

which L-lactide and D-lactide segments are packed parallel and have 3_1 helical conformation [3]). The diffractograms corroborate the trend observed for X_c values calculated from the corresponding DSC thermograms (Table ESI-1a).

3.3. Thermal characteristics of SC-hybrid materials

Differential scanning calorimetry (DSC) was used for analysis of the PLLA/PDLA/LPSQ-R blends. Their melting and crystallization behaviour was studied at temperature ramp of 10 °C/min. DSC heating and cooling curves for the blends of PLLA/PDLA with different LPSQ-R are presented in Fig. 4. No discernible glass transition was found for these materials, showing that the specific molecular packing and interchain interactions characteristic of SC are largely retained.

Various types of crystallites can be formed in a system containing L-chains and D-chains, including homocrystallites (HC) composed solely of L-chains or D-chains. Competitive formation of stereocomplexes and homocomplexes is more common for polylactide of high molecular weight [23]. The molecular mass of PLLA and PDLA samples used in the experiments was, respectively, 6400 and 7200 g/mol. Yet, a small

amount of HC ($X_{mHC} \sim 2\%$) was observed in the product SC-2-1 obtained from solution containing large amount of CH_2Cl_2. A small endotherm related to melting (~ 433 K) indicates the presence of HC built of PLLA or PDLA chains.

For all the studied samples a single characteristic high temperature melting point T_{mSC} (496–498 K) was observed, suggesting predominant formation of SC structures (Table ESI-1 a/b) in all the prepared blends, irrespectively of the synthetic procedure.

T_{cSC} recorded for the blends differ from the temperature of crystallization observed for neat PLLA/PDLA. In the case of smaller amounts of LPSQ-R that can form hydrogen bonds with carbonyl groups in polyester chains, the crystallization of stereocomplex structures in the melt is slightly delayed. For larger amounts of those LPSQ-R one can observe an increase of the T_{cSC} (Fig. 5). The stronger hydrogen bonds the sooner the effect was achieved. It should be stressed that the melting during the second heating run occurred within the same temperature range, for all types and amounts of LPSQ-R (Figure ESI-1, Table ESI-1a).

Templating with LPSQ-(OH)2 proved to be very effective (procedures SC-1 and SC-3) (Fig. 6 and ESI-2, Table ESI-1a/b). The
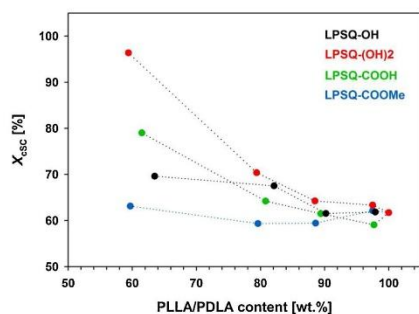
Fig. 6. Changes in X_{cSC} (DSC, 10 K/min, first cooling) of PLLA/PDLA blends containing different amounts of LPSQ-R (procedure SC-3, X_c corrected for neat polylactide).

enthalpy of melting (ΔH_m) and enthalpy of crystallization (ΔH_c) were used to calculate the degree of crystallinity in the blends. A significant improvement of X_{cSC} (corrected for the neat polylactide) was observed in SC-3-(2–4), both for the unprocessed precipitates as well as for the structures formed on cooling from melt (which was confirmed by ΔH_{mSC} during the second heating run). The order of effectiveness can be given as R: OH2 > COOH > OH > COOMe.

Similar dependencies were found for SC-1-(2–4) and SC-2-(2–4). The enthalpy of crystallization of PLLA/PDLA/LPSQ-R decreased with an increasing amount of the additive, yet the degree of crystallinity is significantly higher for hybrid blends containing LPSQ-R (R = OH, (OH)2, COOH) (Table ESI-1a).

However, the opposite effect was observed in the case of LPSQ-COOMe which, as an exception, reduced slightly the extent of stereo-complexation. T_{cSC} of all the blends containing this additive were lowered by about 20 K. The crystallization peak of SC-3-5 is bimodal (Fig. 5). This effect may be attributed to the lack of strong interactions between polylactide chains and LPSQ-COOMe. X_{cSC} decreased in blends containing larger amounts of this additive. Nevertheless, X_{cSC} in experiment SC-3-5 reached 63 %, which means that the weak C–H···O=C hydrogen bonds may also play a role in the templating.

3.4. Thermal stability of PLLA/PDLA/LPSQ-R blends

Thermal stability of the hybrid PLLA/PDLA/LPSQ-R blends was studied in N_2 atmosphere during heating at 10 K/min ramp (Figs. 7, 8, ESI-3) as well as under isothermal conditions (Fig. 9). Both, neat SC PLLA/PDLA and the hybrid blends generally decompose with one major step of weight decrease. However, the rate of weight loss (V_d) decreased on increasing the amount of LPSQ-R. Signifficant increase of both the 10 % weight loss temperature (T_{10}) and the peak temperature of weight loss (T_d) was observed (20−30 K depending on the amount and type of R). Results are given in Table 2. The effect is clear even for very small amounts of LPSQ-R and blends of ratio [R]/[La] ≤ 0.1 which decomposed at higher temperatures than the neat stereocomplex (Fig. 7).
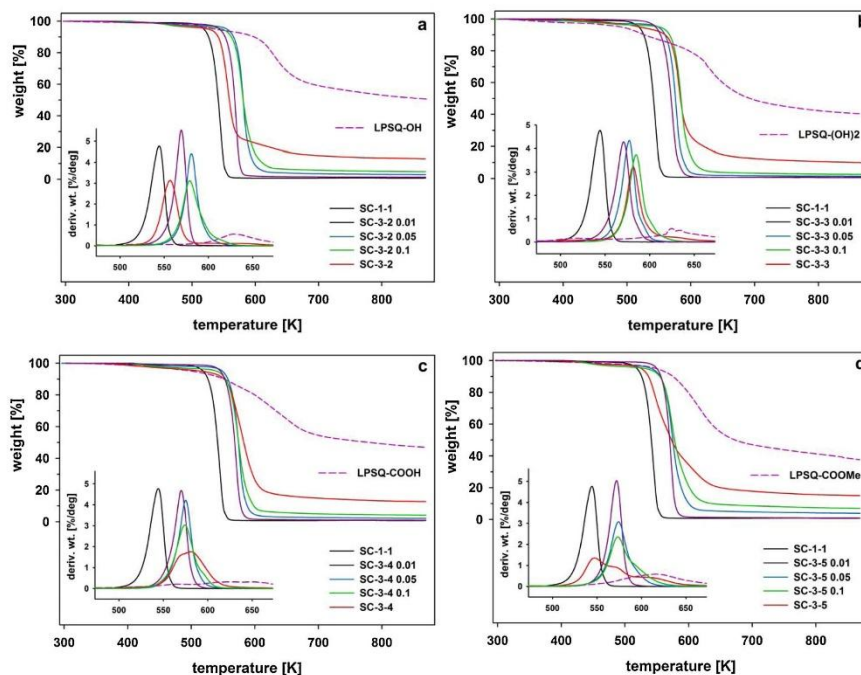

Fig. 7. Comparison of TGA traces recorded for SC-3 blends containing different amounts of LPSQ-OH (a), LPSQ(OH)2 (b), LPSQ-COOH (c) and LPSQ-COOMe (d) (N_2, 10 K/min).
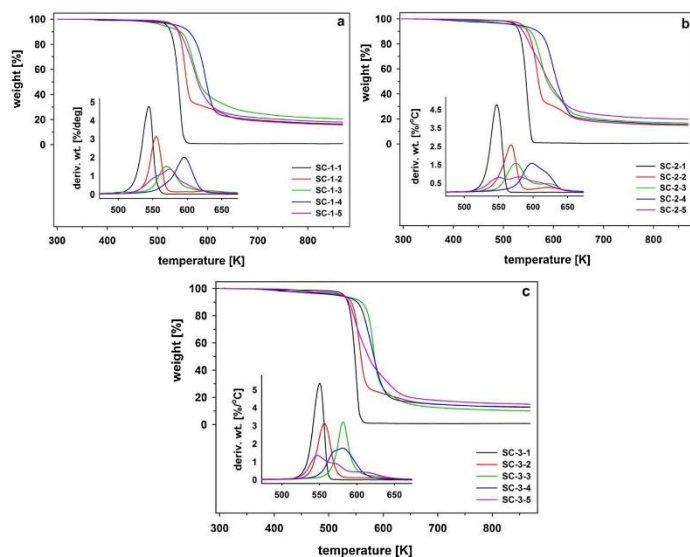
Fig. 8. Comparison of TGA traces recorded for SC-1 (a), SC-2 (b) and SC-3 (c) blends (N_2, 10 K/min).

Thermal stability of blends containing larger amounts of LPSQ-R ([R]/[La] > 0.2) was also high (Figs. 8 and ESI-3). The effect depends on the type of R and the strength of interactions with the polylactide matrix. No relation with the procedure of component mixing was noticed. Comparing to the blends with LPSQ-OH or LPSQ-COOMe, the

degradation of polylactide blends with poly(silsesquioxanes) bearing -COOH or -(OH)2 groups was shifted to higher temperatures, but took place at similar degradation rate V_d.

The used functionalized polysilsesquioxanes are very viscous liquids ($T_g < 263$ K) of good thermal stability both in atmosphere of nitrogen
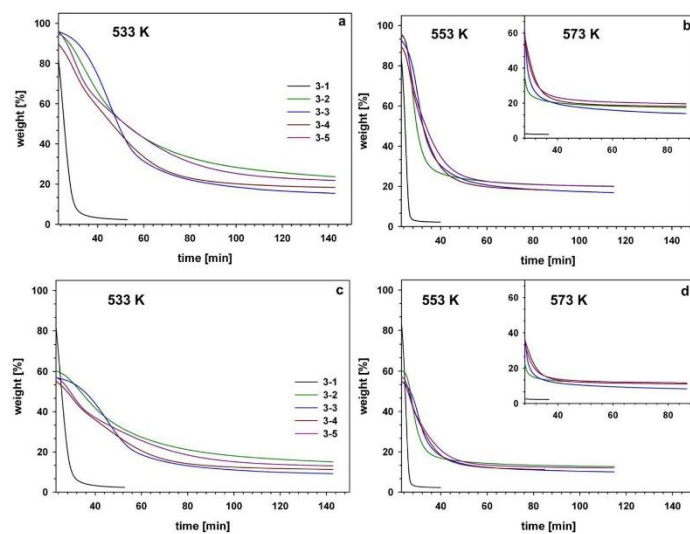

Fig. 9. Degradation of SC-3-(1-5) under isothermal conditions (533 K, 553 K and 573 K); a,b – thermograms of the prepared blends, c,d – thermograms corrected for neat PLLA/PDLA.

Table 3
Assignment of IR bands in amorphous and SC PLA, and functionalized LPSQ-R.

| PLA/PDLA			LPSQ-R				
Vibration mode [cm⁻¹]	amorphous	β-SC	Vibration mode [cm⁻¹]	LPSQ-OH	LPSQ-(OH)2	LPSQ−COOH	LPSQ-COOMe
			ν(OH) (broad band)	3300	3300	3300	–
ν(C-H)	3000-2880	3000-2880	ν(C-H)	2950-2850	2950-2860	2900-2650	2950-2900
ν(C=O)	1751	1746	ν(C=O)	–	–	1700	1734
δ_{as}(CH₃)	1454	1455	δ(OH) in-plane	1410	1409	1417	–
δ_s(CH₃)	1380	1382	δ_{as}(CH₃)	1409	1409	1409	1436
							1412
δ_s(CH₃) + δ(CH)	1361	1367	ν(C-O)	1277	1281	1282	1283
ν_{as}(COC) + τ_{as}(CH₃)	1261	1215	δ_s(Si-CH₃)₃	1254	1254	1253	1254
	1189	1187					
τ_{as}(CH₃)	1132	1130	δ(Si-CH₂)	1180	1179	1181	1182
ν_s(COC)	1085	1087	ν_{as}(SiOSi)	1123	1088	1123	1127
ν(C-CH₃)	1044	1039	ν_s(SiOSi)	1065	1061	1095	1046
				1026	1025	1040	1012
τ(CH₃) + ν(C-COO)	950	954	ν(OH) out-of-plane	944	925	842	–
		908 (β)					
ν(C-COO)	864	875	ρ(Si-CH₃)	758	784	780	800

ν, δ, τ – stretching, bending, rocking modes [asymmetric (as), symmetric (s)].

and air [24]. Comparison of their thermal decomposition as neat materials and after blending with PLLA/PDLA suggests that all the components in the blend may be involved in the major process of sample degradation. It is therefore postulated that thermal degradation of PLLA/PDLA/LPSQ-R blends proceeds through transestrification reactions between LPSQ-R and polylactide chains and subsequent crosslinking of the PLLA/PDLA matrix. Such transestrification may take place for all types of functional groups: −COOH, −OH and also −COOMe. However, the process seems to be slower for LPSQ-COOMe and decomposition of the PLLA/PDLA/LPSQ-COOMe blend ([R]/[La] = 0.26) occurred within a wider temperature range. The shape of the curve representing changes in the weight loss derivative for SC-1-5, SC-2-5 and SC-3-5 suggests that in fact several subsequent processes may occurr during the decomposition of these samples.

Studies on thermal resistance of PLLA/PDLA/LPSQ-R blends under isothermal conditions were carried out for materials prepared following procedure SC-3 ([R]/[La] = 0.26). The hybrid blends were much more stable than neat SC PLLA/PDLA (Fig. 9a–b). The rate of their weigh decrease under the applied conditions is clearly much lower than that of PLLA/PDLA blend. At 533 K the neat SC decomposed almost completely (depolymerization) within 20 min, whereas 60 % weight reduction of the compositions with poly(silsesquioxanes) required 50 min. A similar trend was observed at 553 K despite the faster decomposition. At 573 K polylactide blend completely evaporated but it took almost 30 min before the weight of hybrid blends residue reached a constant level. The effect is retained in thermograms corrected for the content of neat polylactide (Fig. 9c–d).

3.5. FTIR studies on the formation of 3₁ helical structures in PLLA/PDLA/ LPSQ-R blends

Evolution of the stereocomplex structure in PLLA/PDLA and PLLA/PDLA/LPSQ-R blends was studied with FTIR spectroscopy during their isothermal crystallization at 448 K. IR signals were assigned (Table 3) according to the literature data [22]. Changes in peak shapes and positions were observed upon stereocomplexation of polylactide chains in all the studied samples. Polylactide SC crystals of triclinic unit cell packed by one PLLA and PDLA chain both have 3₁ β-helical conformation and exhibit specific IR band frequencies and correlation field splitting [21,22,25]. Weak C−H···O=C hydrogen bonds and dipolar interactions bind PLLA and PDLA chains in SC structures. The interactions may occur in the melt and are the driving force for SC nucleation [26,27]. As a consequence, low-frequency shifts of stretching vibration
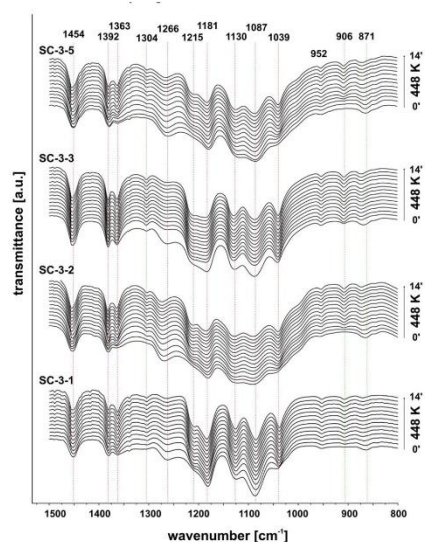
Fig. 10. FTIR spectra (1500–800 cm⁻¹) of hybrid stereocomplexes recorded during isothermal crystallization at 448 K.

modes ν_{as}(CH₃) and ν(C=O) modes with respect to the α-crystals and amorphous materials take place [22]. At room temperature, the vibration modes characteristic of SC β-helix can be found at about 908 cm⁻¹ [τ(CH₃) + ν(C−COO)]. The same mode in homocrystals of PLLA or PDLA (α-helix structure 10₃) is close to 920 cm⁻¹.

The influence of the hybrid silsesquioxane additives was evaluated by the comparison of the intensity of some specific IR modes (Fig. 10). It should be noted that the bending δ_{as}(CH₃) (1455 cm⁻¹) and δ_s(CH₃) (1382 cm⁻¹) modes did not change over the entire time of annealing, which points at rather good stability of samples at high temperature. Intensity of the former vibration mode was used for normalization of
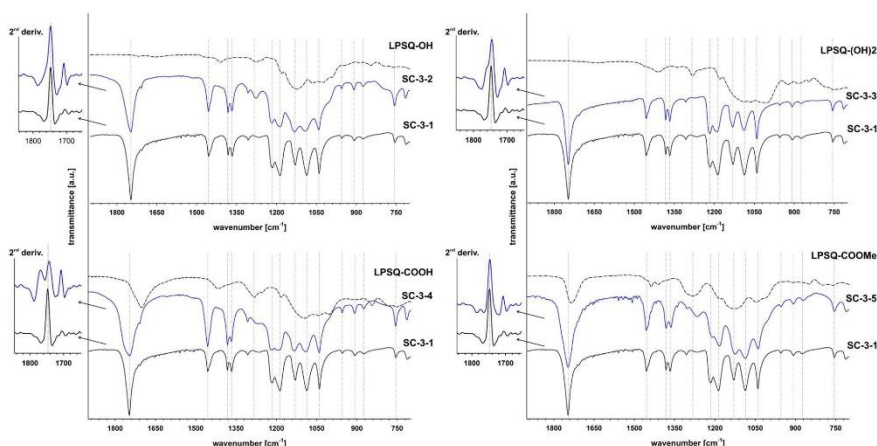
Fig. 11. Comparison of FTIR spectra of SC-3-1, hybrid SC-3-(2-5) (samples crystallized for 30 min at 448 K from melt and cooled to room temperature) and LPSQ-R (thin films). Insets show second derivatives of respective ν(C=O) vibration modes.

the spectra. Isothermal treatment at 523 K for 5 min was required for clearing up all SC crystallites (β-helix vibration mode disappeared). The melted specimens were cooled down to 448 K. Some vibration modes of low intensity in the spectra of amorphous samples become larger on the annealing. The β-helix crystals were formed at different rate in the neat SC-3-1 and hybrid SC-3-(2–5). In sample SC-3-1 the structures appeared after 2 min.

The change of intensity ratio between spectrum components [ν_{as}(COC) + τ_{as}(CH$_3$) at 1215 and 1187 cm^{-1}; τ_{as}(CH$_3$) (1130 cm^{-1}), ν_s (COC) (1087 cm^{-1}) and ν(C-CH$_3$) (1039 cm^{-1})] illustrates adjustment of polymer chains in the formed SC crystals. Intensity of vibration modes δ_s(CH$_3$) + δ(CH) (1367 cm^{-1}) in SC-3-1 depended on the amount of β-helix structures, and was comparable to that of δ_s(CH$_3$) band at 1382 cm^{-1}. The rate of its increase is clearly larger than that of ν_{as}(COC) + τ_{as}(CH$_3$) at 1215 cm^{-1}. This observation corroborates the literature data [3]. In hybrid SC the intensity of δ_s(CH$_3$) + δ(CH) at the beginning of crystallization was lower and the band increased slowly as the crystallization progressed. However, the ester vibration at 1215 cm^{-1} seem to increase more rapidly than for SC-3-1. It suggests an influence of the functionalized silsesquioxanes on the segmental movement in polylactide chains, and may be related to the formation of hydrogen bonds between LPSQ-R and PLLA/PDLA.

A very interesting case is SC-3-3 [PLLA/PDLA/LPSQ-(OH)2]. This sample crystallized rapidly and the vibration modes at 1382 cm^{-1} and 1215 cm^{-1} are strong even at early stages of the process. In the case of its monohydroxy analogue (LPSQ-OH in SC-3-2), the increase of the respective bands (especially the one at 1215 cm^{-1}) is slower. For SC-3-4 and SC-3-5 the evolution of the band is delayed. Surprisingly, formation of β-helix seems to be more effective in the case of LPSQ-COOMe (SC-3-5) than LPSQ–COOH (SC-3-4). The effect can be related to plastification of the PLLA/PDLA by LPSQ-COOMe, that can be only a donor/acceptor of weak C–H···O=C hydrogen bonds, as indicated by slow increase of 1215 cm^{-1} band. Nevertheless, the effect of LPSQ-R on the structure of SC observed after cooling the annealed samples down to room temperature (Fig. 11), can be corelated with the phenomena shown in DSC traces. Intensity of the ν_{as}(COC) + τ_{as}(CH$_3$) mode (1215 cm^{-1}) in SC-3-5 is weak, in comparison with other samples.

We have also studied the relative change of the position of ν(C=O) band and the number of its components in the second derivative spectra (insets in Fig. 11). Hydrogen bonding to C=O groups should result in

low-frequency shifts of the stretching vibration mode ν(C=O). Yet, low-frequency shifts of ν(C=O) in comparison to amorphous PLA also indicate the presence of weak hydrogen bonds between C–H and O=C in SC crystals. Only one main component was present in the second derivative of ν(C=O) in SC-3-1. The structure of 2nd derivative of ν(C=O) in hybrid SC is more complex. The stretching vibrations of C=O group in samples SC-3-2 and SC-3-3 are composed of two overlapping modes (a shoulder and the main SC peak) and accompanied by a small satellite peak at higher frequencies. The intensity of the shoulder is roughly twice as large for LPSQ-(OH)2 as for LPSQ–OH. It suggests that the band may be related to the C=O groups linked with hydrogen bonds donating –OH groups. For SC-3-4 containing LPSQ–COOH the stretching mode ν(C=O) is composed of a set of peaks and all of them are shifted with respect to the ν(C=O) of neat SC. The satellite peak is higher in SC-3-(2–4) due to the overlapping with ν(C=O) of LPSQ–COOH. No shoulder can be observed in the case of SC-3-5, and the main peak is only slightly broadened. It can be linked to the structural similarity of carbonyl groups in lactide segments and –COOMe groups.

4. Conclusions

Addition of functionalized oligomeric ladder silsesquioxanes LPSQ-R (R = COOH, COOMe, OH, (OH)2) to the mixture of poly(L-lactide) and poly(D-lactide) resulted in formation of stereocomplex materials of increased thermal stability. LPSQ-R changed the SC formation process, both during precipitation from solutions and crystallization from melt. The degree of crystallinity of neat polylactide in the hybrid blends was larger than that of SC PLLA/PDLA. Stereocomplexation of PLLA and PDLA chains was not disturbed even in the presence of substantial amounts of polysilsesquioxane additives. In some cases, LPSQ-R exerted a templating effect. The difference can be related to the structure of hydrogen bonds donating/accepting side groups, the type of interactions between functional groups PLA and the experimental procedure. Hybrid blends of PLLA/PDLA and LPSQ-R exhibited increased thermal stability both during isothermal annealing and at 10 K/min ramp. A significant increase of T$_{10}$ (20 – 30 K) was observed, even at very low amount of additives, and V$_d$ decreased linearly on increasing the amounts of LPSQ-R. The results suggest also incorporation of LPSQ-R into the polylactide matrix at high temperatures.

11

CRediT authorship contribution statement

Agata S. Herc: Investigation. **Piotr Lewiński:** Investigation, Writing - review & editing. **Sławomir Kaźmierski:** Investigation, Writing - review & editing. **Joanna Bojda:** Investigation. **Anna Kowalewska:** Conceptualization, Methodology, Supervision, Data curation, Writing - original draft, Writing - review & editing, Funding acquisition.

Declaration of Competing Interest

The authors declare that they have no known competing financial interests or personal relationships that could have appeared to influence the work reported in this paper.

Acknowledgement

Appendix A. Supplementary data

Supplementary material related to this article can be found, in the online version, at doi:https://doi.org/10.1016/j.tca.2020.178592.

References

[1] V. Nagarajan, A.K. Mohanty, M. Misra, Perspective on polylactic acid (PLA) based sustainable materials for durable applications: focus on toughness and heat resistance, ACS Sustain. Chem. Eng. 4 (2016) 2899–2918, https://doi.org/10.1021/acssuschemeng.6b00321.

[2] K. Masutani, Y. Kimura, Present situation and future perspectives of poly(lactic acid), Adv. Polym. Sci. 279 (2018) 1–26, https://doi.org/10.1007/12_2016_16.

[3] H. Tsuji, Poly(lactide) stereocomplexes: formation, structure, properties, degradation, and applications, Macromol. Biosci. 5 (2005) 569–597, https://doi.org/10.1002/mabi.200500062.

[4] M. Hirata, Y. Kimura, Structure and properties of stereocomplex-type poly(lactic acid). Chapter 5 in Poly(lactic acid): Synthesis, structures, properties, processing, and applications, in: R.A. Auras, L.-T. Lim, S.E.M. Selke, H. Tsuji (Eds.), RSC, 2011.

[5] H. Tsuji, Poly(lactic acid) stereocomplexes: a decade of progress, Adv. Drug Deliv. Rev. 107 (2016) 97–135, https://doi.org/10.1016/j.addr.2016.04.017.

[6] H. Tsuji, I. Fukui, Enhanced thermal stability of poly(lactide)s in the melt by enantiomeric polymer blending, Polymer 44 (2003) 2891–2896, https://doi.org/10.1016/S0032-3861(03)00175-7.

[7] H. Ajiro, Y.-J. Hsiao, T.H. Thi, T. Fujiwara, M. Akashi, A stereocomplex of poly (lactide)s with chain end modification: simultaneous resistances to melting and thermal decomposition, Chem. Commun. 48 (2012) 8478–8480, https://doi.org/10.1039/C2CC33589A.

[8] T.M. Quynh, H. Mitomo, L. Zhao, M. Tamada, Properties of a poly(L-lactic acid)/poly(D-lactic acid) stereocomplex and the stereocomplex crosslinked with triallyl isocyanurate by irradiation, J. Appl. Polym. Sci. 110 (2008) 2358–2365, https://doi.org/10.1002/app.28269.

[9] T.M. Quynh, H. Mitomo, M. Yoneyama, N.Q. Hien, Properties of radiation-induced crosslinking stereocomplexes derived from poly(L-lactide) and different poly(D-lactide), Polym. Eng. Sci. 49 (2009) 970–976, https://doi.org/10.1002/pen.21309.

[10] T.M. Quynh, H.H. Mai, P.N. Lan, Stereocomplexation of low molecular weight poly (L-lactic acid) and high molecular weight poly(D-lactic acid), radiation crosslinking PLLA/PDLA stereocomplexes and their characterization, Radiat. Phys. Chem. 83 (2013) 105–110, https://doi.org/10.1016/j.radphyschem.2012.10.002.

[11] H. Bai, H. Liu, D. Bai, Q. Zhang, K. Wang, H. Deng, F. Chen, Q. Fu, Enhancing the melt stability of polylactide stereocomplexes using a solid-state cross-linking strategy during a melt-blending process, Polym. Chem. 5 (2014) 5985–5993, https://doi.org/10.1039/C4PY00700J.

[12] A. Kowalewska, M. Nowacka, A. Tracz, T. Makowski, Supramolecular self-assembly of linear oligosilsesquioxanes on mica-AFM surface imaging and hydrophilicity studies, Soft Matter 11 (2015) 4818–4829, https://doi.org/10.1039/c5sm00787a.

[13] A.S. Herc, M. Włodarska, M. Nowacka, J. Bojda, W. Szymański, A. Kowalewska, Supramolecular interactions between polylactide and model cyclosiloxanes with hydrogen bonding-capable functional groups, eXPRESS Polym. Lett 14 (2020) 134–153, https://doi.org/10.3144/expresspolymlett.2020.12.

[14] A. Kowalewska, M. Nowacka, Synthesis of ladder silsesquioxanes by in situ polycondensation of cyclic tetravinylsiloxanetetraols, Silicon 7 (2015) 133–146, https://doi.org/10.1007/s12633-014-9209-z.

[15] W.L.F. Armarego, Ch.L.L. Chai, Purification of Laboratory Chemicals, Butterworth-Heinemann, Bodmin, 2003, https://doi.org/10.1016/B978-0-7506-7571-0.X5000-5.

[16] C.R. Morcombe, K.W. Zilm, Chemical shift referencing in MAS solid state NMR, J. Magn. Reson. 162 (2003) 479–486, https://doi.org/10.1016/s1090-7807(03)00082-x.

[17] B.M. Fung, A.K. Khitrin, K. Ermolaev, An improved broadband decoupling sequence for liquid crystals and solids, J. Magn. Reson. 142 (2000) 97–101, https://doi.org/10.1006/jmre.1999.1896.

[18] D. Sawai, Y. Tsugane, M. Tamada, T. Kanamoto, M. Sungil, S.-H. Hyon, Crystal density and heat of fusion for a stereo-complex of poly(L-lactic acid) and poly (D-lactic acid), J. Polym. Sci. Part B 45 (2007) 2632–2639, https://doi.org/10.1002/polb.21270.

[19] E.W. Fischer, H.J. Sterzel, G. Wegner, Investigation of the structure of solution grown crystals of lactide copolymers by means of chemical reaction, Kolloid Z. Z. Polym. 251 (1973) 980–990, https://doi.org/10.1007/BF01498927.

[20] H. Tsuji, F. Horii, M. Nakagawa, Y. Ikada, H. Odani, R. Kitamaru, Stereocomplex formation between enantiomeric poly(lactic acid)s. 7. Phase structure of the stereocomplex crystallized from a dilute acetonitrile solution as studied by high-resolution solid-state ^{13}C NMR spectroscopy, Macromolecules 25 (1992) 4114–4118, https://doi.org/10.1021/ma00042a011.

[21] G. Kister, G. Cassanas, M. Vert, Effects of morphology, conformation and configuration on the IR and Raman spectra of various poly(lactic acid)s, Polymer 39 (1998) 267–273, https://doi.org/10.1016/S0032-3861(97)00229-2.

[22] P. Pan, J. Yang, G. Shan, Y. Bao, Z. Weng, A. Cao, K. Yazawa, Y. Inoue, Temperature-variable FTIR and solid-state ^{13}C NMR investigations on crystalline structure and molecular dynamics of polymorphic poly(L-lactide) and poly(L-lactide)/poly(D-lactide) stereocomplex, Macromolecules 45 (2012) 189–197, https://doi.org/10.1021/ma201906a.

[23] H. Bai, S. Deng, D. Bai, Q. Zhang, Q. Fu, Recent advances in processing of stereocomplex-type polylactide, Macromol. Rapid Commun. 38 (2017) 1700454, , https://doi.org/10.1002/marc.201700454.

[24] A.S. Herc, J. Bojda, M. Nowacka, P. Lewiński, W. Maniukiewicz, E. Piórkowska, A. Kowalewska, Crystallization, Structure and Properties of Polylactide/Poly (Silsesquioxane) Blends, (2020) (submitted).

[25] M. Brzeziński, T. Biela, Stereocomplexed polylactides. Encyclopedia of Polymeric Nanomaterials, Springer-Verlag Berlin Heidelberg, 2015, https://doi.org/10.1007/978-3-642-36199-9_394-1.

[26] J. Zhang, H. Sato, H. Tsuji, I. Noda, Y. Ozaki, Infrared spectroscopic study of CH$_3$–O = C interaction during poly(L-lactide)/poly(D-lactide) stereocomplex formation, Macromolecules 38 (2005) 1822–1828, https://doi.org/10.1021/ma047872w.

[27] J. Zhang, H. Sato, H. Tsuji, I. Noda, Y. Ozaki, Differences in the CH$_3$···O = C interactions among poly(l-lactide), poly(l-lactide)/poly(d-lactide) stereocomplex, and poly(3-hydroxybutyrate) studied by infrared spectroscopy, J. Mol. Struct. 735 (2005) 249–257, https://doi.org/10.1016/j.molstruc.2004.11.033.

Hybrid SC-polylactide/poly(silsesquioxane) blends of improved thermal stability.

Electronic Supporting Information

Contents:

1. Synthesis of LPSQ-R:

A mercapto-derivative was added to the solution of LPSQ-Vi in dry THF (containing LPSQ-Vi at 8% wt), placed in a quartz crucible ($[HS]_0/[Vi]_0 = 1.4$). DMPA was added with stirring to the solution of reagents ($[Vi]_0/[DMPA]_0 = 50$). The mixture was irradiated for 15 min with UV light ($\lambda = 365$ nm). ^{1}H NMR analysis of the products thus prepared showed complete conversion of the vinyl groups in LPSQ-Vi. Volatiles were then removed under reduced pressure and the residue was dissolved in a small amount of a good solvent [THF or MeOH in the case of LPSQ-(OH)2] and precipitated into a large amount of hexane/ethyl acetate (1: 1 v/v). The purification procedure was repeated twice. The precipitate was dried under high vacuum at room temperature to the constant weight and characterized with ^{1}H, ^{13}C and ^{29}Si NMR spectroscopy. The spectra were recorded on a Bruker DRX-500 MHz spectrometer using THF-d8 or CD_3OD as the deuterated solvents. Assignment of ^{1}H and ^{13}C resonance lines of LPSQ-OH and LPSQ-(OH)2 was carried out using ^{1}H-^{13}C heteronuclear single quantum correlation (HSQC) and ^{1}H-^{1}H correlation spectroscopy (COSY) techniques.

LPSQ-OH (poly[2-(hydroxyethylthio)-ethylsilsesquioxane]) (Y = 76%)

^{1}H NMR δ [ppm] (CD_3OD): 0.16 (s. $OSiMe_3$), 1.03 (m. $SiCH_2$), 2.67 (m. CH_2S), 2.67 (m. SCH_2), 3.68 (m. CH_2OH)

^{13}C NMR δ [ppm] (THF-d8): 1.05 ($OSiMe_3$), 14.0 (m. $SiCH_2$), 26.3 (CH_2S), 34.2 (m. SCH_2), 61.6 (CH_2OH)

^{29}Si NMR δ [ppm] (CD_3OD): -70.3 ($-CH_2SiO_{3/2}$), 10.7 ($OSiMe_3$)

1

'H-'H COSY LPSQ-OH

'H-¹³C HSQC LPSQ-OH
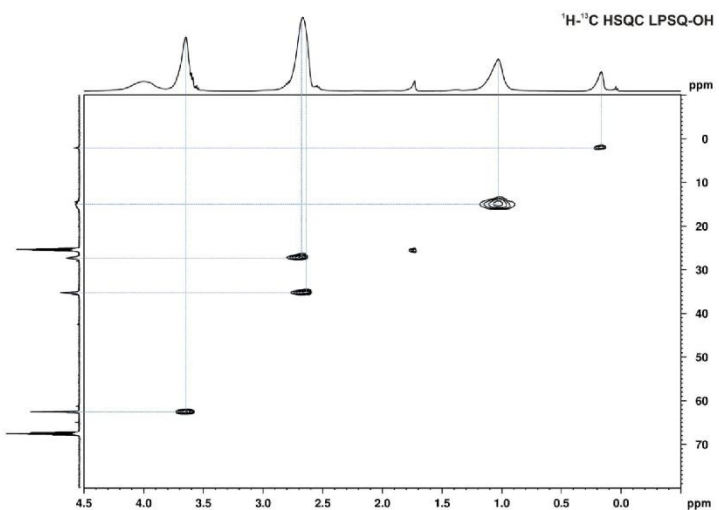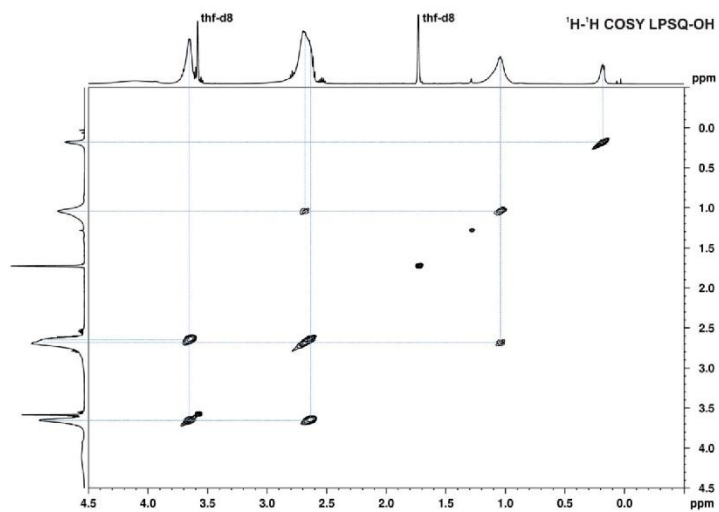
LPSQ-(OH)2 (poly[2-(propane-1,2-diol)-ethylsilsesquioxane) (Y = 82%)

^{1}H NMR δ [ppm] (CD$_3$OD): 0.15 (s. OSiMe$_3$), 1.03 (m. SiCH$_2$), 2.59 (m. CH$_2$S), 2.69 (m. SCH$_2$), 3.75 (m. CHOH), 3.57 (m. CH$_2$OH)

^{13}C NMR δ [ppm] (CD$_3$OD): 0.9 (OSiMe$_3$), 13.0 (m. SiCH$_2$), 26.7 (CH$_2$S), 34.9 (m. SCH$_2$), 71.4 (CHOH), 64.7 (CH$_2$OH)

^{29}Si NMR δ [ppm] (CD$_3$OD): -70.2 (-CH$_2$SiO$_{3/2}$), 10.9 (OSiMe$_3$)

2

¹H-¹H COSY LPSQ-(OH)2
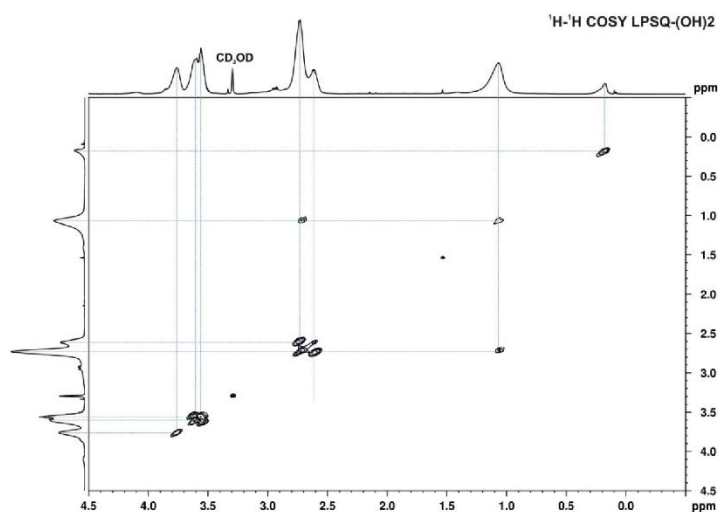
LPSQ-COOMe (poly[2-(methylthioglycolate)-ethylsilsesquioxane]) (91%)

¹H NMR δ [ppm] (THF-d8): 0.16 (s. OSiMe₃), 1.06 (m. SiCH₂), 2.77 (m. CH₂S), 3.25 (m. SCH₂), 3.65 (s. OCH₃)

¹³C NMR δ [ppm] (THF-d8): 0.97 (OSiMe₃), 13.3 (SiCH₂), 26.6 (CH₂S), 32.3 (SCH₂), 51.4 (OCH₃), 170.3 (COO)

²⁹Si NMR δ [ppm] (THF-d8): -70.4 (-CH₂SiO₃/₂), 10.5 (OSiMe₃)

LPSQ-COOH (poly[2-(carboxymethylothio)-ethylsilsesquioxane]) (98%)

¹H NMR δ [ppm] (THF-d8): 0.17 (s. OSiMe₃), 1.08 (m. SiCH₂), 2.79 (CH₂S), 3.20 (m. SCH₂), 8.30 (COOH)

¹³C NMR δ [ppm] (CD₃OD): -0.5 (OSiMe₃), 11.4 (SiCH₂), 25.3 (CH₂S), 31.6 (SCH₂), 170.9 (COOH)

²⁹Si NMR δ [ppm] (CD₃OD): −70.4 (-CH₂SiO₃/₂), 10.9 (OSiMe₃)

2. Synthesis of poly(L-lactide) and poly(D-lactide)

L-lactide (L-LA) and D-lactide (D-LA) (Boehringer-Ingelheim, Germany) were crystallized from dry 2-propanol (analytical grade, Chempur, Poland; distilled from over sodium metal chips), sublimed in vacuum, distributed into glass ampoules with break-seals, dried and sealed off. Tin (2-ethylhexanoate) Sn(Oct)₂ (95%, Aldrich, USA) was first distilled (10⁻³ mbar, 413 K) into a glass ampoule with Rotaflo® stopcock. Next a portion of the catalyst was transferred in vacuum into a heart-shaped flask and distilled (also in vacuum) into glass ampoules with break-seals. Benzyl alcohol (BnzOH) (analytical grade, POCH, Poland) was first distilled under atmospheric pressure, and then on

3

the high vacuum line (at 10^{-3} mbar) into glass ampoules with break-seals. Tetrahydrofuran (POCH, Poland) was kept for several days over KOH, fractionally distilled from sodium metal chips. Next it was again kept over KOH, distilled from sodium metal chips and then distilled in vacuum into glass ampoule with sodium/potassium alloy. Just before use it was distilled in vacuum into the reaction vessel.

The polymerizations were conducted in custom made glass vessels with a polarimetric cell, and three arms with break-seals containing BnzOH (0.1079 g, $1 \cdot 10^{-3}$ mol), L-LA or D-LA (5.9804 g, 0.04 mol) and $Sn(Oct)_2$ (0.2021 g, $5 \cdot 10^{-4}$ mol) attached. The vessels were then connected to high-vac line and THF (36.8 ml) was distilled (in vacuum). Afterwards the vessels were sealed off. After the break-seals were broken and the reagents were mixed at a room temperature, the vessels were placed in 353 K and heated till conversion reached approx. 92%. The PLA samples were isolated by the precipitation into the cold methanol (420 ml; analytical grade, Chempur, Poland; used as received) and filtration. The samples were subsequently washed with cold methanol and dried to a constant weight. PLLA and PDLA were characterized by ^{1}H and ^{13}C NMR spectroscopy in $CDCl_3$ using a Bruker DRX-500 MHz spectrometer. Weight average molar masses of PLLA and PDLA were determined by size-exclusion chromatography (SEC) with a multi-angle laser light scattering (MALLS) detector in CH_2Cl_2 as a mobile phase at a flow rate of $0.8 \, cm^3 \cdot min^{-1}$, using a SEC-MALS instrument composed of an Agilent 1100 isocratic pump, an auto-sampler, a degasser, a thermostatic box for two PLGel 5-μm MIXD-C columns, a MALS DAWN HELEOS photometer Wyatt Technology Corporation, and an Optilab T-rEX differential refractometer Wyatt Technology Corporation. The measurements were conducted at room temperature and normalization was performed using a polystyrene standard ($M_n = 30,000$ g/mol). The dn/dc increment of the refractive index was 0.035.

SEC:

PLLA   RI: M_n = 9300, M_w = 10600 M_w/M_n = 1.14; MALLS: M_n = 4500, M_w = 6400 M_w/M_n = 1.42

PDLA   RI: M_n = 9100, M_w = 10400, M_w/M_n = 1.14; MALLS: M_n = 5300, M_w = 7200, M_w/M_n = 1.36

4

Table ESI-1a. Thermal characteristics of PLLA/PDLA/LPSQ-R blends – stereocomplex structures (DSC, 10 K/min).

sample	[R]/[La]	wt.%	1st heating			1st cooling			2nd heating		
			T_{msc} [K]	ΔH_{msc} [J/g]	$X_{c\text{-}msc}$ [%]	T_{csc} [K]	ΔH_{csc} [J/g]	$X_{c\text{-}csc}$ [%]	T_{msc} [K]	ΔH_{msc} [J/g]	$X_{c\text{-}msc}$ [%]
SC-1-1	0	100.0	498.3	95.6	61.7	436.4	95.6	61.7	495.5	95.6	61.7
SC-1-2	0.25	64.7	498.4	67.0	66.8	432.4	61.0	60.8	493.0	60.6	60.4
SC-1-3	0.50	43.6	497.4	49.5	73.3	430.3	47.7	70.6	495.9	47.7	70.6
SC-1-4	0.25	63.4	498.8	67.9	69.1	429.9	64.8	65.9	496.5	64.3	65.4
SC-1-5	0.25	61.1	498.0	63.9	67.5	408.1	45.8	48.4	492.9	45.8	48.4
SC-2-1	0	100.0	498.9	87.0	56.1	435.3	83.7	54.0	495.1	82.5	53.2
SC-2-2	0.50	47.9	498.9	56.3	75.8	429.5	48.4	65.2	491.1	48.1	64.8
SC-2-3	0.50	43.6	498.2	50.6	74.9	437.3	52.4	77.5	494.1	52.3	77.4
SC-2-4	0.50	45.8	499.7	69.1	97.4	430.8	62.3	87.8	496.7	61.4	86.5
SC-2-5	0.50	43.8	498.5	51.6	76.0	402.5	36.9	54.4	486.3	36.4	53.6
SC-3-1	0	100.0	499.1	93.8	60.5	440.1	95.6	61.7	495.4	95.2	61.4
SC-3-2-0.01	0.01	97.9	499.3	91.8	60.5	439.3	93.8	61.8	497.3	93.4	61.6
SC-3-2-0.05	0.05	90.2	499.1	84.4	60.4	434.6	86.0	61.5	496.9	85.8	61.4
SC-3-2-0.1	0.10	82.1	498.5	87.2	68.5	431.4	85.9	67.5	495.9	85.4	67.1
SC-3-2	0.26	63.5	497.6	73.9	75.1	439.4	68.5	69.6	494.0	68.2	69.3
SC-3-3-0.01	0.01	97.5	499.0	93.1	61.6	437.1	95.7	63.3	496.5	95.8	63.4
SC-3-3-0.05	0.05	88.5	498.5	87.5	63.8	428.0	88.1	64.2	496.4	88.1	64.2
SC-3-3-0.1	0.10	79.4	498.2	86.3	70.1	430.4	86.6	70.4	495.9	86.0	69.9
SC-3-3	0.26	59.4	498.4	88.1	95.7	441.3	88.7	96.3	496.9	88.2	95.8
SC-3-4-0.01	0.01	97.7	498.8	92.9	61.4	426.4	89.4	59.0	496.9	87.8	58.0
SC-3-4-0.05	0.05	89.4	498.7	87.7	63.3	429.5	85.2	61.5	496.5	84.7	61.1
SC-3-4-0.1	0.10	80.8	498.4	83.2	66.4	431.1	80.4	64.2	496.2	80.5	64.3
SC-3-4	0.26	61.5	498.6	76.5	80.3	439.1	75.3	79.0	497.3	74.9	78.6
SC-3-5-0.01	0.01	97.5	499.1	92.5	61.2	436.6	93.9	62.1	497.1	92.9	61.5
SC-3-5-0.05	0.05	88.6	498.2	81.0	59.0	433.7	81.6	59.4	496.2	81.5	59.3
SC-3-5-0.1	0.10	79.6	497.6	80.5	65.3	423.3	73.2	59.3	496.2	72.8	59.0
SC-3-5	0.26	59.7	498.0	69.8	75.4	419.9	58.4	63.1	493.5	58.3	63.0

Table ESI 1-b. Thermal characteristics of PLLA/PDLA/LPSQ-R blends – homocrystals.

sample	[R]/[La]	wt.%	1st heating			1st cooling			2nd heating		
			T_{mSC} [K]	ΔH_{mSC} [J/g]	X_{c-mSC} [%]	T_{cSC} [K]	ΔH_{cSC} [J/g]	X_{c-cSC} [%]	T_{mSC} [K]	ΔH_{mSC} [J/g]	X_{c-mSC} [%]
SC-2-1	0	100.0	429.9	3.4	3.7	362.7	1.2	1.3	421.7	1.9	2.0
SC-2-2	0.50	47.9	428.3	0.7	1.7	-	-	-	-	-	-
SC-2-5	0.50	43.8	427.3	0.5	1.4	-	-	-	-	-	-

[R]/[La] – mixing molar ratio of functional groups R to the amount lactide segments

wt.% – weight content of polylactide in the PLLA/PDLA/LPSQ-R blend

T_{mSC} / T_{mHC} – stereocomplex / homocomplex melting temperature

T_{cSC} / T_{cHC} – stereocomplex / homocomplex crystallization temperature

ΔH_{mSC} / ΔH_{mHC} – stereocomplex / homocomplex enthalpy of melting

ΔH_{cSC} / ΔH_{cHC} – stereocomplex / homocomplex enthalpy of crystallization

X_{c-mSC} / X_{c-mHC} – stereocomplex / homocomplex degree of crystallinity calculated from melting exotherm (corrected for the amount of polylactide)

X_{c-cSC} / X_{c-cHC} – stereocomplex / homocomplex degree of crystallinity calculated from crystallization endotherm (corrected for the amount of polylactide)
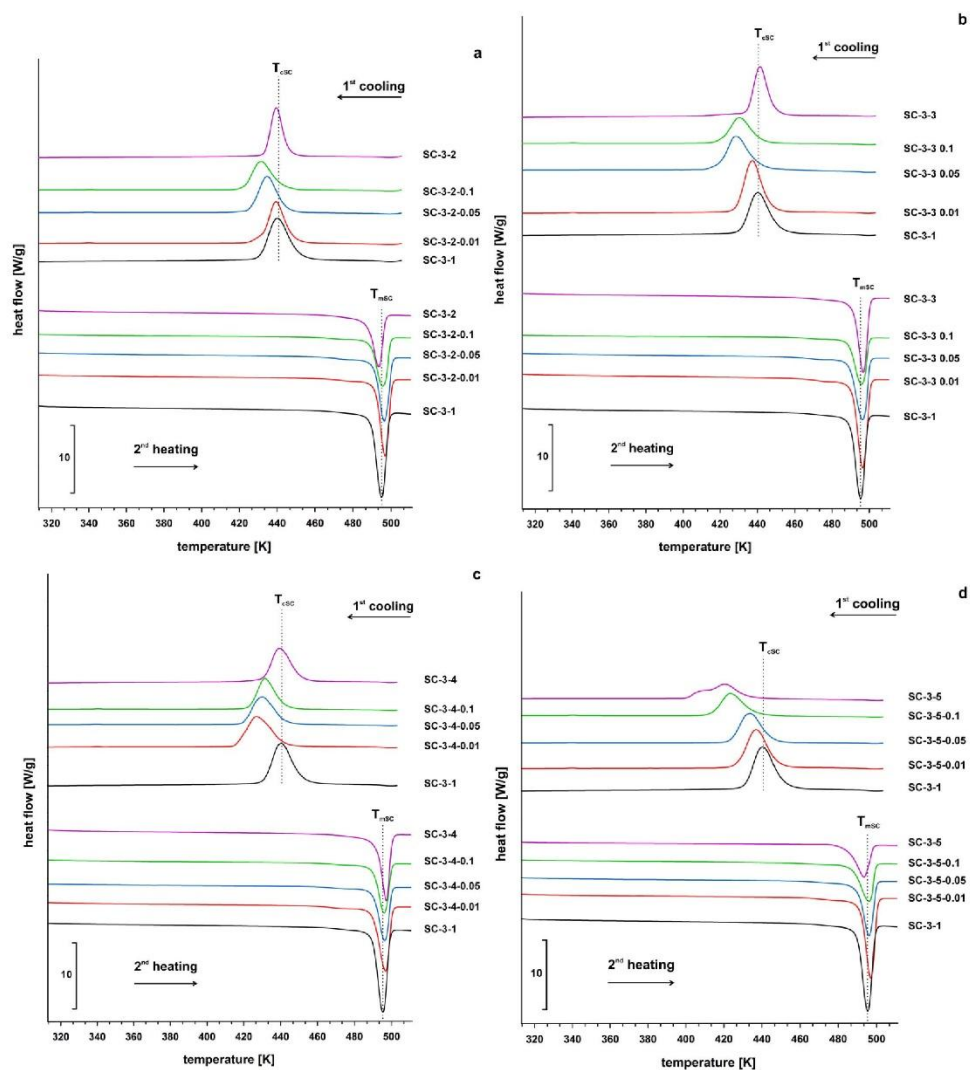
Figure ESI-1. DSC heating/cooling curves (10 K/min) of the SC blends prepared with different amounts of (a) LPSQ-OH, (b) LPSQ-(OH)2, (c) LPSQ-COOH and (d) LPSQ-COOMe.

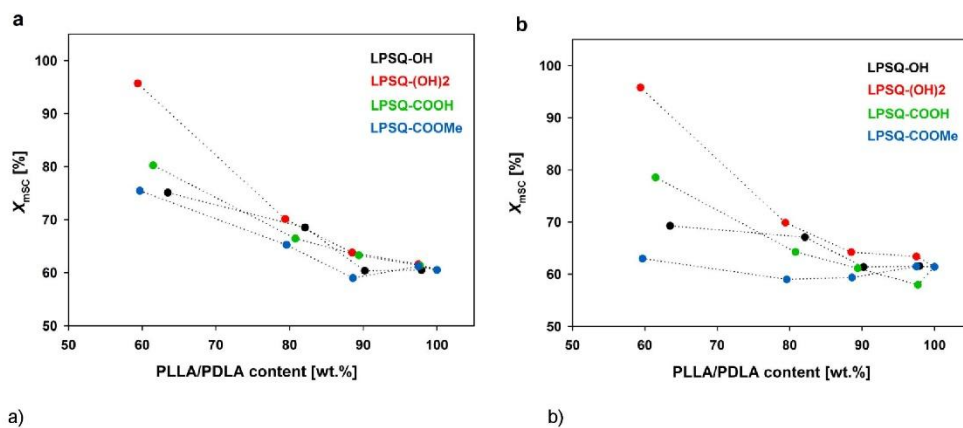**Figure ESI-2.** Changes in X_{mSC} (DSC, 10 K/min) during (a) first and (b) second heating) of PLLA/PDLA blends containing different amounts of LPSQ-R (procedure SC-3).
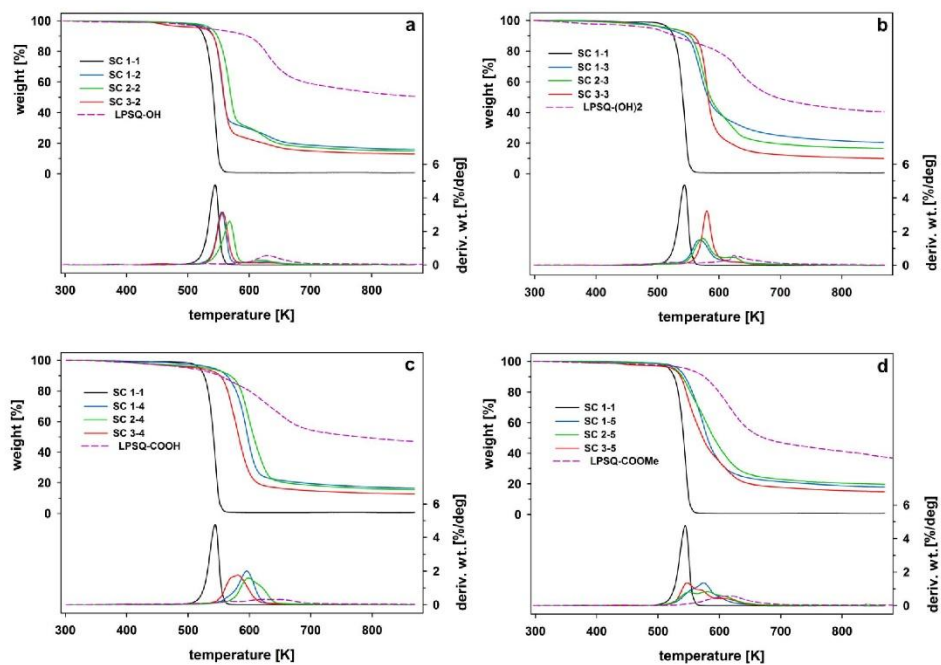
Figure ESI-3. Thermal stability of SC blends and LPSQ-R derivatives used for their preparation (TGA, N₂, 10 K/min).

    (a) blends with LPSQ-OH   (b) blends with LPSQ-(OH)2

    (c) blends with LPSQ-COOH   (d) blends with LPSQ-COMe

Supramolecular interactions between polylactide and model cyclosiloxanes with hydrogen bonding-capable functional groups

A. S. Herc[1], M. Włodarska[2], M. Nowacka[1], J. Bojda[1], W. Szymański[3], A. Kowalewska[1]*

[1]Centre of Molecular and Macromolecular Studies, Polish Academy of Sciences, Sienkiewicza 112, 90-363 Łódź, Poland
[2]Institute of Physics, Lodz University of Technology, Wólczańska 219, 90-924 Łódź, Poland
[3]Institute of Materials Science and Engineering, Lodz University of Technology, Stefanowskiego 1/15, 90-924 Łódź, Poland

Abstract. Interactions between polylactide matrix and additives bearing –COOH and –OH groups were studied for compositions of polylactide (PLA) and functionalized cyclotetrasiloxanes (CX–R, R = OH, COOH, COOMe). Inherent conformational flexibility of cyclotetrasiloxane rings enabled evaluation of supramolecular phenomena between hydrogen bonding-capable functional groups and the polylactide backbone, as well as their role in polymer crystallization. The modification of PLA with CX–R was clearly reflected in the polymer dielectric response, unobscured by interfacial polarization effects frequently observed for other additives. New relaxation processes appeared next to the strong α-relaxation characteristic of the PLA matrix. Addition of CX–R influenced thermally induced crystallization of amorphous matrix as well as isothermal crystallization from melt. Development of crystals with 10_3 helical chain conformation was accelerated at relatively low temperatures in the presence of CX–OH with hydrogen bond donating hydroxyl groups. A specific phase separation that hindered mobility of polymer chains was observed in samples prepared with CX–COOH of strong hydrogen bond donor/acceptor ability. The presented results may be used as a reference for other systems with nanoadditives such as carbon nanotubes (CNT), graphene oxide (GO) or carbon quantum dots, in which interactions between –COOH/–OH groups and the polymer matrix play an important role.

Keywords: material testing, biodegradable polymers, dielectric relaxation, supramolecular interactions, cyclosiloxanes

1. Introduction

Polylactide/poly(lactic acid) (PLA) are well-known biocompatible and biodegradable semicrystalline polymers, that require modification in order to improve their mechanical properties, thermal characteristics and crystallization rate [1–4]. PLA crystallizes typically with a characteristic distorted 10_3 helical chain conformation (orthorhombic α-form and a less ordered α′-form) [5, 6]. Nucleation of PLA crystals is slow, especially if the macromolecules contain a share of isomeric D-lactide units that disturb formation of well-ordered sequences along the chain axis [7, 8]. The induction period before the crystal growth can be reduced and the crystallization kinetics can be improved in the presence of hybrid components that enhance nucleation density, or plasticisers that facilitate chain mobility [8]. The aspect ratio of the hybrid additives and contact area at the interface with polymer matrix is of exceptional significance for the process of crystallization and consequently for thermal, mechanical and gas barrier properties of PLA as well as their biodegradability [3]. Compounds capable of strong supramolecular interactions can change vastly the process of crystallization

---

of PLA. Graphene, carbon nanotubes, carbon nanofibers and carbon quantum dots as low-dimensional carbonaceous nanofillers effectively enhance crystallization of the polymer [9–13]. Interesting results were also obtained with low molecular weight species that crystallize at $T > T_c$ of PLA and are capable of the formation of hydrogen bonds with the polyester backbone. Such compounds (e.g. sorbitol [14], hydrazide [15, 16] and amide [17–19] nucleators) provide nucleation sites in the polymer melt for epitaxial crystallization of PLA.

Broadband dielectric spectroscopy (BDS) studies provided a vast amount of information about the molecular dynamics of PLA and differences in the relaxation processes caused by additives. Local fluctuations below the glass transition temperature (T_g) of neat PLA are reflected in a β dielectric relaxation whereas segmental dynamics (α-relaxation) is increased at $T > T_g$ [20]. Crystallization of PLA was also analysed in details with BDS [21–23]. The relaxation behaviour of the nanocomposites was found to be much more complex than that of neat PLA. For example, addition of organically modified Ni/Al layered double hydroxides resulted in the presence of three additional dielectric active processes, including relaxation of surfactants and water molecules within the layers of inorganic components and interfacial polarization effects at $T > T_g$ [24]. The Maxwell/Wagner/Sillars (MWS) polarization was also observed for PLA nancomposites with montmorillonite [25], graphene oxide (GO) [26] and carboxylated carbon nanotubes (CNT) [27]. The strong effect often overshadows more subtle phenomena connected with the presence of functional groups (–COOH, –OH) on the surface of carbon quantum dots, CNT and GO layers. As a consequence the role of those functional groups in the organization of the polymer matrix, due to their capability of hydrogen bonding to PLA, could not be estimated accurately.

We have found that the isolated effect of supramolecular interactions between PLA chains and carboxyl and hydroxyl groups can be evaluated by employing functionalized cyclotetrasiloxane additives (CX–R) (Figure 1). Species bearing multiple carbonyl/carboxyl or hydroxyl groups were obtained by thiol-ene addition of a range of thiols to 1,3,5,7-tetravinyl-1,3,5,7-tetramethyl-cyclotetrasiloxanes. Owing to the substantial flexibility of siloxane bonds and side alkyl chains, the interactions of PLA with CX–R do
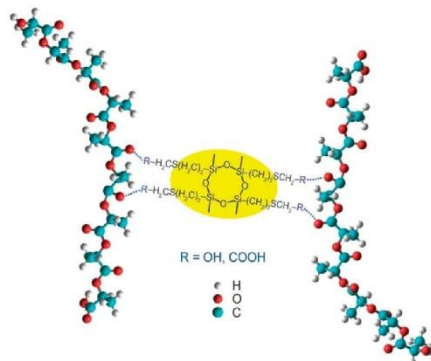
Figure 1. Supramolecular interactions between PLA chains and CX–OH or CX–COOH.

not involve manifestation of any defined interphase effects.

A detailed BDS analysis of interactions between PLA and CX–R is provided. Thermal characteristics and the dynamic behaviour of PLA/CX nanocomposites were also studied using calorimetric (differential scanning calorimetry, DSC) as well as spectroscopic (Fourier-transform infrared spectroscopy, FTIR) techniques. We have found that the specific ability of functional groups to take part in supramolecular interactions with polylactide chains as hydrogen bond donors/acceptors alters strongly the polymer dielectric response. It can be also related to the observed cold crystallization, which is quite interesting taking into account the very low aspect ratio of CX–R additives. The type and amount of CX–R influenced the crystallization of PLA and the rate of 10_3 helical structures formation. The results, combined with no detrimental effect of CX–R on the thermal stability of PLA, and a scarce or small decrease of the polymer light transmittance at low additive loading, make the functionalized cyclosiloxanes interesting models for studies on the impact of hydrogen bonding on PLA matrix. Moreover, there is also a quite important practical aspect of modification of PLA by addition of CX–R. Polylactide is commonly used as a thermoplastic material for fused deposition modelling (FDM) in 3D printing of e.g. scaffolds for regenerative medicine or artificial tissues [28, 29]. The process typically involves extrusion of melted material and then rapid cooling which makes the material brittle. That is why thermal annealing at temperatures corresponding to the cold crystallization

process has to be applied to even out the areas of high and low stress and increase the strength and stiffness of 3D printed parts. Modification of the properties of FDM printed PLA objects by addition of inorganic additives and macromolecules has been described [30, 31]. It can be also expected that shifting cold crystallization of PLA towards lower temperatures in the presence of CX–R can be beneficial in terms of improved physical properties and dimensional stability of the printed objects as well as a lower energy use.

2. Experimental
2.1. Materials

CX–R were prepared by thiol-ene addition of mercapto-compounds: CX–COOH – thioglycolic acid (98%, Sigma-Aldrich, United States), CX–COOMe – methyl thioglycolate (95%, Acros Organics, Belgium), CX–OH – 2-mercaptoethanol (99%, Sigma-Aldrich, United States) and CX–(OH)$_2$ – 1-thioglycerol (99%, Sigma-Aldrich, United States) to vinyl groups of 1,3,5,7-tetravinyl-1,3,5,7-tetramethylcyclotetrasiloxanes (CX–Vi) (97%, a mixture of isomers; ABCR GmbH, Germany) (Figure 2). The synthesis was carried out following earlier reported procedures [32, 33] using 2,2-dimethoxy-2-phenylacetophenone (DMPA) (99%, Acros Organics, Belgium) as the photoinitiator. Solvents used for the experiments were purified following literature procedures [34].

In general a thiol derivative (29.17 mmol) and CX–Vi (6.65 mmol) dissolved in dry tetrahydrofuran (THF) (210 ml) were placed in a quartz vessel. DMPA (0.53 mmol) was added with stirring to the solution of reagents. The mixture was irradiated for 15 min with UV light ($\lambda = 356$ nm). Products were purified by silica gel column chromatography, using ethyl acetate as the mobile phase for CX–COOH, CX–COOMe and CX–OH, or a mixture of ethyl acetate and MeOH for CX–(OH)$_2$. Fractions containing

the desired product were combined and dried over MgSO$_4$. After filtration, volatiles were removed from the solution and the residue was dried to constant weight under high vacuum. Liquid state ^{1}H, ^{13}C and ^{29}Si NMR spectra of all the obtained CX–R were recorded in THF-d8 as a solvent on a Bruker DRX-500 MHz spectrometer (Billerica, Massachusetts, United States).

Polylactide (PLA), commercially available NW 2003D grade from NatureWorks LLC (Minnetonka, MN, United States) used for the study contained 3.2% molar content of D-lactide units ($M_w = 196$ kg·mol^{-1} and dispersity $M_w/M_n = 1.7$). It was purified for the experiments by precipitation using CH$_2$Cl$_2$/MeOH as the solvent/nonsolvent system and carefully dried under high vacuum to constant weight.

PLA/CX–R nanocomposites containing various amounts of CX–R (R = COOH, COOMe, OH, (OH)$_2$ and Vi) were prepared by mixing solutions of PLA in CH$_2$Cl$_2$ ($c = 11$ wt%) with a given amount of CX–R dissolved in THF [or MeOH in the case of CX–(OH)$_2$ due to its insolubility in THF] ($c = 15$ wt%) for 2 h under magnetic stirring. On addition of CX–COOH, CX–OH and CX–(OH)$_2$ the mixtures became cloudy in a short time (less than 3 minutes) and remained turbid on prolonged stirring. The effect was not observed for CX–COOMe and CX–Vi. No increase of viscosity was involved but the turbidity disappeared on sample dilution. The prepared mixtures were then poured into Petri dishes and left for free solvent evaporation. Solid products were dried for 24 h at 80 °C under high vacuum (0.01 Torr). For further studies, thin (0.5 mm) films were compression molded at 190 °C and rapidly quenched at 0 °C.

2.2. Analytic methods

Native PLA NW 2003D and the prepared compositions PLA/CX–R were studied in bulk using a DSC 2920 Modulated thermal analysis system (TA
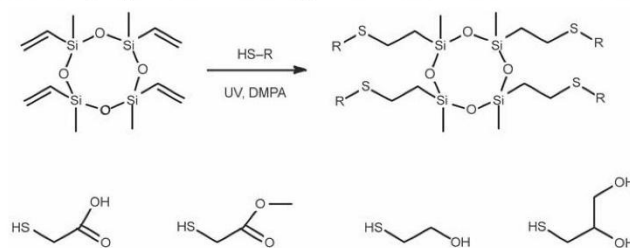

Figure 2. Synthesis and structure of the functionalized CX–R used as additives to PLA.

Instruments; New Castle, DE, United States). Thermograms were taken for samples (sealed in aluminium pans) heated as described in the text. Thermogravimetric analyses were carried out using a Hi-Res TGA 2950 Thermogravimetric Analyzer (TA Instruments; New Castle, DE, United States) under N_2 atmosphere (heating rate $10\,°C\cdot min^{-1}$, resolution 3, sensitivity 3).

Broadband dielectric spectroscopy was performed on samples of initially amorphous polymer matrix in the form of 0.5 mm films placed between brass electrodes in sandwich-type cells. The real and imaginary components of complex permittivity were recorded in a broad frequency range ($10^{-1}\div10^6$ Hz) using a Novocontrol system comprising an Alpha high-resolution dielectric analyser and a Quatro cryosystem (Novocontrol Technologies; Montabaur, Germany). The dielectric profiles were acquired during heating in the temperature range of $20\div150\,°C$. Each frequency sweep took place after temperature stabilization with $0.1\,°C$ accuracy.

Morphological investigations and the distribution of silicon atoms in the studied samples were carried out using a scanning electron microscope (SEM) with energy-dispersive X-ray spectroscopy (EDS) microanalyser (Jeol JSM-6010LA; Tokyo, Japan) operating in the high vacuum mode and at an accelerating voltage 10 kV. The cryo-fractured surfaces were coated with carbon by sputtering in a compact rotary-pumped coating system, Q150R ES (Quorum Technologies; Lewes, Great Britain).

Direct light transmittance through 0.5 mm thick samples of native PLA and the nanocomposites was measured at RT using a UV–VIS SPECORD S 600 diode array spectrophotometer (Analytik Jena AG; Jena, Germany) in the wavelength range from 200 to 1000 nm (0.5 nm resolution) with reference to air. Data were averaged for at least 3 runs.

FTIR spectra were recorded [Nicolet 380 FTIR spectrometer (Thermo Fisher Scientific; Waltham, Massachusetts, United States), equipped with a heated cell and Harrick ATC/low voltage controller (Harrick Scientific Products: Inc. Pleasantville, New York, United States)] for thin films cast on KBr crystal windows from 0.5 wt% solutions of CX–R derivatives, plain PLA and PLA/CX–R nanocomposites in CH_2Cl_2 and dried under high vacuum at room temperature. IR spectra were collected at given intervals by adding 16 scans at $4\,cm^{-1}$ resolution. Isothermal crystallizations were studied for samples melted at 190 °C for complete clearing of crystals. The samples were then cooled down and kept at the desired temperature for 1 hour (procedure I). Alternatively, the melted samples were cooled down to 100 °C and crystallized isothermally as described above. The temperature was then increased ($10\,°C\cdot min^{-1}$) to 110 and then to 120 °C, and samples were crystallized at both respective temperatures for 1 h (procedure II). Comparative analysis was carried out for spectra recorded in transmission mode as well as for their second derivatives.

Nanomechanical properties on the surface and at the cross-section of the compression molded thin (0.5 mm) films of PLA and PLA/CX–R were determined with a G-200 Nano Indenter (MTS Nano Instruments/KLA-Tencor Corporation; Milpitas, California, United States) equipped with TestWorksPro 4 software. The data analysis with the Analyst program was based on Oliver and Pharr's approach [35]. The impressions were made with a Berkovich type indenter with a half angle equal to 65.3° and a radius of roundness <20 nm. The studies were carried out using two methods: CSM (*Continuous Stiffness Measurement*) and BASIC [36]. The CSM method is based on continuous measurement of the stiffness (S) during the material penetration to estimate hardness (H) and modulus of elasticity (E) of the material as a function of penetration depth (h). The test was used to measure the mechanical properties of the specimens from the front with 9 prints per sample (penetration depth 1500 nm). BASIC method was used to map the mechanical properties from the front at the maximum load point. Maps of E and H were obtained with 100 indents in a 10×10 matrix with a step of 20 μm.

3. Results and discussion
3.1. Synthesis of CX–R and preparation of PLA/CX–R blends

Thiol compounds with heterorganic groups being either donors or acceptors of hydrogen bonds (COOH, COOMe, OH), were grafted onto 1,3,5,7-tetravinyl-1,3,5,7-tetramethyl-cyclotetrasiloxane through thiolene addition (Figure 2). All the obtained products were purified by column chromatography and characterized using NMR spectroscopies (Table 1). All CX–R were very viscous liquids that solidified but did not crystallize on cooling.

Cyclotetrasiloxanes with two different substituents at silicon atoms are typically mixtures of four

Table 1. Reaction yields and spectroscopic data for CX–R.

CX–R	Y [%]	δ [ppm]:		
		¹H NMR	¹³C NMR	²⁹Si NMR
CX–COOH	32	0.07–0.14 (s, –Si–$\underline{C}H_3$); 0.84–0.9 (m, –Si–$\underline{C}H_2$–CH₂–S–); 2.6–2.67 (m, –Si–CH₂–$\underline{C}H_2$–S–); 3.2–3.25 (m, –S–$\underline{C}H_2$–COOH)	0.6 (–Si–CH₃); 17.08 (–Si–$\underline{C}$H₂–CH₂–S–); 27.07 (–S–$\underline{C}$H₂–COOH); 33.5 (–Si–CH₂–$\underline{C}$H₂–S–); 176.4 (–$\underline{C}$OOH)	–21.45 (–CH₂SiO₃/₂)
CX–COOMe	62	0.08–0.18 (s, $\underline{C}H_3$–Si–); 0.88–0.92 (m, –Si–$\underline{C}H_2$–CH₂–); 2.67–2.70 (m, –CH₂–$\underline{C}H_2$–S–); 3.17–3.24 (m, –S–$\underline{C}H_2$–C(O)O–); 3.61 (s, –O–$\underline{C}H_3$)	–1.33 ($\underline{C}$H₃–Si–); 17.05 (–Si–$\underline{C}$H₂–CH₂–); 26.7 (–S–$\underline{C}$H₂–C(O)O–); 32.4 (–CH₂–$\underline{C}$H₂–S–); 51.3 (–O–$\underline{C}$H₃); 170.3 ($\underline{C}$(O)O)	–21.49, –23,66 (–CH₂SiO₃/₂)
CX–OH	39	0.07–0.10 (s, –Si–$\underline{C}H_3$); 0.82-0.87 (m, –Si–$\underline{C}H_2$–CH₂–); 2.52–2.58 (m, Si–CH₂–$\underline{C}H_2$–S–$\underline{C}H_2$–); 3.56–3.57 (m, –S–CH₂–$\underline{C}H_2$–OH); 4.22 (s, –CH₂–$\underline{O}H$)	–0.97 ($\underline{C}$H₃–Si–); 17.9 (–Si–$\underline{C}$H₂–CH₂–); 26.2 (–S–$\underline{C}$H₂–CH₂–OH); 34.2 (–CH₂–$\underline{C}$H₂–S–); 61.4 (–S–CH₂–$\underline{C}$H₂–OH)	–21.48 (–CH₂SiO₃/₂)
CX–(OH)₂	48	0.12–0.16 (s, –Si–$\underline{C}H_3$); 0.90–0.91 (m, –Si–$\underline{C}H_2$–); 2.53–2.76 (m, –$\underline{C}H_2$–S–$\underline{C}H_2$–); 3.71–3.72 (m, –CH₂–$\underline{C}H$(OH)–CH₂–); 3.5–3.6 (m, –CH(OH)–$\underline{C}H_2$–OH)	–1.6 (–Si–$\underline{C}$H₃); 17.58 (–Si–$\underline{C}$H₂–CH₂–S–); 26.7 (–S–$\underline{C}$H₂–CH(OH)–); 34.8 (–Si–CH₂–$\underline{C}$H₂–S–); 64.7 (–$\underline{C}$H₂–OH); 71.4 (–CH₂–$\underline{C}$H(OH)–CH₂–)	–21.24 (–CH₂SiO₃/₂)

Y – reaction yield after the column chromatography purification

stereoisomers: *all–cis*, *cis–cis–trans*, *cis–trans–cis*, and *all–trans* [37] of different molar abundance. Yet, owing to the substantial flexibility of siloxane bonds and alkyl chains, this feature is not important for interactions of PLA with CX–R. In the single case of 1,3,5,7-tetra[2-(carboxymethylthio)ethyl]-1,3, 5,7-tetramethyl-cyclotetrasiloxane (CX–COOH), we were able to obtain a fraction (consisting of 91.6% of the total 31.4% yield of CX–COOH after the column separation) enriched in the isomer *cis–cis–trans*.
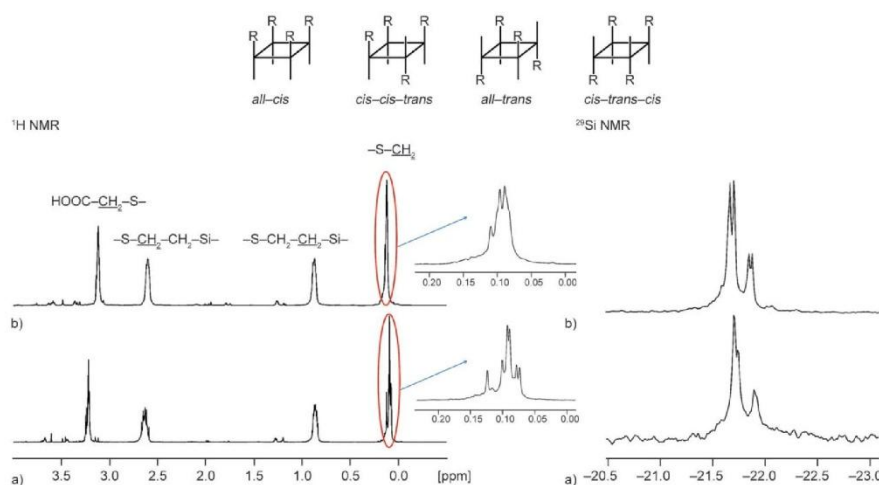
Figure 3. ¹H and ²⁹Si NMR spectra of fractionated CX–COOH: a) fraction enriched in isomer *cis–cis–trans*; b) mixture of isomers.

The assignment was based on the number of resonance lines in ^{1}H and ^{29}Si NMR spectra (Figure 3) and the data published for analogous systems [37–41]. Mixtures of PLA and CX–R were prepared by solution blending. Solutions of PLA became cloudy on addition of CX–COOH, CX–OH and CX–$(OH)_2$ but not in the presence of CX–COOMe or CX–Vi. Small-scale tests showed that the turbidity was not induced by pure solvents (THF or MeOH) at amounts equal to those added with CX–R. Vacuum dried specimens of PLA/CX–R were hot pressed into 0.5 mm thick samples and most of them were fairly clear. Distribution of CX–R was examined using energy dispersive X-ray analysis combined with scanning electron microscopy. SEM-EDS mapping of silicon atoms (Figure 4) showed that samples prepared with CX–COOH contain domains enriched with organosilicon compounds that become more defined on the increase of the amount of CX–COOH. This feature may be explained by interactions of side donor/acceptor carboxyl groups of CX–COOH with both PLA chains and other molecules of CX–COOH. The dimeric structures are more stable than hydrogen bonds with carbonyl groups of PLA chains. CX–Vi, CX–COOMe and CX–OH were well dispersed in the polymer matrix. Distribution of CX–$(OH)_2$ having two hydroxyl moieties at each side group in a 'bidentate' arrangement was quite good. Yet, small domains with slightly higher concentration of this additive can be found in the studied area. The effect may be associated with micro-precipitation of PLA macromolecules hydrogen bonded with CX–$(OH)_2$ (addition of MeOH in the same proportion to PLA and CH_2Cl_2 did not cause a visible precipitation of the polymer).

Direct light transmittance through PLA/CX–R was characterized quantitatively in the range of 200–1000 nm. It depends on the type of functional group R and the concentration of the additive (Figure 5). Transparency of plastic sheets is defined as capability to transmit light within 540–560 nm [42]. Samples of PLA admixed with CX–COOMe at ≤5 wt% were thus as transparent as the native PLA. It was also found that PLA/CX–COOMe absorb light at λ = 250–340 nm. The region is close to the most energetic band of natural UV light (UV-B, 280–315 nm), that is responsible for photochemical degradation of materials. Combination of clarity and absorption of specific wavelength of light are valuable features, e.g. in packing materials. The filter effect can be ascribed
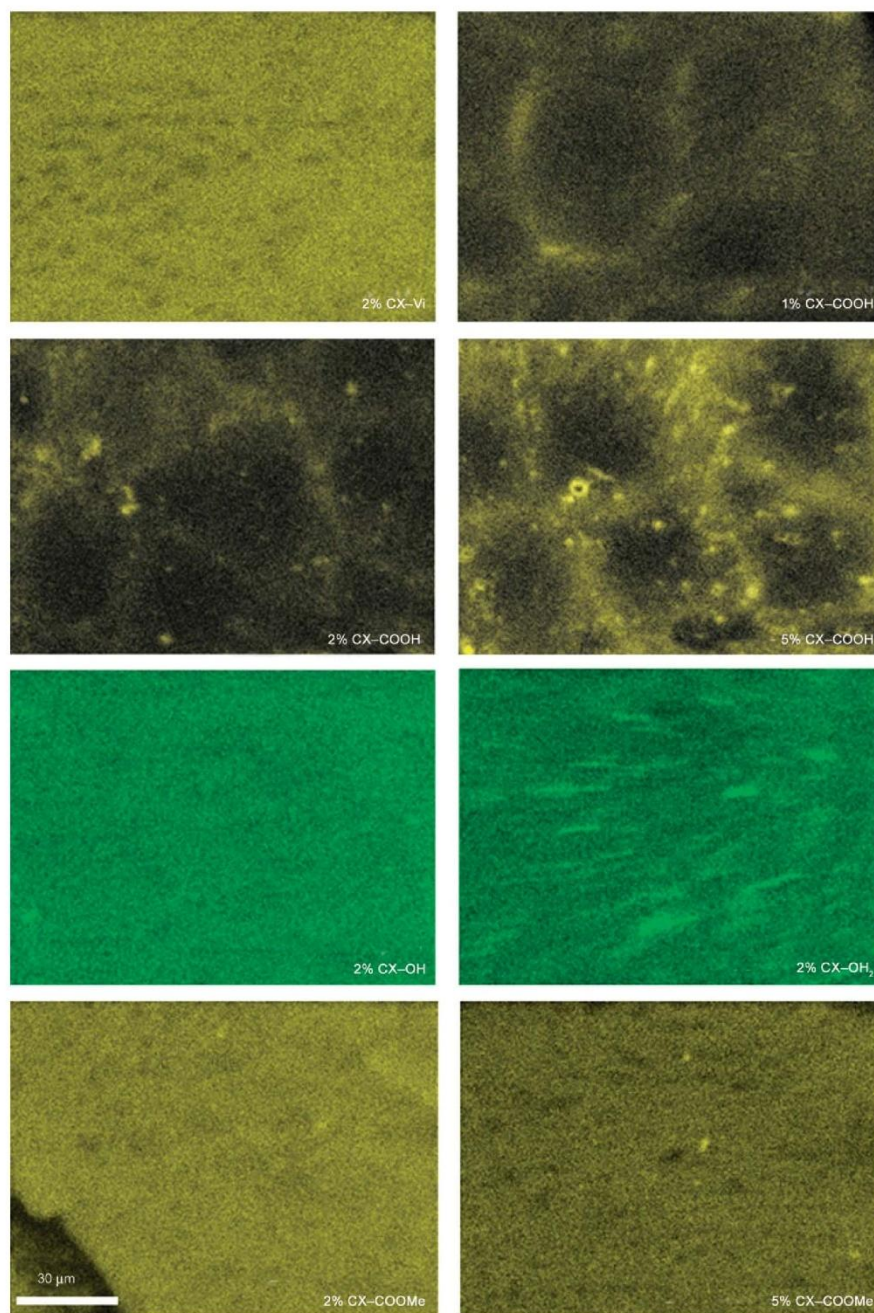
to the presence of carbonyl groups (neat CX–COOMe and CX–COOH absorb light at 250–340 nm). CX–COOH inclusions in PLA, evidenced with SEM-EDS, caused a decrease of light transmission over the studied region of the spectrum. Interestingly, the sample containing 10 wt% of CX–COOH appear to be more transparent to light of λ > 500 nm than the one admixed with 5 wt% of the cyclosiloxane. The observed effect can be explained by an increased phase separation of regions enriched with CX–COOH. Clarity of PLA/CX–Vi (2 wt%) and PLA/CX–OH (1 wt%) is close to that of PLA. Larger amounts of CX–OH (2–4 wt%) made PLA slightly less transparent over the studied wavelength range. CX–$(OH)_2$ caused a substantial decrease of light transmittance through PLA matrix. At 4 wt% it made the polymer opaque over the entire UV/Vis range.

3.2. Broadband dielectric relaxation

Modification of PLA with CX–OH and CX–COOH additives is clearly reflected in the frequency-temperature plots of the imaginary component of complex permittivity (Figure 6), where the characteristic relaxation processes are indicated with arrows. A strong α-relaxation associated with the glass transition is the most prominent feature of the dielectric spectra, with almost identical shape in plain PLA and PLA/CX–R mixtures. Another relaxation (β-process), related to local motion in the polymer matrix, also appears in all the samples. It is hardly visible at this scale and temperature, but it undergoes noticeable modifications depending on the CX–R additive. Modifications of the dielectric response are also visible at high temperatures (>100 °C). They become larger with growing concentration of the CX–R additive, which is why relatively large concentrations were chosen for display in Figure 6 (4 wt% CX–OH and 5 wt% CX–COOH). A distinct case is PLA admixed with a large amount of CX–COOH (5 and 10 wt%), where an additional γ-relaxation appears at low temperatures (Figure 6c). The ε″(f) plots at a few selected temperatures are shown in Figure 7 for better visualization of the observed relaxation processes. The standard Havriliak-Negami formula with conductivity term (Equation (1)) [43] was fitted to the experimental data to support more quantitative analysis:

$$\varepsilon^*(\omega) - \varepsilon_\infty = -i\frac{\sigma_0}{\varepsilon_0 \omega^s} + \sum_k \frac{\Delta\varepsilon_k}{\left(1 + (i\omega\tau_k)^{\alpha_k}\right)^{\beta_k}} \quad (1)$$

139

96

**Figure 4.** Distribution of Si atoms (bright field) in samples of PLA admixed with CX–R, as indicated by SEM-EDS.
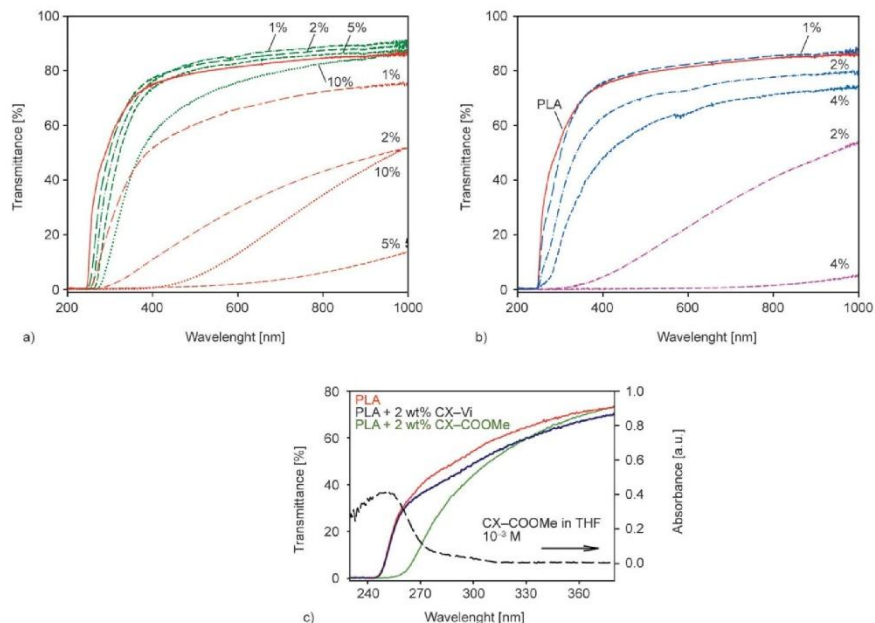
Figure 5. Direct light transmittance measured for the compression molded PLA/CX–R: (a) PLA (—) admixed with CX–COOMe (—) and CX–COOH (—); (b) PLA (—) admixed with CX–OH (—) and CX–(OH)$_2$ (—); (c) comparison of transmittance through selected thin films and absorbance of 10^{-3} M solution of CX–COOMe in THF.

where ε_0 – vacuum permittivity, ω – radial frequency, $\varepsilon_\infty = \varepsilon'$ at $f \rightarrow \infty$, $\Delta\varepsilon$ – difference between the high-frequency and low-frequency values of permittivity for a given relaxation, τ – relaxation time, α and β – shape parameters, σ_0 – direct-current conductivity, s – parameter related to non-ohmic effects.

The α-process, which clearly dominates the response at 60, 65 and 75 °C, is almost identical in pure and admixed PLA. The rapid shift of that process towards low frequencies at temperatures below 47 °C is associated with quenching of cooperative motions and with the vitrification process. A similar behaviour was also observed in other studies of PLA [25]. This frequency-shifting of the α process progresses somewhat slower in PLA/CX–R matrices – *cf.* temperatures 47 and 40 °C in Figures 7a and 7b/7c. After vanishing of the dominant α-process at low temperatures, the secondary processes appear. The β-relaxation visible in all the studied matrices is associated with the motions of local polar groups in PLA. Addition of CX–OH modifies that process, as seen in Figures 7a/7b at 47 and 40 °C. In PLA/CX–COOH, dielectric response at the same temperatures reveals

another relaxation (γ-process) at lower frequencies, which somewhat hides the β-process (Figure 7b). More differences between the dielectric spectra of plain and admixed PLA are visible at high temperatures, where cold crystallization is expected (T = 85, 95 and 115 °C). In plain PLA, cold crystallization is reflected in the modification of the α-process: the frequency shift of that process is slower than at lower temperatures; its amplitude decreases as well (T = 95 °C). These observations are consistent with other studies, where modification of the α-process due to cold crystallization was observed [25]. The effect of the CX–R additives on the α-process in PLA matrix is particularly well visible in the permittivity-temperature plot at high frequencies (Figure 8). The same plot also reveals the influence of concentration of the additive on that relaxation process. For a better insight, dielectric response of PLA admixed with different amounts of the additive is shown at selected low and high temperatures at which the additive has a significant impact on the dielectric response (Figure 9). Figure 9a displays the data for PLA/CX–COOH at four concentration levels (0, 2,

141
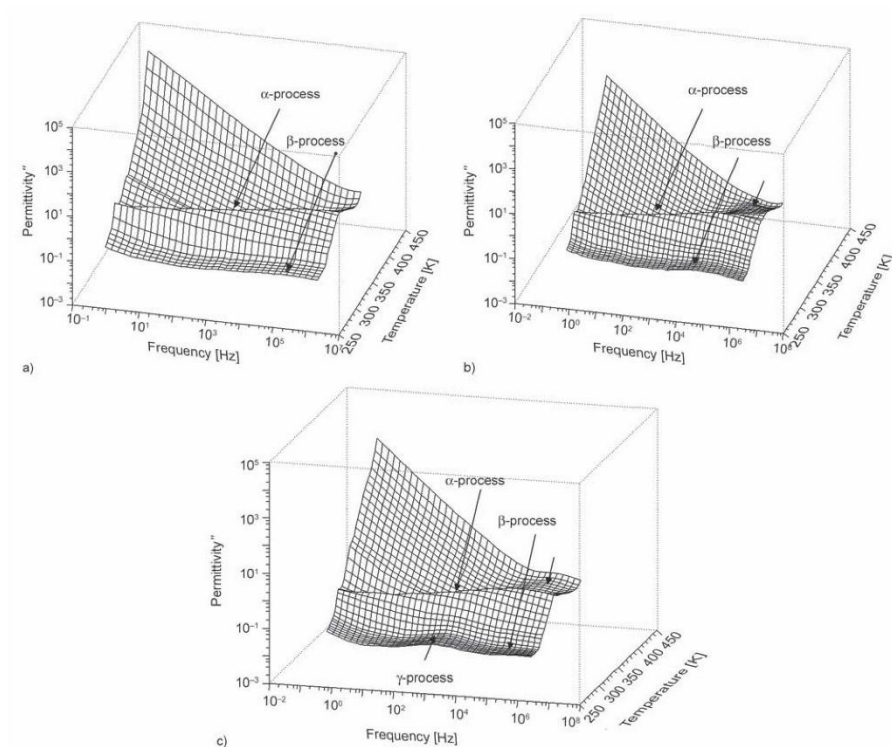
Figure 6. Dielectric response of (a) plain PLA, (b) PLA + 4 wt% CX–OH, and (c) PLA + 5 wt% CX–COOH: the imaginary part of complex permittivity *vs.* frequency and temperature. Arrows indicate the characteristic relaxations.

5 and 10 wt%) and the temperatures of 30 and 115 °C (inset). For comparison, data collected at the same temperatures for PLA/CX–OH at concentrations of 0, 2 and 4 wt% is also presented (Figure 9b). Figure 9a clearly demonstrates the dependence of the strength of the γ-process on the amount of the additive in PLA/CX–COOH. Interestingly, dielectric response at 2% concentration, where both the γ and β-processes occur next to each other, is notably different from the response recorded at higher concentrations. In the mixtures with 5 and 10 wt% of CX–COOH, the γ-process occurs at somewhat different frequency and its amplitude substantially grows with increasing concentration of the additive. The observed process is therefore related to coordination of carboxyl groups in the CX–COOH additive.

The PLA/CX–OH matrix presents a different behaviour (Figure 9b). A modification of the β-process is also visible at low temperatures, but it is not accompanied by any additional processes. At the high-temperature region, where the α-process undergoes a modification along with increasing concentration of CX–OH, lessening of the amplitude of the process occurs at somewhat lower temperature (85 °C) than in plain PLA (95 °C). Thus, a small decrease of cold crystallization temperature due to the additive may be postulated.

Summing up, a small addition of CX–COOH or CX–OH modifies the dielectric response to some extent, both the β-process at low temperatures and the α-process at high temperatures – particularly near 100 °C where the α-relaxation visibly changes with increasing content of CX–OH or CX–COOH. This observation, along with complementary experiments, points towards higher potential for cold crystallization. Larger concentrations of CX–COOH additive (above 2 wt%) display additional relaxation processes at low and high temperatures, whose amplitudes

142

99
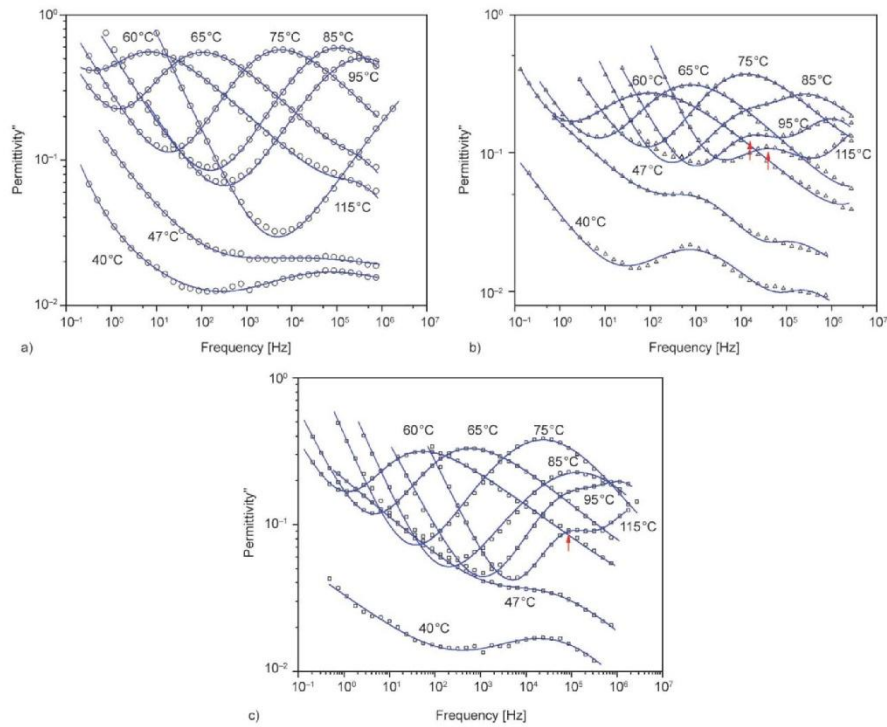
Figure 7. Plots of $\varepsilon''(f)$ at a few selected temperatures, visualizing the relaxation processes: (a) plain PLA, (b) PLA + 5 wt% CX–COOH, (c) PLA + 4 wt% CX–OH.
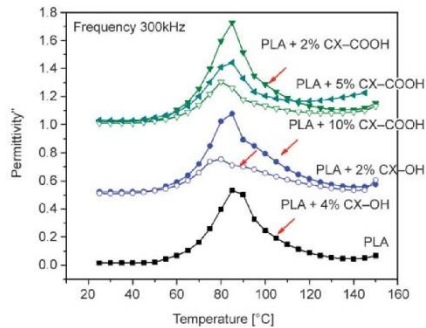

Figure 8. Influence of CX–R additives on the strength of the α-relaxation in PLA. Permittivity-temperature plots at $f = 300$ kHz for a few concentration levels of the additives. Plots for admixed PLA are shifted by the values of 0.5 (PLA/CX–OH) and 1.0 (PLA/CX–COOH).

grow significantly with increasing concentration of CX–COOH. Correlation of this behaviour with the complementary studies (*cf.* Figures 4 and 10) supports interpreting it as a reflection of phase separation and vanishing of cold crystallization.

3.3. Thermal properties of PLA/CX–R blends

The presence of CX–R in PLA matrix led to a range of complex phenomena related to differences in chain dynamics but they did not influence the thermal stability of PLA. Thermogravimetric analysis (not shown) of neat PLA and its mixtures with CX–R indicated that thermal stability of PLA and the composites is the same [$T_{d5} = 330$ °C, $T_{max} = 360$ °C (decomposition rate $10\% \cdot min^{-1}$)] under N_2 at heating rate of 10 °C·min⁻¹. Interesting results were obtained for the behaviour of PLA/CX–R during DSC runs carried out with a temperature ramp. DSC analysis indicated that the native PLA containing ~3% molar
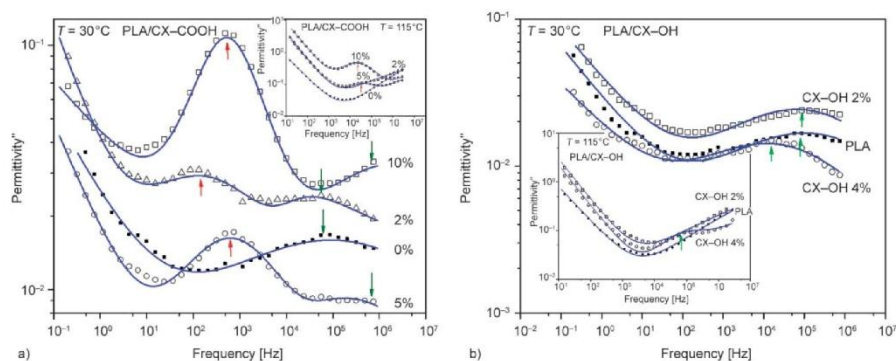
Figure 9. Dielectric response of PLA/CX–R at different concentration levels: (a) PLA/CX–COOH at $T = 30\,°C$ (inset: $T = 115\,°C$); (b) PLA/CX–OH at $T = 30\,°C$ (inset: $T = 115\,°C$).

amount of D-lactide units did not crystallize on cooling from melt at $10\,°C·min^{-1}$ nor $2\,°C·min^{-1}$. Due to the same reason, enthalpy of cold crystallization (ΔH_{cc}) of samples cooled down from melt at $10\,°C·min^{-1}$ and heated again at $10\,°C·min^{-1}$ is very small. The degree of crystallinity (X) achieved under the applied conditions is close to 5% (with respect to the enthalpy of melting of a completely crystallized PLLA; 93.1 J/g [44]).

Addition of CX–R did not improve PLA crystallization from melt, yet their presence clearly influenced the process of cold crystallization. It is known, that nucleation of PLA and the rate of crystal growth are determined, especially at the early stages of the process, by the molecular conformation and chain ordering. Initially formed edge-on lamellar crystals develop straightforward growing both parallel and perpendicular to the film surface evolving finally into flat-on hexagonal crystals and spherulites [45]. Localized binding of 2–4 polymer chains by hydrogen bonding with CX–R can help to the formation of edge-on crystals. Hydrogen bonds are labile at high temperatures and therefore the observed poor nucleating effectiveness of CX–R on cooling since, contrary to the hydrazide or amide nucleators mentioned above, they do not form crystals in the PLA melt. Yet, polymer chains in amorphous samples of PLA/CX–R can gradually gain mobility on heating from $T < T_g$, and the lactide segments bound by supramolecular interactions with CX–R become nuclei of PLA crystals. The combined increase of crystal fraction and lack of a deteriorating effect of CX–R on the thermal resistance and transparency of PLA should be thus stressed. A decrease of thermal stability and poor light transmittance was reported for PLA containing an otherwise effective dihydrazide nucleating agent [46].

Differences in DSC thermograms recorded for samples of PLA/CX–R cooled down at $10\,°C·min^{-1}$ from melt to room temperature and heated at $10\,°C·min^{-1}$ (Figure 10) can be related to the type of CX–R. The test carried out with CX–Vi of no affinity to PLA did not show any strong effects. However, in the presence
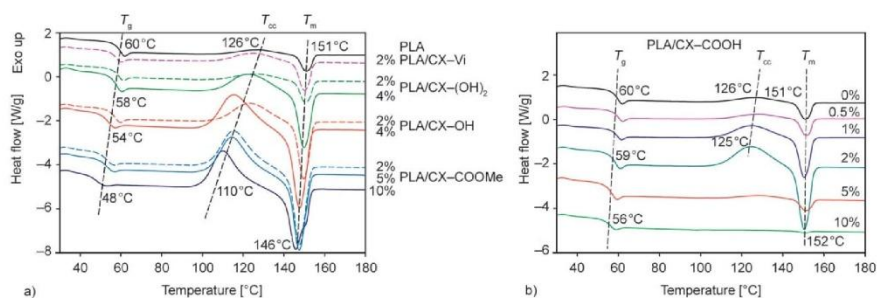
Figure 10. Influence of the type of CX–R for the process of cold crystallization of PLA (DSC, 2nd heating at $10\,°C·min^{-1}$).

144

101

of CX–OH, CX–(OH)$_2$ and CX–COOMe an exothermic peak related to the process of cold crystallization was recorded at 110–140 °C with a maximum shifted to lower temperatures than that characteristic to PLA. The ΔH_{cc} and ΔH_m of the subsequent melting ($T_m \sim$ 150 °C) were the same (within the measurement accuracy), which typically indicates that the crystals were formed exclusively during the heating run.

A shift of the glass transition temperature was observed in the presence of CX–R. The effect points to a slight increase of the segmental movement of PLA chains and depends on the type of functional group and the amount of CX–R. Devitrification takes place at lower temperatures for composites containing larger amounts of the additives. The drop of T_g (ΔT_g) in the presence of 4 wt% CX–(OH)$_2$ is smaller (2 °C) than that noted for 4 wt% CX–OH (6 °C) and for 5 wt% CX–COOMe (6 °C). Yet, crystallinity of PLA admixed with 4 wt% of the hydrogen bond donating CX–OH and CX–(OH)$_2$ was, respectively, 25 and 14%. The poorer nucleation despite multiple hydrogen bonding capability of thioglycerol moieties, suggests that too large amount of hydroxyl groups makes more difficult the proper chain alignment. A more substantial decrease of T_g, proportional to the concentration of the additive, was recorded for PLA compositions with CX–COOMe. Yet the thermally induced crystallinity of samples containing CX–COOMe is almost independent (25–29%) on the amount of the additive (2 to 10 wt%). The phenomenon may be tentatively linked to the ability of –COOMe groups to act as acceptors/donors of weak hydrogen bonds to the carbonyl oxygens of ester groups (CH····O=C). Such interactions play a very important role in stereocomplexes of PLLA and PDLA [47]. Therefore, the total effect of CX–COOMe on PLA would be a resultant of the matrix plastification and supramolecular interactions. The phenomenon will be the subject of extended studies.

An unusual, non-linear effect was noted for mixtures of PLA and CX–COOH. Analogously to the other CX–R, a small amount (0.5–2 wt%) of CX–COOH strongly promoted cold crystallization of the matrix. However, if the concentration of CX–COOH was ≥5 wt%, then crystallization of PLA was hampered. The effect can be related to strong interactions between the –COOH groups and polyester backbone as well as to the phase separation and formation of a hydrogen bonded dual network (shown on SEM-EDS

micrographs – Figure 4, and confirmed by the results obtained with BDS).

3.4. Isothermal crystallization of PLA/CX–R – DSC and FTIR studies

Isothermal crystallization from melt carried out at selected temperatures for PLA admixed with CX–R at 2 wt% suggest that hydrogen bonding from CX–OH and CX–(OH)$_2$ affects the mobility of PLA chains and results in faster crystallization of the polyester matrix within the temperature range 90–120 °C. The estimated crystallization half-times (Figure 11a) show clearly the effect of the cyclosiloxane additives. CX–COOH and CX–COOMe increased the crystallization rate only at high temperatures (120 °C). The isothermal annealing from melt leads to the formation of a thermodynamically preferred polymorph [48–50]. Consequently, a single endothermic peak representing melting of PLA crystals was found for DSC diagrams of samples of PLA and PLA/CX–R crystallized at 110 and 120 °C (Figure 11b). Structures formed at 110 °C melt at slightly lower temperatures (T_m = 149 °C) than those annealed at 120 °C (T_m = 152 °C). Two endothermic peaks that were observed for all samples (PLA and PLA/CX–R) annealed at 90 and 100 °C, reflect the characteristic melt-recrystallization behaviour leading to the perfection of PLA crystals [48, 51]. The undeveloped crystals formed at 90 °C tend to melt at lower temperature ($T_m \sim$ 143 °C) than those obtained at 100 °C ($T_m \sim$ 146 °C). The share of fraction melting at 152 °C is larger in compositions of PLA admixed with CX–OH, CX–(OH)$_2$ and CX–COOH capable of stronger hydrogen bonding to PLA chains. No solid state endothermic disorder-to-order phase transition of α′ to α form [48, 52] was detected.

At T = 120 °C crystallization of PLA is slowed down due to the increased dynamics of polymer chains. Small endotherms of cold crystallization (within 110–120 °C) were noted for PLA/CX–Vi and PLA/CX–COOMe (Figure 11b), indicating that despite long thermal annealing at 120 °C they were not completely crystallized. The respective degree of crystallinity is small (e.g. ~8% for ΔH_{cc} and 28% in total for PLA/CX–COOMe). Composites containing CX–RCX–R that form strong –OH····O=C hydrogen bonds with PLA crystallized effectively at this temperature (achieved degree of crystallinity of ≥40% at $t_{1/2}$ much shorter than that found for neat PLA).
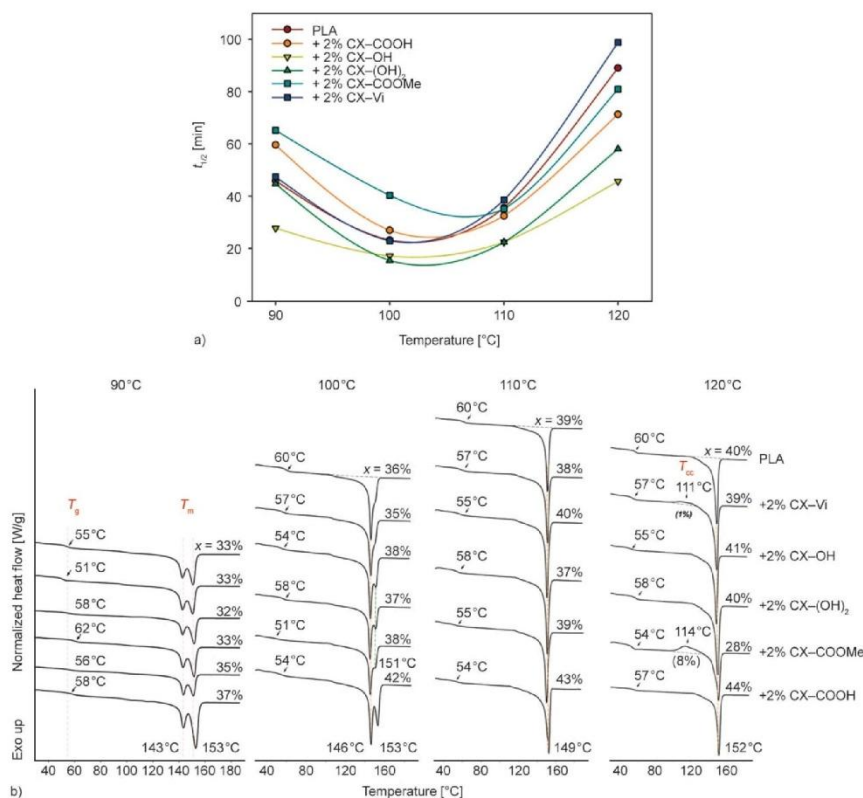
Figure 11. (a) Isothermal crystallization half-times estimated for PLA/CX–R; (b) DSC heating runs (10 °C·min^{-1}) recorded for samples of PLA/2 wt% CX–R crystallized isothermally at 90, 100, 110 and 120 °C.

Interactions between PLA and CX–R (R = COOH, COOMe and OH) were also studied with FTIR in comparison to pure PLA under conditions of isothermal crystallization from melt carried out for one hour after cooling to 100, 110 or 120 °C (procedure I). FTIR spectroscopy is sensitive to the conformation of polymer chains as well as the local molecular environment and crystal packing. The technique is facile and rapid and thus it can be applied for the analysis of PLA crystallization process and structural variations of the formed crystals [49, 53–56]. The amount of CX–R (2 wt%) is small and FTIR spectra of PLA/CX–R and pure PLA consist of the same characteristic vibration modes. They were converted to their second derivatives in order to resolve more precisely the overlapped bands (Figure 12).

The studied region of 1300–700 cm^{-1} contains conformation sensitive vibration modes characteristic of the ester backbone of PLA and the crystalline fraction that were assigned (Table 2) following the published data [49, 50, 53, 55, 57, 58]. Isothermal crystallizations at low temperatures ($T < 100$ °C) and cold crystallization caused by accelerated chain motions result typically in the disordered α′ form whereas tightly packed α crystals are typically obtained at $T \geq 120$ °C [49]. The difference between the chain conformations in α′- and α-crystals is mainly related to the side groups packing. The band at ~920 cm^{-1} associated with $\rho(CH_3)$ vibrations with $\nu(C–COO)$ skeletal stretching modes is an indicator of 10_3 helical chain conformations (α and α′ crystals). Two other indicative bands are combination of $\nu(COC) + \rho(CH_3)$ modes and the stretching $\nu(C–COO)$ [59, 60]. The

146

103
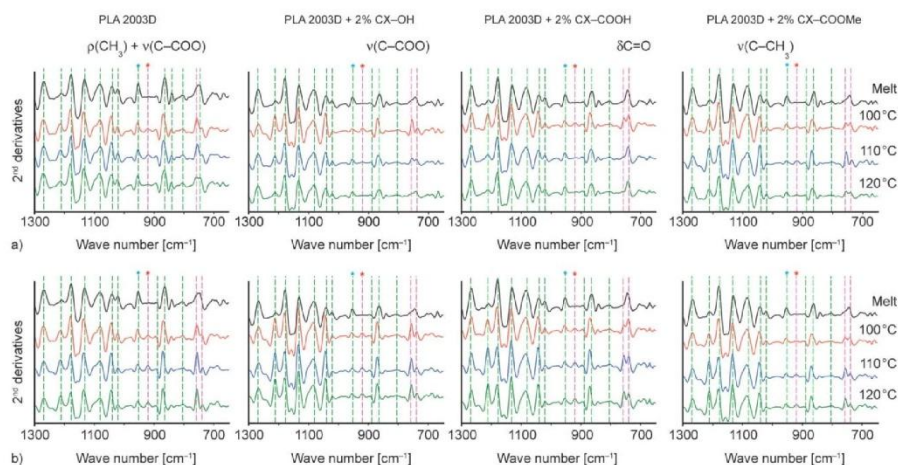
Figure 12. Second derivatives of FTIR spectra of PLA and PLA/CX–R recorded after 1 h of isothermal crystallization: (a) procedure I; (b) procedure II; [ρ(CH₃) + ν(C–COO) *– amorphous; *– 10₃ conformation mode].

shape of the crystal (curved crystals with edge-on orientation vs crystals with flat-on orientation) also affects the intensity of IR spectral bands [57]. Propensity of the native PLA to crystallize from melt under the applied conditions was most significant at 100 and 110 °C – in accordance with the published data as well as the presented isothermal crystallization half-times and the post-crystallization melting curves (Figure 11). The spectra recorded after cooling down to the temperature of 100, 110 and 120 °C are very close, which points to a similar degree of chain order. The intensity of vibration bands at 1213, 1093, 1042 and 757 cm^{-1} increased and the peaks characteristic of the amorphous fraction (1022, 955

and 742 cm^{-1}) decreased with heating. The position of the skeletal stretching vibration band (922 cm^{-1}) at 100 °C, points to the formation of less regular α′ crystals. The peak shifts to 920 cm^{-1} if the crystallization is carried out at 110 °C. However, at 120 °C no signal indicating 10₃ conformations was found around 920 cm^{-1}, which corroborates with the observed large $t_{1/2}$. The vibration bands in the studied region are sharper than those in melt. It was previously explained that the increase of intensity of certain vibration bands should be rather associated with an oriented mesophase and a better packing of macromolecules achieved before the sample crystallization [50, 54, 61].

Table 2. Assignment of PLA IR vibration bands.

| Vibration band	Amorphous	α′	α	Vibration band	Amorphous	α′	α
	Wavenumber [cm^{-1}]				Wavenumber [cm^{-1}]		
δ₂CH	1304	1303	1303	ν(C–CH₃)	1042 1023	1042 1023	1042 1023
δCH + νCOC		1270		ρ(CH₃) + ν(C–COO) amorphous	955	955	955
νas(COC) + ρas(CH₃)	1213 1183	1215 1186	1222 1213 1202 1180	ρ(CH₃) + ν(C–COO) crystalline	–	922	920
ρs(CH₃)	1132	1134	1144 1134	ν(C–COO)	864	868	868
νs(COC)	1081	1093 1081	1093 1081	δC=O	740–760		

Changes in the shape of FTIR spectra of PLA/CX–R during direct isothermal crystallizations from the melt suggest a more rapid formation of crystal nuclei that led to an increase of the overall crystallinity of PLA compositions (Figure 12a). CX–OH induced an extensive crystallization of PLA at 100°C with the skeletal band of $\rho(CH_3) + \nu(C–COO)$ positioned at 920 cm^{-1}. An outstanding increase of the band at 1213 cm^{-1} (C–O stretching E_1 mode – perpendicular to helix axis [57]) was observed with regard to another C–O stretching contribution at 1180 cm^{-1} (A mode – parallel to the helix axis). It was accompanied with a sharp increase of the ν(C–CH$_3$) vibration mode at 1042 cm^{-1}, indicating interactions of adjacent C–CH$_3$ groups in the crystal unit cell and a decrease of intensity of the amorphous phase band at 955 cm^{-1}. A similar effect was observed before but for enantiomerically pure PLLA and only at $T > 110$°C [58, 62]. FTIR studies confirmed a slightly slower crystallization of PLA/CX–OH at 110 and 120°C (corroborated by the estimated $t_{1/2}$). Similar (but less pronounced) effects were observed for CX–COOH. Samples crystallized at 100°C were also thermally annealed at 110°C and then at 120°C (procedure II, Figure 12b). Gradual thermal processing of pre-crystallized samples led to an improvement of the crystal structure. As expected, nuclei formed at 100°C acted as templates for the crystal growth at higher temperatures. Intensity of ν_{as}(CCO–O) + ρ_{as}(CH$_3$) (1213 cm^{-1}) and ρ_s(CH$_3$) (1134 cm^{-1}) was augmented during the annealing. Crystallization of PLA in the presence of CX–COOMe was most rapid at 110°C, both during thermal annealing carried out according to procedures I and II. The organization of polymer matrix was not much improved on heating at 120°C, as it was shown also by results presented on Figure 11.

Traces of interactions between the functional groups of CX–R and PLA backbone may be derived from the small differences in δC=O at ~750 cm^{-1}. In the case of PLA the broad band splits into two peaks (at about 753 and 746 cm^{-1}) of intensity ratio dependent on the crystallization temperature, as earlier reported [63]. For CX–OH and CX–COOMe, the ratio of vibration modes is slightly smaller despite much more intensive skeletal bands of ν_{as}(COC) + ρ_{as}(CH$_3$) (1213 cm^{-1}) and ρ(CH$_3$) + ν(C–COO) (920 cm^{-1}). The effect was most pronounced for PLA/CX–COOH.

3.5. Nanomechanical properties

Depth-sensing indentation (CSM and BASIC methods) was used to evaluate the micro- and nano-scale mechanical properties of amorphous PLA matrices with incorporated additives. Hardness and elastic modulus were derived assuming linear elastic behaviour of the material at the onset of unloading. The extracted data allowed resolving spatially the properties of the heterogeneous nanocomposites, either across the thickness or along the surface. Nanoindentation experiments with moulded and quenched samples were performed at different indentation depths (Figure 13). The change of elastic modulus and hardness of native PLA and PLA/CX–Vi with the indentation depth is typical for viscoelastic polymer materials [64–66]. The effect can be also explained in terms of a surface 'skin'. Larger chain dynamics and lower amount of entanglements at the surface result in changes in properties through sample thickness. A slightly different trend in depth dependence of mechanical properties was noted for CX–R capable of hydrogen bonding with PLA.

Hardness and modulus mapping using the BASIC method allowed for their quantitative determinations with high spatial resolution (Figure 13). Profiles of the local hardness and modulus obtained from the lines of indents on the surface of PLA/CX–R were used. Micromechanical properties were influenced by the mixture composition. It was found that changes of surface stiffness and hardness are uniform for PLA with evenly dispersed CX–OH. More pronounced local variations of the mechanical properties were observed (in accordance with SEM-EDS) for PLA/CX–COOH [and PLA/CX–(OH)$_2$ – not shown]. Changes of surface hardness and elasticity indicate that the accumulated CX–R locally changed PLA properties. It is known that the improvement of mechanical properties of nanocomposites depends on the dispersion of the filler and its interactions with polymer matrix [65]. Inhomogeneous microstructural composition of some PLA/CX–R may be thus responsible for the observed differences in surface hardening. Moreover, the nanoscale properties of semicrystalline polymers can vary due to the presence of amorphous and crystalline domains [67]. Thus, PLA macromolecules linked with nucleating molecules of CX–R can be better organized than the more amorphous part of the sample.
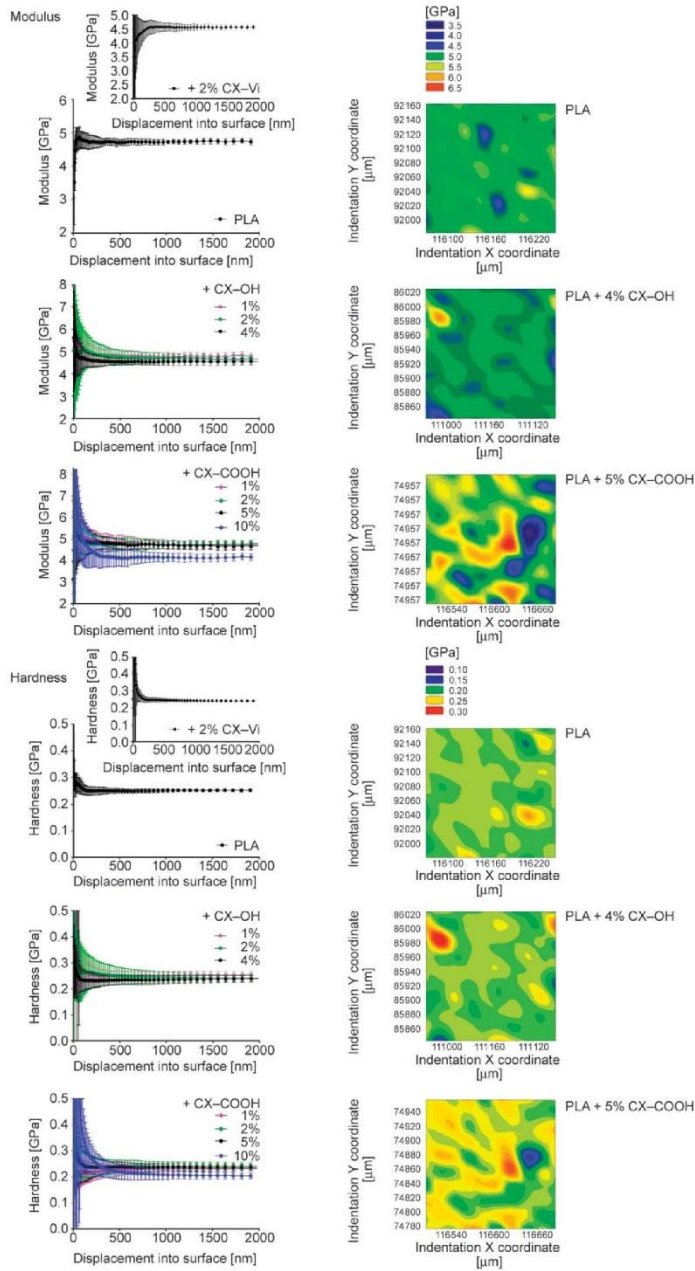
Figure 13. Variation of modulus and hardness with displacement into surface (with exemplary surface maps) of neat PLA and its nanocomposites with CX–OH and CX–COOH (inserts: E and H obtained for PLA admixed with CX–Vi at 2 wt%).

4. Conclusions

Cyclotetrasiloxanes (CX–R) with hydrogen bond accepting/donating functional groups engage in a range of supramolecular interactions with polylactide chains. The nature of those interactions was explored using a combination of complementary analytical methods. Low molecular weight cyclosiloxane compounds were evenly dispersed in the polymer matrix and their presence was clearly reflected in the polymer dielectric response. Distinct relaxation processes associated with different types of hydrogen bonding were observed. It was also found that CX–R, despite their very low aspect ratio, can work efficiently as nucleating agents for PLA. Formation of characteristic crystal structures was determined by the kind and the amount of the additive. CX–OH with hydrogen bond donating hydroxyl groups induced formation of α crystals at temperatures lower than those required for a similar effect with neat PLA, and also lower than those reported for enantiomerically pure PLLA. Samples prepared with CX–COOH of strong hydrogen bond donor/acceptor ability exhibited a specific phase separation at higher loading. Modifications in the long-range chain structure were reflected in variations of the heat flow recorded with DSC and corroborated with changes in the local molecular environment (short-range vibrations) indicated by FTIR.

Acknowledgements

References

[1] Castro-Aguirre E., Iñiguez-Franco F., Samsudin H., Fang X., Auras R.: Poly(lactic acid) – Mass production, processing, industrial applications, and end of life. Advanced Drug Delivery Reviews, **107**, 333–366 (2016). https://doi.org/10.1016/j.addr.2016.03.010

[2] Di Lorenzo M. L., Androsch R.: Synthesis, structure and properties of poly(lactic acid). Springer, Cham (2018). https://doi.org/10.1007/978-3-319-64230-7

[3] Murariu M., Dubois P.: PLA composites: From production to properties. Advanced Drug Delivery Reviews, **107**, 17–46 (2016). https://doi.org/10.1016/j.addr.2016.04.003

[4] Basu A., Nazarkovsky M., Ghadi R., Khan W., Domb A. J.: Poly(lactic acid)-based nanocomposites. Polymers for Advanced Technologies, **28**, 919–930 (2017). https://doi.org/10.1002/pat.3985

[5] De Santis P., Kovacs A. J.: Molecular conformation of poly(S-lactic acid). Biopolymers, **6**, 299–306 (1968). https://doi.org/10.1002/bip.1968.360060305

[6] Wasanasuk K., Tashiro K., Hanesaka M., Ohhara T., Kurihara K., Kuroki R., Tamada T., Ozeki T., Kanamoto T.: Crystal structure analysis of Poly(L-lactic acid) α form on the basis of the 2-dimensional wide-angle synchrotron X-ray and neutron diffraction measurements. Macromolecules, **44**, 6441–6452 (2011). https://doi.org/10.1021/ma2006624

[7] Müller A. J., Ávila M., Saenz G., Salazar J.: Crystallization of PLA-based materials. in 'Poly(lactic acid) science and technology: Processing, properties, additives and applications' (eds.: Jiménez A., Peltzer M., Ruseckaite R.) The Royal Society of Chemistry, Cambridge, RSC Polymer Chemistry Series, **12**, 66–98 (2015). https://doi.org/10.1039/9781782624806-00066

[8] Saeidlou S., Huneault M. A., Li H., Park C. B.: Poly(lactic acid) crystallization. Progress in Polymer Science, **37**, 1657–1677 (2012). https://doi.org/10.1016/j.progpolymsci.2012.07.005

[9] Xu J-Z., Zhong G-J., Hsiao B. S., Fu Q., Li Z-M.: Low-dimensional carbonaceous nanofiller induced polymer crystallization. Progress in Polymer Science, **39**, 555–593 (2014). https://doi.org/10.1016/j.progpolymsci.2013.06.005

[10] Brzeziński M., Biela T.: Polylactide nanocomposites with functionalized carbon nanotubes and their stereocomplexes: A focused review. Materials Letters, **121**, 244–250 (2014). https://doi.org/10.1016/j.matlet.2014.01.159

[11] Xu H., Adolfsson K. H., Xie L., Hassanzadeh S., Pettersson T., Hakkarainen M.: Zero-dimensional and highly oxygenated graphene oxide for multifunctional poly(lactic acid) bionanocomposites. ACS Sustainable Chemistry and Engineering, **4**, 5618–5631 (2016). https://doi.org/10.1021/acssuschemeng.6b01524

[12] Bayer I. S.: Thermomechanical properties of polylactic acid-graphene composites: A state-of-the-art review for biomedical applications. Materials, **10**, 748/1–748/33 (2017). https://doi.org/10.3390/ma10070748

[13] Ege D., Kamali A. R., Boccaccini A. R.: Graphene oxide/polymer-based biomaterials. Advanced Engineering Materials, **19**, 1700627/1–1700627/22 (2017). https://doi.org/10.1002/adem.201700627

[14] Lai W-C.: Thermal behavior and crystal structure of poly(L-lactic acid) with 1,3:2,4-dibenzylidene-*d*-sorbitol. Journal of Physical Chemistry B, **115**, 11029–11037 (2011). https://doi.org/10.1021/jp2037312

[15] Li C., Luo S., Wang J., Wu H., Guo S., Zhang X.: Conformational regulation and crystalline manipulation of PLLA through a self-assembly nucleator. Biomacromolecules, **18**, 1440–1448 (2017). https://doi.org/10.1021/acs.biomac.7b00367

[16] Feng Y., Ma P., Xu P., Wang R., Dong W., Chen M., Joziasse C.: The crystallization behavior of poly(lactic acid) with different types of nucleating agents. International Journal of Biological Macromolecules, **106**, 955–962 (2018).
https://doi.org/10.1016/j.ijbiomac.2017.08.095

[17] Nam J. Y., Okamoto M., Okamoto H., Nakano M., Usuki A., Matsuda M.: Morphology and crystallization kinetics in a mixture of low-molecular weight aliphatic amide and polylactide. Polymer, **47**, 1340–1347 (2006).
https://doi.org/10.1016/j.polymer.2005.12.066

[18] Bai H., Huang C., Xiu H., Zhang Q., Deng H., Wang K., Chen F., Fu Q.: Significantly improving oxygen barrier properties of polylactide *via* constructing parallel-aligned shish-kebab-like crystals with well-interlocked boundaries. Biomacromolecules, **15**, 1507–1514 (2014).
https://doi.org/10.1021/bm500167u

[19] Xie Q., Han L., Shan G., Bao Y., Pan P.: Polymorphic crystalline structure and crystal morphology of enantiomeric poly(lactic acid) blends tailored by a self-assemblable aryl amide nucleator. ACS Sustainable Chemistry and Engineering, **4**, 2680–2688 (2016).
https://doi.org/10.1021/acssuschemeng.6b00191

[20] Mierzwa M., Floudas G., Dorgan J., Knauss D., Wegner J.: Local and global dynamics of polylactides.: A dielectric spectroscopy study. Journal of Non-Crystalline Solids, **307–310**, 296–303 (2002).
https://doi.org/10.1016/S0022-3093(02)01480-1

[21] Brás A. R., Viciosa M. T., Wang Y., Dionísio M., Mano J. F.: Crystallization of poly(L-lactic acid) probed with dielectric relaxation spectroscopy. Macromolecules, **39**, 6513–6520 (2006).
https://doi.org/10.1021/ma061148r

[22] Brás A. R., Malik P., Dionísio M., Mano J. F.: Influence of crystallinity in molecular motions of poly(L-lactic acid) investigated by dielectric relaxation spectroscopy. Macromolecules, **41**, 6419–6430 (2008).
https://doi.org/10.1021/ma800842a

[23] Zhang Y., Li J., Zhang Z., Li H., Meng Y., Jiang S.: Dynamical behaviors of polylactide crystallization. Journal of Polymer Research, **26**, 72/1–72/9 (2019).
https://doi.org/10.1007/s10965-019-1698-4

[24] Leng J., Kang N., Wang D-Y., Falkenhagen J., Thünemann A. F., Schönhals A.: Structure–property relationships of nanocomposites based on polylactide and layered double hydroxides – Comparison of MgAl and NiAl LDH as nanofiller. Macromolecular Chemistry and Physics, **218**, 1700232/1–1700232/12 (2017).
https://doi.org/10.1002/macp.201700232

[25] Pluta M., Jeszka J. K., Boiteux G.: Polylactide/montmorillonite nanocomposites: Structure, dielectric, viscoelastic and thermal properties. European Polymer Journal, **43**, 2819–2835 (2007).
https://doi.org/10.1016/j.eurpolymj.2007.04.009

[26] Klonos P., Kripotou S., Kyritsis A., Papageorgiou G. Z., Bikiaris D., Gournis D., Pissis P.: Glass transition and segmental dynamics in poly(L-lactic acid)/graphene oxide nanocomposites. Thermochimica Acta, **617**, 44–53 (2015).
https://doi.org/10.1016/j.tca.2015.08.020

[27] Yousefzade O., Valenti S., Puiggalí J., Garmabi H., Macovez R.: Segmental relaxation and partial crystallization of chain-extended poly(L-lactic acid) reinforced with carboxylated carbon nanotube. Journal of Polymer Science Part B, Polymer Physics, **57**, 222–233 (2018).
https://doi.org/10.1002/polb.24774

[28] Chiulan I., Frone A. N., Brandabur C., Panaitescu D. M.: Recent advances in 3D printing of aliphatic polyesters. Bioengineering, **5**, 2/1–2/18 (2018).
https://doi.org/10.3390/bioengineering5010002

[29] Baran E. H., Erbil H. Y.: Surface modification of 3D printed PLA objects by fused deposition modeling: A review. Colloids Interfaces, **3**, 43/1–43/25 (2019).
https://doi.org/10.3390/colloids3020043

[30] Coppola B., Cappetti N., Di Maio L., Scarfato P., Incarnato L.: 3D printing of PLA/clay nanocomposites: Influence of printing temperature on printed samples properties. Materials, **11**, 1947/1–1947/17 (2018).
https://doi.org/10.3390/ma11101947

[31] Kaygusuz B., Özcrinç S.: Improving the ductility of polylactic acid parts produced by fused deposition modeling through polyhydroxyalkanoate additions. Journal of Applied Polymer Science, **136**, 48154/1–48154/8 (2019).
https://doi.org/10.1002/APP.48154

[32] Kowalewska A., Nowacka M., Tracz A., Makowski T.: Supramolecular self-assembly of linear oligosilsesquioxanes on mica – AFM surface imaging and hydrophilicity studies. Soft Matter, **11**, 4818–4829 (2015).
https://doi.org/10.1039/C5SM00787A

[33] Nowacka M., Kowalewska A., Makowski T.: Nanostructured surfaces by supramolecular self-assembly of linear oligosilsesquioxanes with biocompatible side groups. Beilstein Journal of Nanotechnology, **6**, 2377–2387 (2015).
https://doi.org/10.3762/bjnano.6.244

[34] Armarego W. L. F., Chai C. L. L.: Purification of laboratory chemicals. Butterworth-Heinemann, Bodmin (2003).
https://doi.org/10.1016/B978-0-7506-7571-0.X5000-5

[35] Oliver W. C., Pharr M. G.: An improved technique for determining hardness and elastic modulus using load and displacement sensing indentation experiments. Journal of Materials Research, **7**, 1564–1583 (1992).
https://doi.org/10.1557/JMR.1992.1564

[36] Li X., Bhushan B.: A review of nanoindentation continuous stiffness measurement technique and its applications. Materials Characterization, **48**, 11–36 (2002).
https://doi.org/10.1016/S1044-5803(02)00192-4

[37] Pelletier E., Harrod J. F.: Cyclosiloxanes as frameworks for multimetallic compounds. 3. Proton NMR spectra of some substituted methylcyclosiloxanes. Organometallics, **3**, 1070–1075 (1984).
https://doi.org/10.1021/om00085a018

[38] Makarova N. N., Petrova I. M., Petrovskii P. V., Kaznacheev A. V., Volkova L. M., Shcherbina M. A., Bessonova N. P., Chvalun S. N., Godovskii Yu. K.: Synthesis of new stereoregular 2,4,6,8-tetraphenylcyclotetrasiloxanes with mesogenic groups and the influence of spatial isomerism on the phase state of individual isomers and their mixtures. Russian Chemical Bulletin, **53**, 1983–1992 (2004).
https://doi.org/10.1007/s11172-005-0059-0

[39] Ryuichi I., Yuriko K., Yusuke K.: Cyclic tetrasiloxanetetraols: Formation, isolation, and characterization. Chemistry Letters, **38**, 364–365 (2009).
https://doi.org/10.1246/cl.2009.364

[40] Pozdnyakova Y. A., Korlyukov A. A., Kononova E. G., Lyssenko K. A., Peregudov A. S., Shchegolikhina O. I.: Cyclotetrasiloxanetetrols with methyl groups at silicon: Isomers all-cis- and cis-trans-cis-[MeSi(O)OH]₄. Inorganic Chemistry, **49**, 572–577 (2010).
https://doi.org/10.1021/ic9017079

[41] Deshmukh M. S., Vijayakanth T., Boomishankar R.: Stereochemically distinct cyclotetrasiloxanes containing 3-pyridyl moieties and their functional coordination polymers. Inorganic Chemistry, **55**, 3098–3104 (2016).
https://doi.org/10.1021/acs.inorgchem.6b00001

[42] ASTM D1746-03: Standard test method for transparency of plastic sheeting (2015).

[43] Havriliak S., Negami S.: A complex plane representation of dielectric and mechanical relaxation processes in some polymers. Polymer, **8**, 161–210 (1967).
https://doi.org/10.1016/0032-3861(67)90021-3

[44] Fischer E. W., Sterzel H. J., Wegner G.: Investigation of the structure of solution grown crystals of lactide copolymers by means of chemical reactions. Kolloid-Zeitschrift und Zeitschrift für Polymere, **251**, 980–990 (1973).
https://doi.org/10.1007/BF01498927

[45] Kikkawa Y., Abe H., Fujita M., Iwata T., Inoue Y., Doi Y.: Crystal growth in poly(L-lactide) thin film revealed by *in situ* atomic force microscopy. Macromolecular Chemistry and Physics, **204**, 1822–1831 (2003).
https://doi.org/10.1002/macp.200350044

[46] Zhao L-S., Cai Y-H.: Investigating the physical properties of poly(L-lactic acid) modified using an aromatics succinic dihydrazide derivative. Polymer Science, Series A, **6**, 777–787 (2018).
https://doi.org/10.1134/S0965545X18070088

[47] Tsui H.: Poly(lactic acid) stereocomplexes: A decade of progress. Advanced Drug Delivery Reviews, **107**, 97–135 (2016).
https://doi.org/10.1016/j.addr.2016.04.017

[48] Zhang J., Tashiro K., Tsuji H., Domb A. J.: Disorder-to-order phase transition and multiple melting behavior of poly(L-lactide) investigated by simultaneous measurements of WAXD and DSC. Macromolecules, **41**, 1352–1357 (2008).
https://doi.org/10.1021/ma0706071

[49] Pan P., Zhu B., Kai W., Dong T., Inoue Y.: Polymorphic transition in disordered poly(L-lactide) crystals induced by annealing at elevated temperatures. Macromolecules, **41**, 4296–4304 (2008).
https://doi.org/10.1021/ma800343g

[50] Wasanasuk K., Tashiro K.: Structural regularization in the crystallization process from the glass or melt of poly(L-lactic acid) viewed from the temperature-dependent and time-resolved measurements of FTIR and wide-angle/small-angle X-ray scatterings. Macromolecules, **44**, 9650–9660 (2011).
https://doi.org/10.1021/ma2017666

[51] Gracia-Fernández C., Gómez-Barreiro S., López-Beceiro J., Naya S., Artiaga R.: New approach to the double melting peak of poly(L-lactic acid) observed by DSC. Journal of Materials Research, **27**, 1379–1382 (2012).
https://doi.org/10.1557/jmr.2012.57

[52] Zhang J., Duan Y., Sato H., Tsuji H., Noda I., Yan S., Ozaki Y.: Crystal modifications and thermal behavior of poly(L-lactic acid) revealed by infrared spectroscopy. Macromolecules, **38**, 8012–8021 (2005).
https://doi.org/10.1021/ma051232r

[53] Kister G., Cassanas G., Vert M.: Effects of morphology, conformation and configuration on the IR and Raman spectra of various poly(lactic acid)s. Polymer, **39**, 267–273 (1998).
https://doi.org/10.1016/S0032-3861(97)00229-2

[54] Meaurio E., Zuza E., López-Rodríguez N., Sarasua J. R.: Conformational behavior of poly(L-lactide) studied by infrared spectroscopy. Journal od Physical Chemistry B, **110**, 5790–5800 (2006).
https://doi.org/10.1021/jp055203u

[55] Pan P., Yang J., Shan G., Bao Y., Weng Z., Cao A., Yazawa K., Inoue Y.: Temperature-variable FTIR and solid-state ¹³C NMR investigations on crystalline structure and molecular dynamics of polymorphic poly(L-lactide) and poly(L-lactide)/poly(D-lactide) stereocomplex. Macromolecules, **45**, 189–197 (2012).
https://doi.org/10.1021/ma201906a

[56] Kang S., Hsu S. L., Stidham H. D., Smith P. B., Leugers M. A., Yang X.: A spectroscopic analysis of poly(lactic acid) structure. Macromolecules, **34**, 4542–4548 (2001).
https://doi.org/10.1021/ma0016026

[57] Meaurio E., López-Rodróguez N., Sarasua J. R.: Infrared spectrum of poly(L-lactide): Application to crystallinity studies. Macromolecules, **39**, 9291–9301 (2006).
https://doi.org/10.1021/ma061890r

109

[58] Pan P., Zhu B., Kai W., Dong T., Inoue Y.: Effect of crystallization temperature on crystal modifications and crystallization kinetics of poly(L-lactide). Journal of Applied Polymer Science, **107**, 54–62 (2008).
https://doi.org/10.1002/app.27102

[59] Zhang J., Tsuji H., Noda I., Ozaki Y.: Weak intermolecular interactions during the melt crystallization of poly (L-lactide) investigated by two-dimensional infrared correlation spectroscopy. Journal of Physical Chemistry B, **108**, 11514–11520 (2004).
https://doi.org/10.1021/jp048308q

[60] Lan Q., Yu J., Zhang J., He J.: Nucleation enhancement in stereodefective poly(L-lactide) by free volume expansion resulting from low-temperature pressure CO_2 preconditioning. Polymers, **10**, 120/1–120/12 (2018).
https://doi.org/10.3390/polym10020120

[61] Xue B., Xie L., Zhang J.: Detailed molecular movements during poly(L-lactic acid) cold-crystallization investigated by FTIR spectroscopy combined with two-dimensional correlation analysis. RSC Advances, **7**, 47017–47028 (2017).
https://doi.org/10.1039/c7ra08921j

[62] Pan P., Liang Z., Zhu B., Dong T., Inoue Y.: Blending effects on polymorphic crystallization of poly(L-lactide). Macromolecules, **42**, 3374–3380 (2009).
https://doi.org/10.1021/ma8024943

[63] Vasanthan N., Ly O.: Effect of microstructure on hydrolytic degradation studies of poly (L-lactic acid) by FTIR spectroscopy and differential scanning calorimetry. Polymer Degradation and Stability, **94**, 1364–1372 (2009).
https://doi.org/10.1016/j.polymdegradstab.2009.05.015

[64] Beyaoui M., Mazeran P-E., Arvieu M-F., Bigerelle M., Guigon M.: Analysis of nanoindentation curves in the case of bulk amorphous polymers. International Journal of Materials Research, **100**, 943–949 (2009).
https://doi.org/10.3139/146.110137

[65] Díez-Pascual A. M., Gómez-Fatou M. A., Ania F., Flores A.: Nanoindentation in polymer nanocomposites. Progress in Materials Science, **67**, 1–94 (2015).
https://doi.org/10.1016/j.pmatsci.2014.06.002

[66] Shirazi R. N., Rochev Y., McHugh P.: Nanoindentation of solvent-cast and compression-moulded poly(lactic-*co*-glycolic acid) to determine elastic modulus and hardness. Polymer Testing, **50**, 111–118 (2016).
https://doi.org/10.1016/j.polymertesting.2016.01.009

[67] Voyiadjis G. Z., Samadi-Dooki A., Malekmotiei L.: Nanoindentation of high performance semicrystalline polymers: A case study on PEEK. Polymer Testing, **61**, 57–64 (2017).
https://doi.org/10.1016/j.polymertesting.2017.05.005

110

POLYMER
TESTING
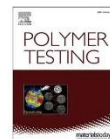
Supramolecular interactions involving fluoroaryl groups in hybrid blends of polylactide and ladder polysilsesquioxanes

Anna Kowalewska [a,*], Agata S. Herc [a], Joanna Bojda [a], Marcin Palusiak [b], Ewa Markiewicz [c], Paweł Ławniczak [c], Maria Nowacka [a], Joanna Sołtysiak [d], Artur Różański [a], Ewa Piorkowska [a]

[a] Centre of Molecular and Macromolecular Studies, Polish Academy of Sciences, Sienkiewicza 112, 90-363, Łódź, Poland
[b] Department of Physical Chemistry, Faculty of Chemistry, University of Lodz, Pomorska 163/165, 90-236, Łódź, Poland
[c] Institute of Molecular Physics Polish Academy of Sciences, Smoluchowskiego 17, 60-179, Poznan, Poland
[d] Industrial Chemistry Research Institute, Rydygiera 8, 01-793, Warsaw, Poland

A B S T R A C T

Linear ladder polysilsesquioxanes (LPSQ-R) bearing fluoroaryl groups [R: *p*-fluorophenyl (F), *p*-tri-fluoromethylphenyl (F$_3$) or pentafluorophenyl (F$_5$)] were used to modify polylactide (PLA). Vibrational spectroscopy analysis suggested specific, non-covalent interactions between C=O of PLA and fluoroaryl groups of LPSQ-R while quantum-chemical modelling performed for representative models indicated that the pattern of possible preferred contacts differs for LPSQ-F$_3$ in respect to LPSQ-F and LPSQ-F$_5$ (H···F hydrogen bonding against n→π* attractive interactions). It may affect interface phenomena in PLA/LPSQ-R systems. Thermal characteristics of PLA/LPSQ-R depended on the type of R and LPSQ-R content. Dielectric relaxation spectroscopy (DRS) studies revealed one relaxation process present in PLA and related to the glass transition. However, for PLA/LPSQ-R blends two processes were identified: glass transition and normal–mode relaxation. The modification with fluorinated macromolecules increased hydrophobicity of amorphous PLA and improved its mechanical and gas barrier properties, which can be of importance for packaging applications.

1. Introduction

Composite multi-layered films made of petroleum derived polymers used for food packaging allow maintenance of a suitable atmosphere for the time of storage. However, technical problems in their recycling increase the interest in other packaging materials, e.g. compostable polymers obtained from renewable natural sources. Materials based on "green" biodegradable polyesters, such as polylactide (PLA) and its composites can be a promising option for environmentally sustainable packaging [1–3]. As recently reviewed, several biobased and biodegradable nucleating agents (orotic acid, humic acids, fulvic acids, nanocellulose, and cyclodextrins) were shown to enhance properties of PLA ("soft templating") [4]. However, oxygen and water barrier properties of polylactide are generally poor. An improvement of barrier properties may be achieved by increasing the path of gas molecules in the polyester matrix [5]. The presence of crystals impermeable for small molecules can enhance polymer barrier properties. However, Guinault et al. [6] showed that the creation of a rigid amorphous fraction including larger free volume produced a pathway of accelerated gas transport around the lamellae of α′-form crystallites in PLLA. Moreover, PLA crystallinity causes a decrease of elongation at break [7,8]. On the other hand an improvement of mechanical properties of PLA achieved e. g. by addition of plasticizers, results in higher polymer chain mobility and can be detrimental for the barrier properties. Tortuosity of the diffusive pathway inside amorphous PLA can be also increased by high aspect ratio fillers or nanofillers. Exfoliated nanoclays [9,10] and graphene or graphene oxide [11] may have a positive impact on barrier properties of PLA, providing that orientation of nanoplatelets is perpendicular to the gas flow, which is quite difficult to achieve. Barrier properties are also improved in PLA-based multilayer materials [12,13]. Another important problem is linked to the fact that polar ester linkages in PLA increase water sorption, despite hydrophobic nature of the polymer matrix. Introduction of fluorine atoms may decrease surface free energy and enhance barrier properties of polymeric blends [14–17]. However, poor compatibility of the components quite often results in deterioration of their mechanical properties.

Noncovalent interactions have a pivotal role in the design of new hybrid materials [18]. Nevertheless, supramolecular contacts involving

---

fluorine atoms are scarcely exploited in materials engineering. Even though the short C–F···H–C contacts are weak, a convincing evidence of their existence has been given [19–23]. Their strength depends on the hybridization of carbon atoms to which fluorine and hydrogen are linked. C (sp3/sp2)–H···F–C (sp3) provides more stabilization than C (sp3/sp2)–H···F–C (sp2) [24]. Fluorine can also display a positive σ-hole effect (acting as a halogen bond donor) when connected to an electron withdrawing atom or organic group [25–27]. It was also observed that replacement of a fluorine atom by –CF₃ moiety in phenyl rings leads to the formation of halogen bonds (C–F···F–C contacts) and C–F···π interactions [28]. Trifluoromethyl group is strongly electron-withdrawing and affects behaviour of neighbouring hydrogen atoms. The presence of σ-hole involving –CF₃ groups was revealed both experimentally and by theoretical charge density analysis [29]. Those data inspired our studies on the synthesis of hybrid polysilsesquioxanes bearing various fluoroaryl groups and their application for modification of PLA. It was recently postulated that hydrogen bond accepting –C=O groups can also connect with a variety of nucleophiles through attractive n→π* interactions [30,31]. Such n→π* contacts have been found in proteins [32], small molecules [33] and transition metal complexes [34]. They may as well be involved in the formation of helical structure of PLA chains [35]. Modification of properties of PLA by addition of components operating through C–F···H–C and n→π* interactions is to our best knowledge unknown.

In this report we present results obtained on modification of PLA with functionalized oligomeric linear ladder polysilsesquioxanes (LPSQ) bearing side 4-fluorophenyl, 4-(trifluoro)phenyl or pentafluorophenyl groups. We have studied their effect with vibrational (FT-IR and Raman) spectroscopies and evaluated the extent of the observed interactions with regard to the properties of the obtained compositions. The supramolecular contacts were modelled with the use of DFT [36] and post-SCF MP2 [37] methods for simplified models being representative for PLA with functionalized LPSQ-R. For the studies we have chosen well defined hybrid macromolecular systems having double-chain silsesquioxane backbones. Due to the specific structure of the LPSQ backbone and local congestion of functional groups R, a localized binding of several lactide segments may be achieved. It resembles the effect of self-organizing templates, e.g. arylamide nucleators [38]. We have previously shown that functionalized LPSQ can form specific self-assembled structures [39–42] and may be successfully applied as additives to polylactide [43]. Contrary to their cyclosiloxane analogues [44], LPSQ-R (R: –OH, –COOH, -COOMe) did not decrease significantly glass transition temperature of PLA. We have found that the postulated interactions involving fluoroaryl groups (Scheme 1) may play an important role in modification of relaxation processes in PLA matrix, which may be correlated with different thermal behaviour of the PLA/LPSQ-R blends. The presence of those additives influences mechanical deformation of PLA/LPSQ-R. Moreover, an increase of the

hydrophobicity and a significant reduction of the oxygen transmission rate (OTR) through PLA/LPSQ-R membranes was observed at room temperature. It should be stressed that the latter effect was noted for completely amorphous samples, which is quite unique and can be of an exceptional importance for packaging materials.

2. Experimental

2.1. Materials

Oligomeric polysilsesquioxanes LPSQ-R of double-strand backbone terminated with trimethylsilyl groups were prepared by photoinitiated thiol-ene addition of selected mercapto-compounds (Scheme 2), analogously to earlier published procedures [39,44]. Three fluoroaryl thiols were grafted to linear poly (vinylsilsesquioxane) precursors (LPSQ-Vi, $M_n = 1$ kg/mol, $M_w/M_n = 1.4$ (SEC/RI) [45]) in the presence of radical initiators: azobisizobutyronitrile [AIBN (98%, Sgma Aldrich, Germany) for FC₆H₄SH and F₅C₆SH] or 2,2-dimethoxy-2-phenylacetophenone [DMPA (99%, POCh, Poland) for F₃CC₆H₄SH] giving respectively LPSQ-F, LPSQ-F5 and LPSQ-F3. Model functionalized cyclotetrasiloxanes (CX–R) were prepared by thiol-ene addition of the mercapto-compounds to vinyl groups of 1,3,5,7-tetravinyl-1,3,5,7-tetramethylcyclotetrasiloxanes (CX–Vi) (97%, a mixture of isomers; ABCR GmbH, Germany). The detailed synthetic procedure and products characterization can be found in ESI. Commercially available reagents were used as received [4-fluorothiophenol (97%, Fluorochem Ltd, UK), 4-(trifluoromethyl)thiophenol (97%, Fluorochem Ltd, UK);
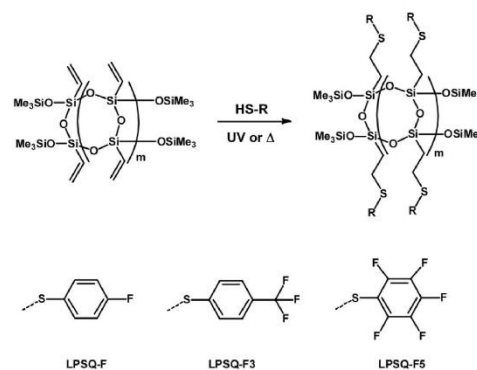
Scheme 2. Synthesis of functionalized LPSQ.
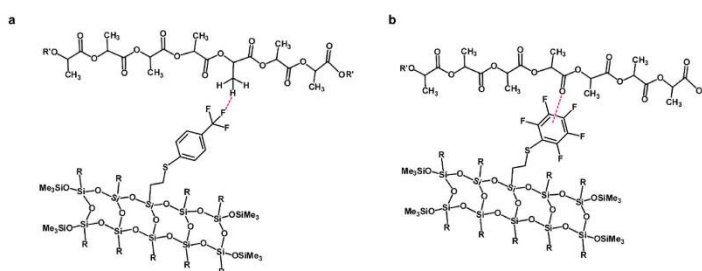
Scheme 1. Postulated C–F···H–C (a) and n→π* (b) interactions between fluoroaryl polysilsesquioxanes and PLA chains (R represents (a) 4-(trifluoromethyl)thiophenyl or (b) pentafluorothiophenyl groups; R' – end groups of PLA).

pentafluorothiophenol (97%, Fluorochem Ltd, UK)]. AIBN was recrystallized from acetone and dried under high vacuum. Solvents (POCh, Poland) were purified following literature procedures [46].

The polyester matrix used for the studies was a commercially available polylactide (PLA) [NW4032D grade from NatureWorks LLC, Minnetonka, MN, $M_n = 130$ kg/mol, $M_w/M_n = 1.9$ (SEC/MALLS)] containing 1.2 mol% of D-lactide units. Compositions of PLA NW4032D with LPSQ-R contents of 1 wt%, 5 wt%, 10 wt% and 20 wt% were prepared. In general, the polyester resin was dissolved in CH_2Cl_2, (c = 10 wt %) and left for 24 h. Then a specific amount of LPSQ-R solution in CH_2Cl_2 (c = 10 wt %) was added dropwise. The mixtures were stirred magnetically for 2 h at room temperature. No viscosity changes or turbidity appearance were observed during that time. The prepared compositions were then poured into Petri dishes and left for free solvent evaporation. Solid products were carefully dried for 24 h at 80 °C under high vacuum (0.01 Torr). For further studies, 1 mm, 0.5 mm and 0.35 mm thick films were compression molded at 190 °C and rapidly quenched at 0 °C. The prepared blends are referred as, for example, P/5-R, where P denotes PLA and the number stands for a respective LPSQ-R weight content. The same procedure was applied for the preparation of PLA/CX-R blends (ESI). Compositions P/100-R containing a large amount of LPSQ-R (the same weight as that of PLA component) were prepared exclusively for the FT-IR and Raman spectroscopic studies. PLA used for those measurements was carefully purified (in order to remove stabilizers) by precipitation of PLA dissolved in CH_2Cl_2 into a large amount of MeOH. The P/100-R blends were prepared by mixing equivolume aliquots of solutions of LPSQ-R and PLA in CH_2Cl_2 (7 wt%). The solvent evaporation and drying was carried out as described above.

2.2. Methodology

Detailed description of the theoretical treatment of complexes stabilized via n→π* interactions and CSD search conditions as well as all the applied analytic techniques (^1H, ^{13}C and ^{29}Si NMR spectroscopy; size-exclusion chromatography (SEC) with multi-angle laser light scattering (MALLS) and refractive index (RI) detection in CH_2Cl_2; FT-IR and Raman spectroscopy; differential scanning calorimetry (DSC); thermogravimetric analysis (TGA); dielectric relaxation spectroscopy (DRS); scanning electron microscopy (SEM); direct light transmittance (DLT); dynamic mechanical thermal analysis (DMTA); tensile tests; oxygen permeability and surface energy measurements) can be found in ESI.

3. Results and discussion

3.1. Synthesis and properties of LPSQ-R

Synthesis of three various fluoroaryl LPSQ-R by modification of LPSQ-Vi with fluorinated tiophenols was based on the thiol-ene addition approach (Scheme 2). Functional groups that have been chosen for the studies - 4-fluorophenyl, 4-(trifluoromethyl)phenyl and pentafluorophenyl - differed by the number of electron withdrawing fluorine atoms and their placement with respect to the phenyl ring. LPSQ-F3 was obtained in the presence of DMPA, following the procedure similar to that used for the preparation of LPSQ-COOH [39]. However, the same strategy was not effective for the addition of 4-fluorothiophenol and pentafluorothiophenol. The synthesis of LPSQ-F and LPSQ-F5 required the use of a thermolabile initiator (AIBN). In both cases the addition to vinyl groups proceeded quantitatively against the Markovnikov rule and the fluoroaryl moieties were bound to silicon atoms by ethylthio-linkers. Their structure was characterized with NMR spectroscopy (Table ESI-1). The functionalized LPSQ are very viscous liquids, well soluble in typical organic solvents. Their specific glass transition temperatures (T_g) can be related to the steric hindrance of the side substituents (Fig. ESI-1); T_gs of LPSQ-F, LPSQ-F3 and LPSQ-F5 were at −31 °C, −9 °C and −10 °C, respectively.

3.2. FTIR/Raman analysis of interactions in PLA/LPSQ-R blends

Spectroscopic studies on supramolecular interactions in PLA/LPSQ blends were carried out for samples containing larger amounts of LPSQ-R (P/100-R). This approach provided a reasonable molar ratio [R]/[C=O] (respectively 0.345, 0.281 and 0.259, for P/100-F, P/100-F3 and P/100-F5) that resulted in detectable shifts of some characteristic IR and Raman vibration modes. Their assignment (Table ESI-2) was based on the literature data [47–50]. FT-IR spectra were recorded in transmission mode for thin films (Fig. ESI-2). A significant part of the spectra of PLA (1200 - 1000 cm^{-1}) was overlapped with those originating from LPSQ-R [especially the broad ν(Si–O) band]. Nevertheless, a reduction of the vibration modes at 1211 cm^{-1} (corresponding to ν_{as} (COC) and $r_{as}CH_3$ in PLA backbone) and 1042 cm^{-1} (r (C–CH$_3$)) can be observed for all P/100-R blends. Those bands typically increase (along with the crystalline skeletal mode at 920 cm^{-1}) with the amount of crystalline fraction in PLA [51], as it was shown in the spectrum of PLA after 30 min isothermal crystallization at 110 °C. Blends P/100-R crystallized slowly owing to the presence of large amounts of additives. Yet, the intensity of peaks at 1042 cm^{-1} and 1211 cm^{-1} almost did not change. The overall effect may suggest changes in the chemical environment of the polyester bonds. A very interesting phenomenon was observed on examination of ν(C=O) band. The mode ν(C=O) (1755 cm^{-1}) became narrow on blending with LPSQ-R. The largest effect was observed for P/100-F5 (ν(C=O) half width of 20.8 cm^{-1}, comparing to 29.5 cm^{-1}, 27.8 cm^{-1}, 26.7 cm^{-1} and 23.8 cm^{-1} for, respectively, neat amorphous PLA, crystallized PLA, P/100-F and P/100-F3). The exact position of component modes was obtained from their second derivatives (Fig. 1).

The C=O stretching band in amorphous PLA contains two major peaks ascribed to gg (1778 cm^{-1}) and gt (1742 cm^{-1}) conformers of lowest energy and largest statistical contribution [51–54]. Their position was only slightly shifted (to, respectively, 1776 cm^{-1} and 1745 cm^{-1}) when PLA was crystallized isothermally at 110 °C. However, a significant red shift of the gt band was noted for P/100-F5 (1750 cm^{-1}) and P/100-F3 (1747 cm^{-1}). The peaks are slightly asymmetric in the spectra of amorphous samples cooled down from melt to 110 °C (Fig. 1a), but the new component became clearly observable after the isothermal treatment and cooling down to room temperature (Fig. 1b). The new band was observed in the range 1760–1757 cm^{-1}. It was found also in the spectrum of P/100-F although its intensity was rather poor. Due to the complexity of the studied system we are not able to definitely ascribe this mode. A band positioned at 1760 cm^{-1} was reported before as a characteristic feature of stereocomplex structures formed by PLLA and PDLA [55]. We suspect that, analogously, the observed effect may correspond with the formation of a supramolecular complex by functional groups R and conveniently arranged part of carbonyl moieties that belong to gt conformers, whereas other gt conformers (not complexed) might experience indirect interactions that changed their chemical environment. This effect requires more detailed experimental studies on simplified model systems.

A relatively small difference (1-2 cm^{-1}) was observed for all LPSQ-R on blending with PLA, concerning the position of ν(C=C) and ν(C–F) vibration modes (Fig. ESI-2). The largest effect was noted for the stretching mode of C–F bonds in LPSQ-F3, which may be correlated with their involvement in the postulated F···H bonds. Those small changes could be also detected by comparative analysis of Raman spectra of neat components and P/100-R blends (Table ESI-2, Fig. ESI-3). Although certain Raman vibrations of PLA and LPSQ-R partially overlapped, weak red shift of vibrations corresponding to ν(C=C) was noted for P/100-F, P/100-F3 and P/100-F5. For the last two a small red shift of the position of –CH$_2$-S-Ar bands was also observed. Interactions between polylactide and pentafluorophenyl groups grafted to LPSQ resulted in red shifts in the aryl ring breathing mode (586 cm^{-1}) as well as C–F in plane [a (511 cm^{-1}) and e (441 cm^{-1}) modes] and out of plane (384 cm^{-1}) deformations.
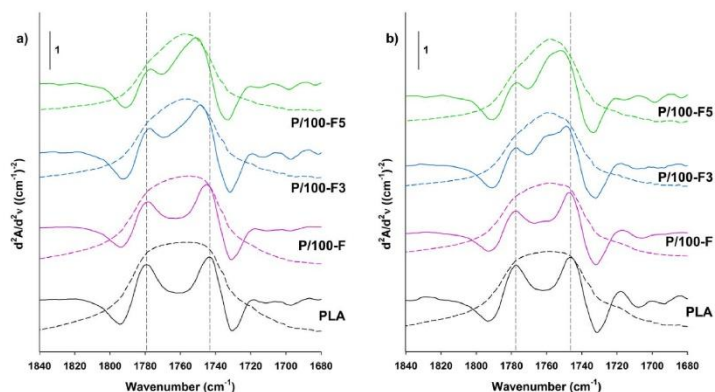
3

Fig. 1. Comparison of ν(C=O) and their second derivatives in PLA and P/100-R blends: (a) cooled down from melt to 110 °C and (b) cooled down to room temperature after 30 min isothermal crystallization at 110 °C.

3.3. Results of quantum-chemistry modelling and analysis of data collected in CSD

In order to check possibility of complexation between carbonyl groups and thiobenzene derivatives, quantum calculations have been done for a set of representative simplified models. See section 2.2 for all technical details in regard of computations.

Three different models were chosen, all towards n→π* interactions

between carbonyl moiety and thiobenzene ring. Model systems have been simplified in respect to experimentally investigated species in order to give possibility of the use of more advanced theoretical level. All were expected to be representative for a complex of carbonyl moiety and thiobenzene fragment in three variants; para-fluorinated (F), penta-fluorinated (F5) and substituted in para position by trifluorometyhyl-group (F3). Apparently, among three model systems in the case of *p*-trifluorometyhyl-thioanisole the expected complexation was not found,
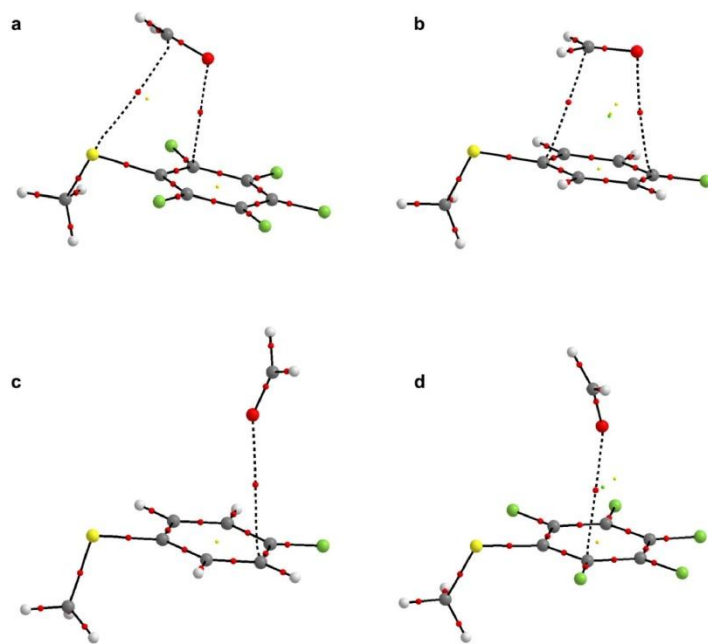
Fig. 2. Molecular graphs of complexes investigated theoretically. See Table 1 and the discussion for information on calculation level and energy of interactions. Bonds are represented with the bond paths, according to Quantum Theory of Atoms in Molecules. Dashed are bond paths corresponding to intermolecular interactions. Colours for elements: C - grey, H - blue, O - red, S - yellow, F - green. (For interpretation of the references to colour in this figure legend, the reader is referred to the Web version of this article.)

4

114

and the optimization procedure led to other pattern of interactions, that is, the H-bonding of S–H⋯O type. (See ESI associated with this article for movie with graphical visualization of optimization procedure for this case. File Mov_F3. gjf.) Therefore in the further discussion of computational results obtained in the context of n→π* interactions only two models, those with fluorinated rings, will be discussed. Fig. 2.

Two general patterns of interactions have been found (see Fig. 2a-d). First one, revealed by post-SCF method (MP2), corresponds to parallel complexation, as shown in Fig. 2 (a) and (b). In the case of complex with F5, (a) in Fig. 2, the oxygen atom of methyl aldehyde approaches one of carbon atoms in the ring, while in the same time carbonyl C of that molecule atom interacts with the sulfur atom of the thiobenzene moiety. The interaction energy of that complexation is of 2.66 kcal/mol (See Table 1 for detailed values). Taking into account distribution of local electron charges in $H_2C{=}O$ molecule one may expect that the electron charge from the sulfur lone pairs is in that case shared with, possessing electron charge deficit, carbon atom in methyl aldehyde. In complex with F, (b) in Fig. 2, the H_2CO molecule is shifted in respect to previous situation and both O and C atoms are linked with carbon atoms 1 and 4 in the benzene ring. This situation may be easily explained when taking into account that the carbon atom 4 in the ring should be the one which has the local deficit of electron charge due to presence of F substituent, while in the same time contribution of resonance structure with isolated formal charges makes the carbon in position 1 of the ring an electron rich due to resonance effect of $-SCH_3$ substituent, thus allows it to share electrons with C in H_2CO. In that case interaction energy is relatively close to that found in previous case, being of 2.27 kcal/mol. For comparison, most recent calculations for water dimer give interaction energy being close to 5 kcal/mol [56].

For DFT-ωB97XD/aug-cc-pVTZ method another pattern of complexation has been identified, namely, a T-shape one shown in Fig. 2 (c) and (d). (Note that in case of all calculations the starting geometry was of T-shape, in MP2 calculations reorientation to parallel complexes took place.) For *p*-fluorinated thiobenzene the complexation is much weaker than in previous cases, with interaction energy lower than 0.3 kcal/mol. Clearly more effective complexation can be observed for penta-fluorinated benzene, for which interaction energy is comparable with those found for parallel MP2-models. Computational methods indicated on possibility of formation of very different geometry complexes, from planar (MP2) to parallel (DFT). Thus, it was justified to check the situation in the crystal state. A search through Crystal Structure Database (CSD) [57] for example interaction between any

penta-fluorinated benzene moiety and any type of carbonyl oxygen shows that in fact both frontier situations with the whole spectrum in between them can be found in crystal state, as shown in Fig. ESI-4, although the individual shortest distances can be noticed for angles between 120 and 150°. The corresponding values of distance and angle for model (d) from Fig. 2 are 3.07A and 158°, respectively, fitting experimental data in region of weaker and closer to linear cases.

As it was mentioned at the beginning of this section, computational methods indicate possibility of formation of n→π* interactions merely in the case of fluorinated thiobenzenes (here analysed F and F5), while in the case of F3 the optimization procedure led to other pattern of interaction. Therefore, other type of interactions should also be considered for F3 in experimental conditions. Fluorine atoms of trifluoromethyl-group clearly may act as lone pairs donors in hydrogen bonding. Even if there are no classic proton-donating groups in experimental conditions, the formation of weak C–H⋯F(C) H-bonds may still be expected. For this reason the CSD collection has been searched again. Two cases have been investigated, with two various C–H type proton donors, namely, with aromatic and methyl-type carbon H-donors, interaction through C–H⋯F bond with F in any F_3C- group. Again, search was limited to high quality crystallographic data. Fig. ESI-5 a-b shows graphics with results. Even when reducing number of searched data to that fulfilling highest quality, the number of entries is large, being of 1518 and 902 for aromatic and methyl carbon donor, respectively. Thus, the C–H⋯F-CF_2 hydrogen bonding is very probable alternative to other type interactions, including those of n→π* type. In fact, they seem to be much more common in crystal state than the n→π* type interactions.

Analysis of theoretical frequencies may give additional information on preferences of interactions formation in experimental conditions, since depending on the type of complexation (parallel vs T-shaped, Fig. 2) there are some evident differences in changes of CO band. The parallel complexation found for MP2, Fig. 2 (a) and (b), results in slight blue shift of CO bond frequency and lowering of the intensity. In T-shaped complexes changes of the band position due to complexation is not so evident, however, a clear increase of its intensity is noticeable. As it was mentioned earlier, for P/100-F5 and P/100-F3 there is a red shift of the main component of the peak, but the additional new component around 1760-1757 cm^{-1} is slightly blue-shifted. This would perhaps correspond to situation where the dominant complexation type is that of T-shaped (P/100-F5) and hydrogen-bonded, but part of CO groups form other type of interactions, like those from Fig. 2 (a,b), which can be associated with the experimentally observed characteristics of the CO band.

3.4. Phase structure and thermal properties of PLA/LPSQ-R blends

The prepared PLA/LPSQ-R were thermally stable and the additives did not change the structure of PLA backbone (Figs. ESI-6 and ESI-7). SEM analysis of samples of PLA/LPSQ-R blends containing various amounts of LPSQ-R indicated phase separated structures. The effect was also dependent on the type of fluoroaryl group; in P/1-F the number and size of the inclusions were the smallest. Exemplary SEM micrographs of the cryo-fractured surfaces are shown on Fig. 3 (and Fig. ESI-8). On the SEM micrographs of P/1-R only very small submicron inclusions are visible, scarcely accompanied by larger ones with a diameter of up 1–2 μm, depending on R. Larger amounts of LPSQ-R (≥5 wt%) formed phase separated inclusions seen on the micrographs of fracture surfaces and accompanied by holes left by the inclusions.

At 5 wt% content of the additive numerous microinclusions (with diameter of approximately 1 μm) of LPSQ-F were evenly distributed in the polyester matrix. LPSQ-F5 and LPSQ-F3 formed, apart from small inclusions, also larger ones of diameter close to 3 μm. In LPSQ-F3 the effect may be augmented by halogen bonds C–F⋯F–C formation, which should increase the strength of interactions between the macromolecules in the polysilsesquioxane phase. Silicon mapping with SEM-EDS evidenced partial miscibility of LPSQ-R with PLA and phase separation

Table 1

Interaction energies estimated for complexes from given in kcal/mol.

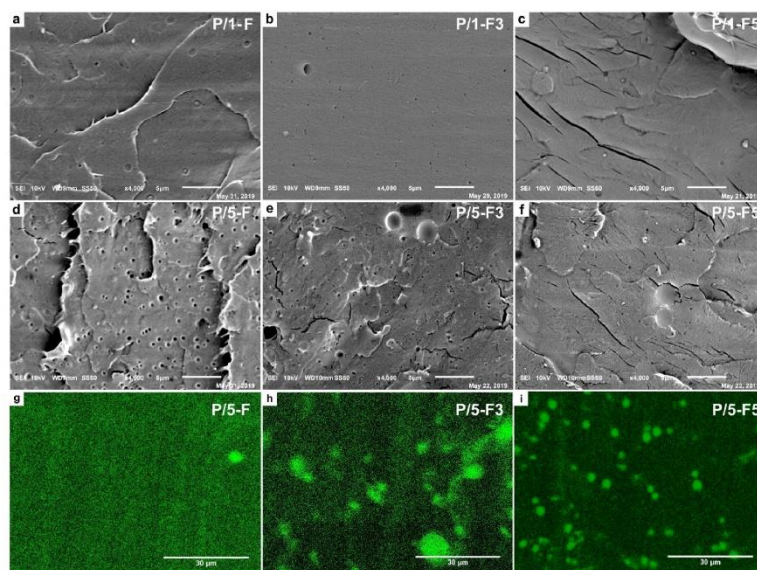| Complex	(a)	(b)	(c)	(d)
Level of calculations	MP2/ 6–311−−G (d,p)	MP2/ 6–311++G (d,p)	ωB97XD/ aug-cc-pVTZ	ωB97XD/ aug-cc-pVTZ
Total interaction energy	−5.79	−5.27	−0.42	−2.64
Interaction energy corrected for BSSE	−2.66	−2.27	−0.29	−2.39
ν(C $=$ O) isolated carbonyl	1761.44	1761.44	1851.20	1851.20
ν(C $=$ O) after complexation	1751.71	1753.04	1852.50	1850.29
I (C $=$ O) isolated carbonyl	73.5755	73.5755	118.6378	118.6378
I (C $=$ O) after complexation	63.0806	51.6524	151.3129	150.7734
$\Delta\nu$ (C $=$ O)	−9.73	−8.4	1.30	−0.91
ΔI (C $=$ O)	−10.4949	−21.9231	32.6751	32.1356
Changes in IR frequencies (cm^{-1}) and intensities (km/mol) $\Delta\nu/\Delta$I	−9.73/ 10.4949	−8.40/- 21.9231	1.30/ 32.6751	−0.91/ 32.1356

Fig. 3. SEM micrographs of samples of PLA admixed with 1 wt% (a–c) and 5 wt% (d–f) of LPSQ-R (cryo-fractured surfaces, scale bar of 10 μm) and distribution of Si atoms (g–i) in blends containing 5 wt% of LPSQ-R (SEM-EDS, scale bar of 30 μm).

of LPSQ-F3 and LPSQ-F5. The polysilsesquioxanes are concentrated in the inclusions but are also dispersed in PLA matrix. The inclusions of LPSQ-F are not seen in Fig. 3g because of their very small size.

The phase structure of the blends and their composition is reflected in their optical properties (Fig. 4). Sample P/1-F was nearly as transparent as the neat PLA owing to the small content of the additive and the small number of the inclusions. The optical clarity of other blends was slightly worse due to light scattering on LPSQ-R rich inclusions dispersed in the polyester matrix. The decrease of transparency was especially striking for LPSQ-F3. A decrease of DLT in the wavelength range of 250–340 nm (UV–B region of light, linked with photochemical degradation of materials) was also observed.

The DMTA results collected in Fig. 5 corroborate microstructure details shown on Fig. 3. E'' temperature dependence of neat PLA exhibits a single peak with a maximum at 63 °C, that corresponds to the glass transition. The two peaks of E'' temperature dependencies of PLA/LPSQ-R and their temperatures evidence partial miscibility and the phase separation in the blends. The main peaks at higher temperatures originate from the glass transition in PLA rich phase. A slight decrease of the E'' peak temperature of the PLA rich phase (5–8 °C comparing to neat PLA) was observed for PLA/LPSQ-R, independently on the type of R. The decrease of the main peak temperature indicates plasticization of PLA by LPSQ-R. It should be stressed that the temperature of E'' peak did not change significantly with the increase of LPSQ-R content. Additional low and broad peaks appeared in a low temperature range of E'' plots of all PLA/LPSQ-R composites containing 1 wt% of the additives, which evidences the phase separation in the blends. The peaks increased and sharpened with increasing LPSQ-R content. The maxima of the low temperature peaks observed for larger amounts of LPSQ-R correspond to T_gs of the polysilsesquioxane components (Fig. ESI-1) as they show glass transitions in domains rich in LPSQ-R, and their positions did not change significantly with the increase of LPSQ-R content. Especially for the
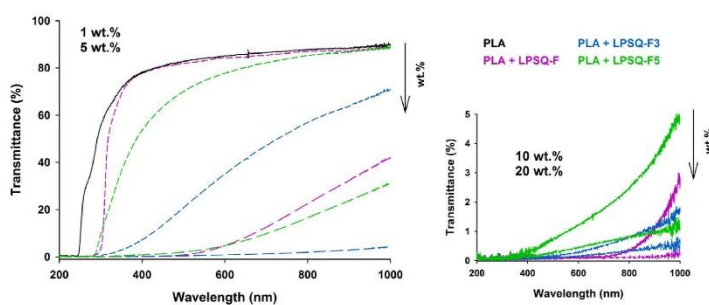

Fig. 4. Direct light transmittance of PLA and PLA/LPSQ-R vs. wavelength.
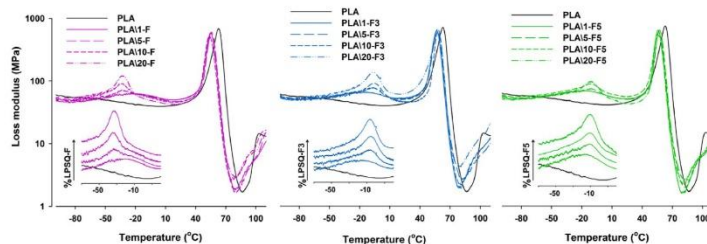
Fig. 5. Loss modulus (*E''*) of neat PLA and PLA/LPSQ-R blends with various contents of the hybrid component vs. temperature.

blends with 5–20 wt% of LPSQ-R.

Storage modulus (E′) of all the studied materials decreases with increasing temperature and drops sharply in the glass transition region (Fig. ESI-9). Up to the 5 wt% content of LPSQ, E′ of the blends is similar to that of neat PLA, although slightly smaller and sharply decreasing at lower temperature due to plasticization of PLA. E′ values of the blends with larger contents of LPSQ-R exceed that of neat PLA in a low temperature range, below T_g of LPSQ-R rich phase, but decrease in the temperature range of glass transition in LPSQ-R content. The stronger decrease occurs in the blends with larger LPSQ-R content. A similar effect was observed for plasticized PLA by others [58]. At 25 °C E′ is equal to 3.3 GPa for P/5-F5, 3.0 GPa for P/10-F5 and 2.6 GPa for P/20-F5 whereas for neat PLA and blends with LPSQ-F and LPSQ-F3 at 20 wt% it is close to 3.4 GPa, 2.9 GPa and 2.8 GPa, respectively. That decrease of E′ of the blends in comparison to that of neat PLA results from plasticization of the matrix, as well as from the presence of phase separated modifier-rich inclusions with low T_g.

The effect of heterorganic hybrid additives on the thermal properties of PLA/LPSQ-R blends can be linked to the differences in the nature of supramolecular interactions between fluoroaryl groups and the polyester matrix. DSC thermograms of PLA and PLA/LPSQ-R (Fig. 6 and Table ESI-3), recorded during the second heating at constant rate of 10 °C/min, illustrate the influence of additives. The thermograms evidence the glass transition in the temperature range similar to T_g of neat PLA (60 °C). This is in contrast to the decrease of the main E″ peak temperature of the blends, as compared to that of neat PLA evidenced by DMTA. The reason can be a different thermal history of samples; additional heating and annealing in DSC could enhance the phase separation. The materials did not crystallize during cooling at 10 °C/min.
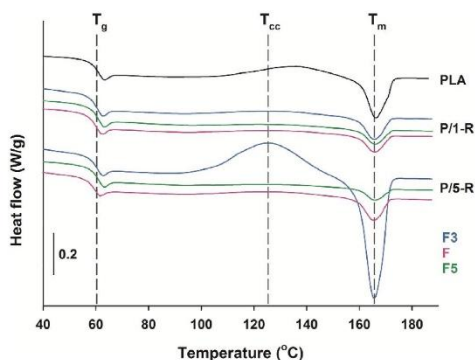

Fig. 6. DSC thermograms of PLA and PLA/LPSQ-R blends (second heating, 10 °C/min, exo up).

The second heating thermograms of PLA/LPSQ-F3 blends containing at least 5 wt% of the additive, above their glass transition display cold-crystallization exotherms and melting endotherms. T_g of PLA/LPSQ-F3 was found in 59–60 °C and 57–59 °C for 1 and 5 wt% blends, respectively. In each case the enthalpy of cold crystallization (ΔH_{cc}) matched exactly the melting enthalpy (ΔH_m), indicating that the materials were amorphous before the heating. The cold-crystallization of PLA/LPSQ-F3 was stronger than neat PLA (ΔH_{cc} of 8 J/g and peak rate temperature (T_{cc}) at 135 °C). The T_{cc} of the cold-crystallization peak shifted to 126 °C (P/5-F3 and P/10-F3) and 132 °C (P/20-F3). The decrease of T_{cc} corresponded with ΔH_{cc} increase. P/5-F3 and P/10-F3 exhibited ΔH_{cc} of 30 J/g_{PLA} and 36 J/g_{PLA}, whereas P/20-F3 of 35.5 J/g_{PLA}, respectively. Clearly, LPSQ-F3 induced cold crystallization of PLA. The promotion of cold crystallization can be ascribed to the hydrogen bonding between fluorine atoms of –CF$_3$ group and hydrogens of methyl or/and methine moieties of PLA. As it was mentioned, C–F···F–C and C–F···π interactions may be observed along with C–H···F–C bonds for species bearing trifluoromethylphenyl groups [28]. Comparative DSC studies carried out for PLA blends with model functionalized cyclosiloxanes CX-R (Table ESI-4, Fig. ESI-10) indicated a similar trend in the induction of cold-crystallization. The most pronounced effect was noted for blend P/5-CX-F3 (yet it was much weaker than that observed for P/5-F3). Regardless the type of R, a significant drop of T_g was observed for P/CX-R.

The melting of cold-crystallized materials did not reflect the range of their T_{cc}. The thermograms of neat PLA and blends with LPSQ-F3 were featured by single melting peaks centred at T_m of 165 °C, despite lower T_{cc} of the blends. The melting peaks of both PLA and the blends are slightly unsymmetrical and seem to contain a high temperature component. It can be attributed to the melt-recrystallization behaviour [59] or the presence of a fraction of thicker crystals formed at higher temperature. It must be also remembered that T_m of crystals in miscible blends can be affected by the presence of the second component. The degree of crystallinity (X_c) of PLA in blends containing 5 wt% or more of LPSQ-F3 and crystallized under the applied conditions is close to 32–39%. The occurrence of cold-crystallization was not clearly visible on the thermograms of PLA blends with LPSQ-F or LPSQ-F5, irrespectively of their contents. Only small melting peaks with T_m of approx. 165 °C were recorded. DSC thermograms did not show any significant change in T_g (59–60 °C) or T_m (165 °C). The effect may be linked to the completely different nature of the interactions between *p*-fluoroaryl and pentafluoroaryl groups and the PLA backbone. The labile contacts between the oxygen atom of carbonyl groups and the electron deficient parts of aromatic rings play the role of attractive interactions. Stabilization from C (sp3)–H···F–C (sp2) interactions is much less effective in this case.

To have a more detailed insight into the thermal behaviour of the blends, their isothermal crystallization was studied and the crystallization half-times were estimated (Fig. 7). The results corroborate data presented above on the thermograms recorded at 10 °C/min. It appears
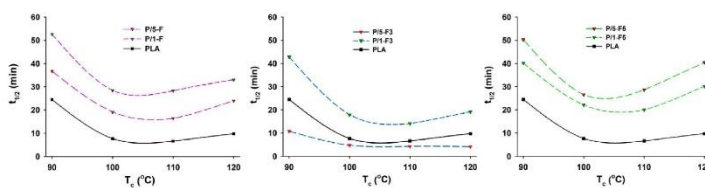
Fig. 7. Isothermal crystallization half-times for PLA/LPSQ-R plotted against crystallization temperature (T_c).

that the crystallization half-times were similar to that of PLA (P/5-F3) or longer (PLA/LPSQ-F and PLA/LPSQ-F5). The slower crystallization process was also noted for P/1-LPSQ-F3 in T_c range of 90–120 °C. It should be stressed that the half-time values at 90 °C are only approximate, since the crystallization might have started before the temperature was stabilized. The slowing down of the overall crystallization process may result from a decrease of the crystal growth rate or/and of the nucleation density. The latter should be similar for all the studied LPSQ-R providing no effect of side groups R. However, the cold-crystallization during heating was enhanced in PLA/LPSQ-F3 blends (Fig. ESI-11). It can be thus postulated that the hydrogen bonds formed between PLA and fluorine atoms of LPSQ-F3 may play a role in enhancement of the low temperature nucleation of PLA crystals.

Thermograms of samples crystallized at 120 °C are plotted in Fig. 8 and ESI-12. Melting behaviour of the isothermally crystallized PLA/LPSQ-F and PLA/LPSQ-F5 was similar to that of PLA. No cold crystallization was observed. Single melting peaks appear with T_m at 165–166 °C and ΔH_m of 44–58 J/g_{PLA}, depending on the additive content. No exothermic pre-melting peaks, typically attributed to transition of the disordered α′ to the ordered α′ form [59], was noted. P/1-F3 crystallized at 120 °C melted in a similar way ($T_m = 165$ °C, $\Delta H_m = 46$ J/g_{PLA}). However, the corresponding melting endotherms of crystallized PLA/LPSQ-F3 blends containing larger amounts of additives exhibited either two peaks (at T_m of 163–164 °C and 168–169 °C, respectively) or a peak with shoulder (T_m of 163 °C) in the case of P/5-F3. The intensity of high temperature peaks increased on the increase of LPSQ-F3 content in samples crystallized at 120 °C. The effect may evidence reorganization in α phase, but also may indicate formation of thicker crystals.

3.5. Dielectric properties of PLA and PLA/LPSQ-R blends

The interactions between the functional groups in LPSQ and PLA matrix through non-covalent bonding are transferred to the dielectric properties of the compounds. Studies were carried out for samples containing 5 wt% of the polysilsesquioxane additives. Fig. 9 shows the dielectric spectra of all investigated samples for several temperatures

from the range 40–120 °C. The spectra are characterized by the steps in the real part of dielectric relaxation permittivity ε' accompanied by the maxima of the imaginary part of dielectric permittivity ε''. Both the steps and the maxima are shifted towards higher frequencies with increasing temperature. The addition of the LPSQ-R does not change significantly the value of ε'. However, it increases the dielectric losses in the low frequency range and the temperature above 80 °C due to the charge separation at the electrodes (Maxwell – Wagner relaxation). The incorporation of LPSQ-R into PLA matrix only slightly increases dielectric losses in higher frequency range and decreases the height of the dielectric losses maxima.

In order to identify the relaxation processes, the experimental results of the dielectric spectrum measurements were fitted using the Cole-Cole equation superimposed to the conductivity term [60].

$$\varepsilon(\omega) = \varepsilon' - i\varepsilon'' = -i\left(\frac{\sigma_{dc}}{\varepsilon_0\omega}\right)^N + \sum_{k=1}^{2}\left[\frac{\Delta\varepsilon_k}{1 + (i\omega\tau_k)^\alpha} + \varepsilon_{\infty k}\right]$$

where: k denotes the number of relaxation processes, Δ — difference between the permittivity value at the lowest and the highest frequency of the dispersion step, ε_∞ — the permittivity value at the highest frequency, ε_0 — the dielectric constant of free space, α — degree of the distribution of relaxation times τ, σ_{dc} — the specific dc conductivity, N — exponent of the frequency dependence of ε''.

Fig. 10 shows the fitting results for all investigated samples at the temperature of 80 °C, as an example. The squares represent the experimental data. The continuous lines drawn over the points are the best fits of the Cole-Cole equation to the obtained results. The dashed line is related to the conductivity term $\left(\frac{\sigma_{dc}}{\varepsilon_0\omega}\right)^N$. The other continuous lines refer to the contributions of separated relaxation processes. Based on the fitting results we found the relationship between the relaxation times τ and the reciprocal of the temperature (Fig. 11). All processes are thermally induced and they show the Vogel-Fulcher-Tammann behaviour described by the equation:
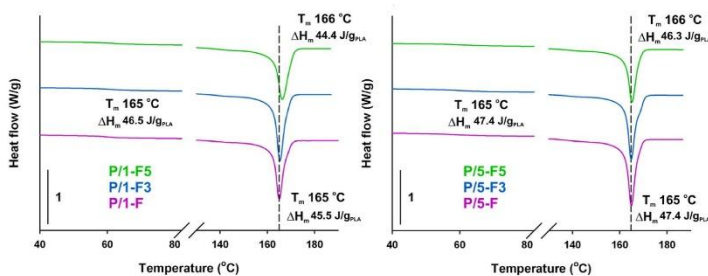

Fig. 8. DSC traces (second heating; 10 °C/min; exo up) of PLA/LPSQ-R samples crystallized isothermally (from melt) at 120 °C.
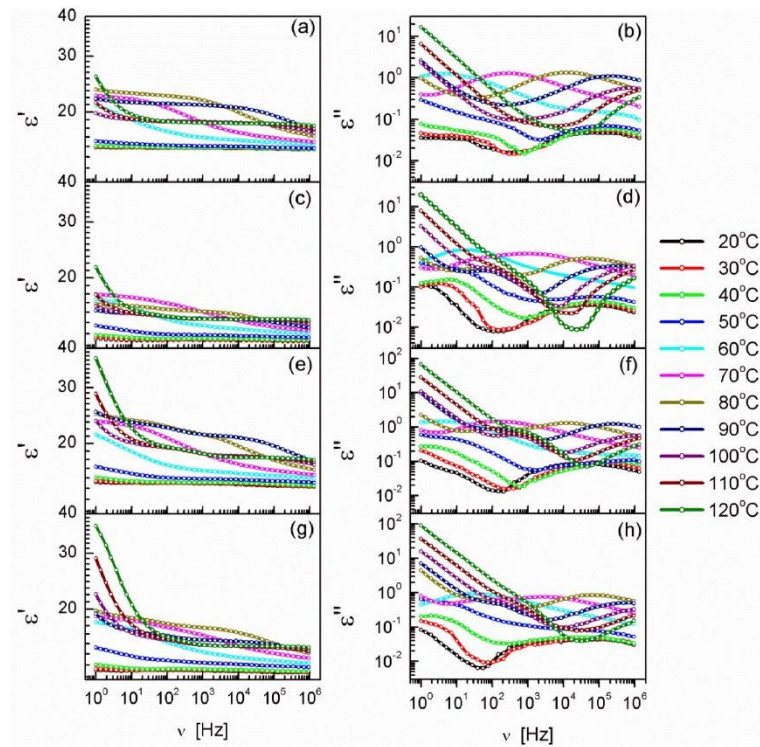
118

Fig. 9. Dielectric spectra for the polylactide PLA (a,b) and the composites: P/5-F (c,d), P/5-F3 (e,f) and P/5-F5 (g,h).

$$\tau = \tau_0 exp\left(\frac{E_a}{T - T_0}\right)$$

where τ is the relaxation time, τ_0 is the relaxation time at very high temperature, E_a is the activation energy and T_0 is the temperature at which the relaxation time becomes extremely large.

The essential difference between the fitting results for PLA and the blends consists in obtaining only one plot for PLA and two plots for the blends. The difference results from the fact that the incorporation of the plasticizers into the PLA matrix leads to higher polymer chain mobility.

The process observed in the case of PLA in the temperature range 60–95 °C is related to the local segmental motion of the polymer chain responsible for the glass transition (α relaxation). The process is observed only at lower temperatures, i.e. below 70 °C for the blends. However, the plots above 70 °C are ascribed to the motions of the whole polymer chain (normal – mode relaxation α_n) which reflect the changes of the end–to–end vector of the chain as the overall dipole moment of the chain is exactly proportional to the end–to–end vector. Thus, the addition of LPSQ-R to PLA releases the cooperative motion of the whole chain which is reflected by appearance of a new normal – mode relaxation α_n. The parameters of both processes are summarized in Table 2.

The temperatures of the onset of the glass transition T_g in the PLA matrix in the vicinity of 60 °C are in good agreement with our results obtained from DMTA and DSC. Moreover, the slight decrease of T_g (5.6–8.8 °C) observed for the blends agrees very well with our dynamic

mechanical analysis results. The lower temperature T_g in comparison with that of PLA matrix was observed for all the studied materials, independently on the type of R. The fact points to the weakening of the interaction between the chains of PLA [61]. On the other hand, for the hybrid blends the lower Vogel's temperatures T_{01} and T_{02} of both α and α_n processes were observed in comparison with that of PLA matrix. The feature is ascribed to the stronger interaction between polymer chains [62,63]. The fact enables us to conclude that non–covalent bonds between PLA chains and LPSQ-R are created, whereas the interaction between PLA chains weakens. In favor of this conclusion is also the decrease of the pre-exponential factors τ_{01} and τ_{02} in the case of the blends. Because, according to the Eyring theory [64], the lower the τ_0 factor the better the cooperativity of the molecular motions. Moreover, the increased activation energies E_{a1} and E_{a2} obtained for the composites correspond to greater number of molecules to be involved in both relaxation processes.

3.6. Mechanical properties

The type of supramolecular interactions, composition and phase structure of the blends was reflected in their mechanical properties (Table ESI-5). Exemplary engineering strain-engineering stress relationships of PLA and PLA/LPSQ-R materials are presented on Fig. 12 and ESI-13. Neat PLA exhibited yield stress (σ_y) of 44 MPa, stress (σ_b) and strain (ε_b) at break of 41 MPa and 30%, respectively. The properties
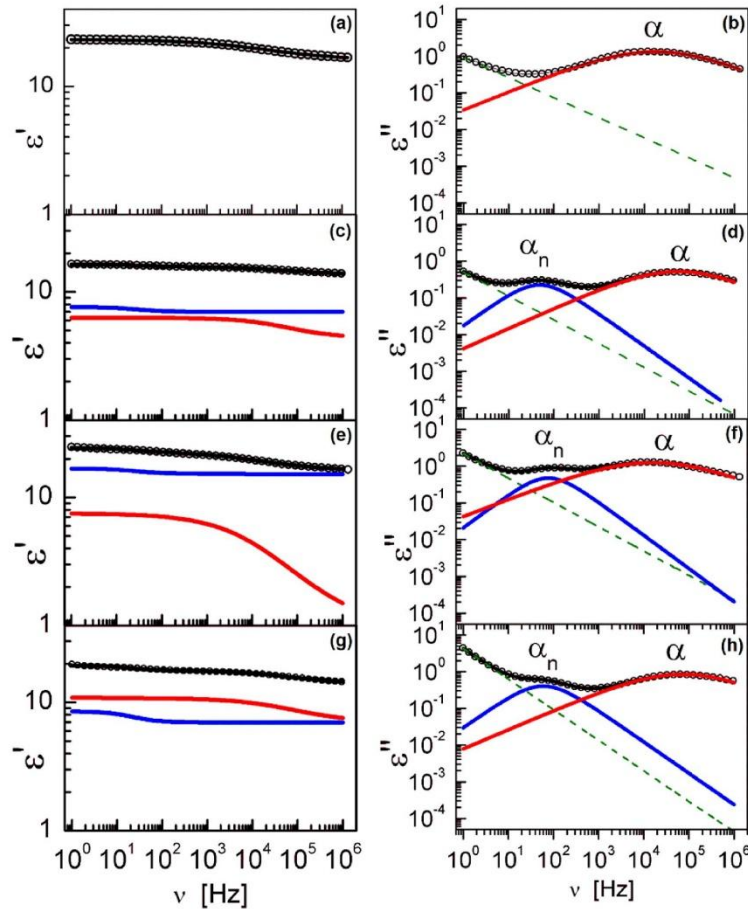
Fig. 10. Frequency dependences of real ε' and imaginary ε'' parts of dielectric permittivity at 80 °C for PLA (a,b) and the composites: P/5-F (c,d), P/5-F3 (e,f) and P/5-F5 (g,h).

of blends with 1 wt% of LPSQ-R were not improved in comparison to those of neat PLA (inset in Fig. 12). The samples yielded at σ_y of 40–43 MPa and fractured early (σ_b of 36–41 MPa, and ε_b of 16–22%). The increase of content of LPSQ-R to 5 wt% resulted in a significant change of the tensile behaviour. For all three types of PLA blends with LPSQ-R a characteristic two-stage plastic deformation was observed. The drop of stress beyond the yield was relatively small and the deformation proceeded without a significant change in the stress until a second stress drop associated with necking.

The mechanism behind the improvement of drawability observed for PLA/LPSQ-R seems to be different than those found for other PLA-based composites and binary mixtures that involved a significant decrease of T_g [65–69]. Two yielding steps, first by crazing and then by shear yielding was only reported before for physically aged graft block co-polymers (BCPs) with poly (4-methyl caprolactone)-*block*-poly (±-lactide) (P4MCL-PLA) side chains [70]. Double yielding on the stress-strain

curve was also found for injection molded PLA/PCL [71], PLLA/PPA and PLLA/PEG/PPA [72]. The effect was ascribed to nano-fibrils made of the additives formed *in situ* and oriented along the melt flow direction. It should be stressed that T_gs of PLA/LPSQ-R were very close to the T_g of neat PLA. Thus, the differences in drawability of samples containing 5 wt% of the fluoroaryl polysilsesquioxane additives cannot be ascribed to the plasticization of the polymer matrix alone. We have previously shown that some functionalized linear polysilsesquioxanes may promote plastic deformation of PLA matrix (ε_b of 230% was reached at σ_b of 22 MPa), retaining the yield strength of nearly 40 MPa [43]. The effect was also achieved without a significant T_g decrease (8 °C).

σ_y of 5 wt% blends was about 41 MPa. For P/5-F the stress decrease beyond the yield was somewhat larger than for two other 5 wt% blends. The stress during post-yield deformation remained close to 36 MPa up to ε of about 35%. A sharp decrease of the stress to 27 MPa preceded the second phase of plastic deformation that was ended with fracture at ε_b of
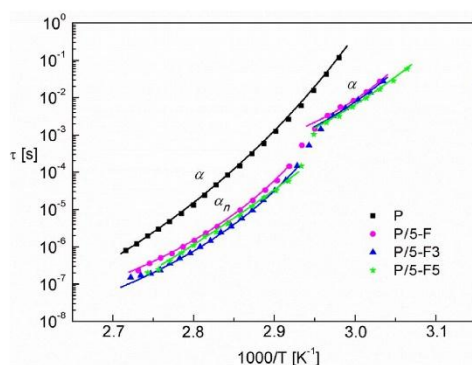
10

Fig. 11. Vogel – Fulcher – Tammann plots obtained for PLA and PLA/LPSQ-R. The points are the experimental results and the lines are the fitting results.

Table 2
Parameters of α and α_n processes in PLA and PLA/LPSQ-R blends (the indexes 1 and 2 are related to α and α_n processes, respectively).

sample	E_{a1} [eV]	E_{a2} [eV]	T_{01} [K]	T_{02} [K]	τ_{01} [s]	τ_{02} [s]	T_g [°C]
PLA	0.17	–	307.5	–	$4.4 \cdot 10^{-16}$	–	62.6
P/5-F	0.02	0.05	304.4	306.8	$1.7 \cdot 10^{-6}$	$1.7 \cdot 10^{-11}$	57.0
P/5-F3	0.04	0.06	294.7	304.8	$5.1 \cdot 10^{-8}$	$4.3 \cdot 10^{-12}$	57.0
P/5-F5	0.09	0.39	273.6	222.7	$3.0 \cdot 10^{-10}$	$3.0 \cdot 10^{-21}$	53.8

E_a – activation energy.
T_O – Vogel's temperature.
τ_O – pre-exponential factor.
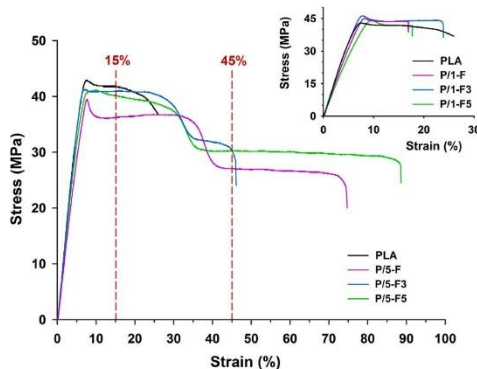T_g – temperature of the onset of the glass transition.

Fig. 12. Exemplary engineering stress vs. engineering strain dependencies of PLA and PLA/LPSQ-R blends at 5 wt% (and 1 wt% - inset) deformed at 25 °C, 5%/min. The gauge region surfaces of samples drawn to 15% and 45% are shown on SEM micrographs (Fig. 13).

63% and σ_b of 25 MPa. An improved drawability and tensile toughness was also observed for P/5-F5 and P/5-F3. The post-yield deformation proceeded at stress of 40 MPa up to ε of 30%. For P/5-F5 the stress/strain curve slightly declined on approaching ε of 30%. During the

second stage of plastic deformation the sample was drawn to break at ε_b of 87% % and σ_b of 28 MPa. The drawability of P/5-F3 was worse despite nearly the same T_g of the blends, most possibly due to the presence of rather large hybrid LPSQ-F3 inclusions. The drop of about 10 MPa in stress and necking occurred for P/5-F3, alike for all the other 5 wt% blends. Yet, a relatively low ε_b 44% was reached at σ_b of 31 MPa.

The submicron size hybrid inclusions might promote plastic deformation of the matrix, thus improving the drawability of the blend without significant decrease of the yield strength. The enhanced ability to plastic deformation of the partially miscible and phase separated blends may be ascribed to the presence of inclusions of LPSQ-R and the fraction of hybrid macromolecules plasticizing the continuous polyester phase. The differences between the blends can be explained in terms of size of inclusions of LPSQ-R in the PLA matrix (Fig. 3). Dispersion of LPSQ-F in PLA was better, that those of two other polysilsesquioxanes, whereas in LPSQ-F3 it was the worst. The observed effects may reflect differences in the interactions between PLA and LPSQ-R, although more extensive studies are required in order to conclude decisively about their nature.

SEM micrographs taken for surfaces of the gauge regions of P/5-F, P/5-F3 and P/5-F5 at 15% and 45% engineering strain show the effects of deformation, depending on the functional groups in LPSQ-R, phase miscibility and the size of inclusions (Fig. 13).

Samples subjected to the 15% strain exhibit cavities that correspond to the presence of LPSQ-R particles. Deformation at low strain is based on the formation and propagation of crazes perpendicular to the drawing direction and originating from the voids, similarly in all 5 wt% blends. Whitening observed at the beginning of the plastic deformation was suggestive of cavitation phenomena. Cavitation may promote the formation of crazes [70,73] or shear bands [74] in PLA blends. The increase in the applied strain to 45% resulted in elongation of the voids in the drawing direction. However, it is known that the smaller the rubber inclusions the higher is the volume strain required for cavitation [75].

Larger contents of LPSQ-F3 did not increase ductility of PLA blends (Fig. ESI-13) despite the decrease of σ_y. The two-stage plastic deformation was clearly visible for P/10-F3, but the stress decreased and sample fractured at σ_b of 27 MPa and ε_b of 49%. Samples containing 20 wt% of LPSQ-F3 fractured at σ_b of 27 MPa and at a very low ε_b of 7%, without pronounced yielding. PLA/LPSQ-F and PLA/LPSQ-F5 blends (P/10-F, P/20-F, P/10-F5 and P/20-F5 in Fig. ESI-13) exhibited decreased σ_y and quite good drawability on the increase of the hybrid additive amount, but the strong stress decrease and necking occurred much earlier than for P/5-F and P/5-F5. P/10-F5 and P/20-F5 fractured at σ_b of 21–23 MPa, and ε_b of 120% and 165%, respectively. P/10-F and P/20-F exhibited higher yield strength and fractured at σ_b of 26–27 MPa and at ε_b of 63% and 150%, respectively.

3.7. Surface and barrier properties of PLA/LPSQ-R

Measurements of barrier properties of the studied materials with regard to the oxygen transmission rate (OTR) were performed for thin PLA/LPSQ-R films conditioned for 24 h at room temperature after their compression molding (Fig. 14, Table ESI-6). The fluoroaryl LPSQ changed significantly the permeability of oxygen through PLA matrix. The observed change of OTR through PLA/LPSQ-R with 1 and 5 wt% of LPSQ-R indicate a significant improvement of the barrier to oxygen in comparison to neat PLA. What is very important, this satisfactory effect was achieved for amorphous samples containing very small amounts of the additive. A difference in OTR depending on the type of R was noticed for compositions containing 1 wt% of the additive. The largest effect was observed for LPSQ-F3. However, a slight OTR increase for P/5-F3 may suggest that the phase separation has an effect for the barrier properties at this composition. Similar effect was noticed for the blends containing LPSQ-F5. A steady decrease of OTR was found in the case of LPSQ-F, which was most miscible with PLA. We have also found that addition of fluorinated polysilsesquioxanes to PLA (at 1 wt% and 5 wt%) resulted
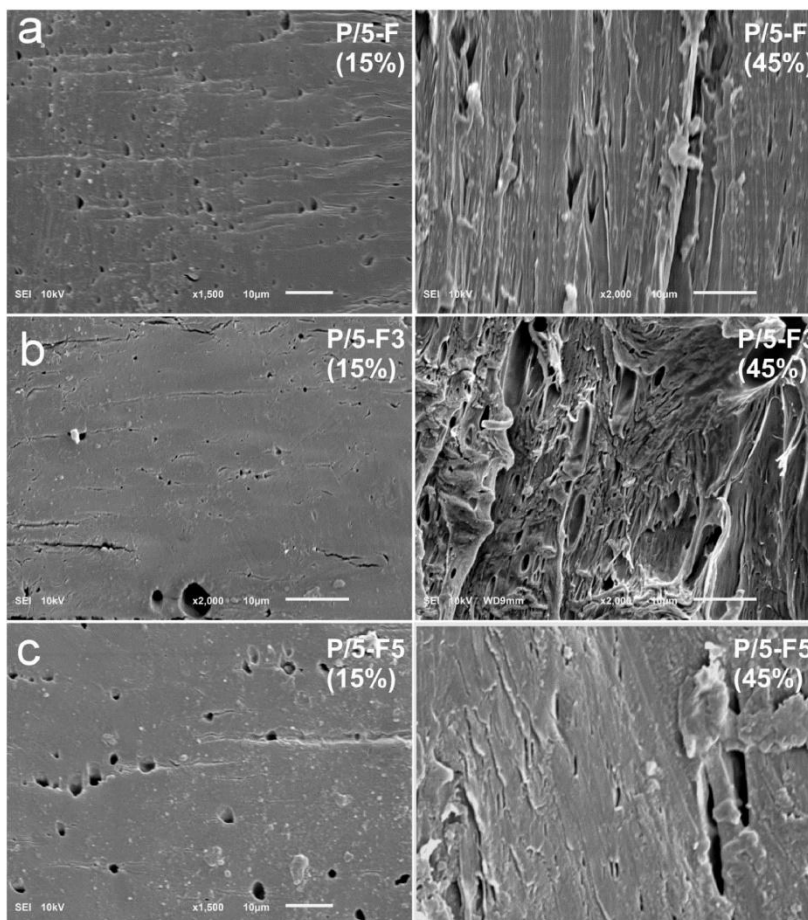
11

121

Fig. 13. SEM micrographs of gauge region surfaces of specimens drawn to the strains of 15% and 45% (a) P/5-F, b) P/5-F3, c) P/5-F5; drawing direction – vertical).

in a decrease of surface free energy (γ_s) with respect to the neat PLA (Fig. 14, inset). The decrease of γ_s does not seem to depend much on the type and amount of the fluorinated LPSQ. A slight increase of the polar component may be related to the presence of silsesquioxane structures.

4. Conclusions

Linear polysilsesquioxanes of ladder-like main chain and functionalized in their side chains with fluoroaryl groups were applied as modifiers in polylactide-based blends. The effect of additives depended on the position of fluorine atoms on phenyl groups. Congestion of substituents along the polysilsesquioxane chains was another factor that should be taken into account. The designed strategy allowed for evaluation of different effects regarding the noncovalent interactions between LPSQ-R and PLA and was aimed at engineering of the structure/properties relationship in the studied system. The blends were partially

miscible and phase separated, depending on the strength of interactions between LPSQ-R and the polyester matrix. DRS studies revealed the presence of the glass transition in PLA and two relaxation processes in the composites PLA/LPSQ-R: glass transition and the normal – mode relaxation. The activation energy of the glass transition in PLA is higher in the case of the blends. The presence of the normal – mode relaxation points to the interaction between the functional groups in LPSQ and PLA matrix. LPSQ with *p*-trifluoromethylphenyl substituents capable of hydrogen and halogen bonding induced effectively the process of cold crystallization in PLA.

The type of supramolecular contacts governed the miscibility and phase structure, which were decisive for the course of plastic deformation in the studied systems. The elongation at break markedly increased for all compositions with LPSQ-R containing at least 5 wt% of the hybrid additives. The ductility of 5 wt% blends was reflected in elongation at break ε_b of up to nearly 90% at σ_b close to 30 MPa, and retaining
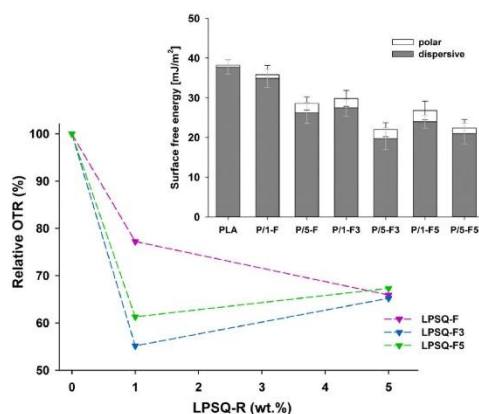
12

122

Fig. 14. Relative changes of the oxygen transmission rate through PLA/LPSQ-R. Inset: Changes of surface energy measured for native PLA and its blends with LPSQ-R.

relatively high yield strength of nearly 40 MPa. Moreover, the studied materials exhibited a significant improvement of barrier properties in the amorphous state (significant decrease of the oxygen transmission rate and increase of hydrophobicity). The unique combination of specific features of PLA/LPSQ-R can be of value in packaging applications.

CRediT author statement

Anna Kowalewska – Conceptualization, Writing – original draft, Supervision, Funding acquisition, Agata S. Herc – Investigation, Formal analysis, Joanna Bojda – Investigation, Formal analysis, Marcin Palusiak – Conceptualization, Investigation, Formal analysis, Writing – original draft, Ewa Markiewicz – Investigation, Writing – original draft, Paweł Ławniczak – Investigation, Formal analysis, Maria Nowacka – Investigation, Writing – review & editing, Joanna Sołtysiak - Investigation, Artur Różański – Investigation, Writing – review & editing, Ewa Piórkowska – Conceptualization, Writing – original draft, Supervision

Declaration of competing interest

The authors declare that they have no known competing financial interests or personal relationships that could have appeared to influence the work reported in this paper.

Acknowledgements

Appendix A. Supplementary data

Supplementary data to this article can be found online at https://doi.org/10.1016/j.polymertesting.2020.107033.

Data availability statement

The raw/processed data are available on request.

References

[1] M.L. Di Lorenzo, R. Androsch (Eds.), Synthesis, Structure and Properties of Poly (lactic Acid). Springer International Publishing AG, 2018, https://doi.org/10.1007/978-3-319-64230-7.
[2] E. Castro-Aguirre, F. Iñiguez-Franco, H. Samsudin, X. Fang, R. Auras, Poly(lactic acid)-Mass production, processing, industrial applications, and end of life, Adv. Drug Deliv. Rev. 107 (2016) 333–366, https://doi.org/10.1016/j.addr.2016.03.010.
[3] K. Hamad, M. Kaseem, M. Ayyoo, J. Joo, F. Deri, Polylactic acid blends: the future of green, light and tough. Progr, Polym. Sci. 85 (2018) 83–127, https://doi.org/10.1016/j.progpolymsci.2018.07.00.
[4] A. Kowalewska, M. Nowacka, Supramolecular interactions in hybrid polylactide blends-the structures, mechanisms and properties, Molecules 25 (2020) 3351, https://doi.org/10.3390/molecules25153351.
[5] S. Domenek, S. Fernandes-Nassar, V. Ducruet, Rheology, mechanical properties, and barrier properties of poly(lactic acid), Adv. Polym. Sci. (2017) 303–341, https://doi.org/10.1007/12_2016_17. Springer International Publishing AG.
[6] A. Guinault, C. Sollogoub, V. Ducruet, S. Domenek, Impact of crystallinity of poly (lactide) on helium and oxygen barrier properties, Eur. Polym. J. 48 (2012) 779–788, https://doi.org/10.1016/j.eurpolymj.2012.01.014.
[7] M. Cocca, M.L. Di Lorenzo, M. Malinconico, V. Frezza, Influence of crystal polymorphism on mechanical and barrier properties of poly(L-lactic acid), Eur. Polym. J. 47 (2011) 1073–1080, https://doi.org/10.1016/j.eurpolymj.2011.02.009.
[8] M.L. Di Lorenzo, R. Androsch, Influence of -crystal polymorphism on properties of poly(L-lactic acid), Polym. Int. 68 (2019) 320–334, https://doi.org/10.1002/pi.5707.
[9] M. Żenkiewicz, J. Richert, A. Różański, Effect of blow moulding ratio on barrier properties of polylactide nanocomposite films, Polym. Test. 29 (2010) 251–257, https://doi.org/10.1016/j.polymertesting.2009.11.008.
[10] A.J. Svagan, A. Åkesson, S. Bulut, J.C. Knudsen, J. Risbo, D. Plackett, Transparent films based on PLA and montmorillonite with tunable oxygen barrier properties, Biomacromolecules 13 (2012) 397–405, https://doi.org/10.1021/bm201438m.
[11] A.M. Pinto, J. Cabral, D.A.P. Tanaka, A.M. Mendes, F.D. Magalhães, Effect of incorporation of graphene oxide and graphene nanoplatelets on mechanical and gas permeability properties of poly(lactic acid) films, Polym. Int. 62 (2013) 33–40, https://doi.org/10.1002/pi.4290.
[12] M. Żenkiewicz, J. Richert, Permeability of polylactide nanocomposite films for water vapour, oxygen and carbon dioxide, Polym. Test. 27 (2008) 835–840, https://doi.org/10.1016/j.polymertesting.2008.06.005.
[13] J.R. Rocca-Smith, R. Pasquarelli, A. Lagorce-Tachon, J. Rousseau, S. Fontaine, F. Debeaufort, T. Karbowiak, Toward sustainable PLA-based multilayer complexes with improved barrier properties, ACS Sustain. Chem. Eng. 7 (2019) 3759–3771, https://doi.org/10.1021/acssuschemeng.8b04064.
[14] A.P. Kharitonov, Practical applications of the direct fluorination of polymers, J. Fluor. Chem. 103 (2000) 123–127, https://doi.org/10.1016/S0022-1139(99)00312-7.
[15] T. Graunke, K. Schmitt, S. Raible, Wöllenstein, towards enhanced gas sensor performance with fluoropolymer membranes, Sensors 16 (2016) 1605, https://doi.org/10.3390/s16101605, 1–20.
[16] F. Carosio, S. Colonna, A. Fina, G. Rydzek, J. Hemmerlé, L. Jierry, P. Schaaf, F. Boulmedais, Efficient gas and water vapor barrier properties of thin poly(lactic acid) packaging films: functionalization with moisture resistant Nafion and clay multilayers, Chem. Mater. 26 (2014) 5459–5466, https://doi.org/10.1021/cm501519c.
[17] Y. Huang, T. He, Y. Pan, L. Jiang, Y. Dan, Study on bulk and surface properties of poly(lactic acid)/fluorinated polymer blends, Polymer-Plastics Techn, Eng. Times 53 (2014) 952–960, https://doi.org/10.1080/03602559.2014.886065.
[18] G.R. Desiraju, T. Steiner, The Weak Hydrogen Bond in Structural Chemistry and Biology, Oxford University Press, Oxford, 1999.
[19] P. Panini, D. Chopra, Understanding of noncovalent interactions involving organic fluorine. Chapter 2, in: Hydrogen Bonded Supramolecular Structures. Lecture Notes in Chemistry 87, 2015.
[20] V.R. Thalladi, H.-C. Weiss, D. Blaser, R. Boese, A. Nangia, G.R. Desiraju, C–H-F interactions in the crystal structures of some fluorobenzenes, J. Am. Chem. Soc. 120 (1998) 8702–8710, https://doi.org/10.1021/ja981198c.
[21] P. Panini, D. Chopra, Quantitative insights into energy contributions of intermolecular interactions in fluorine and trifluoromethyl substituted isomeric N-phenylacetamides and N-methylbenzamides, CrystEngComm 15 (2013) 3711–3733, https://doi.org/10.1039/C3CE40111A.
[22] H.-J. Schneider, Hydrogen bonds with fluorine. Studies in solution, in gas phase and by computations, conflicting conclusions from crystallographic analyses, Chem. Sci. 3 (2012) 1381–1394, https://doi.org/10.1039/C2SC00764A.
[23] P.A. Champagne, J. Desroches, J.-F. Paquin, Organic fluorine as a hydrogen-bond acceptor Recent examples and applications, Synthesis 47 (2015) 306–322, https://doi.org/10.1055/s-0034-1379537.
[24] J.A.K. Howard, V.J. Hoy, D. O'Hagan, G.T. Smith, How good is fluorine as a hydrogen bond acceptor? Tetrahedron 52 (1996) 12613–12622, https://doi.org/10.1016/0040-4020(96)00749-1.

[25] P. Metrangolo, J.S. Murray, T. Pilati, P. Politzer, G. Resnati, G. Terraneo, The fluorine atom as a halogen bond donor, viz. a positive site, Cryst. Eng. Comm. 13 (2011) 6593–6596, https://doi.org/10.1039/C1CE05554B.

[26] P. Metrangolo, J.S. Murray, T. Pilati, P. Politzer, G. Resnati, G. Terraneo, Fluorine centered halogen bonding: a factor in recognition phenomena and reactivity, Cryst. Growth Des. 11 (2011) 4238–4246, https://doi.org/10.1021/cg200888n/.

[27] M.S. Pavan, K.D. Prasad, T.N.G. Row, Halogen bonding in fluorine: experimental charge density study on intermolecular F⋯F and F⋯S donor–acceptor contacts, Chem. Commun. 49 (2013) 7558–7560, https://doi.org/10.1039/c3cc43513j.

[28] P. Panini, D. Chopra, Role of intermolecular interactions involving organic fluorine in trifluoromethylated benzanilides, CrystEngComm 14 (2012) 1972–1989, https://doi.org/10.1039/C2CE06254B.

[29] V.R. Hathwar, D. Chopra, P. Panini, T.N. Guru Row, Revealing the polarizability of organic fluorine in the trifluoromethyl group: implications in supramolecular chemistry, Cryst. Growth Des. 14 (2014) 5366–5369, https://doi.org/10.1021/cg501240r.

[30] R.W. Newberry, R.T. Raines, The n→π* Interaction, Acc. Chem. Res. 50 (2017) 1838–1846, https://doi.org/10.1021/acs.accounts.7b00121.

[31] S.K. Singh, A. Aloke Das, The n→π* interaction: a rapidly emerging non-covalent interaction, Phys. Chem. Chem. Phys. 17 (2015) 9596–9612, https://doi.org/10.1039/e4cp05536e.

[32] A. Rahim, P. Saha, K.K. Jha, N. Sukumar, B.K. Sarma, Reciprocal carbonyl–carbonyl interactions in small molecules and proteins. Nature Commun, 8 78 (2017), https://doi.org/10.1038/s41467-017-00081-x.

[33] S.K. Singh, P.R. Joshi, R.A. Shaw, J.G. Hill, A. Das, Interplay between hydrogen bonding and n→π* interaction in an analgesic drug salicin, Phys. Chem. Chem. Phys. 20 (2018) 18361–18373, https://doi.org/10.1039/c8cp00655e.

[34] J. Echeverría, Intermolecular carbonyl⋯carbonyl interactions in transition-metal complexes, Inorg. Chem. 57 (2018) 5429–5437, https://doi.org/10.1021/acs.inorgchem.8b00392.

[35] R.W. Newberry, R.T. Raines, n→π* interactions in poly(lactic acid) suggest a role in protein folding, Chem. Commun. 49 (2013) 7699–7701, https://doi.org/10.1039/c3cc44317e.

[36] W. Kohn, L.J. Sham, Self-consistent equations including exchange and correlation effects, Phys. Rev. 140 (1965) A1133–A1138, https://doi.org/10.1103/PhysRev.140.A1133.

[37] C. Møller, M.S. Plesset, Note on an approximation treatment for many-electron systems, Phys. Rev. 46 (1934) 618–622, https://doi.org/10.1103/PhysRev.46.618.

[38] C. Li, S. Luo, J. Wang, H. Wu, S. Guo, X. Zhang, Conformational regulation and crystalline manipulation of PLLA through a self-assembly nucleator, Biomacromolecules 18 (2017) 1440–1448, https://doi.org/10.1021/acs.biomac.7b00367.

[39] A. Kowalewska, M. Nowacka, A. Tracz, T. Makowski, Supramolecular self-assembly of linear oligosilsesquioxanes on mica-AFM surface imaging and hydrophilicity studies, Soft Matter 11 (2015) 4818–4829, https://doi.org/10.1039/c5sm00787a.

[40] M. Nowacka, A. Kowalewska, T. Makowski, Nanostructured surfaces by supramolecular self-assembly of linear oligosilsesquioxanes with biocompatible side groups, Beilstein J. Nanotechnol. 6 (2015) 2377–2387, https://doi.org/10.3762/bjnano.6.244.

[41] A. Kowalewska, M. Nowacka, T. Makowski, A. Michalski, Thermal stability of self-assembled surfaces and micropatterns made of ladder polysilsesquioxanes, Polymer 90 (2016) 147–155, https://doi.org/10.1016/j.polymer.2016.03.002.

[42] M. Nowacka, A. Kowalewska, D. Plażuk, T. Makowski, Hybrid polysilsesquioxanes for fluorescence resonance energy transfer, Dyes Pigments 170 (2019) 107622, https://doi.org/10.1016/j.dyepig.2019.107622.

[43] A.S. Herc, J. Bojda, M. Nowacka, P. Lewiński, W. Maniukiewicz, E. Piorkowska, A. Kowalewska, Crystallization, structure and properties of polylactide/ladder poly (silsesquioxane) blends, Polymer 201 (2020) 122563, https://doi.org/10.1016/j.polymer.2020.122563.

[44] A.S. Herc, M. Włodarska, M. Nowacka, J. Bojda, W. Szymański, A. Kowalewska, Supramolecular interactions between polylactide and model cyclosiloxanes with hydrogen bonding-capable functional groups, eXPRESS Polym. Lett. 14 (2020) 134–153, https://doi.org/10.3144/expresspolymlett.2020.12.

[45] A. Kowalewska, M. Nowacka, Synthesis of ladder silsesquioxanes by in situ polycondensation of cyclic tetravinylsiloxanetetraols, Silicon 7 (2015) 133–146, https://doi.org/10.1007/s12633-014-9209-z.

[46] W.L.F. Armarego, L. Chai Ch, Purification of Laboratory Chemicals, Butterworth-Heinemann, Bodmin, 2003, https://doi.org/10.1016/B978-0-7506-7571-0.X5000-5.

[47] G. Kister, G. Cassanas, M. Vert, Effects of morphology, conformation and configuration on the IR and Raman spectra of various poly(lactic acid)s, Polymer 39 (1998) 267–273, https://doi.org/10.1016/S0032-3861(97)00229-2.

[48] S. Kang, S.L. Hsu, H.D. Stidham, P.B. Smith, M.A. Leugers, X. Yang, A spectroscopic analysis of poly(lactic acid) structure, Macromolecules 34 (2001) 4542–4548, https://doi.org/10.1021/ma0016026.

[49] L.J. Bellamy, The Infra-red Spectra of Complex Molecules, third ed., Springer, Dordrecht, 1975 https://doi.org/10.1007/978-94-011-6017-9.

[50] P. Larkin, Infrared and Raman Spectroscopy. Principles and Spectral Interpretation, first ed., Elsevier Inc, 2011 https://doi.org/10.1016/C2010-0-68479-3.

[51] E. Meaurio, N. López-Rodríguez, J.R. Sarasua, Infrared spectrum of poly(L-lactide): application to crystallinity studies, Macromolecules 39 (2006) 9291–9301, https://doi.org/10.1021/ma061890r.

[52] D.A. Brant, A.E. Tonelli, P.J. Flory, The configurational statistics of random poly (lactic acid) chains. II. Theory, Macromolecules 2 (1969) 228–235, https://doi.org/10.1021/ma60009a003.

[53] Y. Sasanuma, D. Togue, Configurational statistics of poly(L-lactide) and poly(DL-lactide) chains, Polymer 55 (2014) 1901–1911, https://doi.org/10.1016/j.polymer.2014.01.059.

[54] E. Meaurio, E. Zuza, N. López-Rodríguez, J.R. Sarasua, Conformational behavior of poly(L-lactide) studied by infrared spectroscopy, J. Phys. Chem. B 110 (2006) 5790–5800, https://doi.org/10.1021/jp055203u.

[55] J. Zhang, H. Sato, H. Tsuji, I. Noda, Y. Ozaki, Infrared spectroscopic study of CH3⋯O=C interaction during poly(L-lactide)/poly(D-lactide) stereocomplex formation, Macromolecules 38 (2005) 1822–1828, https://doi.org/10.1021/ma047872w.

[56] A. Mukhopadhyay, S.S. Xantheas, R.J. Saykally, The water dimer II: theoretical investigations, Chem. Phys. Lett. 700 (2018) 163–175, https://doi.org/10.1016/j.cplett.2018.03.057.

[57] C.R. Groom, I.J. Bruno, M.P. Lightfoot, S.C. Ward, The Cambridge structural database, Acta Crystallogr. B72 (2016) 171–179, https://doi.org/10.1107/S2052520616003954.

[58] M. Pluta, M.-A. Paul, M. Alexandre, P. Dubois, Plasticized polylactide/clay nanocomposites. I. The role of filler content and its surface organo-modification on the physico-chemical properties, J. Polym. Sci., Part B: Polym. Phys. 44 (2006) 299–311, https://doi.org/10.1002/polb.20694.

[59] J. Zhang, K. Tashiro, H. Tsuji, A.J. Domb, Disorder-to-order phase transition and multiple melting behavior of poly(L-lactide) investigated by simultaneous measurements of WAXD and DSC, Macromolecules 41 (2008) 1352–1357, https://doi.org/10.1021/ma0706071.

[60] A.K. Jonscher, Dielectric relaxation in solids, J. Phys. D Appl. Phys. 32 (1999) R57, https://doi.org/10.1088/0022-3727/32/14/201.

[61] P. Xu, H.G. Gui, S.Z. Yang, Y.S. Ding, Q. Hao, Dielectric and conductivity properties of poly(L-lactide) and poly(L-lactide)/Ionic liquid blends, Macromol. Res. 22 (2014) 304–309, https://doi.org/10.1007/s13233-014-2038-5.

[62] F. García, A. García-Bernabé, V. Compañ, R. Díaz-Calleja, J. Guzmán, E. Riande, Relaxation behavior of acrylate and methacrylate polymers containing dioxacyclopentane rings in the side chains, J. Polym. Sci., Part B: Polym. Phys. 39 (2001) 286–299, https://doi.org/10.1002/1099-0488(20010201)39.

[63] V. Compañ, J. Guzmán, R. Díaz-Calleja, E. Riande, Relaxation behavior of methacrylic polymers with bulky hydrophylic groups in their structures, J. Polym. Sci. Part B Polym. 37 (1999) 3027–3037, https://doi.org/10.1002/(SICI)1099-0488(19991101).

[64] S. Glasstone, K.J. Laidler, H. Eyring, The Theory of Rate Processes, McGraw-Hill Book Co., Inc., New York City, 1941.

[65] M. Baiardo, G. Frisoni, M. Scandola, M. Rimelen, D. Lips, K. Ruffieux, E. Wintermantel, Thermal and mechanical properties of plasticized poly(L-lactic acid), J. Appl. Polym. Sci. 90 (2003) 1731–1738, https://doi.org/10.1002/app.12549.

[66] A. Zubrowska, E. Piorkowska, A. Kowalewska, M. Cichorek, Novel blends of polylactide with ethylene glycol derivatives of POSS, Colloid Polym. Sci. 293 (2015) 23–33, https://doi.org/10.1007/s00396-014-3344-3.

[67] M. Nofar, D. Sacligil, P.J. Carreau, M.R. Kamal, M.-C. Heuzey, Poly (lactic acid) blends: processing, properties and applications, Int. J. Biol. Macromol. 125 (2019) 307–360, https://doi.org/10.1016/j.ijbiomac.2018.12.002.

[68] S. Phattarateera, C. Pattamaprom, Comparative performance of functional rubbers on toughness and thermal property improvement of polylactic acid, Materials Today Comm. 19 (2019) 374–382, https://doi.org/10.1016/j.mtcomm.2019.02.012.

[69] M. Pluta, E. Piorkowska, Tough and transparent blends of polylactide with block copolymers of ethylene glycol and propylene glycol, Polym. Test. 41 (2015) 209–218, https://doi.org/10.1016/j.polymertesting.2014.11.011.

[70] I.N. Haugan, B. Lee, M.J. Maher, A. Zografos, H.J. Schibur, S.D. Jones, M. A. Hillmyer, F.S. Bates, Physical aging of polylactide-based graft block polymers, Macromolecules 52 (2019) 8878–8894, https://doi.org/10.1021/acs.macromol.9b01434.

[71] W. Ding, Y. Chen, Z. Liu, S. Yang, In situ nano-fibrillation of microinjection molded poly(lactic acid)/poly(ε-caprolactone) blends and comparison with conventional injection molding, RSC Adv. 5 (2015) 92905–92917, https://doi.org/10.1039/C5RA15402B.

[72] R. Li, L. Wu, B.-G. Li, Poly(L-lactide) materials with balanced mechanical properties prepared by blending with PEG-mb-PPA multiblock copolymers, Ind. Eng. Chem. Res. 56 (2017) 2773–2782, https://doi.org/10.1021/acs.iecr.6b05046.

[73] Z. Bartczak, A. Galeski, M. Kowalczuk, M. Sobota, M. Malinowski, Tough blends of poly(lactide) and amorphous poly([R,S]-3-hydroxy butyrate) - morphology and properties, Eur. Polym. J. 49 (2013) 3630–3641.

[74] C.B. Bucknall, Quantitative approaches to particle cavitation, shear yielding, and crazing in rubber-toughened polymers, J. Polym. Sci., Part B: Polym. Phys. 45 (2007) 1399–1409, https://doi.org/10.1002/polb.21171.

[75] M. Kowalczyk, E. Piorkowska, Mechanism of plastic deformation in biodegradable polylactide/poli(1,4-cis-isoprene) blends, J. Appl. Polym. Sci. 124 (2012) 4579–4589, https://doi.org/10.1002/app.35489.

124

Supramolecular interactions involving fluoroaryl groups in hybrid blends of polylactide and ladder polysilsesquioxanes.

Electronic Supporting Information

Contents:

1. Synthesis and characterization of LPSQ-R and CX-R.
2. Theoretical treatment of complexes stabilized via n→π* interactions and CSD search conditions.
3. Analytic methods.

Schemes, Figures and Tables:

1. Synthesis and characterization of LPSQ-R and CX-R:

LPSQ-F and LPS-F5 were prepared following the general procedure: 4.0 g of LPSQ-Vi (0.045 mol of Vi groups) was placed in a three-necked flask equipped with a condenser and an inlet of dry argon. The polymer was dissolved in 20 ml of dry toluene and admixed with 0.056 mol of fluorinated thiophenol (*p*-fluoro or pentafluoro- derivatives) and 18.5 mg of AIBN. The synthesis was carried out at 80 °C, under argon atmosphere. The reaction course was followed by ^{1}H and ^{19}F NMR. Small amounts of AIBN were added (2 x 9.3 mg) in order to get the complete conversion of vinyl groups.

In the case of LPSQ-F3 derivative, $CF_3C_6H_4SH$ (7.65 ml; 0.057 mol) was added to LPSQ-Vi (4.0 g, 0.045 mol of Vi groups) dissolved in dry THF (70 ml) and placed in a quartz vessel. DMPA (0.23 g; 0.9 mmol) was added with stirring to the solution of reagents. The mixture was irradiated for 30 min with UV light (λ = 356 nm). The reaction course was followed by ^{1}H and ^{19}F NMR. Small amounts of $CF_3C_6H_4SH$ and DMPA were added in order to get the complete conversion of vinyl groups.

The volatiles were removed from the solutions and the crude products were purified by precipitation into hexanes (repeated several times). The residues were dried to constant weight under high vacuum. The products were characterized using NMR spectroscopy (Table ESI-1). Liquid state ^{1}H, ^{13}C and ^{29}Si NMR spectra of LPSQ-R were recorded in CDCl$_3$ as the deuterated solvent on a Bruker DRX-500 MHz spectrometer.

Functionalized cyclosiloxane analogues (CX-R) were obtained using 1,3,5,7-tetravinyl-1,3,5,7-tetramethylcyclotetrasiloxane (CX–Vi) as the precursor, under the same experimental conditions as described above. The obtained liquid products (Scheme ESI-1) were purified by SiO$_2$ column chromatography using ethyl acetate as the eluent.
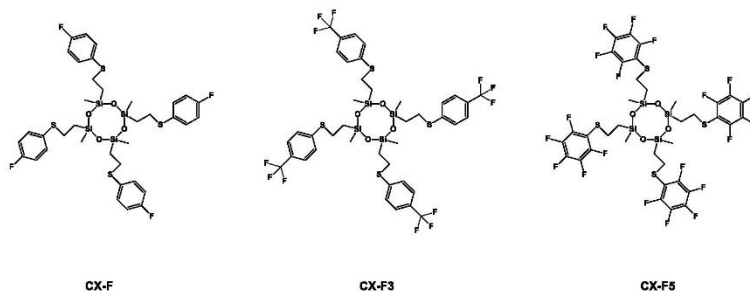
Scheme ESI-1. Structure of cyclosiloxanes used as model compounds for the comparative studies.

2. Theoretical treatment of complexes stabilized via n→π* interactions and CSD search conditions:

Quantum-chemical calculations were performed for selected model system representative for molecular systems shown in Scheme 1. Two quantum chemistry models were used for calculations, that is, DFT [1] and post-SCF MP2 [2] method. In case of DFT calculations two functionals have been tested, commonly used hybrid functional B3LYP [3] and the ωB97XD functional which uses long-range and Grimme's D2 dispersion corrections. Since after the preliminary calculations in the case of B3LYP

model the expected patterns of intermolecular interactions could not be reproduced (probably due to important role of dispersive effects which are not included in B3LYP model description (see ESI associated to this paper for movie being the graphical interpretation of optimization procedure, file Mov_F1_B3LYP.gif). Further calculations were continued merely with the use of ωB97XD and MP2 models in conjunction with aug-cc-pVTZ [4] and 6-311++G(d,p) [5], respectively. Interaction energy was estimated by means of super molecular approach, always with BSSE correction [6]. Gaussian set of codes [7] was used for calculations. Individual interactions have been recognized by means of Quantum Theory of Atoms in Molecules [8]. Electron density critical points and bond paths were localized with use of AIMAll software [9]. Note, that post-SCF densities from MP2 calculations were used when applicable.

For comparative reasons a search through Crystal Structure Database [10] was done for selected structural situations. A general criterion used for the search of specific interactions was the interatomic distance shorter than the sum of corresponding van der Waals radii. Additionally, criteria have been tightened to the highest quality crystallographic data, thus, only these structures were taken into account for which R factor was smaller than 5%, there was no disorder, no errors, polymeric ionic structures were excluded similarly like powder data. Finally, metal-organic structures were also omitted.

3. Analytic methods:

LPSQ-R were characterized with liquid state ^{1}H, ^{13}C and ^{29}Si NMR spectroscopy. The spectra were recorded on a Bruker DRX-500 MHz spectrometer using $CDCl_3$ as the deuterated solvent. The weight average molar masses of LPSQ-R and PLA were determined by size-exclusion chromatography (SEC) with multi-angle laser light scattering (MALLS) and refractive index (RI) detection in CH_2Cl_2.

FT-Infrared spectra of plain PLA, PLA/LPSQ-R (P/100-R) blends or neat LPSQ-R were recorded in transmission mode using Nicolet 380 FTIR spectrometer (Thermo Fisher Scientific; Waltham, Massachusetts, United States), equipped with a heated cell accessory and Harrick ATC/low voltage controller (Harrick Scientific Products, Inc. Pleasantville, New York, United States)] that enabled a programmed temperature change. Thin films were cast on NaCl crystal windows from 0.5 wt% solutions of the studied specimens in CH_2Cl_2. The samples were left for slow solvent evaporation in a desiccator and then dried under high vacuum (0.05 Torr) at room temperature for 16 h. PLA and the blends were melted isothermally at 190 °C (PLA) (5 min) to even out the samples. They were then cooled down to 110 °C and kept at this temperature for 30 minutes to crystalize. The spectra were collected at the beginning of the crystallization and for samples crystalized and cooled down to room temperature by adding 16 scans at 4 cm^{-1} resolution. Comparative analysis was carried out for the spectra recorded in transmission mode as well as for their second derivatives that were used to estimate the position of characteristic IR modes. Spectra of neat LPSQ-R were also measured at room temperature.

FT-Raman spectra of plain PLA, neat LPSQ-R and P/100-R blends (after CH_2Cl_2 evaporation and drying) were recorded on a NTEGRA SPECTRA SOLAR system instrument (NT-MDT Spectrum

Instruments, Moscow, Russia), equipped with a continuous wavelength laser LCM-S-111-20-NP25 (Laser-Expert Co. Ltd, Russia) operating at 532.2 nm wavelength and 20.5 mW power. A Scientific Grade, 1024 x 127 deep depletion spectroscopy CCD camera Andor iDus DV401A-BV-600 (Oxford Instruments) was used as a detector. Samples were fixed on a silicon wafer support and studied on their bottom side to avoid scattering. All samples were measured at room temperature by collecting spectra with 1800/500 diffraction gratings (within 290-1089 cm^{-1} and 1332-2031 cm^{-1}; spectral resolution of 0.8 cm^{-1}). Optimized acquisition time of a single spectrum was 10-240 s (100 μm slit width).

Thermal properties of LPSQ-R and PLA/LPSQ-R blends were studied with a differential scanning calorimetry (DSC) using a DSC 2920 Thermal Analysis System (TA Instruments, New Castle, DE, USA). Neat LPSQ-R were heated from room temperature to 100 °C, cooled down to -100 °C and heated again at 10 °C/min.
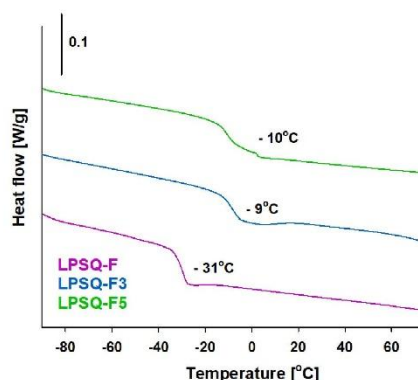
Figure ESI-1. DSC traces of functionalized LPSQ-R (2nd heating runs, 10 °C/min, exo up).

The neat PLA and the blends were heated and cooled down at 10 °C/min within the temperature range from 20 to 190 °C. After the first heating the samples were kept at 190 °C for 5 minutes and then cooled down. The phase transitions were studied during the second heating. To study isothermal crystallization, the specimens were heated to 190 °C, kept at this temperature for 5 min and cooled to selected temperatures at 10 °C/min, crystallized isothermally and then cooled to room temperature at 10 °C/min. Melting of these specimens was analysed during heating at 10 °C/min. The degree of crystallinity (X_c) was estimated from the exothermic cold crystallization and endothermic melting peaks and calculated from the Equation (1):

$$X_c = \frac{\Delta H_m \cdot 100\%}{\Delta H_0} \tag{1}$$

ΔH_m and ΔH_0 are the melting enthalpy of PLA in blends and the crystalline phase of PLA (93 J/g, enthalpy of melting of α-crystals [11]).

4

Thermogravimetric analysis (TGA) was performed using a thermogravimetric analyser (TGA Q50 V20.13 Build 39. Universal V4.5A TA Instruments) at 10 °C/min from 20 to 600 °C under nitrogen atmosphere.

Dielectric Relaxation Spectra (DRS) of PLA and the composite PLA/LPSQ-R samples were measured using an Alpha-A High Performance Frequency Analyzer (Novocontrol GmbH) combined with Quatro Cryosystem for the temperature control. 0.5 mm thick samples with evaporated gold electrodes of 7 mm in diameter were fixed between two additional external electrodes in a sample holder and placed into a cryostat. The measurements were performed in the temperature range from 40 to 120 °C on heating at a rate of 1 °C/min. The frequency varied from 1 Hz to 1 MHz at the oscillation voltage of 1 V. The measured dielectric data were collected and evaluated by WinDETA impedance analysis software and a WinFit V 3.2. program.

Studies of the internal structure of neat and modified PLA were conducted with scanning electron microscopy (SEM). The amorphous films were cryo-fractured, sputtered with gold using a Jeol Fine Coater 1200 (Tokyo, Japan) and analysed using SEM Jeol 5500LV operating in the high vacuum mode at an accelerating voltage of 10 kV. The distribution of silicon atoms of LPSQ-R in the studied samples was examined with SEM equipped with energy dispersive spectroscopy (SEM-EDS, Jeol JSM-6010LA) operating in the high vacuum mode at an accelerating voltage 8 kV. The surfaces were sputtered with carbon using a coater Q150R ES (Quorum Technologies).

Direct light transmittance (DLT) through 0.5 mm thick samples of neat and modified PLA was measured using a UV–VIS SPECORD S 600 diode array spectrophotometer (Analytik Jena AG) in the wavelength (λ) range from 200 to 1000 nm with a resolution of 0.5 nm and using air as a reference. Data were averaged for five runs for each film.

Surface free energy was estimated by contact-angle measurements. Static and advancing contact angles of sessile droplets of reference liquids [diiodomethane (Sigma-Aldrich, ReagentPlus®, 99%) and glycerol (Chempur, pure p.a., anhydrous)] at the film–air interface were taken at room temperature with a Rame-Hart NRL contact-angle goniometer equipped with a video camera JVC KYF 70B and a drop-shape analysis software. The measurements were performed on 0.5 mm thin polymer films. Free surface energies (including their polar and dispersive components) were estimated by the Owens–Wendt method [12]. Static and advancing contact angles were measured right after the deposition of the reference liquid onto the film surface. The values of contact angles are averages of at least four measurements taken on different areas of the same sample and calculated with their standard deviations. The contact angle for each drop was calculated as the arithmetic mean of the left and right angles.

Barrier measurements of the studied materials were performed using gas permeation device Lyssy 100-500 (PBI-Dansensor, Germany), according to PN-EN ISO 2556 standard, 24 h after film preparation by compression moulding. Permeability parameters for 0.35 mm thick films were averaged from five measurements.

Dynamic mechanical thermal analysis (DMTA) was carried out on 1 mm thick rectangular specimens, 17.5 mm x 12 mm, in single cantilever bending mode, using a DMTA TA Q-800 Thermal

5

Analyser (TA Instruments, New Castle, DE, USA) at a frequency of 1 Hz and a heating rate of 2 °C/min from -100 °C to 140 °C.

Tensile properties were measured using Linkam Tensile Stress Testing System TST 350 (Linkam, UK). At least five 0.5 mm thick oar-shaped specimens, with 3.81 mm gauge length and width of 1.59 mm were drawn to fracture at the rate of 5 %/min, at 25 °C. The average values of mechanical parameters were calculated.
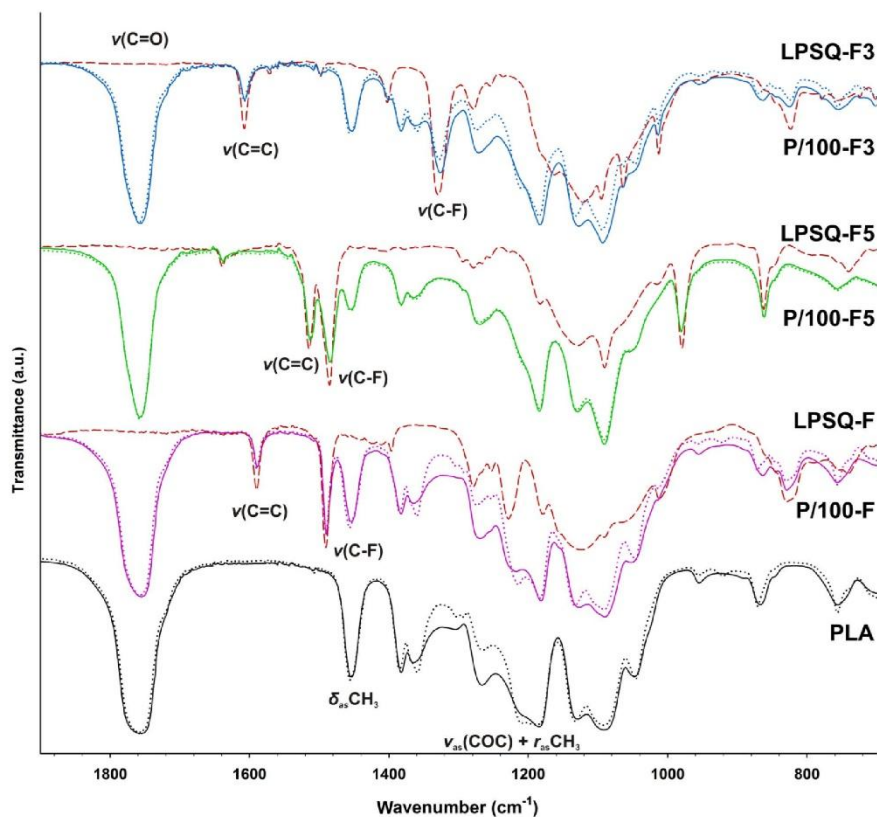
Figure ESI-2. FT-IR spectra of PLA and P/100-R blends (solid line - amorphous samples cooled down from melt to 110 °C; dotted line - samples crystallized for 30 min at 110 °C and cooled down to room temperature; short dash line – LPSQ-R used as additives in P/100-R blends).
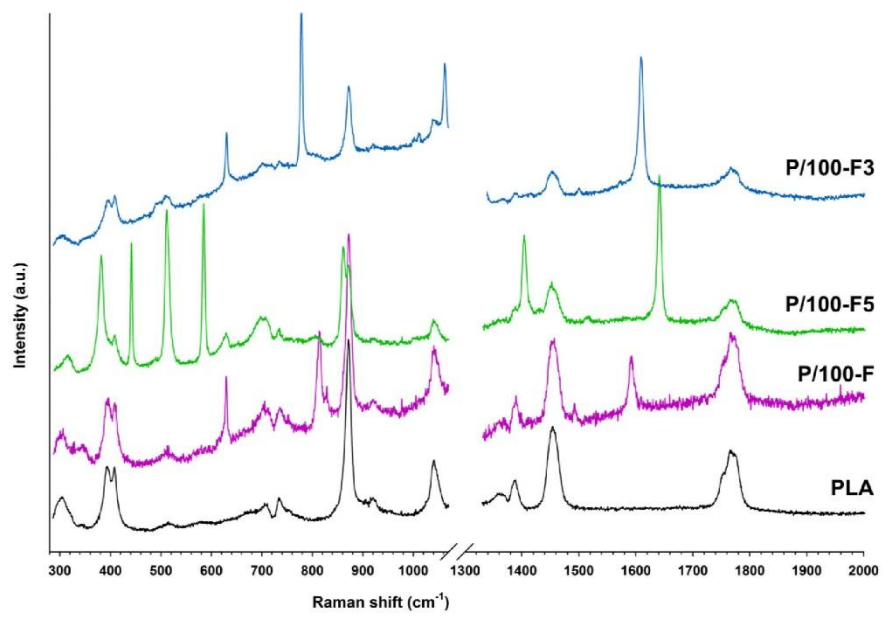
Figure ESI-3. Raman spectra of PLA and P/100-R.

Table ESI-1. NMR resonance shifts of fluoroaryl LPSQ and CX (δ (ppm) in CDCl$_3$), the reaction yield and molecular masses of LPSQ-R.

compound	^{1}H NMR	^{13}C NMR	^{29}Si NMR	^{19}F NMR	Y (%)	M$_{n\,RI}$	PDI$_{RI}$	M$_{n\,MALLS}$	PDI$_{MALLS}$
LPSQ-F	0.10 (s, -Si-$\underline{C}$H$_3$) 1.03 (m,-Si-$\underline{C}$H$_2$-CH$_2$-S-) 2.93 (m,-Si-CH$_2$-$\underline{C}$H$_2$-S-) 7.01 (s,-S-C$_6$H$_4$$\underline{F}$; meta) 7.31 (s,-S-C$_6H_4$$\underline{F}$; ortho)	0.9 (-Si-$\underline{C}$H$_3$) 12.96 (-Si-$\underline{C}$H$_2$-CH$_2$-S-) 28.6 (-Si-CH$_2$-$\underline{C}$H$_2$-S-) 115.4 (-S-C-$\underline{C}_5$H$_4$F; meta); 130.1 (-S-$\underline{C}$-C$_5$H$_4$F; ipso); 131.5 (-S-C$_5$H$_4$F; ortho) 161.2 (-S-C$_5$H$_4$$\underline{C}$-F; para; J(C-F) = 247.0 Hz)	11.1 (-O-Si-CH$_3$) -70.3 (-CH$_2$-SiO$_{3/2}$)	-114.16 (-S-C-C$_5$H$_4$F)	84%	2.0	1.26	2.8	1.45
LPSQ-F3	0.16 (m,-Si-$\underline{C}$H$_3$) 1.22 (m, -Si-$\underline{C}$H$_2$-CH$_2$-S-) 3.13 (m,-Si-CH$_2$-$\underline{C}$H$_2$-S-) 7.27 (m,-S-C$_6$H$_4$-CF$_3$; meta) 7.44 (m,-S-C$_6$H$_4$-CF$_3$; ortho)	0.7 (-Si-$\underline{C}$H$_3$) 12.8 (-Si-$\underline{C}$H$_2$-CH$_2$-S-) 26.8 (-Si-CH$_2$-$\underline{C}$H$_2$-S-) 124.1 (-S-C$_6$H4-$\underline{C}$F$_3$; J(C-F) = 268.7 Hz) 125.8 (-S-C$_6$H4-CF$_3$; meta); 127.0 (-S-$\underline{C}_6$H$_4$-CF$_3$; ortho); 142.0 (-S-$\underline{C}$C$_5$H$_4$C-CF$_3$; ipso)	12.4 (-O-Si-CH$_3$) -70.0 (-CH$_2$-SiO$_{3/2}$)	-61.92 (-S-C$_6$H4-CF$_3$)	92%	2.9	1.25	5.4	1.41
LPSQ-F5	0.12 (s, -Si-$\underline{C}$H$_3$) 1.08 (m, -Si-$\underline{C}$H$_2$-CH$_2$-S-) 3.00 (m,-Si-CH$_2$-$\underline{C}$H$_2$-S-)	0.2 (-Si-$\underline{C}$H$_3$) 13.0 (-Si-$\underline{C}$H$_2$-CH$_2$-S-) 28.4 (-Si-CH$_2$-$\underline{C}$H$_2$-S-) 107.8 (-S-$\underline{C}$-C$_6$F$_5$; ipso) 137.0 (-S-C-$\underline{C}_6$F$_5$; meta; J(C-F) = 254.9 Hz) 140.6 (-S-C-$\underline{C}_6$F$_5$; para; J(C-F) = 258.7 Hz) 146.6 (-S-C-$\underline{C}_6$F$_5$; ortho; J(C-F) = 247.3 Hz)	14.3 (-O-Si-CH$_3$) -70.5 (-CH$_2$-SiO$_{3/2}$)	-160.30 (-S-C$_6$F$_5$; ortho) -151.67 (-S-C$_6$F$_5$; para) -132.68 (-S-C$_6$F$_5$; meta)	70%	2.3	1.23	9.4	1.25
CX-F	0.13 (m,-Si-$\underline{C}$H$_3$) 0.94 (m,-Si-$\underline{C}$H$_2$-CH$_2$-S-) 2.98 (m,-Si-CH$_2$-$\underline{C}$H$_2$-S-) 6.99 (s,-S-C$_6$H$_4$$\underline{F}$; meta) 7.32 (s,-S-C$_6H_4$$\underline{F}$; ortho)	-0.5 (-Si-$\underline{C}$H$_3$) 17.4 (-Si-$\underline{C}$H$_2$-CH$_2$-S-) 29.6 (-Si-CH$_2$-$\underline{C}$H$_2$-S-) 116.0 (-S-C-$\underline{C}_5$H$_4$F; meta; J(C-F) = 21.6 Hz) 131.7 (-S-$\underline{C}$-C$_5$H$_4$F; ipso); 132.1 (-S-C-$\underline{C}_5$H$_4$F; ortho) 161.7 (-S-C$_5$H$_4$$\underline{C}$-F; para; J(C-F) = 245.2 Hz)	-21.4 O-Si(R)Me-O	-114.85 (-S-C-C$_5$H$_4$F)	18%	-	-	-	-
CX-F3	0.21 (m,-Si-$\underline{C}$H$_3$) 1.04 (m, -Si-$\underline{C}$H$_2$-CH$_2$-S-) 3.04 (m,-Si-CH$_2$-$\underline{C}$H$_2$-S-) 7.29 (m,-S-C$_6$H$_4$-CF$_3$; meta) 7.48 (m,-S-C$_6$H$_4$-CF$_3$; ortho)	-0.5 (-Si-$\underline{C}$H$_3$) 16.8 (-Si-$\underline{C}$H$_2$-CH$_2$-S-) 27.0 (-Si-CH$_2$-$\underline{C}$H$_2$-S-) 124.3 (-S-C$_6$H4-$\underline{C}$F$_3$; J(C-F) = 271.6 Hz) 125.7 (-S-$\underline{C}_6$H$_4$-CF$_3$; meta); 127.1 (-S-C$_6$H4-CF$_3$; ortho); 142.7 (-S-$\underline{C}$C$_5$H$_4$C-CF$_3$; ipso)	-21.5 O-Si(R)Me-O	-61.79 (-S-C$_6$H4-CF$_3$)	78%	-	-	-	-
CX-F5	0.15 (s, -Si-$\underline{C}$H$_3$) 1.13 (m,-Si-$\underline{C}$H$_2$-CH$_2$-S-) 3.05 (m,-Si-CH$_2$-$\underline{C}$H$_2$-S-)	-1.3 (-Si-$\underline{C}$H$_3$) 17.8 (-Si-$\underline{C}$H$_2$-CH$_2$-S-) 29.6 (-Si-CH$_2$-$\underline{C}$H$_2$-S-) 109.2 (-S-$\underline{C}$-C$_6$F$_5$; ipso) 137.7 (-S-C-$\underline{C}_6$F$_5$; meta; J(C-F) = 252.8 Hz) 141.1 (-S-C-$\underline{C}_6$F$_5$; para; J(C-F) = 257.3 Hz) 147.3 (-S-C-$\underline{C}_6$F$_5$; ortho; J(C-F) = 247.7 Hz)	-21.6 O-Si(R)Me-O	-160.42 (-S-C$_6$F$_5$; ortho) -152.26 (-S-C$_6$F$_5$; para) -132.39 (-S-C$_6$F$_5$; meta)	9%	-	-	-	-

Y – reaction yield after product purification (precipitation for LPSQ-R and column chromatography for CX-R)

M$_n$ – number average molecular mass of LPSQ-R (kg/mol) estimated with SEC using refractive index (RI) and (MALLS) detectors

PDI – polydispersity index of LPSQ-R (M$_w$/M$_n$) estimated with SEC

8

Table ESI-2. Assignment of characteristic vibration modes in FTIR and Raman spectra (cm⁻¹).

	PLA			LPSQ-F5			LPSQ-F			LPSQ-F3		
mode	mode	FTIR*	Raman	mode	FTIR	Raman	mode	FTIR	Raman	mode	FTIR	Raman
	skeletal torsion	-	~200	out of plane C-F deformation	-	384	out of plane C-F deformation	-	350	-	-	-
	$\delta(COC) + \delta_2 C\text{-}CH_3$	-	300	in plane C-F deformation	-	441 / 511	in plane C-F deformation	-	515	-	-	-
	$\delta(CCO)$	-	392 / 395	ring breathing	-	584	ring breathing	-	629	ring breathing	-	626
	$\delta_s C\text{-}CH_3 + \delta CCO$	-	500	ring vibration	-	693	ring vibration	-	699	ring vibration	-	711
	$\gamma(C=O)$	-	701	$\nu(Si\text{-}C)$	849	-	$\nu(Si\text{-}C)$	824	-	$\nu(Si\text{-}C)$	821	-
	$\delta(C=O)$	740	736	$-CH_2\text{-}S\text{-}Ar$	-	863	$-CH_2\text{-}S\text{-}Ar$	-	815	$-CH_2\text{-}S\text{-}Ar$	-	779
	$\nu(C\text{-}COO)$	864	873		862		CH bending in aromatic rings	829		CH bending in aromatic rings	823	-
	$rCH_3 + \nu CC$	955	950		-			-			-	-
	$r(C\text{-}CH_3)$	1042 / 1023	1042	$\nu_{as}(C\text{-}F)$	979 / 1090		$\nu_{as}(C\text{-}F)$	1008		$\nu_{as}(C\text{-}F)$	1011 / 1062	1062
	$\nu_s(COC)$	1081	1090	-	-	-	trigonal ring breathing in disubstituted benzenes	-	1093	trigonal ring breathing in disubstituted benzenes	-	1095
	$r_{as}CH_3$	1132	1126	$\nu(Si\text{-}O)$ (broad peak)	1030	-	$\nu(Si\text{-}O)$ (broad peak)	1120	-	$\nu(Si\text{-}O)$ (broad peak)	1115	-
	$\nu_{as}(COC) + r_{as}CH_3$	1211 / 1183	1180	-	-	-	CH bending in aromatic rings	1087	1156	CH bending in aromatic rings	1093	1190
	$\delta(CH) + \nu(COC)$	1270	1250	$\nu(Si\text{-}C)$	1183	1244	$\nu(Si\text{-}C)$	1175	1217	$\nu(Si\text{-}C)$	1157	1290
	$\delta_2 CH$	1304	1294	$\nu(C\text{-}F)+ \nu(Si\text{-}C)$	1276	1277	$\nu(C\text{-}F)+ \nu(Si\text{-}C)$	1277	1272	$\nu(C\text{-}F)+ \nu(Si\text{-}C)$	1275	1267
	$\delta_1 CH + \delta_s CH_3$	1355	1349					1226				
	$\delta_s CH_3$	1380	1384									
	$\delta_{as} CH_3$	1450	1452	$\nu(C\text{-}F)aryl$	1485	1403	$\nu(C\text{-}F)aryl$	1490	1410	$\nu_{sym}(C\text{-}F)alkyl$	1327	1327
	$\nu(C=O)$	1755	1767	$\nu(C=C)$	1514	1641	$\nu(C=C)$	1590	1591	$\nu(C=C)$	1607	1607

* - data collected for amorphous PLA
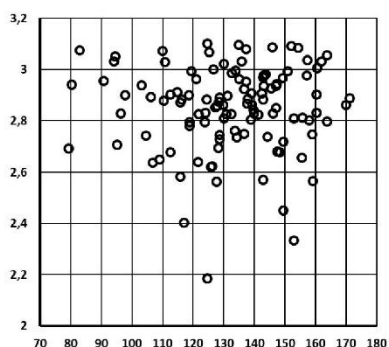
Figure ESI-4. Distance (in Angstroms) between oxygen atom and the plane of pentafluorinated benzene fragment expressed as a function of C=O…Cg angle (in deg.), where Cg is the center of the given ring. Data from CSD search, found for 83 high quality crystal structures in which interaction between carbonyl group and benzene ring was found.

(a)   (b)
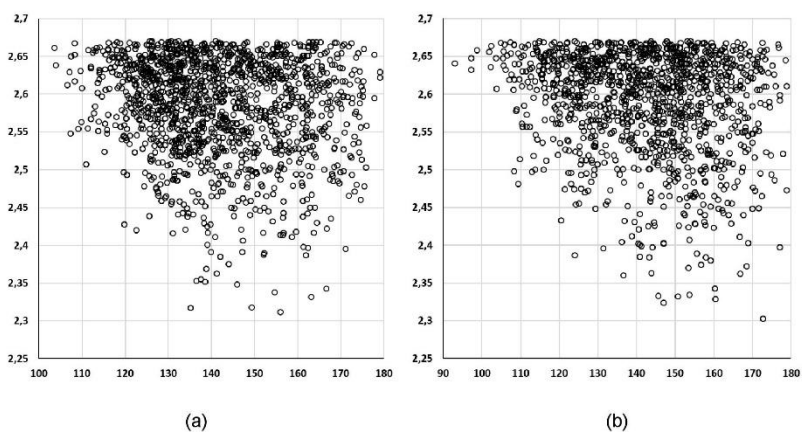
Figure ESI-5. Plot of relation of H…F distance versus C-H…F angle for H-bridges found in CSD data. Any aromatic, (a), and any methyl, (b), carbon donors were considered in the search. There are 1518 and 902 records found for (a) and (b) case, respectively.

10

134
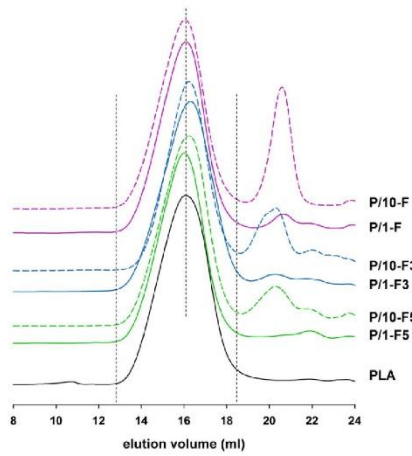
Figure ESI-6. Comparison of SEC (RI) traces of exemplary blends PLA/LPSQ-R.

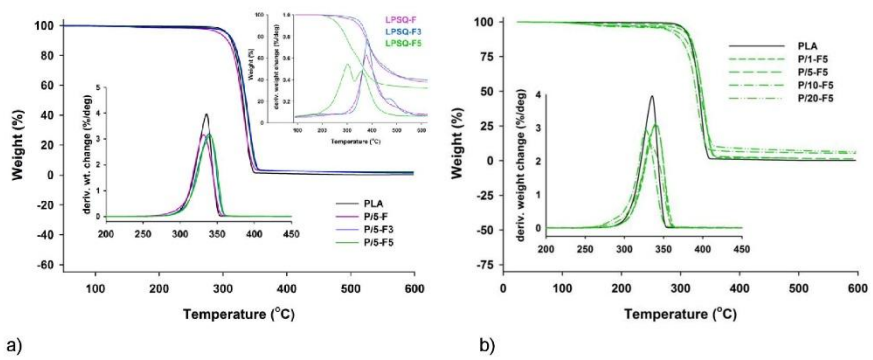a)   b)

Figure ESI-7. Comparison of TGA traces (N_2, 10 °C/min) of exemplary blends PLA/LPSQ-R. Inset in figure ESI-7a shows TGA traces of neat LPSQ-R.

11
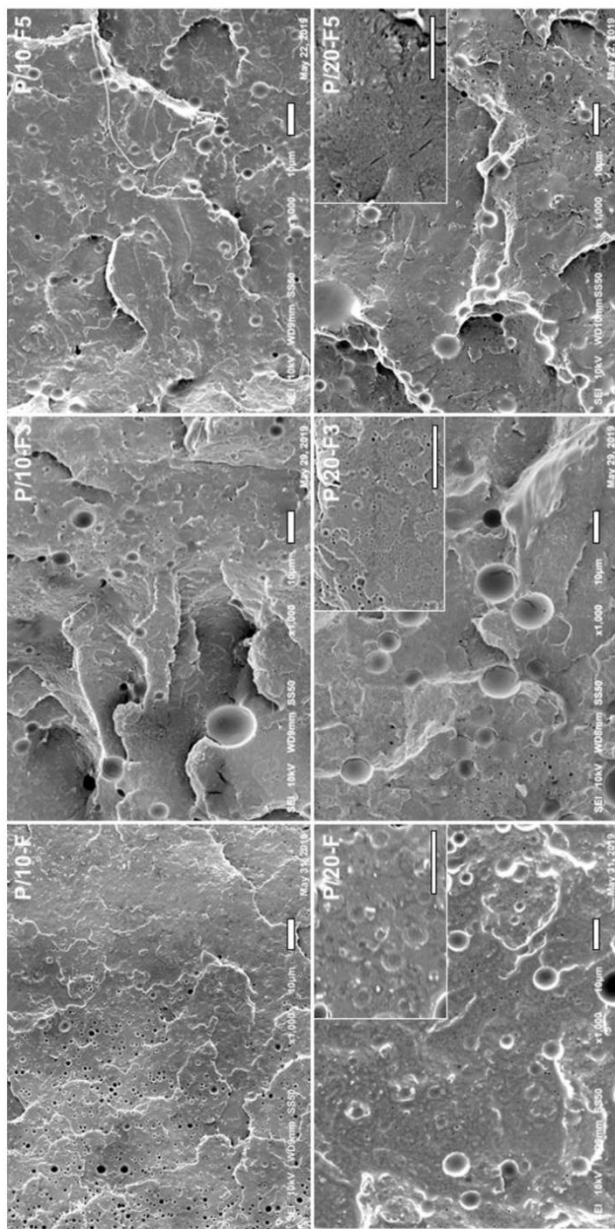
Figure ESI-8. SEM micrographs of samples of P/10-R and P/20-R blends (cryo-fractured surfaces, scale bar of 10 μm). Scale bars in insets correspond to 5 μm.

12

Table ESI-3. Characteristic phase transitions of P/LPSQ-R blends recorded with DSC (10 °C/min).

sample	LPSQ-R (wt%)	1st cooling.	2nd heating				
		T_g (°C)	T_g (°C)	T_{cc} (°C)	ΔH_{cc} (J/g$_{PLA}$)	T_m (°C)	ΔH_m (J/g$_{PLA}$)
PLA	-	55.6	61.5	134.4	8.1	166.3	8.1
P/1-F	1	55.7	60.5	127.5	3.7	166.7	3.7
P/5-F	5	55.8	59.7	127.7	5.3	165.3	5.3
P/10-F	10	53.4	59.9	131.6	2.9	165.5	2.9
P/20-F	20	54.3	59.4	130.8	4.8	165.6	4.8
P/1-F3	1	56.6	60.5	130.6	5.0	165.6	5.1
P/5-F3	5	57.2	60.6	127.0	30.0	165.8	30.0
P/10-F3	10	56.9	59.8	125.6	36.1	165.7	36.1
P/20-F3	20	56.9	59.7	133.8	35.5	165.9	35.5
P/1-F5	1	57.9	61.1	128.2	3.2	166.6	3.2
P/5-F5	5	57.2	61.2	131.7	2.7	165.5	2.7
P/10-F5	10	57.5	61.3	127.4	5.0	165.1	5.0
P/20-F5	20	54.5	60.6	128.4	2.5	165.9	2.5
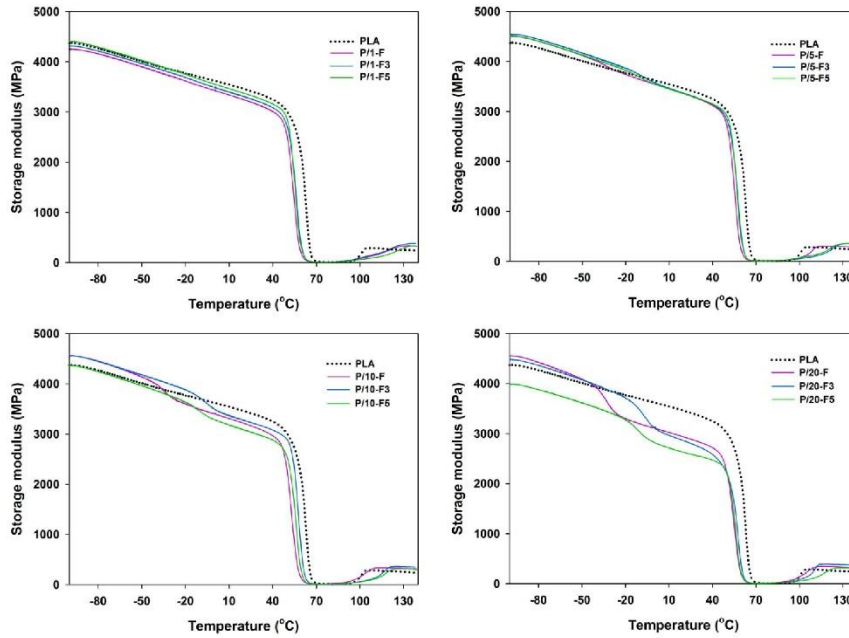
Figure ESI-9. Changes in storage modulus (E') of PLA and PLA/LPSQ-R blends vs. temperature.

13

137

Table ESI-4. Characteristic phase transitions of P/CX-R blends recorded with DSC (10 °C/min).

sample	CX-R (wt%)	1st cooling.	2nd heating				
		T_g (°C)	T_g (°C)	T_{cc} (°C)	ΔH_{cc} (J/g$_{PLA}$)	T_m (°C)	ΔH_m (J/g$_{PLA}$)
PLA	-	55.6	61.5	134.4	8.1	166.3	8.1
P/1-CX-F	1	55.2	60.5	137.5	7.6	166.6	7.6
P/5-CX-F	5	51.0	57.2	133.9	9.2	166.4	9.2
P/1-CX-F3	1	56.1	60.4	132.0	6.5	159.5	6.5
P/5-CX-F3	5	52.5	56.4	134.8	18.0	165.1	18.0
P/1-CX-F5	1	57.0	61.1	137.1	8.8	165.9	8.8
P/5-CX-F5	5	53.7	59.6	131.8	9.1	165.3	9.1
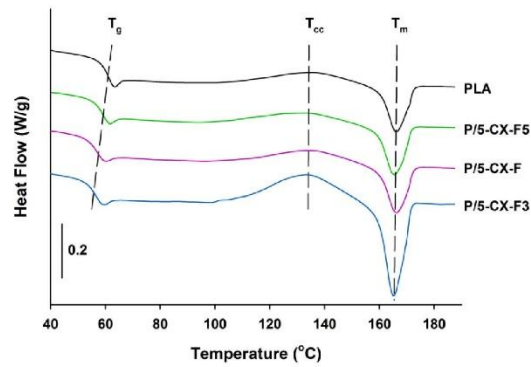
Figure ESI-10. DSC thermograms of PLA and P/5-CX-R (2nd heating, 10 °C/min, exo up).
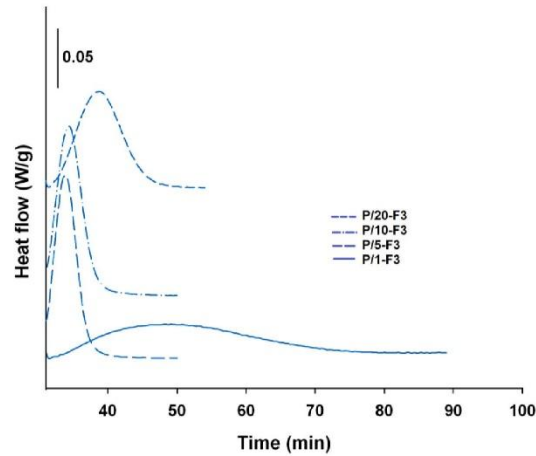
Figure ESI-11. DSC thermograms recorded for PLA/LPSQ-F3 during isothermal crystallization at 120 °C (exo up).
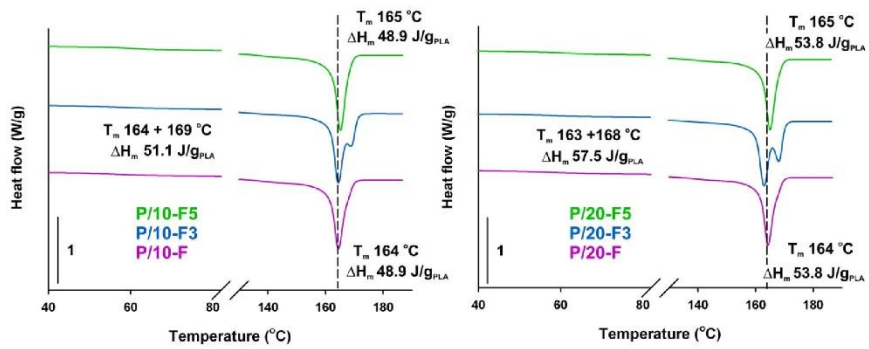
Figure ESI-12. DSC traces (second heating; 10 °C/min; exo up) of samples P/10-R and P/20-R isothermally crystallized (from melt) at 120 °C.
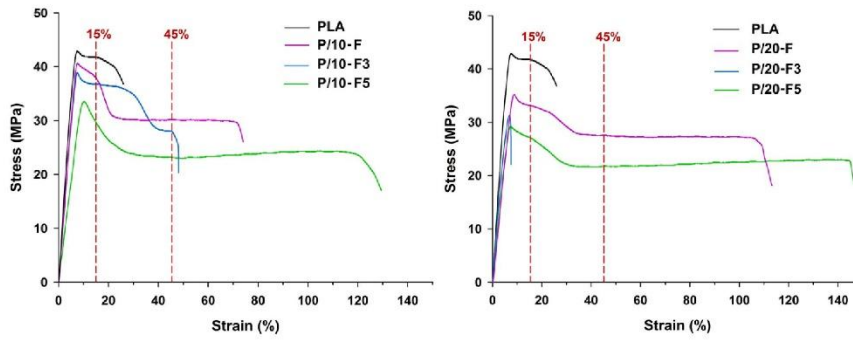
Figure ESI-13. Exemplary stress-strain plots for neat PLA and PLA/LPSQ-R (10 wt% and 20 wt%) uniaxially drawn at 25 °C, 5%/min.

15

139

Table ESI-5. Mechanical properties of PLA/LPSQ-R blends.

sample	Yield Stress (MPa)	Yield Strain (%)	Stress at break (MPa)	Strain at break (%)
P/1-F	42.7 ± 3.4	9.2 ± 1.2	41.4 ± 2.8	16.3 ± 1.8
P/5-F	40.5 ± 2.2	7.8 ± 0.4	25.4 ± 1.1	62.8 ± 10.6
P/10-F	38.1 ± 2.2	7.9 ± 0.4	26.3 ± 1.8	63.5 ± 9.8
P/20-F	36.5 ± 1.0	8.2 ± 0.8	27.1 ± 1.3	150.3 ± 37.7
P/1-F3	42.1 ± 4.6	8.8 ± 1.1	38.9 ± 2.5	18.9 ± 6.7
P/5-F3	41.2 ± 1.7	8.4 ± 2.3	30.8 ± 4.6	44.4 ± 11.8
P/10-F3	36.9 ± 2.0	7.6 ± 0.1	27.0 ± 0.8	49.2 ± 5.2
P/20-F3	28.6 ± 2.3	6.5 ±0.7	27.0 ± 2.3	7.2 ± 0.9
P/1-F5	40.1 ± 5.6	9.0 ± 1.7	36.4 ± 9.2	22.1 ± 3.7
P/5-F5	41.3 ± 4.8	9.1 ± 1.6	27.6 ± 2.2	86.9 ± 22.9
P/10-F5	34.4 ± 2.5	9.5 ± 0.8	22.8 ± 4.3	120.2 ± 16.2
P/20-F5	28.6 ± 0.5	7.6 ± 0.3	21.0 ± 0.8	164.7 ± 28.0

Table ESI-6. Changes in OTR through the studied materials.

Sample	Oxygen transmission rate [ml/(m^2·24h)]
PLA reference	202.73±0.71
P/1-F	156.55±0.63
P/5-F	133.62±0.67
P/1-F3	111.79±0.44
P/5-F3	132.19±0.53
P/1-F5	124.25±0.47
P/5-F5	136.44±0.53

Literature:

[1] Kohn W., Sham L.J., Self-consistent equations including exchange and correlation effects. Phys. Rev., 140 (1965) A1133-A1138. https://doi.org/10.1103/PhysRev.140.A1133

[2] Møller C., Plesset M.S., Note on an approximation treatment for many-electron systems. Phys. Rev., 46 (1934) 618-622. https://doi.org/10.1103/PhysRev.46.618

[3] Becke A.D., Density-functional thermochemistry. III. The role of exact exchange. J. Chem. Phys., 98 (1993) 5648-5652. https://doi.org/10.1063/1.464913

[4] Wilson A.K., van Mourik T., H. Dunning Jr. T., Gaussian basis sets for use in correlated molecular calculations. VI. Sextuple zeta correlation consistent basis sets for boron through neon. J. Mol. Struct. (Theochem), 388 (1996) 339-349 and references therein. https://doi.org/10.1016/S0166-1280(96)80048-0

[5] Krishnan R., Binkley J.S., Seeger R. Pople J.A., Self-consistent molecular orbital methods. 20. Basis set for correlated wave-functions. J. Chem. Phys., 72 (1980) 650-654. https://doi.org/10.1063/1.438955

[6] Boys S.F., Bernardi F., Calculation of small molecular interactions by differences of separate total energies – Some procedures with reduced errors. Mol. Phys., 19 (1970) 553-566. https://doi.org/10.1080/00268977000101561

[7] Gaussian 09, Revision D.01, Frisch M.J., Trucks G.W., Schlegel H.B.,. Scuseria G.E, Robb M.A., Cheeseman J.R., Scalmani G., Barone V., Mennucci B., Petersson G.A., Nakatsuji H., Caricato M., Li X., Hratchian H.P., Izmaylov A.F., Bloino J., Zheng G., Sonnenberg J.L., Hada M., Ehara M., Toyota K., Fukuda R., Hasegawa J., Ishida M., Nakajima T., Honda Y., Kitao O., Nakai H., Vreven T., Montgomery Jr. J.A., Peralta J.E., Ogliaro F., Bearpark M., Heyd J.J., Brothers E., Kudin K.N., Staroverov V.N., Keith T., Kobayashi R., Normand J., Raghavachari K., Rendell A., Burant J.C., Iyengar S.S., Tomasi J., Cossi M., Rega N., Millam J.M., Klene M., Knox J.E., Cross J.B., Bakken V., Adamo C., Jaramillo J., Gomperts R., Stratmann R.E., Yazyev O., Austin A.J., Cammi R., Pomelli C., Ochterski J.W., Martin R.L., Morokuma K., Zakrzewski V.G., Voth G.A., Salvador P., Dannenberg J.J., Dapprich S., Daniels A.D., Farkas O., Foresman J.B., Ortiz J.V., Cioslowski J., Fox D.J., Gaussian, Inc., Wallingford CT, 2013

[8] Bader R.F.W., Atoms in molecules: A quantum theory (1990) Clarendon Press: Oxford.

[9] AIMAll (Version 19.10.12), Todd A. Keith, TK Gristmill Software, Overland Park KS, USA, 2019 (aim.tkgristmill.com)

[10] Groom C.R., Bruno I.J., Lightfoot M.P., Ward S.C., The Cambridge structural database. Acta Cryst., B72 (2016) 171-179. https://doi.org/10.1107/S2052520616003954

[11] Fischer E.W., Sterzel H.J., Wegner G., Investigation of the structure of solution grown crystals of lactide copolymers by means of chemical reaction. Kolloid-Zu Z-Polymer, 251 (1973) 980–990. https://doi.org/10.1007/BF01498927

[12] Owens D.K., Wendt R.C., Estimation of the surface free energy of polymers. J. Appl. Polym. Sci., 13 (1969) 1741–1747. https://doi.org/10.1002/app.1969.070130815.

17
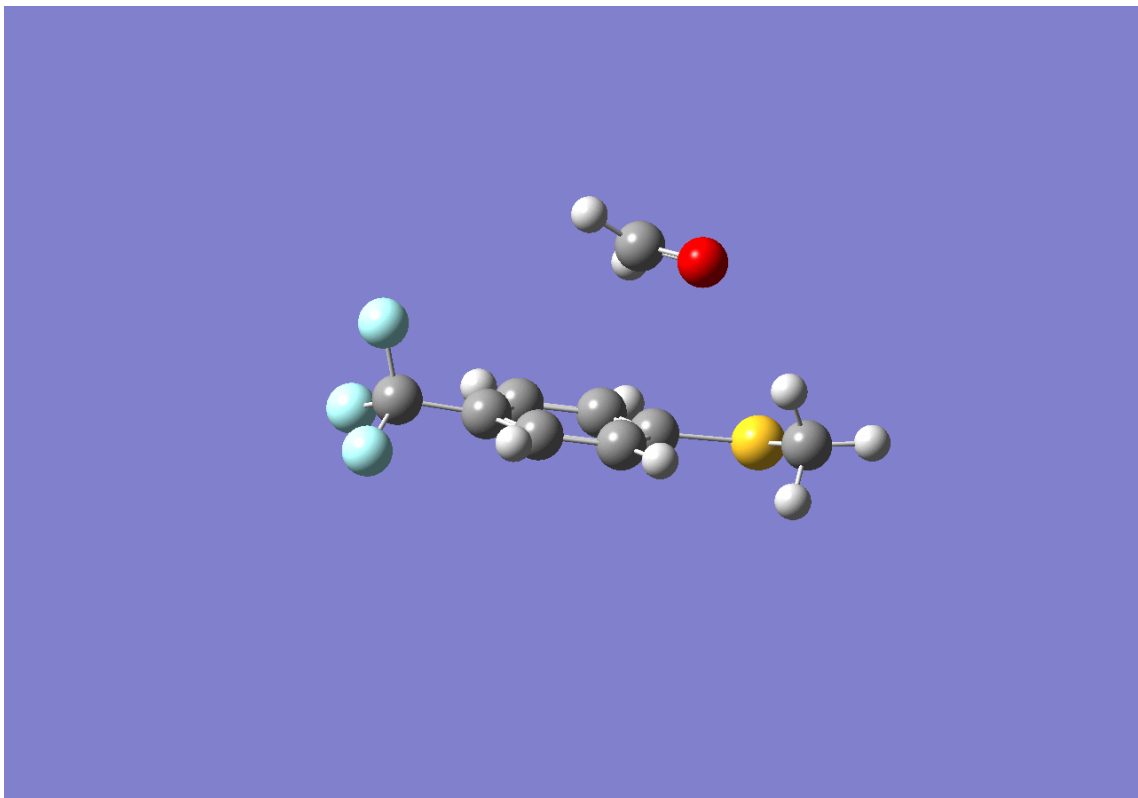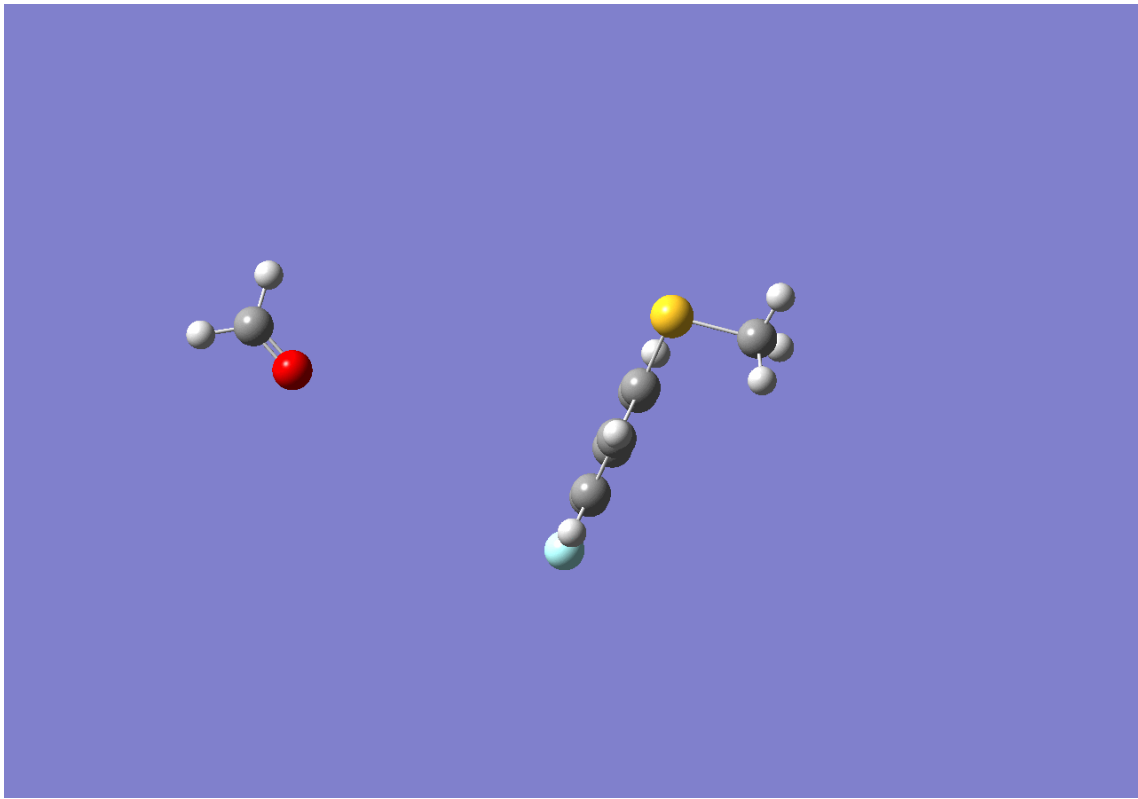
mgr Agata S. Herc

Centrum Badań Molekularnych i Makromolekularnych

Polskiej Akademii Nauk

Sienkiewicza 112

90-363 Łódź

OŚWIADCZENIE WSPÓŁAUTORA

Oświadczam, że w pracach:

1. A.S.Herc, J.Bojda, M.Nowacka, P.Lewiński, W.Maniukiewicz, E.Piorkowska, A.Kowalewska, „Crystallization, structure and properties of polylactide/lader poly(silsesquioxane) blends" *Polymer*, 201 (2020) 122563.

2. A.S.Herc, P.Lewiński, S.Kaźmierski, J.Bojda, A.Kowalewska „Hybrid SC-polylactide/poly(silsesquioxane) blends of improved thermal stability." *Thermochimica Acta*, 687 (2020) 178592.

3. A.S.Herc, M.Włodarska, M.Nowacka, J.Bojda, W.Szymański, A.Kowalewska „Supramolecular interactions between polylactide and model cyclosiloxanes with hydrogen bonding-capable functional groups." *eXPRESS Polym. Lett.*, 14 (2020) 134–153.

4. A.Kowalewska, A.S.Herc, J.Bojda, M.Palusiak, E.Markiewicz, P.Ławniczak, M.Nowacka, J.Sołtysiak; A.Różański, E.Piórkowska „Supramolecular interactions involving fluoroaryl groups in hybrid blends of polylactide and laddder polysilsesquioxanes." *Polymer Testing,* 94 (2021) 107033.

Mój udział w badaniach opisanych w powyższych publikacjach polegał na: wykonaniu syntezy liniowych poli(silseskwioksanów) (na podstawie metod literaturowych) i modyfikacji ich wiązań nienasyconych poprzez addycję eno-tiolową tioglikolanu metylu, 1-tioglicerolu, 2-merkaptoetanolu, 4-(trifluorometylo)tiofenolu, pentafluorotiofenolu i 4-fluorotiofenolu oraz modyfikacji małocząsteczkowych analogów liniowych poli(silseskwioksanów) (cyklosiloksanów); optymalizacji warunków addycji eno-tiolowej, opracowaniu wyników analiz otrzymanych produktów (NMR, TGA, DSC, FTIR, spektroskopia ramanowska), jak również przygotowaniu kompozytów PLA z liniowymi modyfikowanymi poli(silseskwioksanami), kompozytów sc-PLA z liniowymi modyfikowanymi poli(silseskwioksanami) oraz kompozytów PLA z modyfikowanymi cyklosiloksanami, przeprowadzeniu badań właściwości optycznych (UV-Vis) oraz badań strukturalnych (spektroskopia FTIR i Ramana) otrzymanych kompozytów polilaktydu i modyfikowanych liniowych poli(silseskwioksanów) oraz ich analiza, jak również opracowaniu wyników analiz właściwości fizykochemicznych otrzymanych kompozytów (DSC, TGA).

Agata Herc

potwierdzam
Anna Kowalewska

Dr hab. inż. Anna Kowalewska

Profesor Instytutu   Łódź, 26.04.2021

Centrum Badań Molekularnych

i Makromolekularnych PAN

ul. Sienkiewicza 112

90-363 Łódź

Oświadczenie współautora publikacji

Oświadczam, że w ramach przygotowywania artykułu naukowego:

1) Herc, A.S.; Włodarska, M.; Nowacka, M.; Bojda, J.; Szymański, W.; Kowalewska, A. *Supramolecular interactions between polylactide and model cyclosiloxanes with hydrogen bonding-capable functional groups*. eXPRESS Polymer Letters <u>14</u> (2020) 134-153. DOI: 10.3144/expresspolymlett.2020.12

2) Herc, A.S.; Lewiński, P.; Kaźmierski, S.; Bojda, J.; Kowalewska, A. *Hybrid SC-polylactide/poly(silsesquioxane) blends of improved thermal stability*. Thermochimica Acta <u>687</u> (2020) 178592. DOI: 10.1016/j.tca.2020.178592

3) Herc, A.S.; Bojda, J.; Nowacka, M.; Lewiński, P.; Maniukiewicz, W.; Piorkowska, E.; Kowalewska, A. *Crystallization, structure and properties of polylactide/ladder poly(silsesquioxane) blends*. Polymer <u>201</u> (2020) 122563. DOI: 10.1016/j.polymer.2020.122563

4) Kowalewska, A.; Herc, A.S.; Bojda, J.; Palusiak, M.; Markiewicz, E.; Ławniczak, P.; Nowacka, M.; Sołtysiak, J.; Różański, A.; Piorkowska, E. *Supramolecular interactions involving fluoroaryl groups in hybrid blends of polylactide and ladder polysilsesquioxanes*. Polymer Testing <u>94</u> (2021) 107033. DOI: 10.1016/j.polymertesting.2020.10703

dokonywałam merytorycznego nadzoru nad prowadzonymi badaniami, pomagałam w prowadzeniu badań krystalizacji za pomocą FTIR, konsultowałam, tworzyłam i poprawiałam teksty manuskryptów.

dr hab. inż. Anna Kowalewska

profesor Instytutu

Oświadczenie wydane na prośbę:

Mgr. Agaty S. Herc

CBMiM PAN

ul. Sienkiewicza 112

90-363 Łódź

w związku z jej pracą doktorską

144

prof. dr hab. Ewa Piórkowska-Gałęska   7 maja 2021 r.

Centrum Badań Molekularnych i Makromolekularnych

Polskiej Akademii Nauk

Sienkiewicza 112

90-363 Łódź

OŚWIADCZENIE WSPÓŁAUTORA

Oświadczam, że w pracy:

Agata S. Herc, Joanna Bojda, Maria Nowacka, Piotr Lewiński, Waldemar Maniukiewicz, Ewa Piórkowska, Anna Kowalewska „Crystallization, structure and properties of polylactide/lader poly(silsesquioxane) blends" – Polymer, 2020, 201, 122563.

Mój udział na uczestniczeniu w sformułowaniu koncepcji prac, uczestniczeniu w merytorycznym nadzorze nad prowadzonymi badaniami, uczestniczeniu w analizie wyników, a także w przygotowaniu i poprawianiu manuskryptu..

Oświadczam, że w pracy:

Kowalewska A., Herc A.S., Bojda J., Palusiak M., Markiewicz E., Ławniczak P., Nowacka M., Sołtysiak J., Różański A., Piórkowska E. „Supramolecular interactions involving fluoroaryl groups in hybrid blends of polylactide and ladder polysilsesquioxanes" – Polymer Testing, 2021, 94, 107033.

Mój udział polegał na uczestniczeniu w merytorycznym nadzorze nad prowadzonymi badaniami, konsultowaniu, a także na uczestniczeniu w analizie wyników.

E. Piórkowska
~ Gałęska

dr Maria Nowacka

Centrum Badań Molekularnych i Makromolekularnych

Polskiej Akademii Nauk

Sienkiewicza 112

90-363 Łódź

OŚWIADCZENIE WSPÓŁAUTORA

Oświadczam, że w pracach:

1. A.S. Herc, M. Włodarska, M. Nowacka, J. Bojda, W. Szymański, A. Kowalewska* „Supramolecular interactions between polylactide and model cyclosiloxanes with hydrogen bonding-capable functional groups", eXPRESS Polymer Letters 2020, 14, 134–153.

2. Agata S. Herc, Joanna Bojda, Maria Nowacka, Piotr Lewiński, Waldemar Maniukiewicz, Ewa Piórkowska, Anna Kowalewska „Crystallization, structure and properties of polylactide/lader poly(silsesquioxane) blends" – Polymer, 2020, 201, 122563.

3. Kowalewska A., Herc A.S., Bojda J., Palusiak M., Markiewicz E., Ławniczak P., Nowacka M., Sołtysiak J., Różański A., Piórkowska E. „Supramolecular interactions involving fluoroaryl groups in hybrid blends of polylactide and ladder polysilsesquioxanes" – Polymer Testing, 2021, 94, 107033.

Mój udział polegał na:

Ad. 1,2,3. obliczeniu czasów połówkowych krystalizacji PLA/CX-R lub PLA/LPSQ-R i przygotowaniu odpowiednich wykresów.

Ad. 2. syntezie liniowego poli(silseskwioksanu) z grupami 2-(karboksymetylotio)etylowymi w łańcuchach bocznych (LPSQ-COOH);

Ad 3. wykonaniu pomiarów kątów zwilżania, obliczeniu swobodnej energii powierzchniowej filmów PLA oraz mieszanin PLA/LPSQ-R oraz przygotowaniu odpowiedniego wykresu.

dr inż. Waldemar Maniukiewicz

Politechnika Łódzka

Instytut Chemii Ogólnej i Ekologicznej

Żeromskiego 116

90-924 Łódź

OŚWIADCZENIE WSPÓŁAUTORA

Oświadczam, że w pracy:

Agata S. Herc, Joanna Bojda, Maria Nowacka, Piotr Lewiński, Waldemar Maniukiewicz, Ewa Piórkowska, Anna Kowalewska „Crystallization, structure and properties of polylactide/lader poly(silsesquioxane) blends" – Polymer, 2020, 201, 122563.

Mój udział polegał na:

Pomiarze próbek oraz analizie wyników uzyskanych metodą polikrystalicznej dyfrakcji rentgenowskiej.

Podpis

dr Piotr Lewiński

Centrum Badań Molekularnych i Makromolekularnych

Polskiej Akademii Nauk

Sienkiewicza 112

90-363 Łódź

OŚWIADCZENIE WSPÓŁAUTORA

Oświadczam, że w pracy:

Agata S. Herc, Joanna Bojda, Maria Nowacka, Piotr Lewiński, Waldemar Maniukiewicz, Ewa Piórkowska, Anna Kowalewska „Crystallization, structure and properties of polylactide/lader poly(silsesquioxane) blends" – Polymer, 2020, 201, 122563.

Mój udział polegał na: Przeprowadzeniu syntezy próbek poli(L-laktydu)

Oświadczam, że w pracy:

Agata S. Herc, Piotr Lewiński, Sławomir Kaźmierski, Joanna Bojda, Anna Kowalewska „Hybrid S.C.-polylactide/poly(silsesquioxane) blends of improved thermal stability" – Thermochimica Acta, 2020, 687, 178592.

Mój udział polegał na: Przeprowadzeniu syntezy próbek poli(L-laktydu) / poli(D-laktydu); pomocy w edycji i korekcie manuskryptu publikacji

Piotr Lewiński

Piotr Lewiński

dr Piotr Lewiński

Centrum Badań Molekularnych i Makromolekularnych

Polskiej Akademii Nauk

Sienkiewicza 112

90-363 Łódź

OŚWIADCZENIE WSPÓŁAUTORA

Oświadczam, że w pracy:

Agata S. Herc, Joanna Bojda, Maria Nowacka, Piotr Lewiński, Waldemar Maniukiewicz, Ewa Piórkowska, Anna Kowalewska „Crystallization, structure and properties of polylactide/lader poly(silsesquioxane) blends" – Polymer, 2020, 201, 122563.

Mój udział polegał na: Przeprowadzeniu syntezy próbek poli(L-laktydu)

Oświadczam, że w pracy:

Agata S. Herc, Piotr Lewiński, Sławomir Kaźmierski, Joanna Bojda, Anna Kowalewska „Hybrid S.C.-polylactide/poly(silsesquioxane) blends of improved thermal stability" – Thermochimica Acta, 2020, 687, 178592.

Mój udział polegał na: Przeprowadzeniu syntezy próbek poli(L-laktydu) / poli(D-laktydu); pomocy w edycji i korekcie manuskryptu publikacji

Piotr Lewiński

Dr inz. Sławomir Kaźmierski

Centrum Badań Molekularnych i Makromolekularnych

Polskiej Akademii Nauk

Sienkiewicza 112

90-363 Łódź

OŚWIADCZENIE WSPÓŁAUTORA

Oświadczam, że w pracy:

Agata S. Herc, Piotr Lewiński, Sławomir Kaźmierski, Joanna Bojda, Anna Kowalewska „Hybrid S.C.-polylactide/poly(silsesquioxane) blends of improvedthermalstability" – Thermochimica Acta, 2020, 687, 178592.

Mój udział polegał na: rejestracji widm NMR.

Sławomir Kaźmierski

mgr Joanna Bojda

Centrum Badań Molekularnych i Makromolekularnych

Polskiej Akademii Nauk

Sienkiewicza 112

90-363 Łódź

OŚWIADCZENIE WSPÓŁAUTORA

Oświadczam, że w pracy:

Agata S. Herc, Joanna Bojda, Maria Nowacka, Piotr Lewiński, Waldemar Maniukiewicz, Ewa Piórkowska, Anna Kowalewska „Crystallization, structure and properties of polylactide/lader poly(silsesquioxane) blends" – Polymer, 2020, 201, 122563.

Mój udział polegał na zbadaniu struktury fazowej mieszanin za pomocą termicznej dynamicznej analizy mechanicznej (DMTA) oraz skaningowego mikroskopu elektronowego z możliwością badania metodą energodyspersyjnej spektroskopii rentgenowskiej (SEM-EDS). Zbadałam również właściwości termiczne składników mieszanin – sfunkcjonalizowanych poli(silsekwiokasów) - za pomocą skaningowego kalorymetru różnicowego (DSC). Ponadto, przeprowadziłam badania właściwości mechanicznych mieszanin jak również badania izotermicznej krystalizacji mteriałów za pomocą skaningowego kalortmetru różnicowego (DSC) oraz stolika grzejnego Linkam CSS450 zamonowanego na polaryzacyjnym mikroskopie świetlnym. Przeprowadziłam analizę uzyskanych wyników oraz uczestniczyłam w ich interpretacji.

Joanne
Bojda

mgr Joanna Bojda

Centrum Badań Molekularnych i Makromolekularnych

Polskiej Akademii Nauk

Sienkiewicza 112

90-363 Łódź

OŚWIADCZENIE WSPÓŁAUTORA

Oświadczam, że w pracy:

A.S. Herc, M. Włodarska, M. Nowacka, J. Bojda, W. Szymański, A. Kowalewska* „Supramolecular interactions between polylactide and model cyclosiloxanes with hydrogen bonding-capable functional groups", eXPRESS Polymer Letters 2020, 14, 134–153.

Mój udział polegał na zbadaniu struktury fazowej materiałów za pomocą skaningowego mikroskopu elektronowego z możliwością badania metodą energodyspersyjnej spektroskopii rentgenowskiej (SEM-EDS).

Joanna
Bojda

mgr Joanna Bojda

Centrum Badań Molekularnych i Makromolekularnych

Polskiej Akademii Nauk

Sienkiewicza 112

90-363 Łódź

OŚWIADCZENIE WSPÓŁAUTORA

Oświadczam, że w pracy:

Agata S. Herc, Piotr Lewiński, Sławomir Kaźmierski, Joanna Bojda, Anna Kowalewska „Hybrid S.C.-polylactide/poly(silsesquioxane) blends of improved thermal stability" – Thermochimica Acta, 2020, 687, 178592.

Mój udział polegał na zbadaniu struktury krystalicznej materiałów za pomocą szerokokątowego rozpraszania promieni Roentgena (WAXS).

Joanne
Bojda

mgr Joanna Bojda

Centrum Badań Molekularnych i Makromolekularnych

Polskiej Akademii Nauk

Sienkiewicza 112

90-363 Łódź

OŚWIADCZENIE WSPÓŁAUTORA

Oświadczam, że w pracy:

Kowalewska A., Herc A.S., Bojda J., Palusiak M., Markiewicz E., Ławniczak P., Nowacka M., Sołtysiak J., Różański A., Piórkowska E. „Supramolecular interactions involving fluoroaryl groups in hybrid blends of polylactide and ladder polysilsesquioxanes" – Polymer Testing, 2021, 94, 107033.

Mój udział polegał na zbadaniu struktury fazowej mieszanin za pomocą termicznej dynamicznej analizy mechanicznej (DMTA) oraz skaningowego mikroskopu elektronowego z możliwością badania metodą energodyspersyjnej spektroskopii rentgenowskiej (SEM-EDS). Zbadałam również właściwości termiczne składników mieszanin - fluorowanych poli(silsekwiokasów) za pomocą skaningowego kalorymetru różnicowego (DSC). Ponadto, przeprowadziłam badania właściwości mechanicznych mieszanin. Przeprowadziłam analizę uzyskanych wyników oraz uczestniczyłam w ich interpretacji.

Joanne Bojda

dr hab. inż. Magdalena Włodarska
Politechnika Łódzka
Instytut Fizyki
Wólczańska 219
90-924 Łódź

OŚWIADCZENIE WSPÓŁAUTORA

Oświadczam, że w pracy:

A.S. Herc, M. Włodarska, M. Nowacka, J. Bojda, W. Szymański, A. Kowalewska* „Supramolecular interactions between polylactide and model cyclosiloxanes with hydrogen bonding-capable functional groups", eXPRESS Polymer Letters 2020, 14, 134–153.

mój udział polegał na przeprowadzeniu badań dielektrycznych i opracowaniu ich wyników, a także na współredagowaniu rozdziału dotyczącego tych badań.

Magdalena Włodarska

dr inż. Witold Szymański

Politechnika Łódzka

Instytut Inżynierii Materiałowej

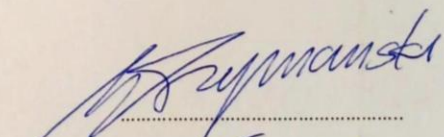Stefanowskiego 1/15

90-924 Łódź

OŚWIADCZENIE WSPÓŁAUTORA

Oświadczam, że w pracy:

A.S. Herc, M. Włodarska, M. Nowacka, J. Bojda, W. Szymański, A. Kowalewska* „Supramolecular interactions between polylactide and model cyclosiloxanes with hydrogen bonding-capable functional groups", eXPRESS Polymer Letters 2020, 14, 134–153.

Mój udział polegał na:

1. Przygotowaniu próbek do badań właściwości mechanicznych w tym: zatopienie próbek w żywicy epoksydowej i wykonanie zgładów.

2. Wykonanie badań nanoindentacji w trybie CSM z użyciem nanoindentera MTS NANO INSTRUMENTS G200.

3. Przygotowanie wykresów twardość/moduł w funkcji zagłębiania się penetratora (CSM)

4. Wykonanie badań nanoindentacji w trybie BASIC z użyciem nanoindentera MTS NANO INSTRUMENTS G200.

5. Przygotowanie map właściwości mechanicznych twardość/moduł (BASIC)

22. II. 2021

dr hab. Artur Różański
Centrum Badań Molekularnych i Makromolekularnych
Polskiej Akademii Nauk
Sienkiewicza 112
90-363 Łódź

OŚWIADCZENIE WSPÓŁAUTORA

Oświadczam, że w pracy:

Kowalewska A., Herc A.S., Bojda J., Palusiak M., Markiewicz E., Ławniczak P., Nowacka M., Sołtysiak J., Różański A., Piórkowska E. „Supramolecular interactions involving fluoroaryl groups in hybrid blends of polylactide and ladder polysilsesquioxanes" – Polymer Testing, 2021, 94, 107033.

Mój udział polegał na wykonaniu pomiarów właściwości barierowych analizowanych materiałów oraz opracowaniu zebranych danych.

Artur Różański

**FACULTY OF
CHEMISTRY**
University of Lodz

prof. dr hab. Marcin Palusiak
Department of Physical Chemistry
Faculty of Chemistry, University of Lodz
Pomorska 163/165, 90-236 Lodz, Poland
mobile phone: +48 504984038
phone: +48 42 6355737
fax: +48 42 6355744
e-mail: marcin.palusiak@chemia.uni.lodz.pl

OŚWIADCZENIE WSPÓŁAUTORA

Oświadczam, że w pracy:

Kowalewska A., Herc A.S., Bojda J., Palusiak M., Markiewicz E., Ławniczak P., Nowacka M., Sołtysiak J., Różański A., Piórkowska E. „Supramolecular interactions involving fluoroaryl groups in hybrid blends of polylactide and ladder polysilsesquioxanes" – Polymer Testing, 2021, 94, 107033.

mój udział nie był wiodący i polegał na wykonaniu obliczeń dla prostych układów modelowych oraz interpretacji tej części wyników.

prof. dr hab. Marcin Palusiak

www.uni.lodz.pl

dr hab. Ewa Markiewicz
Instytut Fizyki Molekularnej
Polskiej Akademii Nauk
Mariana Smoluchowskiego 17
60-179 Poznań

OŚWIADCZENIE WSPÓŁAUTORA

Oświadczam, że w pracy:

Kowalewska A., Herc A.S., Bojda J., Palusiak M., Markiewicz E., Ławniczak P., Nowacka M., Sołtysiak J., Różański A., Piórkowska E. „Supramolecular interactions involving fluoroaryl groups in hybrid blends of polylactide and ladder polysilsesquioxanes" – Polymer Testing, 2021, 94, 107033.

Mój udział polegał na:

Wykonaniu pomiarów przenikalności elektrycznej (wspólnie z dr Pawłem Ławniczakiem) oraz napisaniu odpowiedniego fragmentu publikacji.

Ewa Markiewicz

Ewa Markiewicz

dr inż. Paweł Ławniczak

Instytut Fizyki Molekularnej

Polskiej Akademii Nauk

Mariana Smoluchowskiego 17

60-179 Poznań

OŚWIADCZENIE WSPÓŁAUTORA

Oświadczam, że w pracy:

Kowalewska A., Herc A.S., Bojda J., Palusiak M., Markiewicz E., Ławniczak P., Nowacka M., Sołtysiak J., Różański A., Piórkowska E. *„Supramolecular interactions involving fluoroaryl groups in hybrid blends of polylactide and ladder polysilsesquioxanes"* – Polymer Testing, 2021, 94, 107033.

mój udział polegał na: wykonaniu badań, analizie oraz opisaniu właściwości dielektrycznych opisywanych w pracy polimerów. Badania te wykonane zostały we współpracy z dr. hab. Ewą Markiewicz w Instytucie Fizyki Molekularnej PAN.

Paweł Ławniczak

160

dr inż. Joanna Sołtysiak

Sieć Badawcza Łukasiewicz-Instytut Chemii Przemysłowej

im. Prof. Ignacego Mościckiego

Rydygiera 8

01-793 Warszawa

OŚWIADCZENIE WSPÓŁAUTORA

Oświadczam, że w pracy:

Kowalewska A., Herc A.S., Bojda J., Palusiak M., Markiewicz E., Ławniczak P., Nowacka M., Sołtysiak J., Różański A., Piórkowska E. „Supramolecular interactions involving fluoroaryl groups in hybrid blends of polylactide and ladder polysilsesquioxanes" – Polymer Testing, 2021, 94, 107033.

Mój udział polegał na: analizie TGA polysilseskwiosanów.

J Sołysiak.
19.02.2021

Zestawienie dorobku naukowego

Publikacje niewchodzące w skład rozprawy doktorskiej:

1. A.Kowalewska*, A.S.Herc, J.Bojda, M.Nowacka, E.Piórkowska, W.Kaczorowski, W.Szymański, Phase structure and properties of ternary PLA/PMMA/polysilsesquioxane blends. *Polymers*, 13 (2021) 1033.

2. M.Svyntkivska, T.Makowski*, E.Piorkowska, M.Brzezinski, A.Herc, A.Kowalewska, "Modification of polylactide nonwovens with carbon nanotubes and ladder poly(silsesquioxanes)", *Molecules*, 26 (2021) 1353.

3. M.Nowacka, A.S.Herc, A.Kowalewska*, "Thiol-ene addition of mercaptoalcohols to poly(vinylsiloxanes) under visible light photocatalysis – An approach towards cross-linkable hydrophilic silixones", *Polyhedron*, 185 (2020) 114588.

4. D.Kręgiel*, A.Rygała, B.Kolesińska, M.Nowacka, A.S.Herc, A.Kowalewska, „Antimicrobial and Antibiofilm N-acetyl-L-cysteine Grafted Siloxane Polymers with Potential for Use in Water Systems." *Int. J. Mol. Sci.*, 20 (2019) 2011.

Zgłoszenia patentowe:

1. A.Kowalewska, E.Piórkowska, A.S.Herc, M.Nowacka, J.Bojda „Sfunkcjonalizowane liniowe poli(silseskwioksany), sposób ich wytwarzania oraz ich kompozycje z biodegradowalnymi poliestrami i sposób ich otrzymywania", PL WIPO ST10/C PL429452 (29.03.2019) Polska.

Prezentacje ustne:

1. <u>A.S.Herc</u>, A.Kowalewska, J.Bojda, M.Nowacka, M.Palusiak, P.Lewiński, E.Piórkowska *Functionalized polysilsesquioxanes for polimer science.* 4th International Symposium on Silsesquioxanes-based Functional Materials (SFM2020), 4-7.11.2020, Busan, Korea – komunikat

2. <u>A.Kowalewska</u>, A.S.Herc, J.Bojda, M.Nowacka, P.Lewiński, E.Piórkowska

   Wpływ oddziaływań supramolekularnych na właściwości polilaktydów modyfikowanych za pomocą polisilseskwioksanów wstęgowych. 62. Zjazd PTChem, Warszawa, 2019 – referat sekcyjny

3. <u>A.Kowalewska</u>, M.Nowacka, A.S.Herc *Tetracyclosiloxanolates of alkali metals - precursors for polymeric materials.* 23rd Conference on Organometallic Chemistry (EuCOMC XXIII) Helsinki, Finlandia, 2019 - komunikat

4. <u>J.Bojda</u>, A.Kowalewska, A.S.Herc, E.Piorkowska, A.Rozanski *Poly(lactide) modified with poly(fluoroarylsilsesquioxanes) – structure and properties.* International Conference on Precisely Structured Polymer Materials (PSPM 2019) Łódź, 2019 – komunikat

5. <u>A.Kowalewska</u>, M.Nowacka, A.S.Herc, J.Bojda, *Self-assembly of hybrid poly(silsesquioxanes) for advanced materials*. 3rd International Conference on Biopolymers & Polymer Chemistry, Praga, Czechy, 2018 - wykład na zaproszenie komitetu organizacyjnego konferencji.

6. <u>A.Kowalewska</u>, A.S.Herc, J.Bojda, Nanokompozyty PLA z dodatkiem cyklosiloksanów. 61. Zjazd PTChem, 17-21.09.2018 Kraków - komunikat

Plakaty:

1. <u>A.S. Herc</u>, A. Kowalewska *Interactions of polylactide with fluoroaryl additives.* Eurofillers Polymerblends, Palermo, Włochy, 2019

2. <u>A.Kowalewska</u>, M.Włodarska, A.S.Herc, J.Bojda, M.Nowacka *Influence of hydrogen bonding for dynamics in hybrid polylactide nenocomposites.* Eurofillers Polymerblends, Palermo, Włochy, 2019

3. A.Kowalewska, M.Nowacka, A.S.Herc, S.Kaźmierski *Spectroscopic studies on crystallization of PLA nanocomposites.* 3rd International conference on Advanced Polymer Materials and Nanocomposites ANM 2019, Aveiro, Portugalia, 2019

4. <u>J.Bojda</u>, A.S.Herc, M.Nowacka, P.Lewinski, E.Piorkowska, A.Kowalewska *Crystallization of polylactide blended with novel functionalized oligomeric ladder-like polysilsesquioxanes.* International Discussion Meeting on Polymer Crystallization, San Sebastan, Hiszpania, 2019

5. <u>A.S.Herc</u>, A.Kowalewska *Nanocomposites of PLA and isomeric reactive cyclosiloxanes.* XX International Symposium „Advances in the Chemistry of Heteroorganic Compounds, 23-24.11.2017, Łódź.

Popularyzacja nauki:

1. A.S.Herc „*O pochodzeniu kolorów skóry*" – wykład na XIX Festiwalu Nauki, Techniki i Sztuki, 11.04.2019, Łódź.

2. A.S.Herc „*Pachnidło czy odór? – słów kilka o zapachach i zmyśle powonienia*" – wykład na XVIII Festiwalu Nauki, Techniki i Sztuki, 19.04.2018, Łódź.

3. Udział w Pikniku Naukowym w ramach XVII Festiwalu Nauki, Techniki i Sztuki, 08-09.04.2017, Łódź oraz XIX Festiwalu Nauki, Techniki i Sztuki, 13-14.04.2019, Łódź.

Udział w grantach:

1. Grant NCN, nr 2016/21/B/ST5/03070 OPUS 11 *Badanie oddziaływań supramolekularnych pomiędzy reaktywnymi wstęgowymi nanonapełniaczami nowego typu a matrycami polimerowymi.* – stypendysta/wykonawca (17 02 2017 do 16 08 2021)

2. Grant dla młodych naukowców przyznawany przez CBMiM: *Krzemoorganiczne pochodne tiolaktonów do zastosowań jako nanonapełniacze w hybrydowych nanokompozytach poli(L-laktydu),* 2017.